Discrete Quadratic Time–Frequency Distributions: Definition, Computation, and a Newborn Electroencephalogram Application

John M. O' Toole

A thesis submitted for the degree of Doctor of Philosophy at

The University of Queensland in March 2009

Perinatal Research Centre, University of Queensland Centre for Clinical Research, and
School of Medicine

Declaration by Author

This thesis is composed of my original work, and contains no material previously published or written by another person except where due reference has been made in the text. I have clearly stated the contribution by others to jointly-authored works that I have included in my thesis.

I have clearly stated the contribution of others to my thesis as a whole, including statistical assistance, survey design, data analysis, significant technical procedures, professional editorial advice, and any other original research work used or reported in my thesis. The content of my thesis is the result of work I have carried out since the commencement of my research higher degree candidature and does not include a substantial part of work that has been submitted to qualify for the award of any other degree or diploma in any university or other tertiary institution. I have clearly stated which parts of my thesis, if any, have been submitted to qualify for another award.

I acknowledge that an electronic copy of my thesis must be lodged with the University Library and, subject to the General Award Rules of The University of Queensland, immediately made available for research and study in accordance with the *Copyright Act 1968.*

I acknowledge that copyright of all material contained in my thesis resides with the copyright holder(s) of that material.

John M. O' Toole

Brisbane, January 2009

Statements of Contribution

0.1 Statement of Contributions to Jointly Authored Works

The candidate's and co-authors contribution to the articles for this dissertation is as follows. For articles [R1—R10] in Section 0.4:

- Candidate:
    - contributed to conception and design of research;
    - performed the research;
    - wrote the first drafts;
    - and contributed to editing the articles.
- Mostefa Mesbah:
    - contributed to conception and design of research;
    - and contributed significantly to editing the articles.
- Boualem Boashash:
    - contributed to conception and design;
    - and contributed to editing the articles;

For the article [R8] in Section 0.4 Paul Colditz contributed to the conception and design of the work.

0.2 Statement of Contributions by Others to the Thesis as a Whole

No contributions by others.

0.3 Statement of Parts of the Thesis Submitted to Qualify for the Award of Another Degree

None.

0.4 Published Works by the Author Incorporated into the Thesis

Publications by the candidate and advisory team relevant to the dissertation.

0.4.1 Journal Articles

R1 J. M. O' Toole, M. Mesbah, and B. Boashash, "A new discrete analytic signal for reducing aliasing in the discrete Wigner–Ville distribution," *IEEE Trans. Signal Processing*, vol. 56, no. 11, pp. 5427–5434, Nov. 2008.

- Incorporated in Chapter 3.

R2 J. M. O' Toole, M. Mesbah, and B. Boashash, "Algorithms for discrete quadratic time–frequency distributions," *WSEAS Trans. Signal Processing*, vol. 4, no. 5, pp. 320–329, May 2008.

- Incorporated in Chapter 5.

R3 J. M. O' Toole, M. Mesbah, and B. Boashash, "Improved discrete definition of quadratic time–frequency distributions," *IEEE Trans. Signal Processing, to be published*, Nov. 2008. [Online]. Available: doi:10.1109/TSP.2009.2031287

- Incorporated in Chapter 4.

0.4.2 Conference Articles

R4 J. M. O' Toole, M. Mesbah, and B. Boashash, "A new definition of discrete quadratic time–frequency distributions," in *Proc. Sixteenth European Signal Processing Conf. (EUSIPCO-08)*, Lausanne, Switzerland, Aug., 25–29 2008.

- Incorporated in Chapter 4.

R5 J. M. O' Toole, M. Mesbah, and B. Boashash, "Efficient algorithms for discrete time–frequency distributions," in *Proc. Applied Computing Conf. (ACC'08).* Istanbul, Turkey: World Scientific and Engineering Academy and Society (WSEAS), May, 27–30 2008, pp. 310–315.

- Incorporated in Chapter 5.

R6 J. M. O' Toole, M. Mesbah, and B. Boashash, "A new discrete-time analytic signal for reducing aliasing in discrete time–frequency distributions," in *Proc. Fifteenth European Signal Processing Conf. EUSIPCO-07*, Poznań, Poland, Sept.3–7 2007, pp. 591–595.

- Incorporated in Chapter 3.

R7 J. M. O' Toole, M. Mesbah, and B. Boashash, "A computationally efficient implementation of quadratic time–frequency distributions," in *Proc. Int. Sym. on Signal Processing and its Applications, ISSPA-07*, vol. I, Sharjah, United Arab Emirates, Feb. 12–15 2007, pp. 290–293.

- Incorporated in Chapter 5.

R8 J. M. O' Toole, M. Mesbah, B. Boashash, and P. Colditz, "A new neonatal seizure detection technique based on the time–frequency characteristics of the electroencephalogram," in *Proc. Int. Sym. on Signal Processing and its Applications, ISSPA-07*, vol. III, Sharjah, United Arab Emirates, Feb. 12–15 2007, pp. 132–135.

- Incorporated in Chapter 6.

R9 J. O' Toole, M. Mesbah, and B. Boashash, "A discrete time and frequency Wigner–Ville distribution: properties and implementation," in *Proc. Int. Conf. on Digital Signal Processing and Comm. Systems*, vol. CD-ROM, Dec. 19–21, 2005.

- Incorporated in Chapter 2.

R10 J. O' Toole, M. Mesbah, and B. Boashash, "Neonatal EEG seizure detection using a time–frequency matched filter with a reduced template set," in *Proc. Int. Sym. on Signal Processing and its Applications, ISSPA-05*, Aug. 28–31, 2005, pp. 215–218.

- Incorporated in Chapter 6.

0.5 Additional Published Works by the Author Relevant to the Thesis but not Forming Part of it

None.

Acknowledgements

I could not have done this work without the help of others and I take this opportunity to acknowledge their contribution.

I sincerely thank Prof. Boualem Boashash for providing me with the opportunity to do this research. I appreciate his assistance and guidance over the many years we have worked together. I also sincerely thank Dr. Mostefa Mesbah for his constant willingness to share his time and for tirelessly editing all written manuscripts—not a pleasant task by any stretch of the imagination. His considerable input has helped clarify and focus this document. I thank Prof. Paul Colditz for his helpful guidance and support, open-door policy, and for providing our signal processing research group with a new home at the Perinatal Research Centre.

Thanks also to my fellow researchers, past and present, whom have made the sometimes solidarity pursuit of a Ph.D. much more palatable: Ali, Calvin, Dan, Hamid, James, Luke, Malar, Mohamed, Nathan, and Peggy, to name but a few, thank you.

Outside of the research environment, I am very grateful for Locon and Dawn's assistance and am indebited to my parents for the invaluable support and encouragement throughout the years.

Finally, I thank those who suffered the most during my quest for further formal education: Veronique, Locon, and Iséabeal thank you for your understanding, love, compassion, and—most importantly for a Ph.D.—patience.

Abstract

Most signal processing methods were developed for continuous signals. Digital devices, such as the computer, process only discrete signals. This dissertation proposes new techniques to accurately define and efficiently implement an important signal processing method—the time–frequency distribution (TFD)—using discrete signals.

The TFD represents a signal in the joint time–frequency domain. Because these distributions are a function of both time and frequency they, unlike traditional signal processing methods, can display frequency content that changes over time. TFDs have been used successfully in many signal processing applications as almost all real-world signals have time-varying frequency content. Although TFDs are well defined for continuous signals, defining and computing a TFD for discrete signals is problematic. This work overcomes these problems by making contributions to the definition, computation, and application of discrete TFDs.

The first contribution is a new discrete definition of TFDs. A discrete TFD (DTFD) should be free from the sampling-related distortion known as aliasing and satisfy all the important mathematical properties that the continuous TFD satisfies. Many different DTFD definitions exist but none come close to attaining this ideal. I propose three new components which make up the DTFD: 1) a new discrete Wigner–Ville distribution (DWVD) definition which satisfies all properties, 2) a new discrete analytic signal which minimises aliasing in the DWVD, and 3) a new method to define and convolve the discrete kernel with the DWVD to produce the DTFD. The result: a DTFD definition that, relative to the existing definitions, better approximates the ideal DTFD.

The second contribution is two sets of computationally efficient algorithms to compute the proposed DTFD. The first set of algorithms computes the DTFD exactly; the second set requires less memory than the first set by computing time- and, or frequency-decimated versions of the DTFD. Both sets of algorithms reduce the computational load by exploiting symmetries in the DTFD and by constructing kernel-specific algorithms for four different kernel types.

The third, and final, contribution is a biomedical application for the proposed DTFD and algorithms. This application is to accurately detect seizure events in newborn electroencephalogram (EEG) signals. Existing detection methods do not perform well enough for use in a clinical setting. I propose a new method which is more robust than existing methods and show how using the proposed DTFD, comparative to an existing DTFD, improves detection performance for this method.

In summary, this dissertation makes practical contributions to the area of time–frequency signal processing by proposing an improved DTFD definition, efficient DTFD algorithms, and an improved newborn EEG seizure detection method using DTFDs.

Keywords

algorithms, aliasing, analytic signal, computational complexity, discrete signal processing, electroencephalogram (EEG), newborn, sampling, time–frequency distribution (TFD), Wigner–Ville distribution (WVD)

Australian and New Zealand Standard Research Classifications (ANZSRC)

090609 Signal Processing 80%, 090399 Biomedical Engineering not elsewhere classified 20%

Contents

List of Figures

List of Tables

Acronyms and Symbols

Acronyms

AF	ambiguity function
AF-GDTFD	alias-free generalised discrete time–frequency distribution
ARMA	auto-regressive moving average
AUC	area under curve
DAF	discrete ambiguity function
DAF-A	discrete ambiguity function (definition-A)
DF	Doppler–frequency
DFT	discrete Fourier transform
DL	Doppler–lag
DSP	discrete signal processing
DTFD	discrete time–frequency distribution
DWVD	discrete Wigner–Ville distribution
DWVD-A	discrete Wigner–Ville distribution (definition-A)
EEG	electroencephalogram
FDR	false detection rate
FFT	fast Fourier transform
FIR	finite impulse response
FM	frequency modulation
GDTFD	generalised discrete time–frequency distribution
IC	integrated circuit
IDFT	inverse discrete Fourier transform
IF	instantaneous frequency
LFM	linear frequency modulation signal
LPF	low pass filter
MB	modified-B distribution
MP	matching pursuit

NLFM	nonlinear frequency modulation
PSD	power spectral density
RHS	right hand side
RID	reduced interference distribution
ROC	receiver operator characteristics
ROM	random access memory
SBR	signal to background ratio
SIAF	spectral instantaneous autocorrelation function
SNR	signal to noise ratio
STFT	short-time Fourier transform
TDR	true detection rate
TF	time–frequency
TFD	time–frequency distribution
TFMF	time–frequency matched filter
TIAF	temporal instantaneous autocorrelation function
TL	time–lag
WGN	white Gaussian noise
WVD	Wigner–Ville distribution

Symbols

$x(t)$	real-valued signal
$z(t)$	analytic signal
$X(f)$	frequency-domain signal [Fourier transform of $x(t)$]
$\tilde{X}(f)$	periodic frequency-domain signal
$x(nT)$	discrete signal with sampling period T
$X(\frac{k}{NT})$	discrete, periodic frequency-domain signal
t, f, τ, ν	time t, frequency f, lag τ, and Doppler ν variables
$\rho_z(t,f)$	time–frequency distribution of $z(t)$
$W_z(t,f)$	Wigner–Ville distribution of signal $z(t)$
$K(t,\tau)$	temporal instantaneous autocorrelation function
$R(t,\tau)$	smoothed temporal instantaneous autocorrelation function
$A(\nu,\tau)$	ambiguity function
$S(\nu,\tau)$	smoothed ambiguity function
$\mathcal{K}(\nu,\tau)$	spectral instantaneous autocorrelation function

$\gamma(t,f)$	time–frequency kernel
$g(\nu,\tau)$	Doppler–lag kernel
$G(t,\tau)$	time–lag kernel
$\mathcal{G}(\nu,f)$	Doppler–frequency kernel
$W^{\mathrm{A}}(nT,\frac{k}{2NT})$	DWVD-A (Claasen–Mecklenbräuker)
$W^{\mathrm{B}}(\frac{nT}{2},\frac{k}{4NT})$	DWVD-B (Peyrin–Prost)
$W^{\mathrm{C}}(\frac{nT}{2},\frac{k}{2NT})$	DWVD-C (proposed)
$W^{\mathrm{D}}(nT,\frac{k}{4NT})$	DWVD-D (proposed)
$\rho^{\mathrm{A}}(nT,\frac{k}{2NT})$	generalised DTFD (Boashash–Reilly)
$\rho^{\mathrm{AF}}(nT,\frac{k}{2NT})$	alias-free generalised DTFD (Jeong–Williams)
$\rho^{\mathrm{C}}(\frac{nT}{2},\frac{k}{2NT})$	DTFD (proposed)
$W^{\mathrm{A}}[n,k]$	DWVD-A using sequence notation
$\widetilde{W}^{\mathrm{A}}(nT,f)$	discrete-time, continuous-frequency WVD (definition-A)
$\widetilde{\mathcal{W}}^{\mathrm{A}}(t,k\Lambda)$	continuous-time, discrete-frequency WVD
$\widetilde{K}^{\mathrm{A}}(t,\tau)$	periodic TIAF
$\widetilde{\mathcal{K}}^{\mathrm{A}}(\nu,f)$	periodic SIAF
$z_{\mathrm{c}}(nT)$	discrete analytic signal (Čížek–Bonzanigo)
$z_{\mathrm{p}}(nT)$	discrete analytic signal (proposed)
j	complex number symbol which represents $\sqrt{-1}$
$\mathcal{H}\{\cdot\}$	Hilbert transform
$\mathcal{F}\{\cdot\}$	Fourier transform
$\mathcal{F}^{-1}\{\cdot\}$	inverse Fourier transform
$\mathrm{DFT}\{\cdot\}$	discrete Fourier transform
$\mathrm{IDFT}\{\cdot\}$	inverse discrete Fourier transform
$\Re(\cdot)$	real-part operator
$\Im(\cdot)$	imaginary-part operator
$\mathcal{O}(\cdot)$	order of computational complexity
$z^*(t)$, $\big[z(t)\big]^*$	complex conjugate of $z(t)$
$\underset{t}{*}$	convolution operation in t
$\underset{n}{\circledast}$	circular convolution operation in n
$f_{\mathrm{i}}(t)$	instantaneous frequency
$\tau_{\mathrm{g}}(f)$	group delay

Chapter 1

Introduction

Quadratic time–frequency distributions (TFDs) are usually defined in the continuous domain for continuous signals. To generate a TFD on a computer, or other digital devices, we need to map the distribution from the continuous domain to the discrete domain. This mapping can have unintended consequences—the discrete distribution may not satisfy important mathematical properties that the continuous distribution satisfies, or the discrete distribution may be distorted by aliasing. In addition, because TFDs are two dimensional functions they require a large computational load and a large amount of computer memory to compute and store the discrete distribution.

The work in this dissertation has three broad aims. The first aim is to define a better, comparative to existing methods, discrete TFD definition—a new definition that is not distorted by aliasing and satisfies more important mathematical properties than existing definitions satisfy. The second aim is to design algorithms that minimises the computational load and memory required to compute and store a discrete TFD. The third and final aim is to show how discrete TFDs can be used to solve engineering problems, and more specifically how using a better discrete TFD definition can improve results.

This chapter starts with an introduction to discrete TFDs, relating these signal processing tools to the broader signal processing context. The next two sections presents the aims, contributions, and scope of the work. The chapter concludes with an outline of the dissertation.

1.1 Time–Frequency Signal Processing using Digital Computers

The common approach for implementing signal processing tools is to use personal computers, or similar digital computing devices, to do the processing numerically. (I henceforth use the term *computer* to refer to any digital computing device.) This approach is no different for TFDs. This section gives a brief introduction to signal processing using computers and the specific issues with computing TFDs.

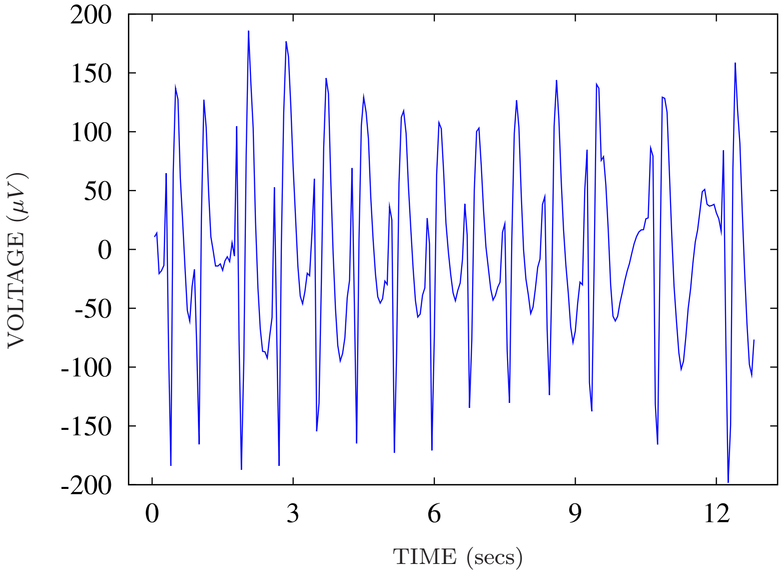

FIGURE 1.1: A time-domain plot of newborn electroencephalogram (EEG), a measurement of electrical activity in the brain.

1.1.1 Signals and Signal Processing

One of the most important aims of signal processing is to extract useful information from signals. Typically, signals are some form of measured quantity, such as sound recorded as a variation in air pressure on a microphone or a measurement of electrical potential between two electrodes attached to the scalp. More generally, any mathematical function of one or more variables is a signal. As signals are recorded on measurement devices over a period of time, they are usually represented as functions of time. Fig. 1.1 shows an example of a signal as a function of time. We shall assume here that all signals are a function of time, although we can easily translate the theory to any variable other than time.

Analysis of the signal in the time domain is known as *time-domain analysis*. For example, note how the signal in Fig. 1.1 is periodic—that is, it has a certain type of waveform which repeats over and over. Although all the information in the signal is contained within the time domain, it may be easier to extract the signal's information by transforming the signal to another domain. A useful analysis domain is the frequency domain. Using *frequency-domain analysis*, we may extract information about the frequency content of the signal. Fig. 1.2 is the frequency domain representation for our time-domain signal in Fig. 1.1. Note that there is a dominant peak, around 1.2 Hz, that represents the frequency for the repetition of the waveform which we previously noted in the time-domain plot. To transform the time-domain signal, $x(t)$, to the frequency domain, we use the Fourier transform [1, pp.7]:

$$X(f) = \int_{-\infty}^{\infty} x(t)\, \mathrm{e}^{-\mathrm{j}2\pi t f}\, \mathrm{d}f \tag{1.1}$$

where $X(f)$ represents the frequency-domain signal.

We can categorise signals into two groups: stationary signals and nonstationary signals. Nonstationary signals have frequency content, or statistical properties, that change

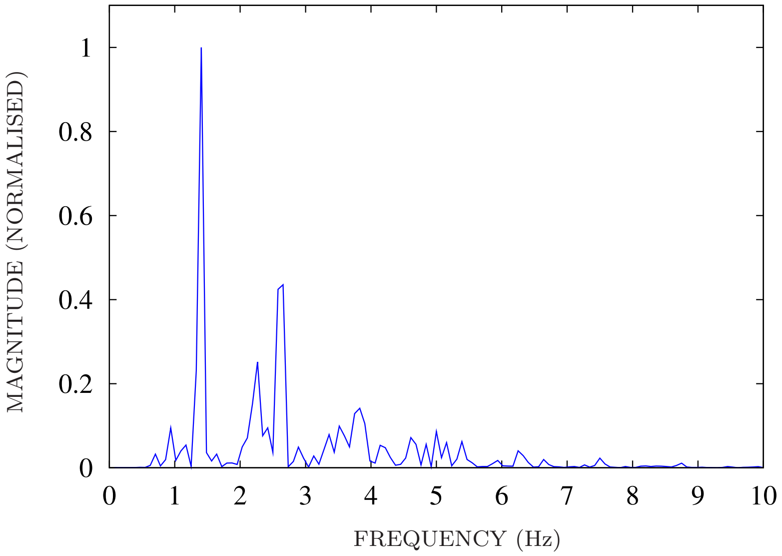

Figure 1.2: A frequency-domain plot of newborn EEG.

over time, unlike stationary signals that have constant frequency, or constant statistical proprieties, over time. For example, holding down one note on a piano produces a sound with constant frequency over time—a stationary signal. Conversely, playing a scale, many different notes in progression, produces a sound with changing frequency over time—a nonstationary signal. Most real-world signals are nonstationary. For the nonstationary signals however, frequency-domain analysis may obscure information as the frequency-domain does not show the time-varying nature of these signal.

1.1.2 Time–Frequency Signal Processing

A more appropriate domain of analysis for nonstationary signals is the joint time–frequency domain. This two-dimensional domain, which is a function of both time and frequency, is able to display the time-varying frequency content of the nonstationary signal. Fig. 1.3 shows our EEG signal in the time–frequency domain. Note how the frequency content of this signal changes over time as the components deviate to the left after about 8 seconds. This time–frequency representation also shows that the EEG signal is composed of a number of separate spectral components.

Representing the Time–Frequency Domain

There are many ways to represent a signal in the time–frequency domain. A problem for many time–frequency representations is that the signal transform from time to time–frequency is not linear. A nonlinear transform can produce artefacts, known as cross-terms, between signal components in the time–frequency representation. These cross-terms can distort signal information or make interpretation of the time–frequency representation difficult.

Probably the simplest method is the short-time Fourier transform (STFT) [2]. The method divides the signal into short-time segments and then Fourier transforms these segments to the frequency domain. This results in an array of Fourier transforms, one for

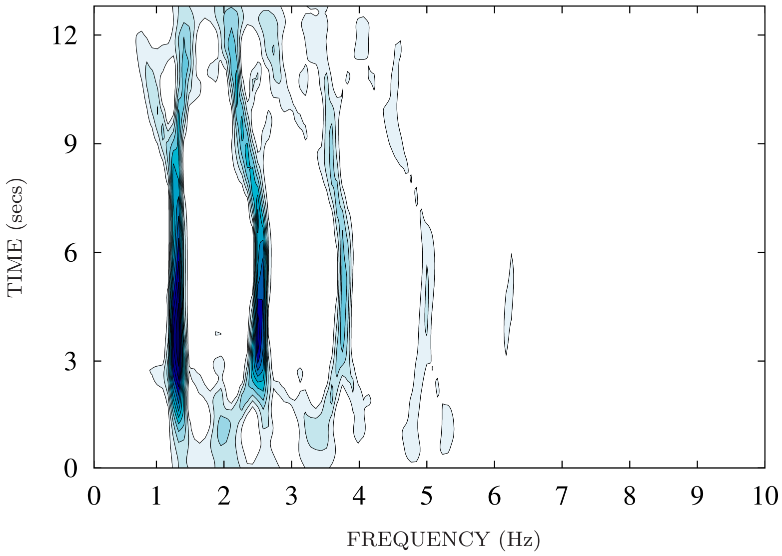

FIGURE 1.3: A time–frequency domain plot of newborn EEG.

each short-time segment. The magnitude squared of the STFT is a real-valued representation called the spectrogram.

The spectrogram is free from cross-terms but suffers from either poor time or poor frequency resolution. The method assumes that each time segment is stationary; when the segment is not stationary, the components in the representation have poor temporal resolution. In addition, if each segment is very short then the components have poor spectral resolution. Thus, there is a trade-off between time and frequency resolution, depending on the segment size. This poor time or frequency resolution limits the use of the spectrogram as not many nonstationary signals can be simply divided up into, sufficiently long, stationary periods.

Another method for generating time–frequency representations is the Wavelet transform [3]. The Wavelet transform decomposes the signal into a set of basis functions that are a function of time and scale. As scale is inversely proportional to frequency, the Wavelet transform can generate a time–frequency representation called the scalogram. The Wavelet transform has had many successful applications including image compression and denosing [4,5]. A limitation of the scalogram is that it does not provide uniform resolution throughout the time–frequency representation, thus making interpretation of the representation difficult. Also, the method is not frequency-shift invariant.

We can also generate a time-varying spectrum using a power spectral density (PSD) estimate method that uses a time-varying auto-regressive moving-average (ARMA) model [6]. This parametric method estimates a PSD, using the ARMA model, at a discrete-time interval of the signal. The method is limited by how accurately the ARMA model describes the signal. In addition, estimating the parameters for the ARMA model is, because of potential convergence and computational complexity problems, not a simple task [6].

Fig. 1.4 shows the three different time–frequency representations using a test signal example. The signal consists of two linear frequency modulated (LFM) components; one component is increasing in frequency and the other component is decreasing in frequency. The ideal representation is a highly resolved “X” shape in the time–frequency plane.

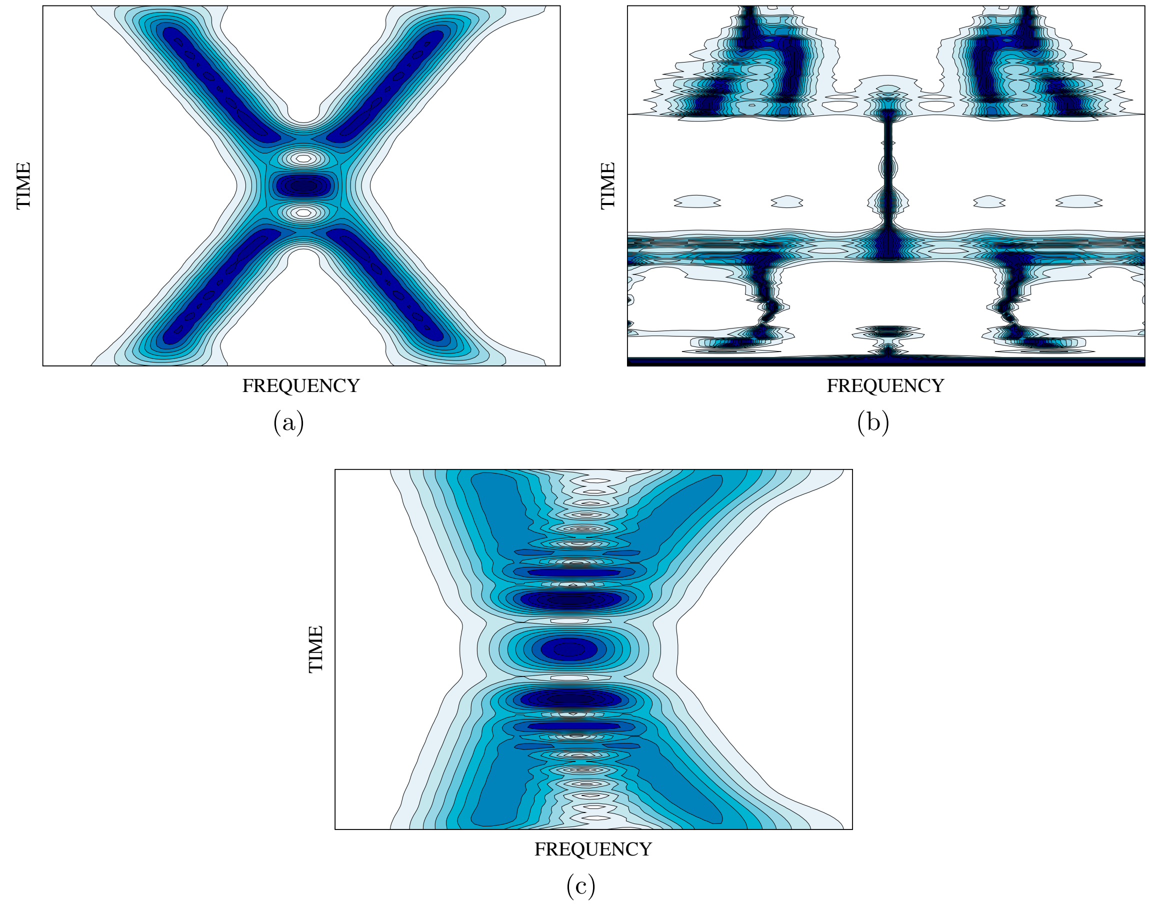

(a)

(b)

(c)

FIGURE 1.4: Time–frequency representations of two LFM components, one increasing with frequency over time and the other decreasing in frequency over time. (a) Spectrogram, (b) time-varying PSD estimation, and (c) scalogram.

Quadratic Time–Frequency Distributions

A quadratic time–frequency distribution is a quadratic transform that maps the signal from the time domain to a time–frequency representation [7,8]. Although there are other classes of TFDs, the quadratic class is probably the most useful and widely cited class in the literature [7,8,9], and is the focus of this dissertation. The quadratic class of TFDs is time- and frequency-shift invariant.

For time-domain signal $s(t)$, the quadratic TFD $\rho_z(t,f)$ has the form

$$\rho_z(t,f) = W_z(t,f) \underset{t}{*} \underset{f}{*} \gamma(t,f). \tag{1.2}$$

where $*_t$ represents the convolution operation in the time direction t and likewise $*_f$ represents the convolution operation in the frequency direction f. There are three steps involved in forming the TFD:

1. transform the real-valued signal $x(t)$ to a complex-valued analytic signal $z(t)$;
2. form the Wigner–Ville distribution (WVD) for $z(t)$:

$$W_z(t,f) = \int_{-\infty}^{\infty} z(t+\tfrac{\tau}{2}) z^*(t-\tfrac{\tau}{2})\, \mathrm{e}^{-\mathrm{j}2\pi\tau f}\, \mathrm{d}\tau \tag{1.3}$$

where $z^*(t)$ represents the complex conjugate of $z(t)$.

3. convolve the WVD, in time and frequency, with the time–frequency kernel $\gamma(t,f)$, as shown in (1.2).

The time–frequency kernel defines the type of TFD. For example, the WVD, which is a member of the quadratic TFD class, has the time–frequency kernel $\gamma(t,f) = \delta(t)\delta(f)$. Lets now look at these three steps in more detail.

Step 1: analytic signal The complex-valued analytic signal $z(t)$ is formed from the real-valued signal $x(t)$ as follows:

$$z(t) = x(t) + \mathrm{j}\mathcal{H}\{x(t)\}$$

where $\mathcal{H}\{\cdot\}$ is the Hilbert transform [1]. In the frequency domain,

$$Z(f) = X(f) + \mathrm{j}\mathcal{F}\left[\mathcal{H}\{x(t)\}\right] \tag{1.4}$$

where $\mathcal{F}[\cdot]$ represents the Fourier transform, $X(f) = \mathcal{F}\left[x(t)\right]$, and $Z(f) = \mathcal{F}\left[z(t)\right]$. The Fourier transform of the Hilbert transform is defined as

$$\mathcal{F}\left[\mathcal{H}\{x(t)\}\right] = \begin{cases} -\mathrm{j}X(f), & f \geq 0, \\ \mathrm{j}X(f), & f < 0. \end{cases} \tag{1.5}$$

Thus, the analytic signal has a zero negative spectrum. No signal information is lost, as $X(f)$ is (conjugate) symmetrical about $f = 0$. We can extract the instantaneous frequency (IF) $f_{\mathrm{i}}(t)$ from the analytic signal, as

$$f_{\mathrm{i}}(t) = \frac{1}{2\pi}\frac{\mathrm{d}\theta(t)}{\mathrm{d}t}$$

where $\theta(t)$ is the phase of $z(t)$. Ville proposed using the analytic signal, rather than the real-valued signal, in the WVD as he showed that the first moment of the WVD equals the IF of $z(t)$ [10]. Boashash described why the analytic is useful [11]: the WVD of the real-valued signal has cross-terms between positive and negative frequency components whereas the WVD of the analytic signal does not. The WVD of the analytic signal is free from positive–negative frequency cross-terms because the analytic signal has zero energy at negative frequencies. Fig. 1.5 shows the difference between the WVDs of the real-valued and analytic signals.

Step 2: Wigner–Ville distribution Ville was the first to apply a function derived by Wigner [12], in a quantum mechanics context, to signal processing. This function became known in the signal processing literature as the Wigner–Ville distribution (WVD). The distribution is a fundamental member of the quadratic TFD class: the WVD satisfies more useful mathematical properties than any other distribution in the class does and it uniquely provides optimal resolution for a one of the most basic types of signals used in signal processing, the sinusoidal signal. In addition, the WVD has been successfully applied to many engineering problems [13, 14, 15, 16, 17, 18, 19, 20].

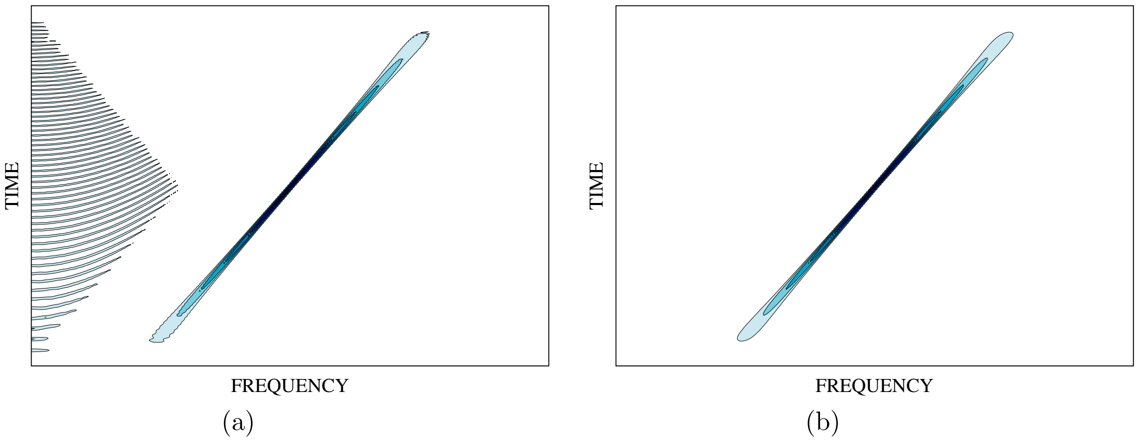

Figure 1.5: Wigner–Ville distribution of an LFM signal. Distribution in (a) uses real-valued signal and distribution in (b) uses analytic associate of signal. Distribution (a) has positive–negative frequency cross-terms.

The WVD has an optimal time–frequency representation for monocomponent linear frequency modulated (LFM) signals [1]. The WVD of an LFM signal with an IF of $f_i(t)$ is

$$W_z(t,f) = \delta(f - f_i(t))$$

where this delta function follows the IF law of the signal. When more than one signal component is present the WVD does not perfectly resolve. Because the transform from time to time–frequency for the WVD is quadratic, the distribution contains cross-terms between the signal's components. Cross-terms are present also for non-linear frequency modulated signals. These cross-terms make the interpretation of the WVD difficult, as they add spurious components to the distribution and many even distort signal components. Convolving the WVD with the time–frequency kernel $\gamma(t,f)$ can suppress, or even eliminate, the cross-terms.

Step 3: time–frequency distribution Quadratic TFDs can be expressed as smoothed WVDs, as shown in (1.2). By convolving the WVD with a kernel, cross-terms can be suppressed, leaving just the signal components in the distribution. Smoothing, however, will reduce the resolution of the signal's components and may result in a loss of a number of mathematical properties.

Fig. 1.6 shows an example of the WVD compared with a TFD, a smoothed WVD, using the same LFM signal shown in Fig. 1.4. The WVD in this example resolves the signal components well but contains many cross-terms around the "X" shaped signal components; the TFD suppresses the cross-terms but also smears the signal components. [The TFD in this example uses a kernel of the form $\gamma(t,f) = g_1(t)G_2(f)$, where $g_1(t)$ are $G_2(f)$ are Fourier transforms of Tukey windows [21] of different lengths.] Thus there is a trade off between time–frequency resolution of signal components on one hand, and suppression of cross-terms and possible loss of mathematical properties on the other hand.

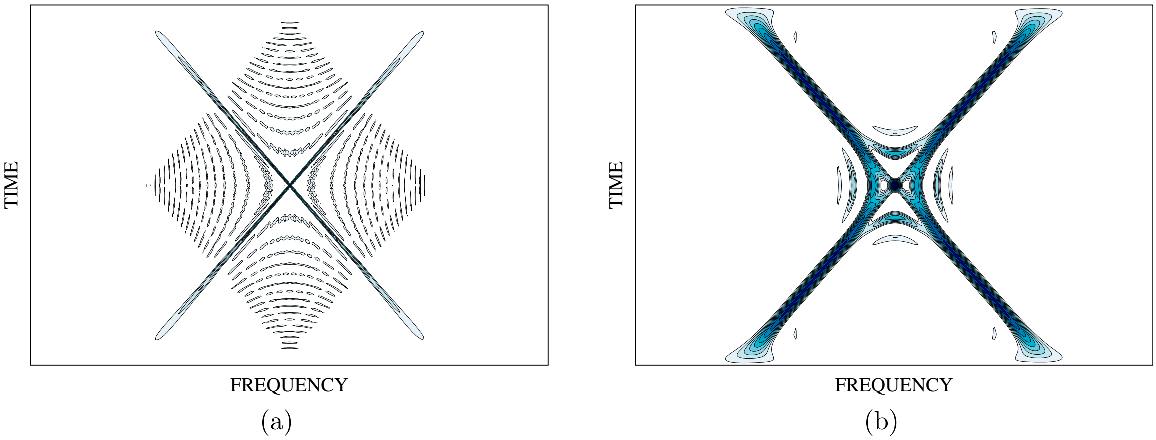

(a) (b)

FIGURE 1.6: Quadratic time–frequency distributions. (a) WVD and (b) TFD with smoothing kernel.

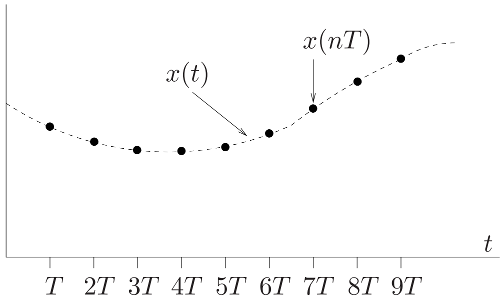

FIGURE 1.7: Discrete signal $x(nT)$ defined as sample points from the continuous signal $x(t)$.

1.1.3 Digital Signal Processing

The signal processing platform has—over time—changed from pen and paper, to mechanical devices, to analog circuits, and more recently, to digital devices. The transition from analog circuits to digital devices started in the 1950's with the introduction of the integrated circuit (IC). The IC brought circuit design into the industrialised age: ICs were mass produced and had the advantage of reliability and cost over the analog circuit. Soon the microprocessor, a self-contained IC processing unit, was developed. Today, microprocessors are integrated into many common devices such as computers, mobile phones, digital cameras, and personal music players.

To process a signal on a microprocessor, the signal must be discrete. A discrete signal is a sequence of numbers rather than a continuous function. Digital signal processing (DSP), a new branch of signal processing, emerged with the advent of the microprocessor.

Sampling Continuous signals

As most real-world signals are continuous, we first need to transform the signal into a discrete set of points. This process, known as sampling, takes discrete points at a constant time interval T from a continuous signal. Thus, the discrete signal $x(nT)$ equals $x(t)$ at $t = nT$. Fig. 1.7 shows an example of a discrete signal.

Intuitively, we can tell that the time spacing or period T between the sample points is

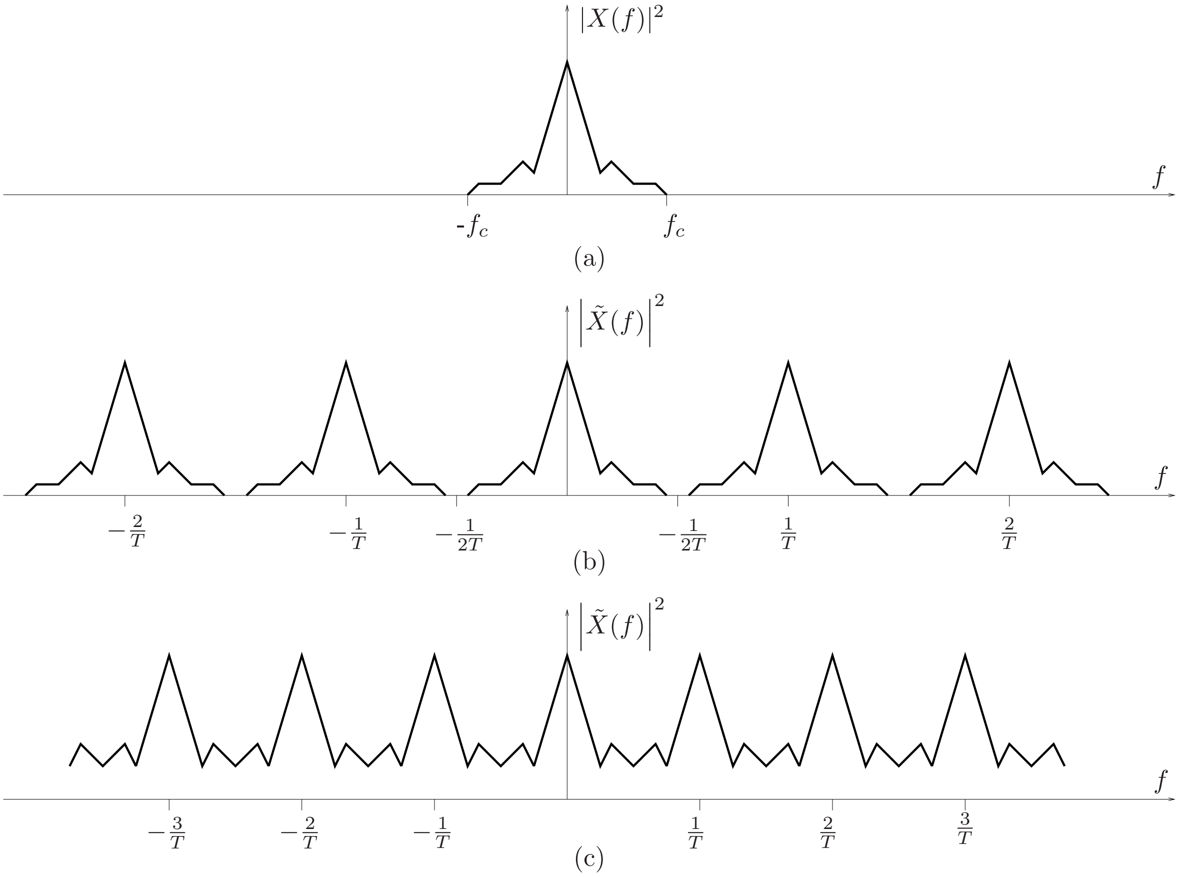

Figure 1.8: Effect of time-domain sampling: (a) $X(f)$, Fourier transform of continuous-time signal $x(t)$ with bandwidth $2f_c$, (b) $\tilde{X}(f)$, Fourier transform of discrete-time signal $x(nT)$, when $1/(2T) > f_c$, and (c) $\tilde{X}(f)$ when $1/(2T) < f_c$.

important—the larger this value is the more information we may loose from the continuous signal. Shannon formalised this [22]: he stated that the sampling frequency $1/T$, must be greater than or equal to twice the highest frequency component f_c in the signal; that is, $1/T \geq 2f_c$. Fig. 1.8 shows the effect that sampling has on the frequency domain—the spectrum of the discrete signal $x(nT)$ contains multiple frequency-shifted copies of the spectrum. Note that if we compare Fig. 1.8a with Fig. 1.8b, the spectrum within the range $|f| \leq 1/(2T)$ remains the same. This periodic spectrum $\tilde{X}(f)$ equals the nonperiodic spectrum $X(f)$ within this range because, for the example in Fig. 1.8b, $1/T > 2f_c$. Fig. 1.8c shows what happens when $1/T < 2f_c$: periodic copies in the spectrum overlap distorting the spectrum within the range $|f| \leq 1/(2T)$. This undesirable effect is known as aliasing.

Discrete Fourier transform

Sampling both the time-domain $x(t)$ and frequency-domain $X(f)$ signals results in the discrete and periodic signals $\tilde{x}(nT)$ and $\tilde{X}(k/NT)$, for $n, k = 0, 1, \ldots, N-1$. The discrete Fourier transform (DFT), the discrete version of the Fourier transform in (1.1), transforms between $\tilde{x}(nT)$ and $\tilde{X}(k/NT)$, as

$$\tilde{X}(\tfrac{k}{NT}) = \sum_{n=0}^{N-1} \tilde{x}(nT)\, \mathrm{e}^{-\mathrm{j}2\pi nk/N}.$$

The properties for the Fourier transform simply translate to the DFT [23]. In addition, there are computationally efficiently algorithms to compute the DFT [24].

Discrete TFDs

Forming the discrete TFD follows the same three steps as that for the continuous TFD—namely, form the analytic signal, then the WVD, and finally the TFD. There is an extra step for the DTFD, which is how to efficiently compute the DTFD. I pose questions at the end of each segment to highlight the limitations of the existing methods. The work in this dissertation addresses each of these questions.

Step 1: discrete analytic signal The discrete analytic is usually formed, using a discrete version of the frequency-domain method in (1.4) and (1.5), as follows [25, 26]:

1. DFT $\tilde{x}(nT)$ to $\tilde{X}(k/NT)$;
2. zero negative-frequency samples: let $\tilde{X}(k/NT) = 0$ for $k = N/2, ...N-1$;
3. Inverse DFT (IDFT) back to time domain and call this signal $\tilde{z}(nT)$.

The WVD of the discrete analytic signal $\tilde{z}(nT)$ is free from artefacts between positive–negative frequency components. To avoid aliasing in the WVD however, the discrete signal must satisfy two conditions [27]:

$$\tilde{z}(nT) = 0, \qquad N/2 \leq n \leq N-1, \tag{1.6}$$

$$\tilde{Z}(\tfrac{k}{NT}) = 0, \qquad N/2 \leq k \leq N-1, \tag{1.7}$$

By construction, the discrete analytic signal $\tilde{z}(nT)$ satisfies the second condition but not the first. To satisfy the first condition without losing signal information, we can zero-pad $\tilde{z}(nT)$ from length-N to $2N$ and replace N with $2N$ in (1.6) and (1.7). In doing so however, the DFT of the $2N$-point $\tilde{z}(nT)$ is no longer zero at negative frequencies as some spectral energy will leak into the negative-frequency range [27]. Now,

$$\begin{aligned} \tilde{z}(nT) &= 0, \qquad && N \leq n \leq 2N-1, \\ \tilde{Z}(\tfrac{k}{2NT}) &\approx 0, \qquad && N \leq k \leq 2N-1, \end{aligned} \tag{1.8}$$

where this approximation represents the spectral leakage caused by the zero-padding of $\tilde{z}(nT)$. Because $\tilde{Z}(k/2NT)$ does not have an exactly zero negative spectrum, the WVD of $\tilde{z}(nT)$ will not be completely alias free. In fact, the conditions in (1.6) and (1.7), for a finite-time and finite-frequency bandwidth signal, are mutually exclusive [28].

Question 1 Although it is not possible to completely eliminate aliasing from the WVD of a discrete signal, can we improve on the approximation in (1.8) to minimise this aliasing?

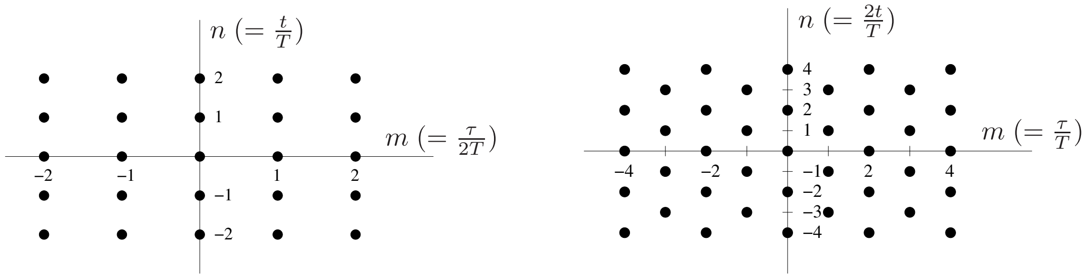

(a) (b)

FIGURE 1.9: Discrete time–lag grids with sampling period T for length $N = 5$ signal: (a) uniform discrete grid, and (b) nonuniform discrete grid. The black dots represent the time–lag locations of the sample points.

Step 2: discrete Wigner–Ville distribution The WVD of $\tilde{z}(nT)$ is discrete in both time and frequency. This discrete-time, discrete-frequency WVD is known simply as a discrete WVD (DWVD) [29]. Forming the DWVD from $\tilde{z}(nT)$ is problematic: how can we generate a discrete version of the time–lag function $K(t,\tau) = \tilde{z}(t + \tau/2)\tilde{z}^*(t - \tau/2)$ as the discrete signal $\tilde{z}(nT/2)$ does not exist for odd values of n? There are two approaches to tackling this problem. The first approach [30] forms the discrete time–lag function

$$K^{\mathrm{A}}(nT, 2mT) = \tilde{z}((n+m)T)\tilde{z}^*((n-m)T).$$

This method is equivalent to sampling $K(t,\tau)$ in time t with period T and τ with period $2T$. Fig. 1.9a shows the shape of this discrete time–lag grid.

The second approach [31,27] uses a nonuniform discrete grid, shown in Fig. 1.9b, to form

$$\begin{aligned} K^{\mathrm{A}}(nT, 2mT) &= \tilde{z}((n+m)T)\tilde{z}^*((n-m)T) \\ K^{\mathrm{A}}((n+\tfrac{1}{2})T, 2(m+\tfrac{1}{2})T) &= \tilde{z}((n+m+1)T)\tilde{z}^*((n-m)T). \end{aligned}$$

Although this methods still samples in τ with a period of $2T$, it also samples in t with a period of $T/2$, unlike the first method which samples in t with a period of T.

The DWVD is the DFT of the discrete time–lag function. Thus, we have two DWVD definitions, one which uses K^{A}, and the other, which uses K^{B}. Lets call the first definition [30] the DWVD-A and the second [27] the DWVD-B. DWVD-B, comparative to DWVD-A, retains more mathematical properties of the WVD—a consequence of the denser sampling grid, and therefore more signal information, in K^{B} compared with that for K^{A}. But DWVD-B requires $4N^2$ discrete sample points to compute, compared with N^2 for DWVD-A, and hence DWVD-B requires four times the computational load of DWVD-A.

Question 2 Can we define a DWVD that retains all important mathematical properties of the WVD and contains less than $4N^2$ sample points?

Step 3: discrete time–frequency distribution The discrete time–frequency distribution (DTFD) can be formed by convolving a DWVD with a discrete kernel. There are two commonly-used approaches for defining a DTFD. The first, known as the generalised DTFD (GDTFD) [32, 33, 34, 35], convolves DWVD-A with a discrete kernel:

$$\rho^{\mathrm{A}}(nT, \tfrac{k}{2NT}) = W^{\mathrm{A}}(nT, \tfrac{k}{2NT}) \underset{n}{\circledast} \underset{k}{\circledast} \gamma^{\mathrm{A}}(nT, \tfrac{k}{2NT}).$$

The second method, known as the alias-free GDTFD (AF-GDTFD), is a function of DWVD-B [36, 37, 29]:

$$\rho^{\mathrm{AF}}(nT, \tfrac{k}{2NT}) = \left[W^{\mathrm{B}}(\tfrac{n'T}{2}, \tfrac{k'}{4NT}) \underset{n'}{\circledast} \underset{k'}{\circledast} \gamma^{\mathrm{AF}}(\tfrac{n'T}{2}, \tfrac{k'}{4NT}) \right] \Bigg|_{n'=n/2, k'=k/2} .$$

The AF-GDTFD may, depending on the structure of the kernel, be aliased. There are two sources to this aliasing—aliasing from periodic overlap in the DWVD and aliasing from the discrete analytic signal's approximation in (1.8). In contrast, the GDTFD contains only minimal aliasing from the discrete analytic signal's approximation in (1.8). The AF-GDTFD, however, satisfies more mathematical properties that the GDTFD does. Nonetheless, the AF-GDTFD, which contains $4N^2$ sample points, requires four times the computational load to compute compared with the load for the GDTFD, which contains N^2 samples points. In addition, the AF-GDTFD does not satisfy the time- or frequency-support properties.

Question 3 Can we define a DTFD that satisfies all important mathematical properties, including the time- and frequency-support properties, contains only minimal aliasing, and contains less than $4N^2$ sample points?

Step 4: computing DTFDs To generate a DTFD using a computer, the algorithm uses a finite number of additions and multiplications, known as the computational load, and a finite number of memory points to compute and store the DTFD. A DTFD algorithm requires an approximate computational load of $\mathcal{O}(aN^2 \log_2 N)$ and aN^2 memory points [26], where a depends on the particular DTFD definition. This is a large computational load in comparison to DFT algorithms; DFT algorithms require a computational load of $\mathcal{O}(N \log_2 N)$ and N memory points to compute and store the DFT [38].

Reducing computational time and memory to compute a DTFD would help make the DTFD a more useful tool for signal processing. All digital devices are constrained by processing power and memory. Successful signal processing algorithms respect these limitations—for example the fast Fourier transform, a DFT algorithm, has been applied successfully in many practical engineering problems.

Question 4 Can we reduce the computational load and memory required to compute a DTFD?

1.2 Aims

This dissertation aims to improve on existing methods of implementing TFDs on a computer—how to define and efficiently compute a DTFD. More specifically, the dissertation addresses the questions from the previous section for the four stages involved with implementing TFDs. An extra, final stage, of this dissertation is to apply DTFDs to solve real-world signal processing problems. This application is a nonstationary detection problem—detecting seizure periods in newborn electroencephalogram (EEG) data.

I divide the aims of this dissertation into the following goals.

- *Goal 1:* To understand existing DWVD definitions by answering the following:
  - what is the relation between the continuous and discrete WVD definitions?
  - what properties do the DWVD definitions satisfy?
  - to what extent are the different DWVD definitions aliased?
  - are the DWVD definitions related to each other?
- *Goal 2:* To define a new DWVD definition, using the analysis from Goal 1, that improves—in terms of properties, aliasing, and computational load—on existing DWVD definitions.
- *Goal 3:* To define a DTFD that minimises aliasing and satisfies all the important properties of the continuous TFD.
- *Goal 4:* To design efficient DTFD algorithms that minimise the computational load and memory requirements for computing and storing the DTFD.
- *Goal 5:* To show how DTFDs can be used to solve practical signal processing problems. In particular, to use DTFDs to improve newborn EEG seizure detection methods.

1.3 Contributions and Scope

Addressing the goals of the previous section, the following lists the contributions of the dissertation. In addition, when appropriate, I describe the scope of this research:

- Addressing Goal 1
  - *Contribution:* Section 2.4.7 describes the relations between the DWVD definitions and the WVD. Section 2.5 details aliasing, mathematical properties, and the relations among the different DWVD definitions.
  - *Scope:* I derive the DWVD definitions using an impulse-train sampling approach [39], although other derivation approaches could be used, such as the group theory approach presented by Richman *et al.* [40]. Also, the properties examined in Chapter 2 and 4 are a set of mathematical properties that commonly appear in the literature [41, 31, 40, 42, 43, 44, 34, 36, 29, 45, 46]; I do not consider every mathematical property.
- Addressing Goal 2
  - *Contribution:* I propose a new DWVD definition in Section 2.6 [43]. This DWVD retains all the important mathematical properties of the WVD; contains minimal aliasing; and requires, comparative to the equivalent existing

  definition, only one-half of the computational load required to compute the distribution.

  To further minimise aliasing in the DWVD, I propose a new discrete analytic signal in Section 3.3. This analytic signal, relative to the commonly used discrete analytic signal, reduces aliasing in the DWVD by approximately 50%. This new signal also retains the useful attributes of the commonly-used analytic signal [47,46].

  - *Scope:* I compare aliasing in the DWVD with the commonly-used analytic signal [11,48,26,43] only; I do not compare aliasing with other analytic signal definitions.
  - *Scope:* I quantify aliasing, caused by the discrete analytic signal, in the DWVD and not in the more general DTFD form.

- Addressing Goal 3

  - *Contribution:* I propose a new DTFD definition in Section 4.3 that minimises aliasing and satisfies more important proprieties than other existing DTFD definitions [49,50]. This proposed DTFD definition uses the proposed DWVD and proposed discrete analytic signal.
  - *Scope:* The proposed DTFD definition is for the quadratic class of TFDs only; I do not consider other classes of TFDs.

- Addressing Goal 4

  - *Contribution:* I propose a set algorithms in Section 5.3 to minimise the computational time and memory needed to compute and store the proposed DTFD [45,51,52].
  - *Scope:* I do not compare the proposed algorithms with the sum-of-spectrogram algorithms [53,54] that generate only approximate DTFDs, not exact DTFDs.

- Addressing Goal 5

  - *Contribution:* I propose a newborn EEG seizure detection method, based on an existing time–frequency method, in Section 6.5.2 [55,56]. The method uses the proposed DTFD definition and the proposed algorithms.
  - *Scope:* I have not compared the proposed detection method with all other existing detection methods. I leave this analysis to future work.

1.4 Outline

The rest of the dissertation is organised, chapter by chapter, as follows.

- *Chapter 2: Discrete Wigner–Ville Distributions* This chapter presents a detailed analysis of two existing DWVD definitions and proposes two new DWVD definitions. This analysis includes a rigorous derivation for the DWVDs, presents the relations between the discrete and continuous domains, and examines the mathematical properties of the DWVD. Then, I show that the two existing definitions are fundamental DWVD definitions as most other existing DWVD definitions are simply related to them. Next, I propose two new DWVD definitions. One of the proposed DWVD definitions, like one of the existing DWVD definitions, retains all the important properties of the continuous WVD. The proposed DWVD, however, requires only one-half of the computational load and memory to compute and store the distribution compared with that for the existing DWVD.

- *Chapter 3: Discrete Analytic Signals* This chapter proposes a new discrete analytic signal that minimises aliasing in the DWVD. Unfortunately, the two conditions on the signal for an alias-free DWVD are mutually exclusive. The proposed analytic signal, however, better approximates these conditions compared with the commonly-used, or *conventional*, discrete analytic signal's approximation. The proposed analytic signal retains the two useful attributes of the conventional analytic signal: it satisfies the signal recovery and orthogonality properties and it can be computed simply. Results in this chapter show that the DWVD of the proposed analytic signal has 50% less aliasing than that for the DWVD of the conventional analytic signal.

- *Chapter 4: Discrete Time–Frequency Distributions* This chapter proposes a DTFD definition that minimises aliasing and satisfies all important properties. The chapter begins with a review of two popular DTFD definitions, the generalised DTFD (GDTFD) [34] and the alias-free GDTFD (AF-GDTFD) [29]. I show why the AF-GDTFD is not always alias-free and may contain significant aliasing depending on the kernel structure; the GDTFD, in comparison, has minimal aliasing. The proposed DTFD definition is closely related to the GDTFD—the GDTFD is a time-decimated version of the proposed DTFD. The advantage of the proposed DTFD is that it satisfies more important properties than the GDTFD or AF-GDTFD does and, like the GDTFD, contains only minimal aliasing.

- *Chapter 5: Efficient Algorithms for Discrete Time–Frequency Distributions* This chapter proposes algorithms that aim to minimise the computational time and memory required to compute and store the proposed DTFD. The chapter presents two different approaches to this. The first approach presents four different algorithms, for four different kernel types, that minimises the computational load. For three of the four kernel types, the memory used to generate the DTFD is also minimised. This first approach computes the DTFD exactly. The second approach again presents four different algorithms for the four different kernel types but this time it generates a decimated version of the DTFD. We can use this second approach for computing the DTFD for long signals to avoid running out of memory. In addition, this second set of algorithms minimise the computational load.

- *Chapter 6: Neonatal Electroencephalogram Seizure Detection* This chapter proposes a newborn EEG seizure detection method. The method, which uses the proposed DTFD from Chapter 4 and the proposed algorithms from Chapter 5, is based on the time–frequency matched filter. One of the limitations to the existing time–frequency matched filter is that it requires a predefined template set. The performance of the matched filter is sensitive to how we define the template set. The proposed method generates a time–frequency matched filter without the need for a predefined template set. This makes the method more robust to variability in different newborn's EEG. The new detection method has promising results. Also, performance is increased when the method uses the proposed DTFD definition compared to using the GDTFD.

- *Chapter 7: Conclusions* This chapter presents conclusions—the importance, limitations, and significance—of the contributions in this dissertation. Also, the chapter presents some recommendations for future work.

Chapter 2

Discrete Wigner–Ville Distributions

2.1 Introduction

The Wigner–Ville distribution (WVD) is an important member of the quadratic class of TFDs. The WVD is known as the fundamental distribution, as all quadratic TFDs can be expressed as a function of the WVD and a time–frequency kernel [1]. Also, the WVD satisfies more desirable mathematical properties than any other distribution in the quadratic class [30, 1]. Computing a WVD on a digital device, such as a computer, requires a discrete version of the WVD. The discrete WVD (DWVD) is generated by transforming the discrete time-domain signal to a discrete two-dimensional WVD function. Two difficulties arise with this process.

The first problem for the DWVD is aliasing—a distortion of the DWVD's representation of the continuous WVD. An alias-free DWVD requires that the discrete signal $x(nT)$ satisfies the two mutually exclusive conditions (1.6) and (1.7) from Chapter 1, where $x(nT)$ is a Nyquist sampled signal with sampling period T. To approximate these conditions without losing signal information, we set the negative frequencies of $X(k/NT)$, the discrete Fourier transform of $x(nT)$, to zero and then zero-pad $x(nT)$ from length-N to $2N$ [41, 11]. The resultant signal $z(nT)$ has the form:

$$\begin{aligned} z(nT) &= 0, & N \leq n \leq 2N-1, \\ Z(\tfrac{k}{2NT}) &\approx 0, & N \leq k \leq 2N-1. \end{aligned} \tag{2.1}$$

Because of the approximation in this equation the DWVD of the $2N$-point $z(nT)$ will never be completely free from aliasing. Nonetheless, for this chapter I shall assume that $z(nT)$ provides a good approximation in (2.1) [27, 57, 46] and thus refer to the DWVD of $z(nT)$ as a pseudo-alias–free DWVD. Likewise, I shall refer to the DWVD of $x(nT)$ as an aliased DWVD because $x(nT)$ does not approximate the conditions.

The second problem for the DWVD is mathematical properties—does the DWVD satisfy all the important mathematical properties that the WVD satisfies? The DWVD may not satisfy all of these properties because of the problem with defining the discrete version of the time–lag function $K_z(t, \tau)$, where

$$K_z(t,\tau) = z(t + \tfrac{\tau}{2}) z^*(t - \tfrac{\tau}{2}).$$

[The WVD equals the Fourier transform of $K_z(t, \tau)$, as shown in (1.3).] Specifically, the problem lies in attaining the $\tau/2$ samples from the discrete signal $z(nT)$ as the sample points at $z(nT/2)$ are not available. Incorrect sampling of the discrete time–lag function can results in a loss of mathematical properties for the DWVD.

Many different DWVD definitions have been proposed [41,31,27,42,58,44] to tackle the aliasing and properties problems. Among these different definitions, there are two fundamental DWVD definitions, which I shall refer to as DWVD-A and DWVD-B. Claasen and Mecklenbräuker [41] proposed the first DWVD definition, DWVD-A; soon after, Chan [31] proposed the other definition, DWVD-B, which was later further developed by Peyrin and Prost [27]. Most other DWVD definitions are linear combinations of DWVD-A or DWVD-B [59, 60, 44].

This chapter provides a detailed analysis of DWVD-A and DWVD-B. This analysis includes a rigorous and unified derivation for the two definitions; a description of the properties of DWVD-A and DWVD-B; and details the relation between the two definitions and other DWVD definitions. The analysis shows that DWVD-B preserves all important properties of the WVD whereas DWVD-A does not. Computing DWVD-B, however, requires four times the computational load and computer memory compared with that for DWVD-A.

Additionally, at the end of the chapter, I propose two new DWVD definitions that are closely related to DWVD-B. One of these new DWVD definitions satisfies all important properties and requires only one-half of the computational load and memory to compute compared with that for DWVD-B.

The layout of this chapter is as follows. Section 2.2 introduces the continuous WVD and lists a set of important WVD properties. Section 2.4 presents the derivation of DWVD-A and DWVD-B. This section starts by reviewing the formulation of the discrete Fourier transform, which forms the basis of the method which I use to derive the DWVDs. Section 2.5 presents the sufficient conditions for the pseudo-alias–free DWVD. Also this section presents the set of important properties for the DWVD definitions and shows the relation between existing DWVD definitions. The last section proposes the two new DWVD definitions, which are time- and frequency-decimated versions of DWVD-B.

2.2 Continuous Wigner–Ville Distribution

We start with some definitions. The continuous Wigner–Ville Distribution (WVD) is defined in terms of the time–lag function $K(t,\tau)$ as [1]

$$W_x(t,f) = \int K_x(t,\tau)\,\mathrm{e}^{-\mathrm{j}2\pi f\tau}\,\mathrm{d}\tau. \tag{2.2}$$

The function $K_x(t,\tau)$, called the temporal instantaneous autocorrelation function (TIAF), is a function of the time-domain signal $x(t)$,

$$K_x(t,\tau) = x(t+\tfrac{\tau}{2})x^*(t-\tfrac{\tau}{2}). \tag{2.3}$$

The WVD can also be defined in terms of the Doppler–frequency function $\mathcal{K}_X(\nu,f)$ as

$$\mathcal{W}_X(t,f) = \int \mathcal{K}_X(\nu,f)\,\mathrm{e}^{\mathrm{j}2\pi\nu t}\,\mathrm{d}\nu. \tag{2.4}$$

---

[1] Assume that all integration and summation limits are from $-\infty$ to ∞ unless otherwise stated.

The function $\mathcal{K}_X(\nu, f)$, called the spectral instantaneous autocorrelation function (SIAF), is a function of the frequency-domain signal $X(f)$,

$$\mathcal{K}_X(\nu, f) = X(f + \tfrac{\nu}{2})X^*(f - \tfrac{\nu}{2}). \tag{2.5}$$

where $X(f)$ represents the Fourier transform of $x(t)$. Although the two expressions in (2.2) and (2.4) are equal—that is, $W(t, f) = \mathcal{W}(t, f)$—different notation is used here as it is needed later.

We can also use the TIAF to define the ambiguity function (AF) as

$$A_x(\nu, \tau) = \int K_x(t, \tau)\, \mathrm{e}^{-\mathrm{j}2\pi t\nu}\, \mathrm{d}t. \tag{2.6}$$

The AF represents the Doppler–lag (ν, τ) domain. The AF, as a function of the SIAF, is

$$\mathcal{A}_X(\nu, \tau) = \int \mathcal{K}_X(\nu, f)\, \mathrm{e}^{\mathrm{j}2\pi f\tau}\, \mathrm{d}f$$

where $\mathcal{A}_X(\nu, \tau) = A_x(\nu, \tau)$.

The four functions in (2.2), (2.3), (2.5) and (2.6), which represent four different domains, are linearly related by the Fourier transform as follows:

$$\begin{tikzcd}
& W(t,f) \arrow[r, "\underset{t\to\nu}{\mathcal{F}}"] & \mathcal{K}(\nu,f) & X(f) \arrow[l] \\
x(t) \arrow[r] & K(t,\tau) \arrow[u, "\underset{\tau\to f}{\mathcal{F}}"] \arrow[r, "\underset{t\to\nu}{\mathcal{F}}"] & A(\nu,\tau) \arrow[u, "\underset{\tau\to f}{\mathcal{F}}"] &
\end{tikzcd} \tag{2.7}$$

This diagram also highlights the relation of these functions with $x(t)$ and $X(f)$: the TIAF $K(t, \tau)$ is a function of $x(t)$ whereas the SIAF $\mathcal{K}(\nu, f)$ is function of $X(f)$. Thus, we can form the WVD or AF from either the time- or frequency-domain signal.

Note on Time-Domain Signals Throughout this chapter, we use two types of signals: the real-valued signal $x(t)$ and its analytic associate $z(t)$. The analytic signal $z(t)$, which is complex valued, has zero energy at negative frequencies [1, 61]. Therefore, the analytic signal has half the frequency bandwidth of the real-valued signal. The WVD of the analytic signal is free from cross-term artefacts—present when the real-valued signal is used—between the positive- and negative-frequency components in the WVD [11]. In addition, as we shall see later, using the analytic signal in the WVD significantly reduces aliasing in DWVD.

Also note that although the term Wigner–Ville distribution usually [8] implies that the distribution uses the analytic signal rather than the real-valued signal, in this dissertation I refer to the Wigner–Ville distribution as a distribution that uses either the analytic or real-valued signal.

2.2.1 Properties

The WVD satisfies more mathematical properties than any other quadratic distribution. I now introduce and explain a set of properties for the WVD. These properties, which are of practical importance, often appear in the literature [41,31,40,42,43,44,34,36,29,45,46]. All these properties are applicable to either the real-valued signal $x(t)$ or the analytic signal $z(t)$.

- **Quadratic form:** The WVD, as a member of the quadratic TFD class, has the general quadratic form

  $$W(t,f) = \int\int x(t_1)x^*(t_2)H(t_1,t_2;t,f)\,\mathrm{d}t_1\,\mathrm{d}t_2$$

  where the function $H(t_1,t_2;t,f)$ is

  $$H(t_1,t_2;t,f) = \delta(t - \tfrac{t_1+t_2}{2})\,\mathrm{e}^{-\mathrm{j}2\pi(t_1-t_2)f}.$$

- **Realness:** The WVD $W_x(t,f)$ is real valued for any signal $x(t)$.

- **Time–frequency covariance:** The WVD is invariant to time and frequency shifts. That is, a shift in time or frequency in the time-domain signal produces an equivalent shift in time or frequency in the WVD. A signal of the form

  $$y(t) = x(t-t_0)\,\mathrm{e}^{\mathrm{j}2\pi f_0 t}$$

  produces a shift in the WVD as follows:

  $$W_y(t,f) = W_x(t-t_0, f-f_0).$$

- **Time marginal:** Integrating the WVD over frequency gives the instantaneous power:

  $$\int W_x(t,f)\,\mathrm{d}f = |x(t)|^2$$

- **Frequency marginal:** Integrating the WVD over time gives the spectral density:

  $$\int W_x(t,f)\,\mathrm{d}t = |X(f)|^2$$

- **Time support:** If the signal $x(t)$ is time limited to $x(t)=0$ for $t<t_1$ and $t>t_2$, then the WVD is likewise time limited:

  $$W_x(t,f) = 0, \qquad \text{for } t<t_1 \text{ and } t>t_2.$$

- **Frequency support:** If the signal $X(f)$ is frequency limited to $X(f)=0$ for $f<f_1$ and $f>f_2$, then the WVD is likewise frequency limited:

  $$W_x(t,f) = 0, \qquad \text{for } f<f_1 \text{ and } f>f_2.$$

- **Instantaneous frequency:** The first moment, with respect to frequency, of the WVD is equal to the instantaneous frequency (IF):

  $$\frac{\int f W_z(t,f)\,\mathrm{d}f}{\int W_z(t,f)\,\mathrm{d}f} = f_i(t)$$

  The IF $f_i(t)$ is defined as

  $$f_i(t) = \frac{1}{2\pi}\frac{\mathrm{d}\phi(t)}{\mathrm{d}t}$$

  where $\phi(t)$ is the instantaneous phase of the analytic signal $z(t)$.

- **Group delay:** The first moment, with respect to time, of the WVD is equal to the group delay:

  $$\frac{\int t W_z(t,f)\,\mathrm{d}t}{\int W_z(t,f)\,\mathrm{d}t} = \tau_g(f).$$

  The group delay $\tau_g(f)$ is defined as

  $$\tau_g(f) = \frac{1}{2\pi}\frac{\mathrm{d}\Theta(f)}{\mathrm{d}f}$$

  where $\Theta(f)$ is the phase of the frequency-domain signal $Z(f)$.

- **Moyal's formula:** This property, also known as unitarity or inner-product invariance, states that the inner product of the WVDs of two signals $x(t)$ and $y(t)$ is equal to the magnitude squared of the inner product of the two time-domain signals:

  $$\int\int W_x(t,f)W_y(t,f)\,\mathrm{d}t\,\mathrm{d}f = \left|\int x(t)y^*(t)\,\mathrm{d}t\right|^2.$$

- **Signal recovery:** We can recover the time-domain signal, up to a constant phase, from the WVD:

  $$\int W_x(\tfrac{t}{2},f)\,\mathrm{e}^{\mathrm{j}2\pi f t}\,\mathrm{d}f = x(t)x^*(0).$$

A notable omission from the preceding list of properties is the nonnegativity property. For most signal types, the WVD contains negative values. The nonnegativity property is important for the physical interpretation of the WVD as an energy density function. Even though the WVD does not satisfy this property, it has many useful engineering applications [62, 63, 13, 14, 15, 16, 17, 18, 19, 20].

2.3 Discrete Fourier Transform

The Fourier transform maps a time-domain signal to the frequency domain; the WVD maps a time-domain signal to the time–frequency domain—hence the Fourier transform and the WVD are, in a limited sense, alike. In fact, the WVD contains a Fourier transform. As (2.2) shows, the WVD Fourier transforms the time–lag function to the time–frequency domain. More generally, all four two-dimensional domains in (2.7) are related by Fourier

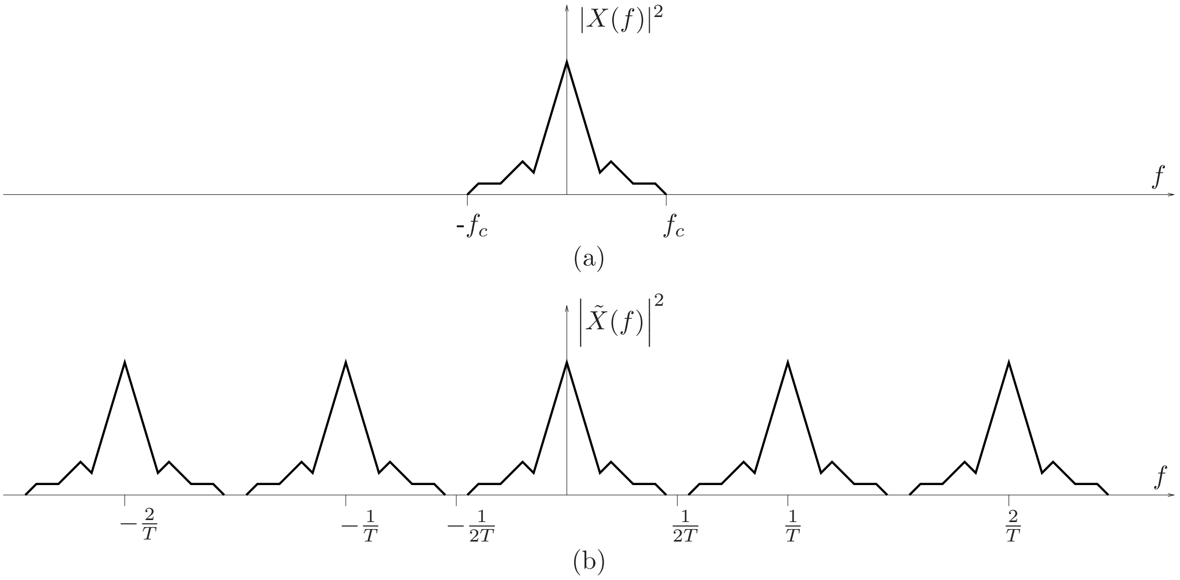

FIGURE 2.1: Effect of time-domain sampling: (a) $X(f)$, Fourier transform of continuous-time signal, and (b) $\tilde{X}(f)$, Fourier transform of discrete-time signal. In this example $X(f)$ is band limited to $|f| < f_c$ with $f_c < 1/(2T)$.

transforms. For these reasons, before defining the discrete WVD, we shall review the discrete Fourier transform.

The Fourier transform $X(f)$ of continuous time-domain signal $x(t)$ is defined as

$$X(f) = \int x(t)\, \mathrm{e}^{-\mathrm{j}2\pi tf}\, \mathrm{d}t. \tag{2.8}$$

The inverse Fourier transforms of the continuous frequency-domain signal $X(f)$ is

$$x(t) = \int X(f)\, \mathrm{e}^{\mathrm{j}2\pi tf}\, \mathrm{d}f. \tag{2.9}$$

Let us consider the effects of sampling a continuous signal. Let $x(nT)$ be a discrete time-domain signal sampled from $x(t)$ at a discrete set of sample points n separated in time by T. The Fourier transform of $x(nT)$ is $\tilde{X}(f)$, which is equal to an infinite sum of scaled and shifted copies of $X(f)$:

$$\tilde{X}(f) = \frac{1}{T} \sum_n X(f - \tfrac{n}{T}). \tag{2.10}$$

Fig. 2.1 illustrates the difference between the two frequency-domain signals. Thus, $\tilde{X}(f)$ is a periodic version of $X(f)$. The theory behind this relation is in Appendix A.1.

Similarly, let $X(k\Lambda)$ be a discrete frequency-domain signal sampled from $X(f)$ at a discrete set of sample points k separated in frequency by Λ. The inverse Fourier transform of $X(k\Lambda)$ is $\tilde{x}(t)$, where $\tilde{x}(t)$ is an infinite sum of scaled and shifted copies of $x(t)$ (see Appendix A.3 for details):

$$\tilde{x}(t) = \frac{1}{\Lambda} \sum_k x(t - \tfrac{k}{\Lambda}).$$

Thus, $\tilde{x}(t)$ is a periodic version of $x(t)$.

A computer requires both a discrete-time and discrete-frequency signal, as it cannot compute a continuous signal. We must sample, therefore, in both domains. Setting the frequency-domain sampling rate to $1/\Lambda = NT$ [23], then the discrete signals are related to the continuous signals as follows (see Appendix A.4 for details):

$$\begin{aligned}\tilde{X}(\tfrac{k}{NT}) &= \frac{1}{T}\sum_n X((k-nN)\tfrac{1}{NT}),\\ \tilde{x}(nT) &= NT\sum_k x((n-kN)T),\end{aligned}$$

The discrete signals do not equal samples of the continuous signals but, rather, equal scaled and shifted copies of the continuous signals. Thus, when $X(f)$ is not band limited then $\tilde{X}(f)$ is aliased; likewise, when $x(t)$ is not band limited then $\tilde{x}(nT)$ is aliased.

Now, if we assume that $x(t)$ is band limited to $0 < t < NT$ and $X(f)$ is band limited to $|f| < f_c$, then the discrete signals $\tilde{x}(nT)$ and $\tilde{X}(k/NT)$ should, ideally, equal samples of the continuous signals $x(t)$ and $X(f)$ in one period:

$$\begin{aligned}\tilde{x}(nT) &= x(nT), & 0 \le n \le N-1,\\ \tilde{X}(\tfrac{k}{NT}) &= X(\tfrac{k}{NT}), & 0 \le k \le N-1.\end{aligned} \tag{2.11}$$

when $f_c \le 1/(2T)$. This relation is not possible however—the assumption that both the time-domain and frequency-domain signals are both band limited is not valid [28] as a finite bandwidth in one domain must have an infinite bandwidth in the other domain.

In practice we assume that $x(t)$ is band limited and $X(f)$ is approximately band limited [28, 23]—that is, $x(t) = 0$ for $t < 0$ and $t > NT$ and $X(f) \approx 0$ for $|f| > 1/2T$—and therefore

$$\begin{aligned}\tilde{x}(nT) &= x(nT), & 0 \le n \le N-1,\\ \tilde{X}(\tfrac{k}{NT}) &\approx X(\tfrac{k}{NT}), & 0 \le k \le N-1,\end{aligned}$$

when $f_c \le 1/(2T)$. Because the discrete frequency-domain signal does not exactly equal samples of the continuous signal, $\tilde{X}(k/NT)$ is aliased. The extent of this aliasing, however, is controlled by the sampling frequency $1/T$; as $1/T$ increases, the period for shifted copies of $X(f)$ increases, as expressed by the relation (2.10). Thus, increasing the sampling frequency reduces aliasing and for most practical applications, this aliasing is assumed to be negligible and is usually ignored.

The discrete-time, discrete-frequency Fourier transform, known as the discrete Fourier transform (DFT), for band limited signals is defined as [23]

$$\begin{aligned}\tilde{X}(\tfrac{k}{NT}) &= \sum_{n=0}^{N-1} \tilde{x}(nT)\,\mathrm{e}^{-\mathrm{j}2\pi nk/N}\\ \tilde{x}(nT) &= \sum_{k=0}^{N-1} \tilde{X}(\tfrac{k}{NT})\,\mathrm{e}^{\mathrm{j}2\pi kn/N}.\end{aligned} \tag{2.12}$$

Fig. 2.2 shows two examples for $\tilde{X}(k/NT)$, assuming that $X(f)$ is band limited to $|f| < f_c$. The signal $\tilde{X}(k/NT)$ is alias free when $1/(2T) \ge f_c$, known as the Nyquist rate, and aliased when $1/(2T) < f_c$.

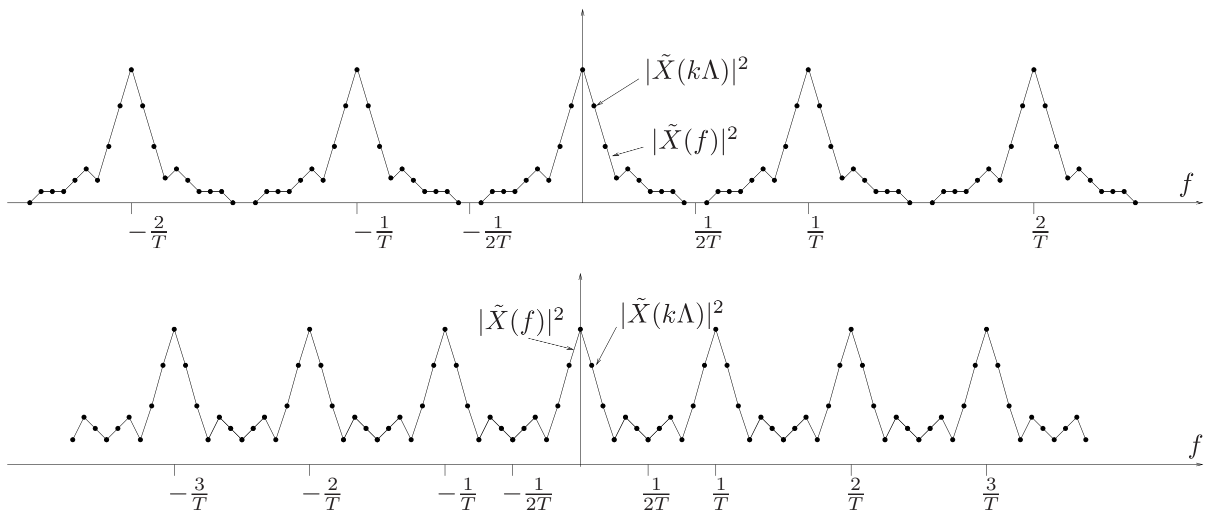

FIGURE 2.2: Discrete, periodic frequency-domain signal $\tilde{X}(k/NT)$. (a) Alias free as $1/(2T) > f_c$ and (b) aliased as $1/(2T) < f_c$ assuming that $X(f)$ is band limited to $|f| < f_c$. Each dot represents the sample point k separated by $1/NT$ in frequency.

2.4 Discrete Wigner–Ville Distribution

The following sections present derivations for the discrete WVD (DWVD), a discrete-time, discrete-frequency version of the WVD. The derivation methods use a two-dimensional sampling grid to sample in the time–lag and Doppler–frequency domains. The details for deriving a DWVD is more complicated than that for the DFT because the DWVD is a function of two variables and has four Fourier-related domains, but the process is essentially the same. Sampling in the two-dimensional time–lag domain and the two-dimensional Doppler–frequency domain produces a DWVD that is periodic in both the time and frequency directions.

Even though we sample the TIAF and SIAF directly, we must be able to form the discrete TIAF from $x(nT)$ and the discrete SIAF from $X(k/NT)$. Otherwise the resultant DWVD will not be able to fulfil its purpose—to transform time- or frequency-domain signals to the time–frequency domain.

The two-dimensional sampling-grid method was originally proposed by Nuttall in the appendix of his report [39]. I extend his method by using two types of two-dimensional sampling grids, one denser than the other. The outcome of using two different sampling grids is two different DWVD definitions. Both these DWVD definitions are existing definitions that were proposed using different derivations.

The purpose of presenting the following rigorous derivation is to provide a unified method for deriving DWVDs, something missing in current literature [30, 31, 64, 27, 57, 40, 42, 44]. I also apply the two-dimensional sampling approach to define discrete-Doppler, discrete-lag AFs.

2.4.1 Discrete-Time Wigner–Ville Distribution

If we sample only in the time–lag domain, then map this discrete TIAF to the time–frequency domain, the resultant distribution will be a discrete-time, continuous-frequency

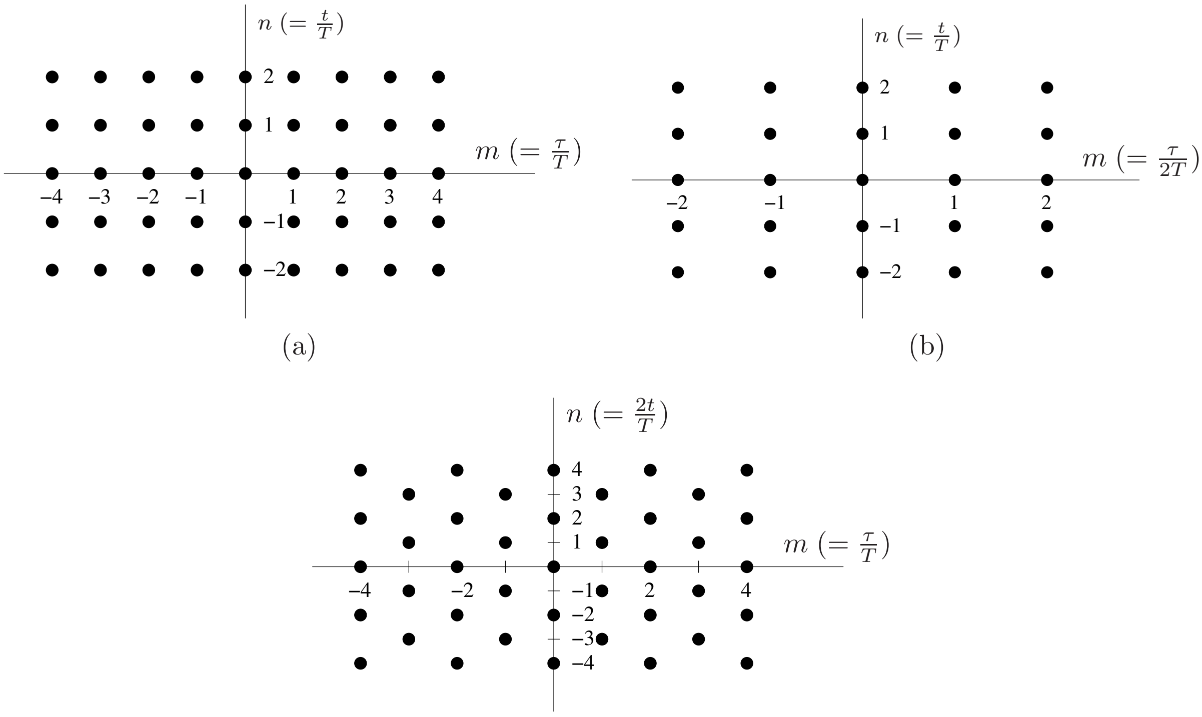

(a) (b)

(c)

FIGURE 2.3: Different time–lag (t, τ) sampling grids with sampling period T for length $N = 5$ signal: (a) ideal discrete grid (nT, mT), (b) discrete grid A $(nT, 2mT)$, and (c) discrete grid B $(nT/2, mT)$.

WVD. Here, we shall examine two different approaches for sampling the TIAF. Each approach results in a different discrete-time WVD definition, and also a different discrete-lag AF definition. Before we examine the two sampling approaches, we look at an ideal sampling approach for the TIAF—an approach we could use if we were not constrained to forming the TIAF from the discrete-time signal.

The derivations for most of the expressions in this section are in Appendix B.1.

The ideal approach is to sample the TIAF $K(t, \tau)$ in time and lag with sampling frequency $1/T$. Fig. 2.3a illustrates this sampling grid. This discrete TIAF, in terms of the discrete-time signal $x(nT)$, is

$$K^{\text{ideal}}(nT, mT) = x((n + \tfrac{m}{2})T)x^*((n - \tfrac{m}{2})T). \tag{2.13}$$

Unfortunately, we cannot generate this function because we only have samples of $x(nT)$ when n is an integer and do not have access to the sample points at $x(nT/2)$.

TIAF Sampling Approach A

Claasen and Mecklenbräuker [41] proposed a simple alternative to the ideal sampling approach by just ignoring the lag samples in (2.13) when m is odd. This procedure samples the TIAF in t with sample period T and in τ with sample period $2T$; Fig. 2.3(b) illustrates this sample grid.

Unlike the ideal discrete TIAF, we can generate this discrete TIAF $K^{\mathrm{A}}(nT, 2mT)$ from the discrete-time signal:

$$K^{\mathrm{A}}(nT, 2mT) = x((n+m)T)x^*((n-m)T).$$

Note that this discrete TIAF $x(aT)x^*(bT)$, where $a = n+m$ and $b = n-m$, uses only half of the outer product of this matrix $x(aT)x^*(bT)$ [36].

To form the discrete-time WVD, we simply take the discrete-time Fourier transform of $K^{\mathrm{A}}(nT, 2mT)$:

$$\widetilde{W}^{\mathrm{A}}(nT, f) = 2T \sum_m K^{\mathrm{A}}(nT, 2mT)\, \mathrm{e}^{-\mathrm{j}4\pi mTf}. \tag{2.14}$$

(The symbol $\widetilde{W}^{\mathrm{A}}$ represents the discrete-time WVD using sampling approach A.) This discrete-time WVD is related to the WVD as follows:

$$\widetilde{W}^{\mathrm{A}}(nT, f) = \sum_m W(nT, f - \tfrac{m}{2T}) \tag{2.15}$$

see Appendix B.1.1 for the proof. Thus, the discrete-time WVD equals shifted copies of the WVD, similar to the relation between the discrete-time Fourier transform and Fourier transform in (2.10); although the discrete-time WVD is periodic in $1/(2T)$ whereas the discrete-time Fourier transform is periodic in $1/T$. This result was first noted by Claasen and Mecklenbräuker [41].

TIAF Sampling Approach B

We now look at a different sampling approach, first presented by Chan [31]. Chan claimed that his discrete-time WVD was alias free—a claim disproved a year later by Claasen and Mecklenbräuker [59].

So why should we consider this sampling approach? Chan realised that by using this approach more signal information is used to the form the discrete TIAF, which results in a discrete-time WVD that satisfies more important properties than the distribution $\widetilde{W}^{\mathrm{A}}$.

Chan's method uses a nonuniform sampling grid, illustrated in Fig. 2.3c. The gird samples in time t with a period of $T/2$ and in lag τ with a period T. The discrete TIAF, as a function of $x(nT)$, for n and $(n + 1/2)$ sample values is

$$\begin{aligned} K^{\mathrm{B}}(nT, 2mT) &= x((n+m)T)x^*((n-m)T) \\ K^{\mathrm{B}}((n+\tfrac{1}{2})T, 2(m+\tfrac{1}{2})T) &= x((n+m+1)T)x^*((n-m)T). \end{aligned} \tag{2.16}$$

Because $K^{\mathrm{B}}(nT/2, mT)$ has a nonuniform discrete grid, the function is not defined at the sample points $(nT, 2(m+1/2)T)$ or $((n+1/2)T, 2mT)$. At n sample values, the TIAF is equal to $K^{\mathrm{A}}(nT, 2mT)$. In the matrix form $x(aT)x^*(bT)$, the discrete TIAF in (2.16), unlike the $K^{\mathrm{A}}(nT, 2mT)$, uses the full outer product. This sampling approach, therefore, uses more signal information compared with that for approach A. We can confirm this by comparing the density of the two sampling grids in Fig. 2.3b and Fig. 2.3c.

To form the discrete-time WVD, we take the discrete-time Fourier transform of this discrete TIAF,

$$\widetilde{W}^{\mathrm{B}}(\tfrac{nT}{2}, f) = 2T \sum_m K^{\mathrm{B}}(\tfrac{nT}{2}, mT)\, \mathrm{e}^{-\mathrm{j}2\pi mTf}.$$

For n and $(n+1/2)$ sample values this equates to

$$\begin{aligned}\widetilde{W}^{\mathrm{B}}(nT,f) &= \sum_m K^{\mathrm{B}}(nT,2mT)\,\mathrm{e}^{-\mathrm{j}4\pi mTf}\\ \widetilde{W}^{\mathrm{B}}((n+\tfrac{1}{2})T,f) &= \sum_m K^{\mathrm{B}}((n+\tfrac{1}{2})T,2(m+\tfrac{1}{2})T)\,\mathrm{e}^{-\mathrm{j}4\pi mTf}\,\mathrm{e}^{-\mathrm{j}2\pi Tf}\end{aligned} \tag{2.17}$$

Note, from (2.17), that $\widetilde{W}^{\mathrm{B}}(nT,f) = \widetilde{W}^{\mathrm{A}}(nT,f)$.

The relation between the discrete-time WVD and the continuous WVD (see Appendix B.1.1 for details) is

$$\widetilde{W}^{\mathrm{B}}(\tfrac{nT}{2},f) = \sum_m (-1)^{nm} W(\tfrac{nT}{2}, f - \tfrac{m}{2T}). \tag{2.18}$$

Thus, similar to the DWVD $\widetilde{W}^{\mathrm{A}}$, the DWVD $\widetilde{W}^{\mathrm{B}}$ is periodic in frequency with a period of $1/(2T)$. The periodic copies for W^{B}, however, alternate between positive and negative values depending on the values of n and m because of the $(-1)^{nm}$ term in (2.18).

2.4.2 Periodic Doppler–Frequency Domain

The discrete-time, discrete-lag TIAF results in periodicity, in Doppler and frequency, in the Doppler–frequency domain. Examining this continuous Doppler–frequency domain helps us understand aliasing in the discrete-time WVD.

Assuming that $X(f)$ is band limited to $|f| < 1/(2T)$ then the SIAF $\mathcal{K}(\nu,f)$, as defined in (2.5), is band limited to

$$|f \pm \tfrac{\nu}{2}| \leq \frac{1}{2T}.$$

This results in the diamond shaped SIAF [39, 57] illustrated in Fig. 2.4a. If we use the analytic signal $z(t)$ instead of the real-valued signal $x(t)$, where $Z(f)$ is band limited to $0 < f < 1/(2T)$, then this diamond shaped SIAF reduces to

$$f \pm \tfrac{\nu}{2} \leq \frac{1}{2T}.$$

Fig. 2.4b shows this region of support for the SIAF. Note we assume at this point that $x(t)$ and $z(t)$ have infinite length.

First, we look at sample approach A. The discrete-time Fourier transform of the discrete-time WVD results in the periodic SIAF, that is,

$$\widetilde{\mathcal{K}}^{\mathrm{A}}(\nu,f) = \sum_n \widetilde{W}^{\mathrm{A}}(nT,f)\,\mathrm{e}^{-\mathrm{j}2\pi\nu nT}.$$

This periodic function $\widetilde{\mathcal{K}}^{\mathrm{A}}$ is related to $\mathcal{K}$ as follows (see Appendix B.2 for details):

$$\widetilde{\mathcal{K}}^{\mathrm{A}}(\nu,f) = \frac{1}{T}\sum_n \sum_m \mathcal{K}(\nu - \tfrac{n}{T}, f - \tfrac{m}{2T}). \tag{2.19}$$

Fig. 2.5 displays the periodic SIAFs for both the real-valued signal $x(nT)$ and the analytic signal $z(nT)$. Periodic overlap distorts the SIAF of the real-valued signal whereas the

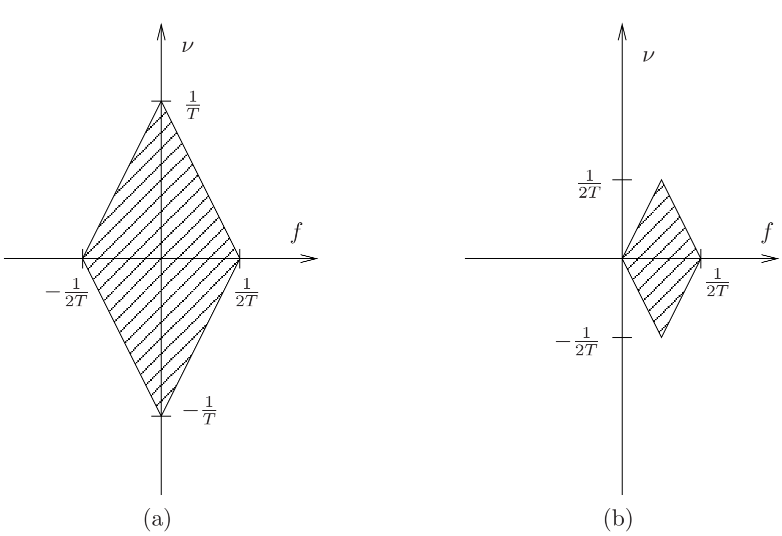

(a) (b)

FIGURE 2.4: Regions of support for the continuous bandlimited SIAF $\mathcal{K}(\nu, f)$ formed from (a) a real signal, and (b) an analytic signal.

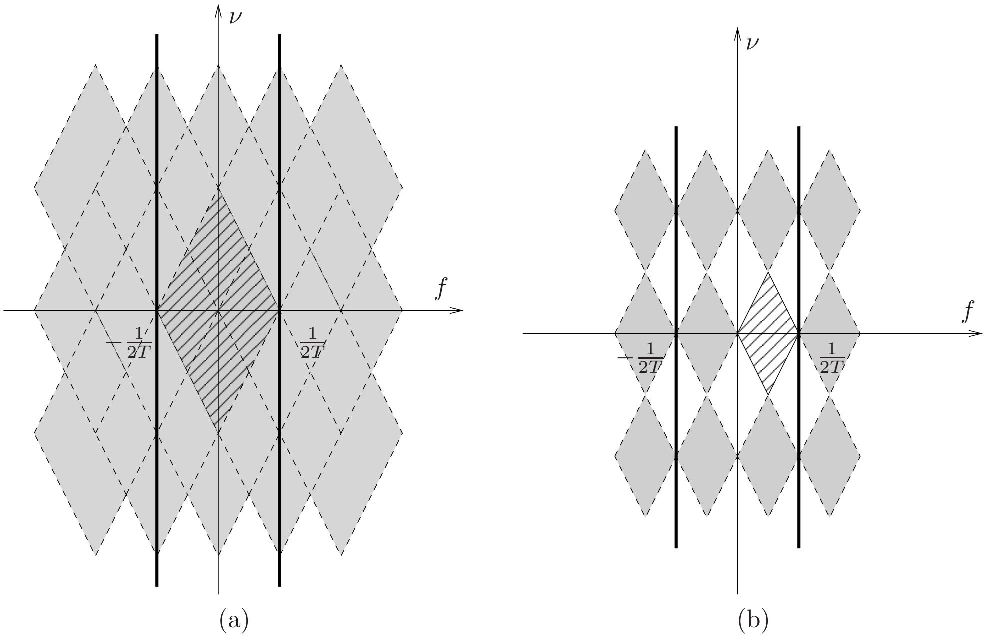

(a) (b)

FIGURE 2.5: Periodic SIAF $\widetilde{\mathcal{K}}^{\mathrm{A}}(\nu, f)$ for a (a) real and (b) analytic signal. The periodicity of the function is due to the sampling in the temporal domain. The signals are band limited in the frequency domain and infinite extent in the time domain. The two dark lines in each diagram represents the frequency extent of the discrete-time WVD, which is $|f| < 1/(2T)$.

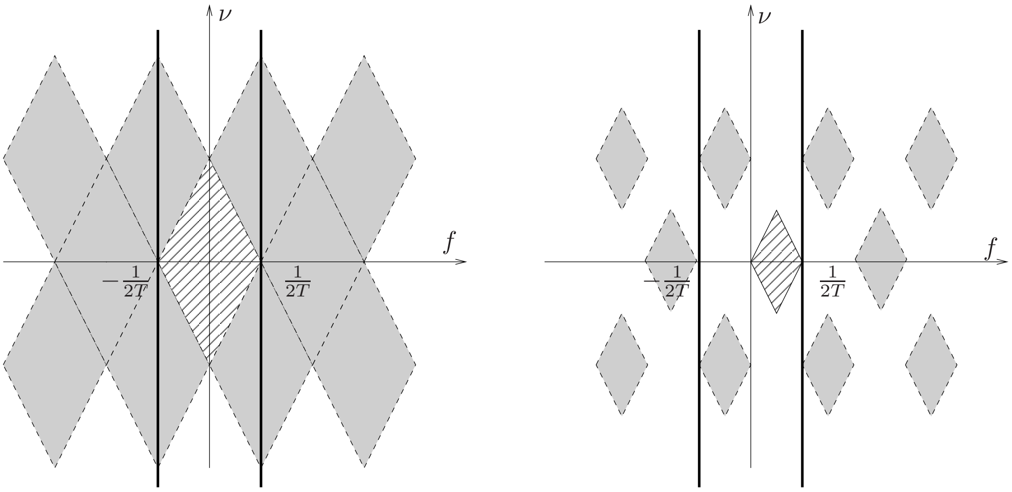

(a)

(b)

Figure 2.6: Periodic SIAF $\widetilde{\mathcal{K}}^{\mathrm{B}}(\nu,f)$ for (a) a real and (b) an analytic signal. The signals are band limited in the frequency domain and infinite extent in the time domain. The two dark lines in each diagram represents the frequency extent of the discrete-time WVD, which is $|f|<1/(2T)$.

SIAF of the analytic signal is free from periodic overlap. Both SIAFs, however, results in an aliased discrete-time WVD. This is because the SIAF for the analytic signal is not zero in the region $-1/(2T)<f<0$, and therefore the discrete-time WVD will not be zero in this region.

Now we look at sample approach B using a similar approach. The function $\widetilde{\mathcal{K}}^{\mathrm{B}}(\nu,f)$ is periodic as follows (see Appendix B.2.2):

$$\widetilde{\mathcal{K}}^{\mathrm{B}}(\nu,f)=\frac{2}{T}\underset{n+m\ \text{even}}{\sum_{n}\sum_{m}}\mathcal{K}(\nu-\tfrac{n}{T},f-\tfrac{m}{2T}). \tag{2.20}$$

This result was also noted by Nuttall [39].

Fig. 2.6 illustrates this periodicity for both the real and analytic signal. Compared with the SIAF $\widetilde{\mathcal{K}}^{\mathrm{A}}$, the SIAF $\widetilde{\mathcal{K}}^{\mathrm{B}}$ is more *spread-out*, and therefore we may be tempted to conclude that $\widetilde{W}^{\mathrm{B}}$ contains less aliasing than $\widetilde{W}^{\mathrm{A}}$. Yet within the region required to form the discrete-time WVD, which is bounded by $|f|\leq 1/(2T)$, periodic copies are present when we use either the real or analytic signal. Thus the discrete-time $\widetilde{W}^{\mathrm{B}}$ will be aliased, as (2.18) confirms.

The following example illustrates the difference between the two discrete-time WVDs $\widetilde{W}^{\mathrm{A}}$ and $\widetilde{W}^{\mathrm{B}}$. In this example, we use a linear frequency modulated (LFM) analytic signal. The two discrete-time WVDs are plotted in Fig. 2.7, where we see that both discrete-time WVDs are aliased. For the analytic signal, the aliased component is contained within the negative frequency range, as this region is zero for the continuous WVD. From (2.15) and (2.18), we can see that the two discrete-time WVDs are related differently to the WVD; in particular, the periodic copies for $\widetilde{W}^{\mathrm{B}}$ oscillate between positive and negative values, depending on the parity of n. This is caused by the $(-1)^{nm}$ term in (2.18), which is not present in (2.15).

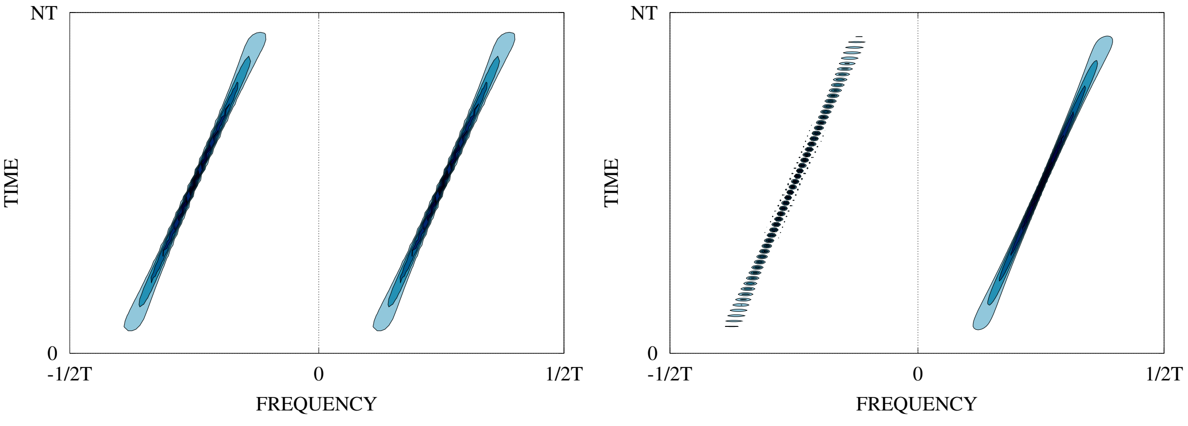

(a) (b)

FIGURE 2.7: Discrete-time WVD of analytic LFM signal. (a) Discrete-time WVD produced using sampling approach A, and (b) discrete-time WVD produced using sampling approach B.

We can apply the two sampled TIAF functions $K^{\mathrm{A}}(nT, 2mT)$ and $K^{\mathrm{B}}(nT/2, mT)$ to define a discrete–lag AF; the details are in Appendix C.1.

2.4.3 Discrete-Frequency Wigner Distribution

We now look at sampling the SIAF using a method similar to that in the previous section for the discrete TIAF. The derivations for most of the expressions in this section are in Appendix B.3.

SIAF Sampling Approach A

Sampling the SIAF in frequency f with sampling period Λ and in Doppler ν with sampling period 2Λ results in the discrete SIAF $\mathcal{K}^{\mathrm{A}}$,

$$\mathcal{K}^{\mathrm{A}}(2l\Lambda, k\Lambda) = X((k+l)\Lambda)X^*((k-l)\Lambda).$$

The discrete-frequency WVD is the inverse discrete-frequency Fourier transform, scaled by 2Λ, of the discrete SIAF,

$$\widetilde{\mathcal{W}}^{\mathrm{A}}(t, k\Lambda) = 2\Lambda \sum_{l} \mathcal{K}^{\mathrm{A}}(2l\Lambda, k\Lambda)\, \mathrm{e}^{\mathrm{j}4\pi l\Lambda t}. \tag{2.21}$$

The discrete-frequency WVD is related to the WVD as follows (see Appendix B.3.1 for details):

$$\widetilde{\mathcal{W}}^{\mathrm{A}}(t, k\Lambda) = \sum_{l} W(t - \tfrac{l}{2\Lambda}, k\Lambda). \tag{2.22}$$

Thus, the discrete-frequency WVD is periodic in time direction with a period of $1/(2\Lambda)$.

SIAF Sampling Approach B

Similar to K^{B}, we apply a nonuniform sampling grid to form the discrete SIAF $\mathcal{K}^{\mathrm{B}}$ as follows:

$$\begin{aligned}\mathcal{K}^{\mathrm{B}}(2l\Lambda, k\Lambda) &= X((k+l)\Lambda)X^*((k-l)\Lambda)\\ \mathcal{K}^{\mathrm{B}}(2(l+\tfrac{1}{2})\Lambda, (k+\tfrac{1}{2})\Lambda) &= X((k+l+1)\Lambda)X^*((k-l)\Lambda)\end{aligned}$$

The inverse discrete-frequency Fourier transform of this discrete SIAF $\mathcal{K}^{\mathrm{B}}$ is the discrete-frequency WVD $\widetilde{\mathcal{W}}^{\mathrm{B}}$,

$$\widetilde{\mathcal{W}}^{\mathrm{B}}(t, \tfrac{k\Lambda}{2}) = 2\Lambda \sum_l \mathcal{K}^{\mathrm{B}}(l\Lambda, \tfrac{k\Lambda}{2})\, \mathrm{e}^{\mathrm{j}2\pi l\Lambda t}.$$

For k and $(k+1/2)$ sample values, the preceding relation equates to

$$\begin{aligned}\widetilde{\mathcal{W}}^{\mathrm{B}}(t, k\Lambda) &= 2\Lambda \sum_l \mathcal{K}^{\mathrm{B}}(2l\Lambda, k\Lambda)\, \mathrm{e}^{\mathrm{j}4\pi l\Lambda t}\\ \widetilde{\mathcal{W}}^{\mathrm{B}}(t, (k+\tfrac{1}{2})\Lambda) &= 2\Lambda \sum_l \mathcal{K}^{\mathrm{B}}(2(l+\tfrac{1}{2})\Lambda, (k+\tfrac{1}{2})\Lambda)\, \mathrm{e}^{\mathrm{j}4\pi l\Lambda t}\, \mathrm{e}^{\mathrm{j}2\pi\Lambda t}.\end{aligned} \tag{2.23}$$

This discrete-frequency WVD is related to the WVD as follows (see Appendix B.3.2 for details):

$$\widetilde{\mathcal{W}}^{\mathrm{B}}(t, \tfrac{k\Lambda}{2}) = \sum_l (-1)^{kl} \mathcal{W}(t - \tfrac{l}{2\Lambda}, \tfrac{k\Lambda}{2}). \tag{2.24}$$

Thus, this discrete-frequency WVD $\widetilde{\mathcal{W}}^{\mathrm{B}}$, similar to $\widetilde{\mathcal{W}}^{\mathrm{A}}$, is periodic in time with a period of $1/(2\Lambda)$. The periodic copies for $\widetilde{\mathcal{W}}^{\mathrm{B}}$, however, alternate between positive and negative values, depending on the values of k and l, because of the $(-1)^{kl}$ term in (2.24).

2.4.4 Periodic Time–Lag Domain

Sampling in the temporal domain causes periodicity in the continuous spectral domain, as discussed in Section 2.4.2. Likewise, sampling in the spectral domain causes periodicity in the continuous temporal domain.

If $x(t)$ is time-limited to $|t| \leq 1/(2\Lambda)$, with an infinite frequency bandwidth, the continuous TIAF is bounded by

$$|t + \tfrac{\tau}{2}| \leq \frac{1}{2\Lambda}$$

resulting in the diamond shaped function illustrated in Fig. 2.8. This region of support is the same for both the real and analytic signal.

The periodic $\widetilde{K}^{\mathrm{A}}(t,\tau)$ is related to K as follows (see Appendix B.4.1 for details):

$$\widetilde{K}^{\mathrm{A}}(t,\tau) = \frac{1}{\Lambda} \sum_k \sum_l K(t - \tfrac{l}{2\Lambda}, \tau - \tfrac{k}{\Lambda}). \tag{2.25}$$

and the periodic $\widetilde{K}^{\mathrm{B}}(t,\tau)$ is related to K as follows (see Appendix B.4.2 for details):

$$\widetilde{K}^{\mathrm{B}}(t,\tau) = \frac{2}{\Lambda} \sum_{\substack{k \\ k+l \text{ even}}} \sum_l K(t - \tfrac{l}{2\Lambda}, \tau - \tfrac{k}{\Lambda}). \tag{2.26}$$

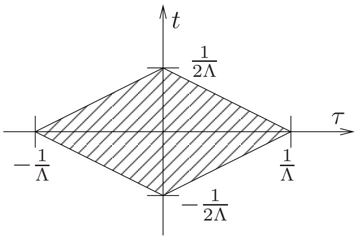

FIGURE 2.8: Region of support for the continuous-time TIAF $K(t,\tau)$ for either the real-valued or analytic signal.

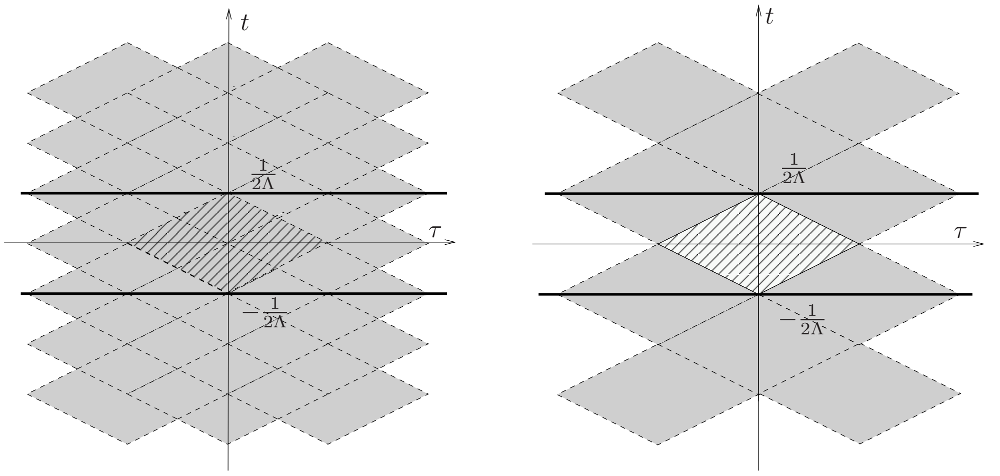

(a) (b)

FIGURE 2.9: The periodic continuous TIAF (a) $\widetilde{K}^{\mathrm{A}}(t,\tau)$, and (b) $\widetilde{K}^{\mathrm{B}}(t,\tau)$ of either the real-valued or analytic signal. The signals are band limited in the time domain and have an infinite extent in the frequency domain. The two dark lines in each diagram represents the time extent of the discrete-frequency WVD, which is $|t| < 1/(2\Lambda)$.

Both these periodic TIAFs are illustrated in Fig. 2.9.

Unlike the TIAF $\widetilde{K}^{\mathrm{A}}$, the TIAF $\widetilde{K}^{\mathrm{B}}$ does not have overlapping periodic components. The region, however, used to form the discrete-frequency WVD $\widetilde{\mathcal{W}}^{\mathrm{B}}$, bounded by $|t| \leq 1/(2\Lambda)$, does contain periodic components, as shown in Fig. 2.9b. Thus the discrete-frequency WVD $\widetilde{\mathcal{W}}^{\mathrm{B}}$ will be aliased, as supported by the relation (2.24).

To highlight the differences between the two discrete-frequency WVDs, the distributions are plotted in Fig. 2.10 using the same LFM analytic signal used in Fig. 2.7. The periodic copies for the discrete-frequency WVDs overlap in the time direction. For the discrete-frequency WVD $\widetilde{\mathcal{W}}^{\mathrm{B}}$, these periodic copies oscillate between positive and negative values depending on the parity of k.

We can form the discrete-Doppler AF using the two discrete SIAFs $\mathcal{K}^{\mathrm{A}}$ and $\mathcal{K}^{\mathrm{B}}$; Appendix C.2 contains the details.

2.4.5 Discrete-Time, Discrete-Frequency Wigner Distribution

To form a DWVD, which is discrete in time and frequency, we use either the discrete, periodic TIAF or discrete, periodic SIAF. The discrete, periodic TIAF is formed from the

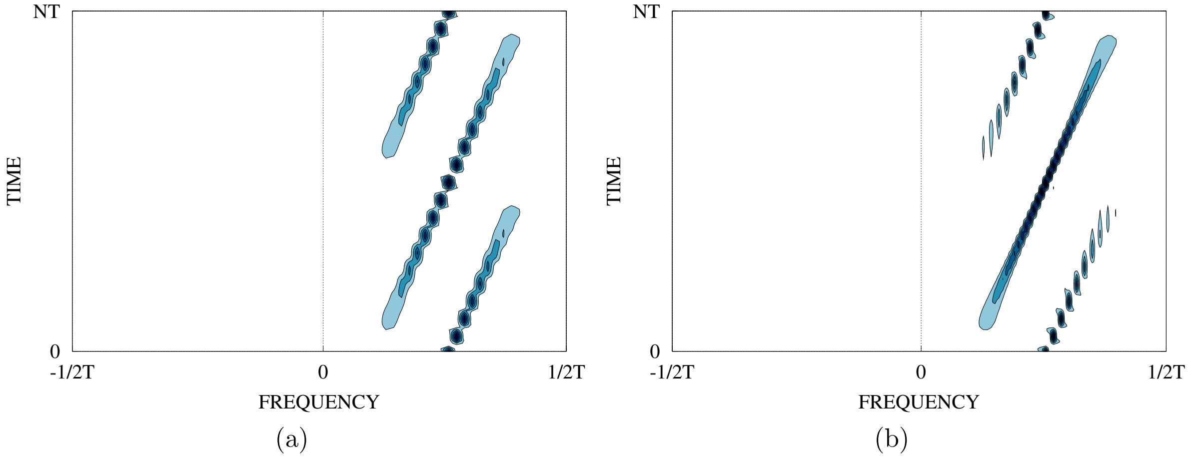

(a) (b)

Figure 2.10: Discrete-frequency WVD of analytic LFM signal. (a) Discrete-frequency WVD produced using sampling approach A, and (b) discrete-frequency WVD produced using sampling approach B.

discrete, periodic signal $\tilde{x}(nT)$; and likewise, the discrete, periodic SIAF is formed from the discrete, periodic signal $\widetilde{X}(k\Lambda)$.

Assume that $\tilde{x}(nT)$ is an alias-free signal of length NT and the frequency domain sampling rate is $\Lambda = 1/NT$, as discussed in Section 2.3. This signal will be used to form the discrete, periodic TIAF or SIAF. We examine the former first. The following analysis assumes that N is even. Derivations for this section are in Appendix B.5.

TIAF Sampling Approach A

The discrete and periodic TIAF $\widetilde{K}^{\mathrm{A}}(nT, 2mT)$ is formed by sampling the periodic TIAF $\widetilde{K}^{\mathrm{A}}(t,\tau)$ using sample approach A. This function, in terms of the discrete and periodic signal $\tilde{x}(nT)$, is

$$\widetilde{K}^{\mathrm{A}}(nT, 2mT) = \tilde{x}((n+m)T)\tilde{x}^*((n-m)T) + \tilde{x}((n+m+\tfrac{N}{2})T)\tilde{x}^*((n-m-\tfrac{N}{2})T)$$

for $|n| < N/4$ and $|m| < N/4$, which represents one period of the function.

The DWVD is the DFT, scaled by $2/N$, of the TIAF $\widetilde{K}^{\mathrm{A}}(nT, 2mT)$,

$$W^{\mathrm{A}}(nT, \tfrac{k}{NT}) = \frac{2}{N} \sum_{|m|<N/4} \widetilde{K}^{\mathrm{A}}(nT, 2mT)\, \mathrm{e}^{-\mathrm{j}4\pi mk/N}. \tag{2.27}$$

(I do not use the tilde accent—used thus far to denote periodicity—in the DWVD symbol W^{A} to distinguish the DWVD W^{A} from the discrete-time WVD $\widetilde{W}^{\mathrm{A}}$ or the discrete-frequency WVD $\widetilde{\mathcal{W}}^{\mathrm{A}}$. Irrespective of this notation, this discrete distribution W^{A} is periodic in both the time and frequency directions.)

The DWVD W^{A} is related to the WVD as follows:

$$W^{\mathrm{A}}(nT, \tfrac{k}{NT}) = \sum_{m}\sum_{l} W((n - \tfrac{lN}{2})T, (k - \tfrac{mN}{2})\tfrac{1}{NT}) \tag{2.28}$$

The derivation is in Appendix B.5.1.

TIAF Sampling Approach B

Sampling the periodic TIAF $\widetilde{K}^{\mathrm{B}}(t,\tau)$ with sampling approach B results in the discrete, periodic TIAF $\widetilde{K}^{\mathrm{B}}(nT/2, mT)$. This function, in terms of $\tilde{x}(nT)$, is

$$\begin{aligned} \widetilde{K}^{\mathrm{B}}(nT, 2mT) &= \tilde{x}((n+m)T)\tilde{x}^*((n-m)T) \\ \widetilde{K}^{\mathrm{B}}((n+\tfrac{1}{2})T, 2(m+\tfrac{1}{2})T) &= \tilde{x}((n+m+1)T)\tilde{x}^*((n-m)T) \end{aligned} \tag{2.29}$$

for $|n| < N$ and $|m| < N$, which represents one period.

The DWVD is the DFT transform, scaled by $1/N$, of the discrete TIAF $\widetilde{K}^{\mathrm{B}}(nT/2, mT)$,

$$W^{\mathrm{B}}(\tfrac{nT}{2}, \tfrac{k}{2NT}) = \frac{1}{N} \sum_{|m|<N} \widetilde{K}^{\mathrm{B}}(\tfrac{nT}{2}, mT)\, \mathrm{e}^{-\mathrm{j}\pi mk/N}. \tag{2.30}$$

and this DWVD is related to the WVD as follows:

$$W^{\mathrm{B}}(\tfrac{nT}{2}, \tfrac{k}{2NT}) = \sum_{l} \sum_{m} (-1)^{nm+lk-lmN} W((n-lN)\tfrac{T}{2}, (k-mN)\tfrac{1}{2NT}). \tag{2.31}$$

The derivation is in Appendix B.5.2.

We could also derive the DWVD by sampling the discrete, periodic SIAF. I show this in Appendix B.5.3 and Appendix B.5.4.

2.4.6 Periodic Time–Frequency Domain

Here we look at the relation between the discrete WVD definitions and the continuous WVD definitions for both the analytic and real-valued signals.

Real-valued Signal

Assume that the real-valued signal $x(t)$ has a finite time bandwidth of NT and an approximate finite frequency bandwidth $1/T$; that is,

$$\begin{aligned} x(t) &= 0, \quad |t| > \frac{NT}{2}, \\ X(f) &\approx 0, \quad |f| > \frac{1}{2T}. \end{aligned} \tag{2.32}$$

The approximation in (2.32) is because of the mutually exclusive constraints of finite time and frequency bandwidth [28]. Thus, the continuous WVD of $x(t)$ has the form [27]

$$W(t,f) \approx 0, \quad \text{for } |t| > \frac{NT}{2} \text{ or } |f| > \frac{1}{2T}. \tag{2.33}$$

Within the signal's time–frequency region—that is, within the region $|t| \leq NT/2$ and $|f| \leq 1/(2T)$—the two DWVD definitions W^{A} and W^{B} are related to the continuous WVD as follows:

$$W^{\mathrm{A}}(nT, \tfrac{k}{NT}) \approx \sum_{m=-1}^{1} \sum_{l=-1}^{1} W((n - \tfrac{lN}{2})T, (k - \tfrac{mN}{2})\tfrac{1}{NT}) \tag{2.34}$$

$$W^{\mathrm{B}}(\tfrac{nT}{2}, \tfrac{k}{2NT}) \approx \sum_{m=-1}^{1} \sum_{l=-1}^{1} (-1)^{nm+lk-lmN} W((n-lN)\tfrac{T}{2}, (k-mN)\tfrac{1}{2NT}). \tag{2.35}$$

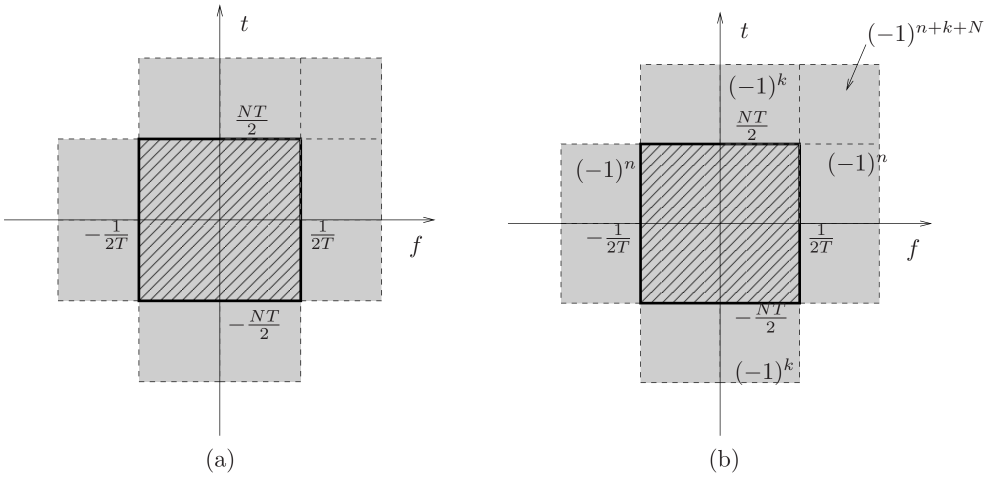

FIGURE 2.11: The DWVD (a) W^{A} and (b) W^{B} represented as a sum of time and frequency shifted WVD copies using the real-valued signal $x(t)$. The region for the WVD of the signal is represented by the area occupied by the slanted lines. For clarity only a subset of the terms in the summations in (2.36) are used. The terms $(-1)^n$, $(-1)^k$ and $(-1)^{n+k+N}$ in (b) are multiplicative factors for the shifted WVD copies.

The approximation sign in the preceding expressions is because $W(t, f)$ is not exactly zero outside of the signal's time and frequency band limits, as described in (2.33). Irrespective of this approximation, both DWVDs are aliased—Fig. 2.11 illustrates. The DWVD W^{A} is (an approximate) sum of WVDs which overlap in both the time and frequency direction. For the DWVD W^{B}, similar aliasing occurs, although for this DWVD definition the shifted WVD copies contain the multiplicative factor $(-1)^{nm+lk-lmN}$. Otherwise, they are aliased to the same extent.

Analytic Signal

Assume that complex-valued analytic signal $z(t)$ has a finite time bandwidth of NT and an approximate frequency bandwidth of $1/(2T)$; that is,

$$\begin{aligned} z(t) &= 0, \quad |t| > \frac{NT}{2}, \\ Z(f) &\approx 0, \quad f > \frac{1}{2T} \text{ or } f < 0. \end{aligned}$$

Thus, similar to the real-valued signal bandwidths in (2.32), the analytic signal has only an approximate finite frequency bandwidth. The WVD of $z(t)$, therefore, is zero outside the signal's time–frequency area; that is,

$$W(t, f) \approx 0, \quad \text{for } |t| > \frac{NT}{2}, \, f > \frac{1}{2T}, \text{ or } f < 0,$$

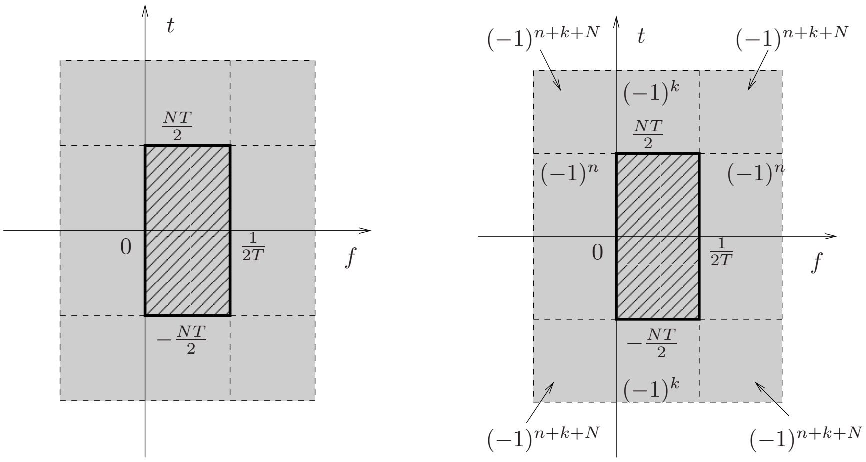

(a) (b)

FIGURE 2.12: The DWVD (a) W^{A} and (b) W^{B} represented as a sum of some time and frequency shifted WVD copies using an analytic signal. For clarity only a subset of the terms in the summations in (2.36) are used. The terms $(-1)^n$, $(-1)^k$ and $(-1)^{n+k+N}$ in (b) are multiplicative factors for the shifted WVD copies.

Within the signal's time–frequency region—that is, within the region $|t| \leq NT/2$ and $0 \leq f \leq 1/(2T)$—the two DWVDs are related to the continuous WVD as follows:

$$\begin{aligned} W^{\mathrm{A}}(nT, \tfrac{k}{NT}) &\approx \sum_{l=-1}^{1} W((n - \tfrac{lN}{2})T, \tfrac{k}{NT}) \\ W^{\mathrm{B}}(\tfrac{nT}{2}, \tfrac{k}{2NT}) &\approx \sum_{l=-1}^{1} (-1)^{lk} W((n - lN)\tfrac{T}{2}, \tfrac{k}{2NT}). \end{aligned} \tag{2.36}$$

Again, both DWVD definitions are aliased—Fig. 2.12 illustrates. Note that because the nonzero region for the WVD of the analytic signal $z(t)$ is smaller than that for the WVD of the real-valued signal $x(t)$, the extent of the periodic overlap, or aliasing, is smaller for the DWVD of the analytic signal as aliasing is present in the time direction only within the region $|t| \leq NT/2$ and $0 \leq f \leq 1/(2T)$.

This section concludes with an example. Fig. 2.13 shows the two DWVDs W^{A} and W^{B} of a LFM analytic signal. We see that aliasing is present in both the time and frequency directions but note that within the region $|t| \leq NT/2$ and $0 \leq f \leq 1/(2T)$, aliasing is present only in the time direction. Note also that both DWVDs are aliased to the same extent.

2.4.7 Key Results: Relation Between Continuous and Discrete Domains

To understand the characteristics of a discrete function, we must first understand the relation between the discrete and continuous function. This section highlights important results from Section 2.4.1, Section 2.4.3, Section 2.4.5, and Appendix C. Some, but not all, of these results have been presented by others [31, 59, 27, 57, 39, 36, 65].

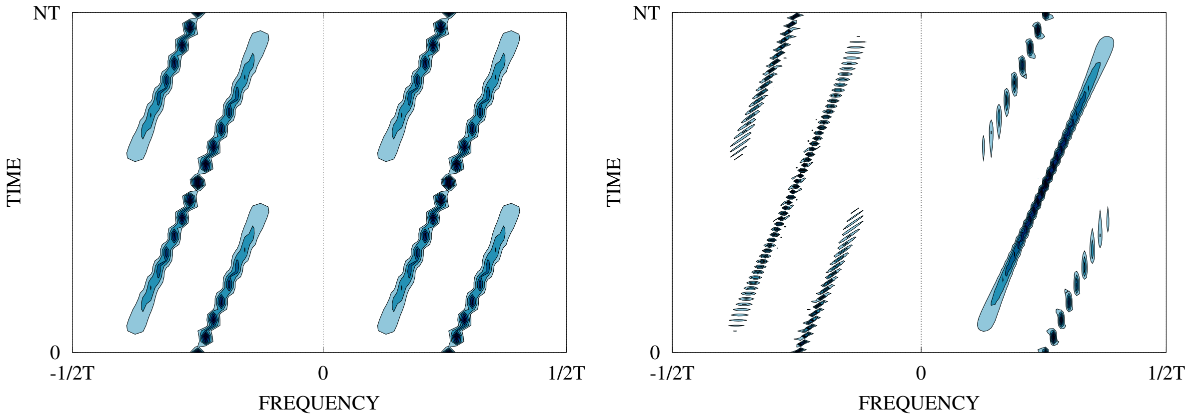

(a) (b)

Figure 2.13: DWVD of analytic LFM signal. (a) DWVD produced using sampling approach A, and (b) DWVD produced using sampling approach B.

Table 2.1: Discrete–continuous relations due to sampling in the time–lag domain.

Domain[a]	Sampling Approach A	Sampling Approach B
TL	$K^{\mathrm{A}}(nT, 2mT)$	$K^{\mathrm{B}}(\frac{nT}{2}, mT)$
DF	$\widetilde{\mathcal{K}}^{\mathrm{A}}(\nu, f) = \frac{1}{T}\sum_n \sum_m \mathcal{K}(\nu - \frac{n}{T}, f - \frac{m}{2T})$	$\widetilde{\mathcal{K}}^{\mathrm{B}}(\nu, f)$ $= \frac{2}{T}\sum_n \sum_m \mathcal{K}(\nu - \frac{n}{T}, f - \frac{m}{2T})$ $n+m$ even
TF	$\widetilde{W}^{\mathrm{A}}(nT, f) = \sum_m W(nT, f - \frac{m}{2T})$	$\widetilde{W}^{\mathrm{B}}(\frac{nT}{2}, f)$ $= \sum_m (-1)^{nm} W(\frac{nT}{2}, f - \frac{m}{2T})$
DL	$\widetilde{A}^{\mathrm{A}}(\nu, 2mT) = \sum_n A(\nu - \frac{n}{T}, 2mT)$	$\widetilde{A}^{\mathrm{B}}(\nu, mT)$ $= \sum_n (-1)^{nm} A(\nu - \frac{n}{T}, mT)$

[a] Legend TF: time–frequency, TL: time–lag, DF: Doppler–frequency, and DL: Doppler–lag.

Table 2.1 shows the relation between discrete and continuous domains from sampling in the time–lag domain. Table 2.2 shows the discrete–continuous relations from sampling in the Doppler–frequency domain. Table 2.3 and Table 2.4 show the discrete–continuous relations from sampling in both the time–lag and Doppler–frequency domains.

2.5 Aliasing, Properties, and other DWVD Definitions

For this section we shall examine how to avoid aliasing and the mathematical properties for two DWVD definitions. In addition, we shall present other existing DWVD definitions

TABLE 2.2: Discrete–continuous relations due to sampling in the Doppler–frequency domain.

Domain[a]	Sampling Approach A	Sampling Approach B
DF	$\mathcal{K}^{\mathrm{A}}(2l\Lambda, k\Lambda)$	$\mathcal{K}^{\mathrm{B}}(l\Lambda, \frac{k\Lambda}{2})$
TL	$\widetilde{K}^{\mathrm{A}}(t,\tau) = \frac{1}{\Lambda}\sum_k \sum_l K(t-\frac{l}{2\Lambda}, \tau-\frac{k}{\Lambda})$	$\widetilde{K}^{\mathrm{B}}(t,\tau) = \frac{2}{\Lambda}\underset{k+l\ \text{even}}{\sum_k \sum_l} K(t-\frac{l}{2\Lambda}, \tau-\frac{k}{\Lambda})$
TF	$\widetilde{\mathcal{W}}^{\mathrm{A}}(t, k\Lambda) = \sum_l W(t-\frac{l}{2\Lambda}, k\Lambda)$	$\widetilde{\mathcal{W}}^{\mathrm{B}}(t, \frac{k\Lambda}{2}) = \sum_l (-1)^{kl} W(t-\frac{l}{2\Lambda}, \frac{k\Lambda}{2})$
DL	$\widetilde{\mathcal{A}}^{\mathrm{A}}(2l\Lambda, \tau) = \sum_k A(2l\Lambda, \tau-\frac{k}{\Lambda})$	$\widetilde{\mathcal{A}}^{\mathrm{B}}(l\Lambda, \tau) = \sum_k (-1)^{kl} A(l\Lambda, \tau-\frac{k}{\Lambda})$

[a] Legend TF: time–frequency, TL: time–lag, DF: Doppler–frequency, and DL: Doppler–lag.

TABLE 2.3: Discrete–continuous relations due to sampling in the both the time–lag and Doppler–frequency domains using sampling approach A.

Domain	Sampling Approach A
TL	$\widetilde{K}^{\mathrm{A}}(nT, 2mT) = NT \sum_k \sum_l K((n-\frac{lN}{2})T, (2m-kN)T)$
DF	$\widetilde{\mathcal{K}}^{\mathrm{A}}(\frac{2l}{NT}, \frac{k}{NT}) = \frac{1}{T}\sum_n \sum_m \mathcal{K}((2l-nN)\frac{1}{NT}, (k-\frac{mN}{2})\frac{1}{NT})$
TF	$W^{\mathrm{A}}(nT, \frac{k}{NT}) = \sum_m \sum_l W((n-\frac{lN}{2})T, (k-\frac{mN}{2})\frac{1}{NT})$
DL	$A^{\mathrm{A}}(\frac{2l}{NT}, 2mT) = \sum_n \sum_k A((2l-nN)\frac{1}{NT}, (2m-kN)T)$

[a] Legend TF: time–frequency, TL: time–lag, DF: Doppler–frequency, and DL: Doppler–lag.

TABLE 2.4: Discrete–continuous relations due to sampling in both the time–lag and Doppler–frequency domains using sampling approach B.

Domain	Sampling Approach B
TL	$\widetilde{K}^{\mathrm{B}}(\frac{nT}{2}, mT) = 2NT\underset{k+l\ \text{even}}{\sum_k \sum_l} K((n-lN)\frac{T}{2}, (m-kN)T)$
DF	$\widetilde{\mathcal{K}}^{\mathrm{B}}(\frac{l}{NT}, \frac{k}{2NT}) = \frac{2}{T}\underset{n+m\ \text{even}}{\sum_n \sum_m} \mathcal{K}((l-nN)\frac{1}{NT}, (k-mN)\frac{1}{2NT})$
TF	$W^{\mathrm{B}}(\frac{nT}{2}, \frac{k}{2NT}) = \sum_l \sum_m (-1)^{nm+lk-lmN} W((n-lN)\frac{T}{2}, (k-mN)\frac{1}{2NT})$
DL	$A^{\mathrm{B}}(\frac{l}{NT}, mT) = \sum_n \sum_k (-1)^{nm+lk-knN} A((l-nN)\frac{1}{NT}, (m-kN)T)$

[a] Legend TF: time–frequency, TL: time–lag, DF: Doppler–frequency, and DL: Doppler–lag.

and relate them to the two presented DWVD definitions.

2.5.1 Aliasing

We saw in Section 2.4.6 that the DWVD of the real-valued signal $\tilde{x}(nT)$ or analytic signal $\tilde{z}(nT)$ is aliased. For the DWVD of the analytic signal, however, aliasing only occurs in the time direction within the region $|t| \leq NT/2$ and $0 \leq f \leq 1/(2T)$. Thus, if we halve the time-bandwidth of the signal, then the DWVD would be free from aliasing within this region [27]. To do this, lets define a discrete analytic signal $\tilde{z}_{\text{pad}}(nT)$ that equals the N-point signal $\tilde{z}(nT)$ zero-padded to length $2N$:

$$\tilde{z}_{\text{pad}}(nT) = \begin{cases} \tilde{z}(nT), & 0 \leq n \leq N-1, \\ 0, & N \leq n \leq 2N-1. \end{cases} \tag{2.37}$$

This signal $\tilde{z}_{\text{pad}}(nT)$ is periodic with a period of $2N$. A consequence of zero-padding $\tilde{z}(nT)$ is spectral leakage into the ideally-zero negative frequency region of $\tilde{Z}_{\text{pad}}(k/2NT)$, where $\tilde{Z}_{\text{pad}}(k/2NT)$ is the DFT of $\tilde{z}_{\text{pad}}(nT)$. Thus,

$$\begin{aligned} \tilde{z}_{\text{pad}}(nT) &= 0, & N \leq n \leq 2N-1 \\ \tilde{Z}_{\text{pad}}(\tfrac{k}{2NT}) &\approx 0, & N \leq k \leq 2N-1. \end{aligned} \tag{2.38}$$

This relation mirrors the continuous domain relation of (2.32). The next chapter present a new method for defining the discrete analytic signal that improves on the approximation in (2.38).

The DWVD of $\tilde{z}_{\text{pad}}(nT)$ is related to the continuous WVD as follows:

$$W^{\text{A}}_{z_{\text{pad}}}(nT, \tfrac{k}{2NT}) \approx W_{z_{\text{pad}}}(nT, \tfrac{k}{2NT}) \tag{2.39}$$

$$W^{\text{B}}_{z_{\text{pad}}}(\tfrac{nT}{2}, \tfrac{k}{4NT}) \approx W_{z_{\text{pad}}}(\tfrac{nT}{2}, \tfrac{k}{4NT}) \tag{2.40}$$

within the signal's time–frequency region of extent—that is, for $|t| \leq NT/2$ and $0 \leq f \leq 1/(2T)$. Hence these DWVDs are approximately alias free and I therefore refer to them as pseudo-alias–free DWVDs rather than alias-free DWVDs. I use the term *pseudo-alias free* to differentiate between the aliased DWVDs—such as the DWVDs of $\tilde{z}(nT)$ in (2.36), or the DWVDs of $\tilde{x}(nT)$ in (2.34) and (2.35)—and the approximately alias-free DWVDs in (2.39) and (2.40).

Assume henceforth that all DWVD definitions, unless otherwise stated, use the $2N$-point analytic signal $\tilde{z}_{\text{pad}}(nT)$ and are therefore pseudo-alias–free definitions. Also, we shall refer to the DWVD definition W^{A} as DWVD-A, and the DWVD definition W^{B} as DWVD-B. Likewise, we shall refer to the DAF definition A^{A} as DAF-A, and the DAF definition A^{B} as DAF-B.

2.5.2 Periodic Discrete Functions

Using the definitions for DWVD-A and DAF-A in (2.27) and (C.9), we find that the four discrete domains have the following periodic relations:

$$\begin{aligned}
W^{\mathrm{A}}((n+pN)T,(k+qN)\tfrac{1}{2NT}) &= W^{\mathrm{A}}(nT,\tfrac{1}{2NT})\\
A^{\mathrm{A}}((l+pN)\tfrac{1}{NT},(m+qN)2T) &= A^{\mathrm{A}}(\tfrac{l}{NT},2mT)\\
\widetilde{K}^{\mathrm{A}}((n+pN)T,(m+qN)2T) &= \widetilde{K}^{\mathrm{A}}(nT,2mT)\\
\widetilde{\mathcal{K}}^{\mathrm{A}}((l+pN)\tfrac{1}{NT},(k+qN)\tfrac{1}{2NT}) &= \widetilde{\mathcal{K}}^{\mathrm{A}}(\tfrac{l}{NT},\tfrac{k}{NT})
\end{aligned}$$

where p and q are integers. Fig. 2.14 illustrates this periodicity; the illustration ignores any periodic overlap caused by the approximation in (2.38).

Using the definitions for DWVD-B and DAF-B in (2.30) and (C.11), we find the following periodic relations:

$$\begin{aligned}
W^{\mathrm{B}}((n+p2N)\tfrac{T}{2},(k+q2N)\tfrac{1}{4NT}) &= (-1)^{pk+qn+pq2N}W^{\mathrm{B}}(\tfrac{nT}{2},\tfrac{k}{4NT})\\
A^{\mathrm{B}}((l+p2N)\tfrac{1}{2NT},(m+q2N)T) &= (-1)^{pm+ql+pq2N}A^{\mathrm{B}}(\tfrac{l}{2NT},mT) \qquad (2.41)\\
\widetilde{K}^{\mathrm{B}}((n+p2N)\tfrac{T}{2},(m+q2N)T) &= \widetilde{K}^{\mathrm{B}}(\tfrac{nT}{2},mT), \qquad \text{for } p+q \text{ even only,}
\end{aligned}$$

$$\widetilde{\mathcal{K}}^{\mathrm{B}}((l+p2N)\tfrac{1}{2NT},(k+q2N)\tfrac{1}{4NT}) = \widetilde{\mathcal{K}}^{\mathrm{B}}(\tfrac{l}{2NT},\tfrac{k}{4NT}), \qquad \text{for } p+q \text{ even only.} \tag{2.42}$$

Fig. 2.15 illustrates this periodicity; again, the illustration ignores any periodic overlap caused by the leaked energy in the approximation (2.38).

2.5.3 Relation Between Definitions

DWVD-A and DWVD-B are closely related: DWVD-A is a decimated, in time and frequency, version of DWVD-B:

$$W^{\mathrm{A}}(nT,\tfrac{k}{2NT}) = 2W^{\mathrm{B}}(\tfrac{2nT}{2},\tfrac{2k}{4NT}). \tag{2.43}$$

The proof is in Appendix B.5.5.

DAF-A and DAF-B are similarly related:

$$A^{\mathrm{A}}(\tfrac{l}{NT},2mT) = 2A^{\mathrm{B}}(\tfrac{2l}{2NT},2mT).$$

The proof is in Appendix C.3.2.

2.5.4 Relation Between Different Domains

The four different domains for DWVD-A are related by the DFT as follows:

$$\begin{tikzcd}
\frac{N}{2}W^{\mathrm{A}}(nT,\frac{k}{NT}) & \widetilde{K}^{\mathrm{A}}(nT,2mT) \arrow[l, "\substack{\mathrm{DFT}\\ m\to k}"'] \arrow[d, "\substack{\mathrm{DFT}\\ n\to l}"'] \\
\widetilde{\mathcal{K}}^{\mathrm{A}}(\frac{2l}{NT},\frac{k}{NT}) \arrow[u, "\substack{\mathrm{IDFT}\\ l\to n}"] \arrow[r, "\substack{\mathrm{IDFT}\\ k\to m}"] & \frac{N}{2}A^{\mathrm{A}}(\frac{2l}{NT},2mT)
\end{tikzcd} \tag{2.44}$$

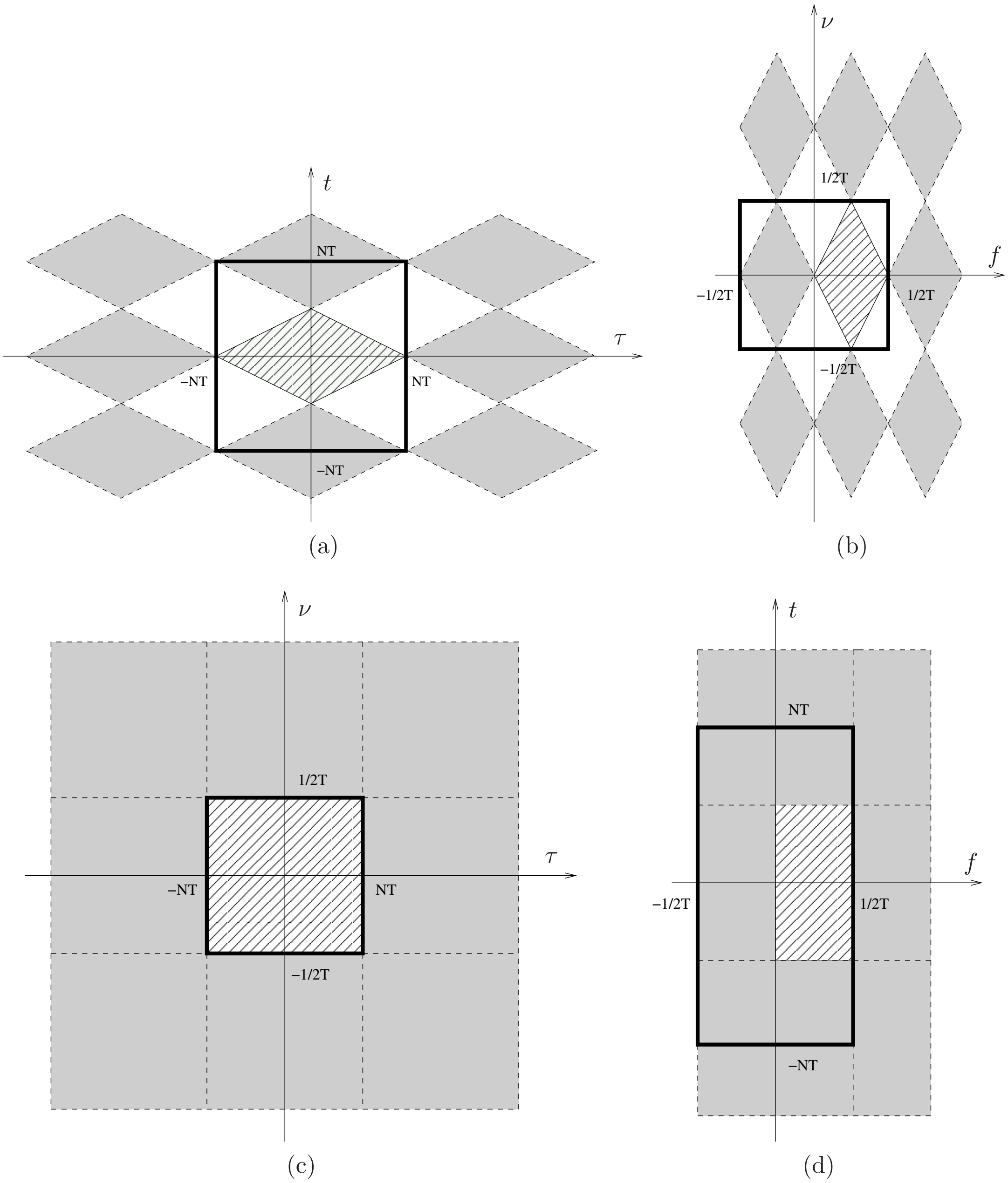

Figure 2.14: The DWVD-A using the analytic signal $\tilde{z}_{\mathrm{pad}}(nT)$ in the four Fourier-related domains. (a) Discrete TIAF, (b) discrete SIAF, (c) discrete AF, DAF-A, and (c) discrete WVD, DWVD-A. The dark-lined rectangular boxes define the limits for the full time–frequency extent of the signal, $|t| < NT$ and $|f| < 1/(2T)$.

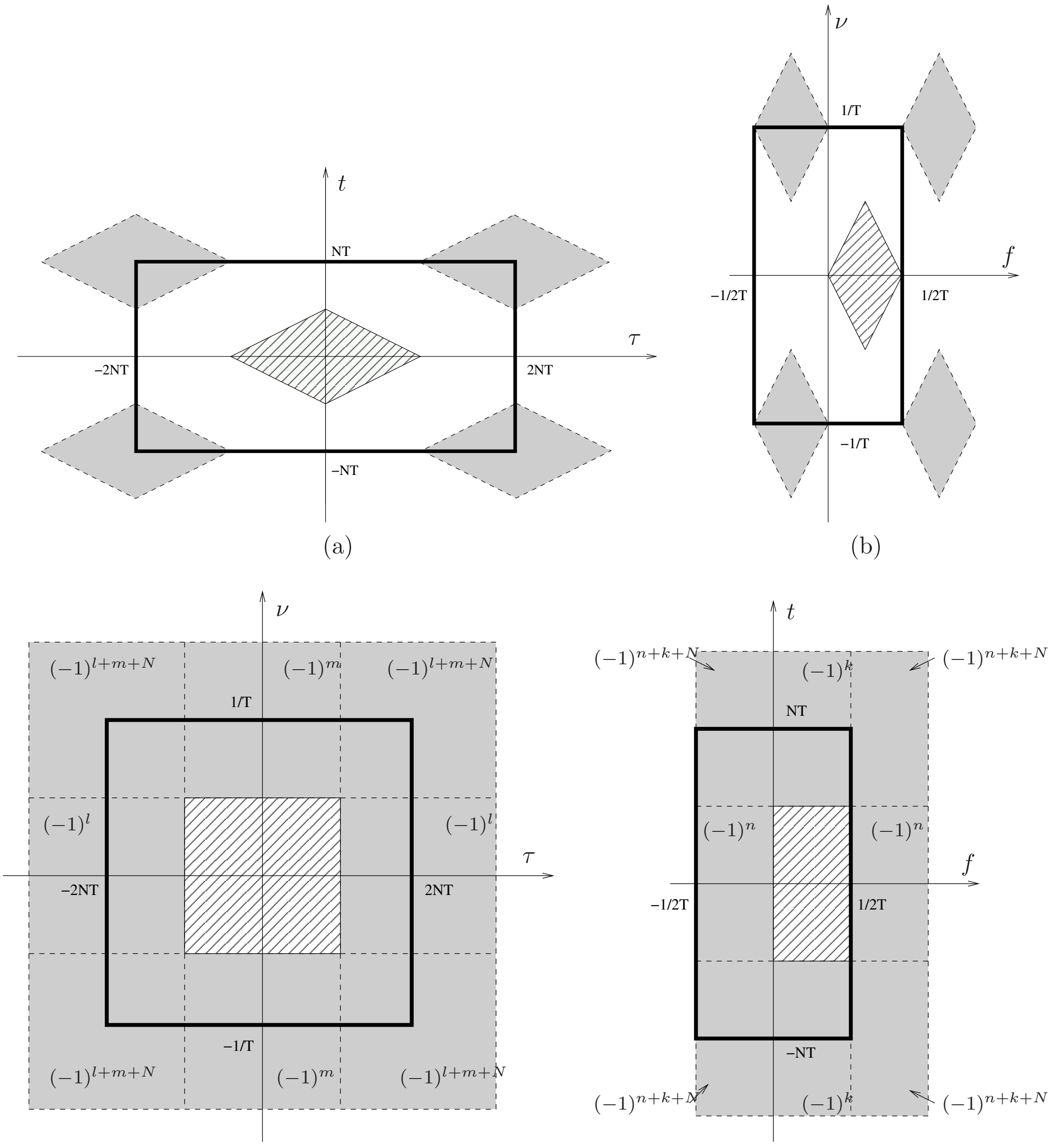

(a) (b)

(c) (d)

FIGURE 2.15: The DWVD-B using the analytic signal $\tilde{z}_{\text{pad}}(nT)$ in the four Fourier-related domains. (a) Discrete TIAF, (b) discrete SIAF, (c) discrete AF, DAF-B, and (c) discrete WVD, DWVD-B. The dark-lined rectangular boxes define the limits for the full time–frequency extent of the signal, $|t| < NT$ and $|f| < 1/(2T)$.

Also, the four different domains for DWVD-B are related as follows:

$$\begin{tikzcd}
NW^{\mathrm{B}}(\frac{nT}{2}, \frac{k}{2NT}) & \underset{\text{for odd } n \text{ only}}{\times\ \mathrm{e}^{-\mathrm{j}\pi k/N}} \arrow[l] & \widetilde{K}^{\mathrm{B}}(\frac{nT}{2}, mT) \arrow[l, "\underset{m\to k}{\text{DFT}}"'] \arrow[d, "\underset{n\to l}{\text{DFT}}"'] \\
\underset{\text{for odd } k \text{ only}}{\times\ \mathrm{e}^{\mathrm{j}\pi n/N}} \arrow[u] & & \underset{\text{for odd } m \text{ only}}{\times\ \mathrm{e}^{-\mathrm{j}\pi l/N}} \arrow[d] \\
\widetilde{\mathcal{K}}^{\mathrm{B}}(\frac{l}{NT}, \frac{k}{2NT}) \arrow[u, "\underset{l\to n}{\text{IDFT}}"] \arrow[r, "\underset{k\to m}{\text{IDFT}}"] & \underset{\text{for odd } l \text{ only}}{\times\ \mathrm{e}^{\mathrm{j}\pi m/N}} \arrow[r] & NA^{\mathrm{B}}(\frac{l}{NT}, mT)
\end{tikzcd} \tag{2.45}$$

The multiplication, indicated by the × symbol, with the complex exponentials is because of the nonuniform discrete grids for the TIAF and SIAF, whereas both the DWVD and DAF have uniform discrete grids.

The direction in (2.44) and (2.45) could be reversed by replacing the DFT with the IDFT and, likewise, replacing the IDFT with the DFT.

2.5.5 DWVD Properties

Ideally, the DWVD should satisfy all the properties from Section 2.2.1 for the continuous WVD. The DWVD-B, but not the DWVD-A, satisfies all of these properties. Here, I list the discrete version of the properties from Section 2.2.1, and show why the DWVD-A fails to satisfy the relevant properties. The properties are altered to accommodate the discrete, periodic signal [27,36,40]. Assume that the signals $\tilde{z}(nT)$, $\tilde{s}(nT)$, and $\tilde{y}(nT)$ are $2N$-point discrete analytic signals of the form in (2.38).

- **Quadratic form:** The DWVD can be written as

$$\sum_{a=0}^{N-1}\sum_{b=0}^{N-1} \tilde{z}(aT)\tilde{z}^*(bT)H(a,b;n,k) \tag{2.46}$$

  where, for DWVD-B, function H is defined as

$$H(a,b;n,k) = \frac{1}{2N}\,\mathrm{e}^{-\mathrm{j}\pi k(a-b)/(2N)}\delta(b-n+a).$$

  The DWVD-A does not satisfy this property because it has the following form:

$$W^{\mathrm{A}}(nT, \tfrac{k}{2NT}) = \sum_{\substack{a=0 \\ a+b \text{ even}}}^{N-1}\sum_{b=0}^{N-1} \tilde{z}(aT)\tilde{z}^*(bT)H_1(a,b;n,k)$$

  where a and b only exists for a, b both even or both odd.

- **Realness:** Both the DWVD-A and DWVD-B are real valued.

- **Time–frequency covariance:** Both DWVD definitions are invariant to time and frequency shifts. The signal

  $$\tilde{y}(nT) = \tilde{s}((n-n_0)T)\,\mathrm{e}^{\mathrm{j}\pi k_0 n/N}$$

  which is periodic in time with period $2NT$ and in frequency with a period of $1/T$, produces the following time–frequency shifts:

  $$\begin{aligned} W_y^{\mathrm{A}}(nT, \tfrac{k}{2NT}) &= W_s^{\mathrm{A}}((n-n_0)T, (k-k_0)\tfrac{1}{2NT}) \\ W_y^{\mathrm{B}}(\tfrac{nT}{2}, \tfrac{k}{4NT}) &= W_s^{\mathrm{B}}((n-2n_0)\tfrac{T}{2}, (k-2k_0)\tfrac{1}{4NT}). \end{aligned}$$

  Because the DWVDs are discrete in both time and frequency, the time–frequency shifts are circular rather than linear and therefore the DWVDs are shift covariant in a periodic sense [23]. The two DWVD definitions are periodic as follows:

  $$\begin{aligned} W^{\mathrm{A}}((n+pN)T, (k+qN)\tfrac{1}{2NT}) &= W^{\mathrm{A}}(nT, \tfrac{k}{2NT}) \\ W^{\mathrm{B}}((n+p2N)\tfrac{T}{2}, (k+q2N)\tfrac{1}{4NT}) &= (-1)^{pk+qn} W^{\mathrm{B}}(\tfrac{nT}{2}, \tfrac{k}{4NT}) \end{aligned}$$

  where p, q are integers. Note that DWVD-B is not, because of the $(-1)^{pk+qn}$ term in the preceding relation, periodic in the usual sense.

- **Time marginal:** We obtain the instantaneous power of the signal, for both DWVD definitions, by summing the DWVD over frequency:

  $$\begin{aligned} \sum_{k=0}^{N-1} W_z^{\mathrm{A}}(nT, \tfrac{k}{2NT}) &= |\tilde{z}(nT)|^2 \\ \sum_{k=0}^{2N-1} W_z^{\mathrm{B}}(\tfrac{2nT}{2}, \tfrac{k}{4NT}) &= |\tilde{z}(nT)|^2. \end{aligned}$$

- **Frequency marginal:** We obtain the spectral energy of the signal, for DWVD-B only, by summing over time:

  $$\sum_{n=0}^{2N-1} W_z^{\mathrm{B}}(\tfrac{nT}{2}, \tfrac{2k}{4NT}) = \frac{1}{2N}\left|\tilde{Z}(\tfrac{k}{2NT})\right|^2$$

  using only even values of k. DWVD-A does not satisfy this property because

  $$\sum_{n=0}^{N-1} W_z^{\mathrm{A}}(nT, \tfrac{k}{2NT}) = \frac{1}{2N}\left[\left|\tilde{Z}(\tfrac{k}{2NT})\right|^2 + \tilde{Z}((k+N)\tfrac{1}{2NT})\tilde{Z}^*((k-N)\tfrac{1}{2NT})\right]$$

- **Time support:** If the signal $\tilde{z}(nT)$ is time limited to $\tilde{z}(nT) = 0$ for $n < n_1$ and $n > n_2$, then the DWVD definitions are likewise time limited:

  $$\begin{aligned} W_z^{\mathrm{A}}(nT, \tfrac{k}{2NT}) &= 0, \qquad \text{for } n < n_1 \text{ and } n > n_2, \\ W_z^{\mathrm{B}}(\tfrac{nT}{2}, \tfrac{k}{4NT}) &= 0, \qquad \text{for } n < 2n_1 \text{ and } n > 2n_2. \end{aligned}$$

- **Frequency support:** If the signal $\tilde{Z}(k/2NT)$ is frequency limited to $\tilde{Z}(k/2NT) = 0$ for $k < k_1$ and $k > k_2$, then the DWVD definitions are likewise frequency limited:

$$\begin{aligned} W_z^{\mathrm{A}}(nT, \tfrac{k}{2NT}) &= 0, && \text{for } k < k_1 \text{ and } k > k_2, \\ W_z^{\mathrm{B}}(\tfrac{nT}{2}, \tfrac{k}{4NT}) &= 0, && \text{for } k < 2k_1 \text{ and } k > 2k_2. \end{aligned}$$

- **Instantaneous frequency:** The first moment, with respect to frequency, of the two DWVD definitions are equal to the instantaneous frequency (IF). For the discrete case, I use the central finite difference of the phase of the analytic signal $\tilde{z}(nT)$ to define the IF $f_{\mathrm{i}}(nT)$ [66, pp. 462], where

$$f_{\mathrm{i}}(nT) = \frac{1}{4\pi T}\left(\left\{\arg\left[\tilde{z}((n+1)T)\right] - \arg\left[\tilde{z}((n-1)T)\right]\right\} \mod 2\pi\right). \tag{2.47}$$

  Thus for a signal of the form $\tilde{z}(nT) = A(nT)\,\mathrm{e}^{\mathrm{j}\varphi(nT)}$ then this discrete IF equates to

$$f_{\mathrm{i}}(nT) = \frac{1}{2\pi T}\left[\frac{\varphi((n+1)T) - \varphi((n-1)T)}{2} \mod \pi\right].$$

  For the DWVD-A and DWVD-B,

$$f_{\mathrm{i}}(nT) = \frac{1}{4\pi T}\left\{\arg\left[\sum_{k=0}^{N-1} W^{\mathrm{A}}(nT, \tfrac{k}{2NT})\,\mathrm{e}^{\mathrm{j}2\pi k/N}\right] \mod 2\pi\right\}$$

$$f_{\mathrm{i}}(nT) = \frac{1}{4\pi T}\left\{\arg\left[\sum_{k=0}^{2N-1} W^{\mathrm{B}}(\tfrac{2nT}{2}, \tfrac{k}{4NT})\,\mathrm{e}^{\mathrm{j}\pi k/N}\right] \mod 2\pi\right\}.$$

  using the discrete periodic moment of the DWVDs [41] [66, pp. 463].

- **Group delay:** The first moment, with respect to time, of the DWVD-B is equal to the group delay (GD). Similar to the discrete IF, I use the central finite difference of the spectral phase to define the discrete group delay $\tau_d(k/2NT)$, where

$$\tau_d(\tfrac{k}{2NT}) = -\frac{N}{2\pi}\left(\left\{\arg\left[\tilde{Z}_1((k+1)\tfrac{1}{2NT})\right] - \arg\left[\tilde{Z}_1((k-1)\tfrac{1}{2NT})\right]\right\} \mod -2\pi\right). \tag{2.48}$$

  Thus for a signal of the form $\tilde{Z}(k/2NT) = a(k)\,\mathrm{e}^{\mathrm{j}\theta(k)}$ then this discrete GD equates to

$$\tau(\tfrac{k}{2NT}) = -\frac{NT}{T}\left[\frac{\theta(k+1) - \theta(k-1)}{2} \mod -\pi\right].$$

  For the DWVD-B,

$$\tau_d(\tfrac{k}{2NT}) = -\frac{N}{2\pi}\left\{\arg\left[\sum_{n=0}^{2N-1} W_{z_1}^{\mathrm{B}}(\tfrac{nT}{2}, \tfrac{2k}{4NT})\,\mathrm{e}^{-\mathrm{j}\pi n/N}\right] \mod -2\pi\right\}$$

The DWVD-A does not satisfy this property because the first moment equates to

$$-\frac{N}{2\pi}\Bigg\{\arg\Big[\ \tilde{Z}_1((k+1)\tfrac{1}{2NT})\tilde{Z}_1^*((k-1)\tfrac{1}{2NT}) \\ +\ \tilde{Z}_1((k+1+N)\tfrac{1}{2NT})\tilde{Z}_1^*((k-1-N)\tfrac{1}{2NT})\Big] \quad \mathrm{mod}\ -2\pi\Bigg\}$$

- **Moyal's formula:** For the DWVD-B, the inner product of the two DWVDs of $\tilde{s}(nT)$ and $\tilde{y}(nT)$ equals the magnitude squared of the inner product of the signal in the time domain:

$$\sum_{n=0}^{2N-1}\sum_{k=0}^{2N-1} W_s^{\mathrm{B}}(\tfrac{nT}{2},\tfrac{k}{4NT})W_y^{\mathrm{B}}(\tfrac{nT}{2},\tfrac{k}{4NT}) = \frac{1}{2N}\left|\sum_{m=0}^{N-1}\tilde{s}(mT)\tilde{y}^*(mT)\right|^2 .$$

The DWVD-A does not satisfy this property because

$$\sum_{n=0}^{N-1}\sum_{k=0}^{N-1} W_s^{\mathrm{A}}(nT,\tfrac{k}{2NT})W_y^{\mathrm{A}}(nT,\tfrac{k}{2NT}) = \frac{1}{N}\left|\sum_{m=0}^{N/2-1}\tilde{s}(2mT)\tilde{y}^*(2mT)\right|^2 \\ +\frac{1}{N}\left|\sum_{m=0}^{N/2-1}\tilde{s}(2(m+\tfrac{1}{2})T)\tilde{y}^*(2(m+\tfrac{1}{2})T)\right|^2$$

- **Signal recovery:** We can recover the time-domain signal, up to a constant phase, from the DWVD-B,

$$\sum_{k=0}^{2N-1} W^{\mathrm{B}}(\tfrac{nT}{2},\tfrac{k}{4NT})\,\mathrm{e}^{\mathrm{j}\pi kn/(2N)} = \tilde{z}(nT)\tilde{z}^*(0)$$

The DWVD-A does not satisfy this property because we only obtain a decimated version of $\tilde{z}(nT)$; that is,

$$\sum_{k=0}^{N-1} W^{\mathrm{A}}(nT,\tfrac{k}{2NT})\,\mathrm{e}^{\mathrm{j}2\pi kn/N} = \tilde{z}(2nT)\tilde{z}^*(0)$$

2.5.6 Other DWVD Definitions

Thus far, we have looked at two important DWVD definitions: the DWVD-A and the DWVD-B. I presented these definitions first because almost all other DWVD definitions are related to the DWVD-A or DWVD-B.

Some of these definitions use different signals types, all derived from $\tilde{x}(nT)$, which I now define:

- $\tilde{x}(nT)$ is a real-valued signal of length N;
- $\tilde{z}(nT)$ is an analytic associate of $\tilde{x}(nT)$ also of length N;

- $\tilde{x}_{\text{pad}}(nT)$ is equal to $\tilde{x}(nT)$ zero padded to length $2N$;
- $\tilde{z}_{\text{pad}}(nT)$ is equal to $\tilde{z}(nT)$ zero padded to length $2N$.
- $\tilde{x}_{\text{pad1}}(nT/2)$ is an interpolated, by a factor of two, version of $\tilde{x}(nT)$; it is then zero padded to length $4N$;
- $\tilde{x}_{\text{pad2}}(nT/2)$ is an interpolated, by a factor of two, version of $\tilde{x}_{\text{pad}}(nT)$ and thus is length $4N$.

In 1980 Claasen and Mecklenbräuker [41] presented the first discrete version of the WVD for a discrete-time signal $\tilde{x}_{\text{pad}}(nT)$. The authors noted that the distribution was aliased unless either the $2N$-point analytic signal $\tilde{z}_{\text{pad}}(nT)$ or the $4N$-point interpolated signal $\tilde{x}_{\text{pad1}}(nT/2)$ was used. This DWVD is the DWVD-A.

Chan, in 1982 [31], realised that this distribution did not use all the available signal information from $\tilde{x}_{\text{pad}}(nT)$. Motivated to create a DWVD that satisfies the properties of the continuous WVD, Chan proposed a discrete-time WVD $W^{\text{B}}(nT/2, f)$—that is, a discrete-time, continuous-frequency version of DWVD-B. The author claimed that this distribution was alias free. Addressing this claim, Claasen and Mecklenbräuker in 1983 [59] related the DWVD-B to the DWVD-A and showed that the DWVD-B was aliased. Claasen and Mecklenbräuker also proposed three new DWVDs, which they defined as linear combinations of DWVD-A and DWVD-B using the real-valued signal $\tilde{x}_{\text{pad}}(nT)$. Their aim was to reduce the effects of aliasing by an averaging process.

In 1986 Peyrin and Prost [27] presented the discrete-frequency version of Chan's distribution—that is, the DWVD-B. The authors noted that either $\tilde{z}_{\text{pad}}(nT)$ or $\tilde{x}_{\text{pad1}}(nT/2)$ was required to avoid aliasing.

Nuttall, in 1989, presented a thorough analysis of a DWVD and its Fourier-related domains [39]; Appendix B is partly based on his analysis method. He applied sampling approach B to the TIAF and SIAF to form the DWVD using only the real-valued signal. The DWVD he presented, however, is best expressed as the DWVD-A of $\tilde{x}_{\text{pad2}}(nT/2)$.

In 1993 Beiker [60] introduced three discrete-time WVD definitions, as linear combinations of DWVD-A and DWVD-B, similar in approach to the DWVDs proposed by Claasen and Mecklenbräuker in [59]. These distributions attempted to reduced aliasing by averaging the different distributions. In 2005 Chassante-Mottin and Pai [44] presented a discrete-frequency version of one of the distributions presented by Bekir in [60].

Richman *et al.* [40] proposed a DWVD using group representation theory in 1998. A year later O' Neill *et al.* [42] proposed the same DWVD derived differently. The proposed DWVD is described as

$$W^{\text{ON}}(nT, \tfrac{k}{NT}) = \sum_{m=0}^{N-1} \tilde{x}((n+cm)T)\tilde{x}((n-cm)T)\, \mathrm{e}^{-\mathrm{j}2\pi mk/N} \tag{2.49}$$

where $c = (N+1)/2$ and $\tilde{x}(nT)$ is the N-point real-valued or complex-valued signal. This DWVD definition, however, exists for N odd *only.* As the signal $\tilde{x}(nT)$ is not zero padded in the time direction this DWVD is always aliased. This definition is not related to either the DWVD-A or DWVD-B because these definitions assume that N is even. (Note this does not limit DWVD-A or DWVD-B as we use the $2N$-point zero-padded signal to avoid aliasing.)

Table 2.5 displays the relation between these existing DWVD definitions and the DWVD-A and DWVD-B. I have omitted the O'Neill definition of (2.49) because, as I previously mentioned, it is not directly related to either DWVD-A or DWVD-B.

TABLE 2.5: DWVD definitions in terms of DWVD-A and DWVD-B

Definition	DWVD
CM	$W^{\mathrm{A}}(nT, \frac{k}{2NT})$
CH	$W^{\mathrm{B}}(\frac{nT}{2}, f)$
CM1	$\frac{1}{2}\left[W^{\mathrm{A}}(nT, f) + W^{\mathrm{B}}((n-\frac{1}{2})T, f)\right]$
CM2	$\frac{1}{2}\left[W^{\mathrm{A}}(nT, f) + W^{\mathrm{B}}((n+\frac{1}{2})T, f)\right]$
CM3	$\frac{1}{2}\left[2W^{\mathrm{A}}(nT, f) + W^{\mathrm{B}}((n-\frac{1}{2})T, f) + W^{\mathrm{B}}((n+\frac{1}{2})T, f)\right]$
PP	$W^{\mathrm{B}}(\frac{nT}{2}, \frac{k}{4NT})$
BE[a]	$\frac{1}{2}\left[W^{\mathrm{A}}(nT, f) + W^{\mathrm{B}}((n+\frac{1}{2})T, f)\right]$, for n even
	$\frac{1}{2}\left[2W^{\mathrm{A}}(nT, f) + W^{\mathrm{B}}((n-\frac{1}{2})T, f) + W^{\mathrm{B}}((n+\frac{1}{2})T, f)\right]$, for n odd
NT	$W^{\mathrm{A}}(\frac{nT}{2}, \frac{k}{4NT})$
CP	$\frac{1}{2}\left[W^{\mathrm{A}}(nT, \frac{k}{2NT}) + W^{\mathrm{B}}((n+\frac{1}{2})T, \frac{k}{2NT})\right]$, for n even
	$\frac{1}{2}\left[2W^{\mathrm{A}}(nT, \frac{k}{2NT}) + W^{\mathrm{B}}((n-\frac{1}{2})T, \frac{2k}{4NT}) + W^{\mathrm{B}}((n+\frac{1}{2})T, \frac{2k}{4NT})\right]$, for n odd.

[a] Bekir proposed 3 DWVD definitions in [60]; I show only one here as an example.
Legend: CM: Claasen and Mecklenbräuker in [41]; CH: Chan in [31]; CM(1–3): Claasen and Mecklenbräuker in [59]; PP: Peyrin and Prost in [27]; BE: Bekir in [60]; NT: Nuttall in [39]; CP: Chassande-Mottin and Pai in [44].

2.5.7 Limitations of Existing Definitions

I consider only pseudo-alias–free definitions in this dissertation. Therefore, I do not consider the definitions of Claasen and Mecklenbräuker in [59], Bekir [60], O' Neill *et al.* [42], or Chassande-Mottin and Pai [44] because they are aliased. That leaves us with DWVD-A and DWVD-B which, because they are pseudo-alias–free definitions, contain only minimal aliasing.

The DWVD-B satisfies all important properties; the DWVD-A does not. The DWVD-A, as we saw in Section 2.5.2, is periodic in the time and frequency direction in N; thus, one period of the DWVD-A contains $N \times N$, or N^2, sample points. The DWVD-B, on the other hand, is periodic in the time and frequency direction in $2N$ and thus contains $2N \times 2N$, or $4N^2$ sample points. The consequence of this larger array size is that the DWVD-B requires four times as much computational load and memory to compute compared with that required for the DWVD-A.

2.6 Proposed DWVD Definitions

Here I propose two new DWVD definitions that are closely related to DWVD-A and DWVD-B. To the best of my knowledge, these definitions have not been formally proposed before.

The definitions are based on the decimation relation between DWVD-B and DWVD-A in (2.43): the first DWVD, which I call the DWVD-C, is a frequency-decimated version of DWVD-B [43],

$$W^{\mathrm{C}}(\tfrac{nT}{2}, \tfrac{k}{2NT}) = W^{\mathrm{B}}(\tfrac{nT}{2}, \tfrac{2k}{4NT}) \tag{2.50}$$

and the second DWVD W^{D}, which I call the DWVD-D, is a time-decimated version of DWVD-B,

$$W^{\mathrm{D}}(nT, \tfrac{k}{4NT}) = W^{\mathrm{B}}(\tfrac{2nT}{2}, \tfrac{k}{4NT}). \tag{2.51}$$

Note that both these definitions contain only $2N^2$ sample points, compared with the DWVD-B which contains $4N^2$ samples and therefore have a computational advantage over the DWVD-B.

2.6.1 Formulation of Proposed DWVDs

Here I define the proposed DWVDs as functions of the discrete, periodic TIAFs and SIAFs.

DWVD-C

The DWVD-C W^{C}, in terms of the SIAF $\widetilde{\mathcal{K}}^{\mathrm{C}}$, is

$$W^{\mathrm{C}}(\tfrac{nT}{2}, \tfrac{k}{2NT}) = \frac{1}{2N} \sum_{l=0}^{2N-1} \widetilde{\mathcal{K}}^{\mathrm{C}}(\tfrac{l}{NT}, \tfrac{k}{2NT})\, \mathrm{e}^{\mathrm{j}\pi l n/N}$$

where the SIAF $\widetilde{\mathcal{K}}^{\mathrm{C}}$ is

$$\begin{aligned}\widetilde{\mathcal{K}}^{\mathrm{C}}(\tfrac{l}{NT},\tfrac{k}{2NT}) &= \widetilde{\mathcal{K}}^{\mathrm{B}}(\tfrac{l}{NT},\tfrac{2k}{4NT})\\ &= \tilde{Z}((k+l)\tfrac{1}{2NT})\tilde{Z}^{*}((k-l)\tfrac{1}{2NT}).\end{aligned}$$

The signal $\tilde{z}(nT)$ is the $2N$-point discrete analytic signal of the form (2.38).

In terms of the TIAF,

$$W^{\mathrm{C}}(\tfrac{nT}{2},\tfrac{k}{2NT}) = \frac{1}{2N}\sum_{m=0}^{2N-1}\widetilde{K}^{\mathrm{C}}(\tfrac{nT}{2},mT)\,\mathrm{e}^{-\mathrm{j}\pi mk/N}$$

where the TIAF $\widetilde{K}^{\mathrm{C}}$ is a folded, in the lag direction, version of the TIAF for DWVD-B, as

$$\widetilde{K}^{\mathrm{C}}(\tfrac{nT}{2},mT) = \widetilde{K}^{\mathrm{B}}(\tfrac{nT}{2},mT) + \widetilde{K}^{\mathrm{B}}(\tfrac{nT}{2},(m+N)T)$$

which in terms of $\tilde{z}(nT)$ is

$$\begin{aligned}\widetilde{K}^{\mathrm{C}}(nT,2mT) &= \tilde{z}((n+m)T)\tilde{z}^{*}((n-m)T)\\ &\quad+\tilde{z}((n+m+N)T)\tilde{z}^{*}((n-m-N)T)\\ \widetilde{K}^{\mathrm{C}}((n+\tfrac{1}{2})T,2(m+\tfrac{1}{2})T) &= \tilde{z}((n+m+1)T)\tilde{z}^{*}((n-m)T)\\ &\quad+\tilde{z}((n+m+1+N)T)\tilde{z}^{*}((n-m-N)T).\end{aligned}$$

Because, from (2.38), $\tilde{z}(nT)=0$ for $N\le n\le 2N-1$, we can rewrite the previous expression as

$$\begin{aligned}\widetilde{K}^{\mathrm{C}}(nT,2mT) &= \tilde{z}((n+m)T)\tilde{z}^{*}((n-m)T)\\ \widetilde{K}^{\mathrm{C}}((n+\tfrac{1}{2})T,2(m+\tfrac{1}{2})T) &= \tilde{z}((n+m+1)T)\tilde{z}^{*}((n-m)T).\end{aligned}$$

Thus the frequency decimation process in (2.50) results in removing the zeros from the TIAF $\widetilde{K}^{\mathrm{B}}$ and therefore the DWVD-C does not lose any signal information from DWVD-B. Consequently, as I show in the next section, DWVD-C satisfies all the desirable properties that DWVD-B satisfies.

DWVD-D

The DWVD-D W^{D}, in terms of the TIAF $\widetilde{K}^{\mathrm{D}}$, is

$$W^{\mathrm{D}}(nT,\tfrac{k}{4NT}) = \frac{1}{2N}\sum_{m=0}^{2N-1}\widetilde{K}^{\mathrm{D}}(nT,2mT)\,\mathrm{e}^{-\mathrm{j}\pi mk/N}$$

with

$$\begin{aligned}\widetilde{K}^{\mathrm{D}}(nT,2mT) &= \widetilde{K}^{\mathrm{B}}(\tfrac{2nT}{2},2mT)\\ &= \tilde{z}((n+m)T)\tilde{z}^{*}((n-m)T).\end{aligned}$$

The decimation in time by a factor of two leads to a folding in the Doppler direction in the SIAF. That is, the complementary folded SIAF $\widetilde{\mathcal{K}}^{\mathrm{D}}$ is defined as

$$\widetilde{\mathcal{K}}^{\mathrm{D}}(\tfrac{l}{NT},\tfrac{k}{4NT}) = \widetilde{\mathcal{K}}^{\mathrm{B}}(\tfrac{l}{NT},\tfrac{k}{4NT}) + \widetilde{\mathcal{K}}^{\mathrm{B}}((l+N)\tfrac{1}{NT},\tfrac{k}{4NT})$$

which in terms of $\tilde{Z}(k/2NT)$ is

$$\begin{aligned}\widetilde{\mathcal{K}}^{\mathrm{D}}(\tfrac{2l}{NT},\tfrac{2k}{4NT}) &= \tilde{Z}((k+l)\tfrac{1}{2NT})\tilde{Z}^{*}((k-l)\tfrac{1}{2NT})\\ &\quad+\tilde{Z}((k+l+N)\tfrac{1}{2NT})\tilde{Z}^{*}((k-l-N)\tfrac{1}{2NT})\\ \widetilde{\mathcal{K}}^{\mathrm{D}}(\tfrac{(2l+1)}{NT},\tfrac{2k+1}{4NT}) &= \tilde{Z}((k+l+1)\tfrac{1}{2NT})\tilde{Z}^{*}((k-l)\tfrac{1}{2NT})\\ &\quad+\tilde{Z}((k+l+1+N)\tfrac{1}{2NT})\tilde{Z}^{*}((k-l-N)\tfrac{1}{2NT}),\end{aligned}$$

Because of the approximation in (2.38), we cannot assume that $\tilde{Z}(k/2NT)=0$ for $N\le k\le 2N-1$. Thus, this SIAF folding process for DWVD-D will lose signal information from DWVD-B and consequently, as I show in the next section, DWVD-D does not satisfy all desirable properties that DWVD-B satisfies.

In terms of the SIAF,

$$W^{\mathrm{D}}(nT,\tfrac{k}{4NT})=\frac{1}{2N}\sum_{l=0}^{2N-1}\widetilde{\mathcal{K}}^{\mathrm{D}}(\tfrac{l}{NT},\tfrac{k}{4NT})\,\mathrm{e}^{\mathrm{j}\pi ln/N}.$$

2.6.2 Properties

Here I list the discrete properties from Section 2.5.5 and show that DWVD-C satisfies all presented properties whereas DWVD-D fails to satisfy all properties. Assume again that $\tilde{z}(nT)$, $\tilde{s}(nT)$, and $\tilde{y}(nT)$ are $2N$-point discrete analytic signals of the form in (2.38).

- **Quadratic form:** DWVD-C has the quadratic form

  $$W^{\mathrm{C}}(\tfrac{nT}{2},\tfrac{k}{2NT})=\sum_{a=0}^{N-1}\sum_{b=0}^{N-1}\tilde{z}(aT)\tilde{z}^{*}(bT)H(a,b;n,k)$$

  with

  $$H(a,b;n,k)=\frac{1}{2N}\,\mathrm{e}^{-\mathrm{j}\pi k(a-b)/(2N)}\delta(b-n+a).$$

  DWVD-D does not satisfy this property because it has the following form:

  $$W^{\mathrm{A}}(nT,\tfrac{k}{2NT})=\sum_{\substack{a=0\\a+b\text{ even}}}^{N-1}\sum_{b=0}^{N-1}\tilde{z}(aT)\tilde{z}^{*}(bT)H_1(a,b;n,k)$$

  where a and b only exist for a,b both even or both odd.

- **Realness:** Both the DWVD-C and DWVD-D are real valued.

- **Time–frequency covariance:** Both DWVD definitions are invariant to time and frequency shifts. The signal

  $$\tilde{y}(nT)=\tilde{s}((n-n_0)T)\,\mathrm{e}^{\mathrm{j}\pi k_0 n/N}$$

  produces the following time–frequency shifts:

  $$\begin{aligned}W_y^{\mathrm{C}}(\tfrac{nT}{2},\tfrac{k}{2NT})&=W_s^{\mathrm{C}}((n-2n_0)\tfrac{T}{2},(k-k_0)\tfrac{1}{2NT})\\ W_y^{\mathrm{D}}(nT,\tfrac{k}{4NT})&=W_s^{\mathrm{D}}((n-n_0)T,(k-2k_0)\tfrac{1}{4NT}).\end{aligned}$$

These time–frequency shifts are circular, rather than linear and the two DWVD definitions have the following periodicity:

$$W^{\mathrm{C}}((n+p2N)\tfrac{T}{2},(k+qN)\tfrac{1}{2NT}) = (-1)^{qn}W^{\mathrm{C}}(\tfrac{nT}{2},\tfrac{k}{2NT})$$
$$W^{\mathrm{D}}((n+pN)T,(k+q2N)\tfrac{1}{4NT}) = (-1)^{pk}W^{\mathrm{D}}(nT,\tfrac{k}{4NT})$$

where p, q are integers.

- **Time marginal:** We obtain the instantaneous power of the signal, for both DWVD definitions, by summing over frequency:

$$\sum_{k=0}^{N-1} W^{\mathrm{C}}(\tfrac{2nT}{2},\tfrac{k}{2NT}) = |\tilde{z}(nT)|^2$$
$$\sum_{k=0}^{2N-1} W^{\mathrm{D}}(nT,\tfrac{k}{4NT}) = |\tilde{z}(nT)|^2.$$

- **Frequency marginal:** We obtain the spectral energy of the signal, for DWVD-C only, by summing over time:

$$\sum_{n=0}^{2N-1} W^{\mathrm{C}}(\tfrac{nT}{2},\tfrac{k}{2NT}) = \frac{1}{2N}\left|\tilde{Z}(\tfrac{k}{2NT})\right|^2.$$

DWVD-D does not satisfy this property because

$$\sum_{n=0}^{N-1} W^{\mathrm{D}}(nT,\tfrac{2k}{4NT}) = \frac{1}{4N}\left[\left|\tilde{Z}(\tfrac{k}{2NT})\right|^2 + \tilde{Z}((k+N)\tfrac{1}{2NT})\tilde{Z}^*((k-N)\tfrac{1}{2NT})\right].$$

- **Time support:** If the signal $\tilde{z}(nT)$ is time limited to $\tilde{z}(nT) = 0$ for $n < n_1$ and $n > n_2$, then the two DWVD definitions are likewise time limited:

$$W^{\mathrm{C}}(\tfrac{nT}{2},\tfrac{k}{2NT}) = 0, \qquad \text{for } n < 2n_1 \text{ and } n > 2n_2,$$
$$W^{\mathrm{D}}(nT,\tfrac{k}{2NT}) = 0, \qquad \text{for } n < n_1 \text{ and } n > n_2.$$

- **Frequency support:** If the signal $\tilde{Z}(k/2NT)$ is frequency limited to $\tilde{Z}(k/2NT) = 0$ for $k < k_1$ and $k > k_2$, then the DWVD definitions are likewise frequency limited:

$$W^{\mathrm{C}}(\tfrac{nT}{2},\tfrac{k}{2NT}) = 0, \qquad \text{for } k < k_1 \text{ and } k > k_2,$$
$$W^{\mathrm{D}}(nT,\tfrac{k}{4NT}) = 0, \qquad \text{for } k < 2k_1 \text{ and } k > 2k_2.$$

- **Instantaneous frequency:** The discrete periodic moment, with respect to frequency, of the two definitions equal the discrete IF,

$$\frac{1}{4\pi T}\left\{\arg\left[\sum_{k=0}^{N-1} W^{\mathrm{C}}(\tfrac{2nT}{2},\tfrac{k}{2NT})\,\mathrm{e}^{\mathrm{j}2\pi k/N}\right] \mod 2\pi\right\} = f_{\mathrm{i}}(nT)$$
$$\frac{1}{4\pi T}\left\{\arg\left[\sum_{k=0}^{2N-1} W^{\mathrm{D}}(nT,\tfrac{k}{4NT})\,\mathrm{e}^{\mathrm{j}\pi k/N}\right] \mod 2\pi\right\} = f_{\mathrm{i}}(nT).$$

where the discrete IF function $f_{\mathrm{i}}(nT)$ is defined in (2.47).

- **Group delay:** The discrete periodic moment, with respect to time, of the DWVD-C equals the discrete GD,

$$-\frac{N}{2\pi}\left\{\arg\left[\sum_{n=0}^{2N-1} W^{\mathrm{C}}(\tfrac{nT}{2},\tfrac{k}{2NT})\,\mathrm{e}^{-\mathrm{j}\pi n/N}\right] \mod -2\pi\right\} = \tau_d(\tfrac{k}{2NT})$$

  where the discrete GD function $\tau_d(k/2NT)$ is defined in (2.48).

  DWVD-D does not satisfy this property because the first moment equates to

$$\begin{aligned}-\frac{N}{2\pi}\Big\{\arg\Big[\;&\tilde{Z}((k+1)\tfrac{1}{2NT})\tilde{Z}^*((k-1)\tfrac{1}{2NT})\\&+\;\tilde{Z}((k+1+N)\tfrac{1}{2NT})\tilde{Z}^*((k-1-N)\tfrac{1}{2NT})\Big] \mod -2\pi\Big\}\end{aligned}$$

- **Moyal's formula:** For DWVD-C,

$$\sum_{n=0}^{2N-1}\sum_{k=0}^{N-1} W_s^{\mathrm{C}}(\tfrac{nT}{2},\tfrac{k}{2NT})W_y^{\mathrm{C}}(\tfrac{nT}{2},\tfrac{k}{2NT}) = \frac{1}{4N}\left|\sum_{m=0}^{N-1}\tilde{s}(mT)\tilde{y}^*(mT)\right|^2 .$$

  DWVD-D does not satisfy this property because

$$\begin{aligned}\sum_{n=0}^{N-1}\sum_{k=0}^{2N-1} W_s^{\mathrm{D}}(nT,\tfrac{k}{4NT})W_y^{\mathrm{D}}(nT,\tfrac{k}{4NT}) &= \frac{1}{2N}\left|\sum_{m=0}^{N/2-1}\tilde{s}(2mT)\tilde{y}^*(2mT)\right|^2\\&+\frac{1}{N}\left|\sum_{m=0}^{N/2-1}\tilde{s}(2(m+\tfrac{1}{2})T)\tilde{y}^*(2(m+\tfrac{1}{2})T)\right|^2\end{aligned}$$

- **Signal recovery:** For DWVD-C,

$$\sum_{k=0}^{2N-1} W^{\mathrm{C}}(\tfrac{nT}{2},\tfrac{k}{2NT})\,\mathrm{e}^{\mathrm{j}\pi kn/N} = \tilde{z}(nT)\tilde{z}^*(0)$$

  DWVD-D does not satisfy this property because

$$\sum_{k=0}^{2N-1} W^{\mathrm{D}}(nT,\tfrac{k}{4NT})\,\mathrm{e}^{\mathrm{j}\pi kn/(2N)} = \tilde{z}(2nT)\tilde{z}^*(0)$$

Table 2.6 summaries these results and also includes the results from Section 2.5.5 for DWVD-A and DWVD-B. Both DWVD-C and DWVD-B satisfy all desirable properties. The DWVD-C has a computational advantage however—the $2N \times N$ DWVD-C requires only one-half of the computational load and memory required to compute the distribution compared with that for the $2N \times 2N$ DWVD-B.

TABLE 2.6: Discrete properties for the four different DWVD definitions.

Properties	DWVD-A	DWVD-B	DWVD-C	DWVD-D
quadratic form		✓	✓	
realness	✓	✓	✓	✓
time–frequency covariance	✓	✓	✓	✓
time marginal	✓	✓	✓	✓
frequency marginal		✓	✓	
time support	✓	✓	✓	✓
frequency support	✓	✓	✓	✓
instantaneous frequency	✓	✓	✓	✓
group delay		✓	✓	
Moyal's formula		✓	✓	
signal recovery		✓	✓	

2.7 Summary and Conclusions

Defining a discrete WVD is not a trivial task. The DWVD should, ideally, be alias free and retain all the important mathematical properties from the continuous WVD. Unfortunately, the DWVD will always contain some level of aliasing and the DWVD may not satisfy all important properties. Thus, an optimal DWVD definition is one with minimal aliasing, which I called a pseudo-alias–free DWVD, and satisfies all important properties. Also, because the DWVD is a two-dimensional function, it requires a large computational load and section of memory to compute and store the distribution; reducing this required load and memory would make the DWVD a more applicable signal processing tool.

This chapter presented a thorough analysis of two important DWVD definitions, DWVD-A and DWVD-B. This analysis included a rigorous derivation which details the relation between the discrete and continuous domains and a study of discrete properties for DWVD-A and DWVD-B. After this, I proposed two new DWVD definitions, DWVD-C and DWVD-D.

All four definitions are pseudo-alias–free DWVDs. Both the proposed DWVD-C the existing DWVD-B satisfy all important properties whereas the proposed DWVD-D and existing DWVD-A fail to satisfy all properties. The proposed DWVD-C has $2N^2$ sample points, whereas the existing DWVD-B definition has $4N^2$ sample points. Hence the DWVD-C requires only one-half of the computational load and memory to compute and store the DWVD compared with that for the DWVD-B. (Algorithm details are in Chapter 5.) For these three reasons—aliasing, properties, and computational load—I propose the DWVD-C as an optimal DWVD definition.

Chapter 3

Discrete Analytic Signals

3.1 Introduction

A completely alias-free DWVD requires that the discrete analytic signal satisfies two constraints. Unfortunately, these two constraints are mutually exclusive. This chapter presents a new discrete analytic signal that improves on the commonly-used discrete analytic signal's approximation of these two constraints—and therefore further reduces aliasing in the DWVD.

The analytic signal, unlike the real-valued signal, has zero energy at negative frequencies. No signal information is lost when the forming the analytic signal from the real-valued signal, as the spectrum of the real-valued signal $X(f)$ is conjugate symmetrical about the origin; that is, $X(-f) = X^*(f)$. The continuous WVD uses the analytic signal to avoid the cross-term artefacts—present when the real-valued signal is used—between the positive and negative frequency components [11]. The analytic signal has another use—it minimises aliasing in the DWVD. To completely eliminate aliasing from the DWVD however, the $2N$-point discrete analytic signal $z(nT)$ must satisfy the following two constraints:

$$z(nT) = 0, \qquad N \leq n \leq 2N-1, \tag{3.1}$$

$$Z(\tfrac{k}{2NT}) = 0, \qquad N \leq k \leq 2N-1. \tag{3.2}$$

These two constraints are mutually exclusive [28]. Any violation of the two constraints, however, will produce some aliasing in the DWVD. We shall refer to (3.1) as the time-constraint and (3.2) as the frequency-constraint. (Note that I drop the tilde accent, which I used in previous chapters to signify a periodic signal, for all discrete signals. Thus, $z(nT)$ is a discrete, periodic signal with a period of $2NT$.)

The commonly-used discrete analytic signal [25], which we shall refer to as the *conventional* analytic signal, satisfies the time-constraint of (3.1) but not the frequency constraint of (3.2). The conventional analytic signal is popular because it can be computed simply using DFTs and it satisfies two important properties—namely, its real part is equal to the original real-valued signal and that its real and imaginary parts are orthogonal [25].

In this chapter, I propose a new discrete analytic signal to better approximate the frequency-constraint of (3.2) and therefore reduce aliasing in the DWVD. To assess the performance of this proposed signal, I compare the proposed and conventional signals' approximation of the frequency-constraint in (3.2). I measure this approximation by quantifying the amount of energy in the ideally-zero region in (3.2). Then, I numerically compare, using a number of test signals, the amount of aliasing energy in the DWVD of the two signals. I use the proposed DWVD-C from the previous chapter for this numerical analysis.

The results show that the DWVD of the proposed analytic signal has approximately 50% less aliasing than that for the DWVD of the conventional analytic signal. This agrees with my initial result—that the proposed signal, relative to the conventional signal, better approximates the frequency-constraint of (3.2). Furthermore, the proposed signal retains the useful attributes of the conventional signal: it satisfies the signal recovery and orthogonality property and can be simpled computed using DFTs.

3.2 Review

There is no unique definition for a discrete analytic signal. (I use the term *discrete analytic signal* to refer to a discrete version of the continuous analytic signal, even though the discrete signal is not an analytic function of a continuous complex variable [25].) This section presents different definitions and some important mathematical properties of discrete analytic signals.

3.2.1 Desirable Properties

The discrete definition should conserve as many properties of the continuous analytic signal as possible. Marple [25] proposed that a discrete analytic signal should at least satisfy the recovery and orthogonality properties, which I now describe.

For a discrete analytic signal $z(nT)$, associated with the N-point real-valued signal $s(nT)$, the recovery property is

$$\Re\big[z(nT)\big] = s(nT), \qquad \text{for } 0 \le n \le N-1 \tag{3.3}$$

and orthogonality property is

$$\sum_{n=0}^{N-1} \Re\big[z(nT)\big]\,\Im\big[z(nT)\big] = 0. \tag{3.4}$$

The function $\Re[a]$ represents the real part of a and $\Im[a]$ represents the imaginary part of a. (We shall refer to the discrete analytic signal simply as an analytic signal when the context is clear.)

3.2.2 Existing Methods

We can classify existing methods for forming analytic signals as either time- or frequency-domain based methods. First, lets look at two time-domain based methods. One method uses dual quadrature FIR filters to jointly produce the real and imaginary parts of $z(nT)$, as described in [61]. The resultant analytic signal satisfies the orthogonality property but not the recovery property [25]. The other method forms the analytic signal using the relation $z(nT) = s(nT) + \mathrm{j}\mathcal{H}\{s(nT)\}$, by approximating the Hilbert transform operation $\mathcal{H}\{\cdot\}$ with an FIR filter [61]. The resultant analytic signal satisfies the recovery property but not the orthogonality property.

Next, lets look at two frequency-domain based methods. One method forms the analytic signal by setting the negative frequency samples to zero [25]. This method, originally proposed in discrete Hilbert transform form by Čížek [67] and Bonzanigo [68], uses the DFT and inverse DFT (IDFT) to switch between the time and frequency domains. The method, which we shall refer to as the Čížek–Bonzanigo method, satisfies both properties. The other frequency-domain based method [69] is a modified version of the Čížek–Bonzanigo method; it has the additional step of zeroing an extra single value of the continuous spectrum in the negative frequency range. The method satisfies the recovery property but not the orthogonality property.

Comparative to the other methods, the analytic signal produced by the Čížek–Bonzanigo method is particularly attractive for the following reasons:

- its negative frequency samples are exactly zero;
- it preserves the recovery and orthogonality properties;
- it has a simple implementation [25]—no filter design [61] or selection of an arbitrary frequency point [69] is necessary.

The commonly-used procedure for obtaining an analytic signal for a DWVD uses the Čížek–Bonzanigo method. The complete procedure, for the N-point real-valued signal $s(nT)$, is as follows [11, 48, 26, 43]:

1. take the DFT of signal $s(nT)$ to obtain $S(k/NT)$;
2. let
$$\widehat{Z}_{\mathrm{c}}(k/NT) = \widehat{H}_{\mathrm{c}}(k/NT)S(k/NT)$$
where
$$\widehat{H}_{\mathrm{c}}(\tfrac{k}{NT}) = \begin{cases} 1, & k = 0 \text{ and } k = \frac{N}{2}, \\ 2, & 1 \leq k \leq \frac{N}{2} - 1, \\ 0, & \frac{N}{2} + 1 \leq k \leq N - 1; \end{cases}$$
3. take the IDFT of $\widehat{Z}_{\mathrm{c}}(k/NT)$ to obtain $\hat{z}_{\mathrm{c}}(nT)$ (of length N);
4. let $z_{\mathrm{c}}(nT)$ equal $\hat{z}_{\mathrm{c}}(nT)$ zero-padded to length $2N$; we call $z_{\mathrm{c}}(nT)$ the *conventional* analytic signal.

The last step ensures that $z_{\mathrm{c}}(nT)$ satisfies the time-constraint of (3.1), and therefore not the frequency-constraint of (3.2). In addition, the Čížek–Bonzanigo method does not zero the Nyquist frequency term, which further violates the frequency-constraint.

3.3 Proposed Discrete Analytic Signal

While developing algorithms for DTFDs using linear convolution [45], I used two methods to generate the analytic signal. Both these methods are different to the Čížek–Bonzanigo method, the difference being the order of applying the analytic generating function and zero-padding operations. I noticed that the three signals, the conventional analytic signal and two from [45], all had different levels of non-zero energy in the ideally-zero regions. After some theoretical and experimental analysis, I was able to show that one of these analytic signals better approximates, comparative to the conventional analytic signal, the frequency-constraint. This signal is the discrete analytic signal I propose here.

The procedure to form the proposed analytic signal $z_{\mathrm{p}}(nT)$ [47,46], from the N-point real-valued signal $s(nT)$, is as follows:

1. zero-pad $s(nT)$ to length $2N$; call this $s_{\mathrm{a}}(nT)$;
2. take the DFT of $s_{\mathrm{a}}(nT)$ to obtain $S_{\mathrm{a}}(k/2NT)$;
3. let
$$Z_{\mathrm{a}}(\tfrac{k}{2NT}) = H_{\mathrm{a}}(\tfrac{k}{2NT})S_{\mathrm{a}}(\tfrac{k}{2NT}) \tag{3.5}$$
where $H_{\mathrm{a}}(k/2NT)$ is defined as
$$H_{\mathrm{a}}(\tfrac{k}{2NT}) = \begin{cases} 1, & k=0 \text{ and } k=N, \\ 2, & 1 \le k \le N-1, \\ 0, & N+1 \le k \le 2N-1; \end{cases} \tag{3.6}$$
4. take the IDFT of $Z_{\mathrm{a}}(k/2NT)$ to obtain $z_{\mathrm{a}}(nT)$;
5. and lastly, force the second half of $z_{\mathrm{a}}(nT)$ to zero
$$z_{\mathrm{p}}(nT) = \begin{cases} z_{\mathrm{a}}(nT), & 0 \le n \le N-1, \\ 0, & N \le n \le 2N-1. \end{cases} \tag{3.7}$$

Steps 2 to 4 implements the Čížek–Bonzanigo method on the zero-padded signal $s_{\mathrm{a}}(nT)$ [45]. We, therefore, do the zero-padding process before we generate the signal $z_{\mathrm{a}}(nT)$, unlike the procedure for $z_{\mathrm{c}}(nT)$, where we do the zero-padding process last. The last step ensures that $z_{\mathrm{p}}(nT)$ satisfies the time-constraint of (3.1), although at the expense of the frequency-constraint of (3.2).

The proposed analytic signal satisfies the recovery and orthogonality properties from Section 3.2.1. The following explains why. From (3.7), $z_{\mathrm{p}}(nT) = z_{\mathrm{a}}(nT)$ for $0 \le n \le N-1$; from [25], $\Re\big[z_{\mathrm{a}}(nT)\big] = s(nT)$ for $0 \le n \le N-1$; therefore

$$\Re\big[z_{\mathrm{p}}(nT)\big] = s(nT), \qquad 0 \le n \le N-1$$

and thus the proposed signal satisfies the signal recovery property.

From (3.7),

$$\sum_{n=0}^{2N-1} \Re\big[z_{\mathrm{p}}(nT)\big]\,\Im\big[z_{\mathrm{p}}(nT)\big] = \sum_{n=0}^{N-1} \Re\big[z_{\mathrm{a}}(nT)\big]\,\Im\big[z_{\mathrm{a}}(nT)\big]\,.$$

Because $z_{\mathrm{a}}(nT)$ satisfies the orthogonality property [25] the proposed analytic signal therefore satisfies the orthogonality property.

3.3.1 Time-Domain Analysis

The two analytic signals are related to the $2N$-point real-valued signal $s_{\mathrm{a}}(nT)$ as follows:

$$z_{\mathrm{c}}(nT) = \big[s_{\mathrm{a}}(nT) \circledast h_{\mathrm{c}}(nT)\big]\, u_{\mathrm{t}}(nT) \tag{3.8}$$

$$z_{\mathrm{p}}(nT) = \big[s_{\mathrm{a}}(nT) \circledast h_{\mathrm{a}}(nT)\big]\, u_{\mathrm{t}}(nT) \tag{3.9}$$

where $\circledast$ represents circular convolution. The time-reversed and time-shifted step function $u_{\mathrm{t}}(nT)$ is defined as $u_{\mathrm{t}}(nT) = u((N-1-n)T)$, where $u(nT)$ represents the unit step function. The impulse function $h_{\mathrm{a}}(nT)$ is the IDFT of the frequency-response function $H_{\mathrm{a}}(k/2NT)$, defined in (3.6). We can show that this impulse function equates to

$$h_{\mathrm{a}}(nT) = \begin{cases} \delta(n), & n \text{ even}, \\ \frac{\mathrm{j}}{N}\cot\left(\frac{\pi n}{2N}\right), & n \text{ odd}, \end{cases}$$

where $\delta(n)$ is the Kronecker delta function. The relation between the two convolving functions $h_{\mathrm{c}}(nT)$ and $h_{\mathrm{a}}(nT)$ is

$$h_{\mathrm{c}}(nT) = h_{\mathrm{a}}(nT) + h_{\mathrm{a}}((n+N)T). \tag{3.10}$$

The presence of $u_{\mathrm{t}}(nT)$ in (3.8) and (3.9) guarantees that $z_{\mathrm{c}}(nT)$ and $z_{\mathrm{p}}(nT)$ both satisfy the time-constraint.

To highlight the differences between the two analytic signals, we use the N-point impulse signal $s(nT) = \delta(nT)$ as an example. As both analytic signals preserve the real-valued signal, only the imaginary parts for the signals are plotted in Fig. 3.1. As expected, the imaginary parts of $z_{\mathrm{c}}(nT)$ and $z_{\mathrm{p}}(nT)$ are zero for $N \leq n \leq 2N-1$, because the presence of $u_{\mathrm{t}}(nT)$ in (3.8) and (3.9) guarantee that both signals satisfy the time-constraint. Also, $z_{\mathrm{c}}(nT)$ has a significant negative component around $n = N-1$, whereas $z_{\mathrm{p}}(nT)$ does not. The relation in (3.10) explains this difference.

3.3.2 Frequency-Domain Analysis

In the frequency domain, the two analytic signals as a function of $S_{\mathrm{a}}(k/2NT)$ are

$$Z_{\mathrm{c}}(\tfrac{k}{2NT}) = \Big[S_{\mathrm{a}}(\tfrac{k}{2NT})H_{\mathrm{c}}(\tfrac{k}{2NT})\Big] \circledast U_{\mathrm{t}}(\tfrac{k}{2NT}) \tag{3.11}$$

$$Z_{\mathrm{p}}(\tfrac{k}{2NT}) = \Big[S_{\mathrm{a}}(\tfrac{k}{2NT})H_{\mathrm{a}}(\tfrac{k}{2NT})\Big] \circledast U_{\mathrm{t}}(\tfrac{k}{2NT}). \tag{3.12}$$

where $S_{\mathrm{a}}(k/2NT)$ is the DFT of $s_{\mathrm{a}}(nT)$ and $U_{\mathrm{t}}(k/2NT)$ is the DFT of $u_{\mathrm{t}}(nT)$. The frequency-response function $H_{\mathrm{c}}(k/2NT)$ is

$$H_{\mathrm{c}}(\tfrac{k}{2NT}) = \begin{cases} 2H_{\mathrm{a}}(\tfrac{k}{2NT}), & k \text{ even}, \\ 0, & k \text{ odd}, \end{cases} \tag{3.13}$$

with $H_{\mathrm{a}}(k/2NT)$ defined in (3.6). Because of the convolution with $U_{\mathrm{t}}(k/2NT)$ in (3.11) and (3.12), neither $Z_{\mathrm{c}}(k/2NT)$ nor $Z_{\mathrm{p}}(k/2NT)$ satisfy the frequency-constraint.

To illustrate the difference between the two analytic signals' spectra, we use the impulse signal once more. These results are displayed in Fig. 3.2. For this signal

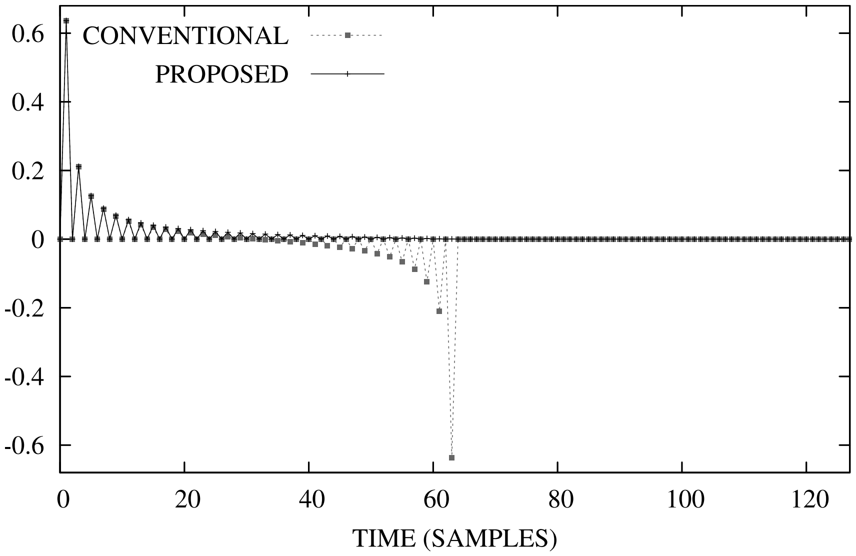

FIGURE 3.1: Imaginary part of the conventional and proposed analytic signals formed from the N-point impulse signal, where $N = 64$.

$S_{\mathrm{a}}(k/2NT) = 1$ for all values of k. Neither signal satisfies the frequency-constraint. The conventional analytic signal's approximation—comparative to the proposed analytic signal—of the frequency-constraint, however, is marred by significant oscillation between the odd and even values of k. The oscillatory nature of $H_{\mathrm{c}}(k/2NT)$, described in (3.13), causes this behaviour.

3.4 Performance of Proposed Analytic Signal

We shall now examine the relative performance of the proposed analytic signal at approximating the frequency-constraint in (3.2).

3.4.1 Relative Performance

I use the signals' spectral energy, at the Nyquist and negative frequencies, as a relative performance measure. The following proposition describes this measure.

Proposition 1 *The spectral energy relation of $Z_{\mathrm{p}}(k/2NT)$ and $Z_{\mathrm{c}}(k/2NT)$, at Nyquist and negative frequencies, is*

$$\sum_{k=N}^{2N-1} \left| Z_{\mathrm{p}}\left(\tfrac{k}{2NT}\right) \right|^2 = \frac{1}{2} \sum_{k=N}^{2N-1} \left| Z_{\mathrm{c}}\left(\tfrac{k}{2NT}\right) \right|^2 + \frac{1}{2} \left(\left| Z_{\mathrm{p}}\left(\tfrac{N}{2NT}\right) \right|^2 - \left| \widehat{Z}\left(\tfrac{0}{2NT}\right) \right|^2 - C \right) \tag{3.14}$$

where $\widehat{Z}(k/2NT) = Z_{\mathrm{a}}(k/2NT) - Z_{\mathrm{p}}(k/2NT)$, with $Z_{\mathrm{a}}(k/2NT)$ defined in (3.5), and

$$C = \begin{cases} 0, & N \text{ even}, \\ 2\left| \widehat{Z}\left(\tfrac{N}{2NT}\right) \right|^2, & N \text{ odd}. \end{cases}$$

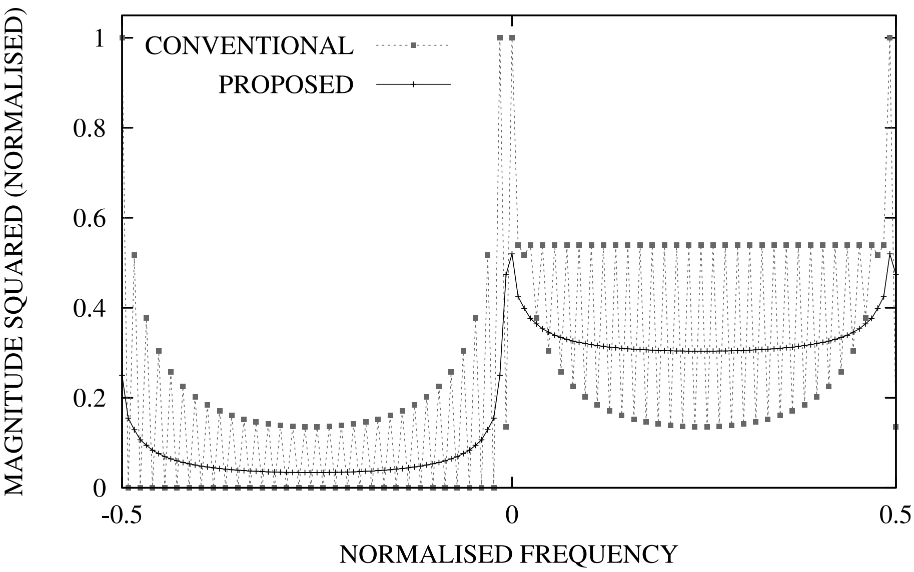

FIGURE 3.2: Discrete spectra of the two analytic signals formed from the test impulse signal.

Proof: See Appendix D. ■

From (3.14), we see that the energy relation between $Z_{\rm p}(k/2NT)$ and $Z_{\rm c}(k/2NT)$ is dependent on the value of $Z_{\rm a}(k/2NT)$ and $Z_{\rm p}(k/2NT)$ at $k = 0$ and $k = N$. If the second term in the right hand side of (3.14) is small, relative to the first term, then we can rewrite (3.14) as

$$\sum_{k=N}^{2N-1} \left| Z_{\rm p}\left(\tfrac{k}{2NT}\right) \right|^2 \approx \frac{1}{2} \sum_{k=N}^{2N-1} \left| Z_{\rm c}\left(\tfrac{k}{2NT}\right) \right|^2 . \tag{3.15}$$

This equation states that the spectral energy for $Z_{\rm p}(k/2NT)$ is approximately half of the spectral energy for $Z_{\rm c}(k/2NT)$ in the specified range. I numerically verify this approximation in the next subsection using a number of test signals.

3.4.2 Numerical Examples

This section provides examples to confirm the approximation in (3.15). To start, I define the ratio

$$\eta = \frac{\sum_{k=N}^{2N-1} \left| Z_{\rm p}\left(\tfrac{k}{2NT}\right) \right|^2}{\sum_{k=N}^{2N-1} \left| Z_{\rm c}\left(\tfrac{k}{2NT}\right) \right|^2}.$$

Next, I compute this ratio with six different signal types: an impulse function, a step function, a sinusoidal signal, a nonlinear frequency modulated signal (NLFM) signal, white Gaussian noise (WGN), and a real-world signal. This last signal is an electroencephalogram (EEG) recording from a newborn baby. The length N for each signal was arbitrarily set to even values between 14 and 2048; 1 was added to this value to obtain N odd.

The results, in Table 3.1, for most of the test signals confirm the approximation stated in (3.15). The exceptions to this include the WGN realisations, where the mean ratio value is < 0.6, and the sinusoidal signal when N is odd, where the ratio value is also < 0.6.

TABLE 3.1: Performance ratio measures comparing the proposed with the conventional analytic signal.

Signal Type	η (N even)	η (N odd)
Impulse	0.5078	0.4711
Step	0.4137	0.4136
Sinusoid	0.4595	0.5709
NLFM	0.5055	0.4999
WGN[a]	0.5883 (0.0976)	0.5319 (0.0983)
EEG[b]	0.4184 (0.0671)	0.4155 (0.0650)

[a] 1000 realisations used.

[b] 1000 epochs used. [a,b] Values are in the form, mean (standard deviation).

In addition, I plot, in Fig. 3.3, the spectra of the conventional and proposed analytic signals using two of the tests signals: the sinusoidal signal with $N = 14$, and an EEG epoch with $N = 99$. Note, from Fig. 3.3 and Fig. 3.2, that the amount of energy in the negative spectral region is signal dependent, but the ratio η comparing the analytic signals remains approximately the same.

3.5 Reduced Aliased DWVD

This section compares the performance of the analytic signals by their contribution to aliasing in the DWVD. I use the DWVD-C definition from Chapter 2 to quantify the aliasing, although either of the four DWVD definitions from Chapter 2 will produce the same results because of their close relation in (2.43) and (2.50). We may write the DWVD-C from the relation in (2.50), for spectral signal $Z(k/2NT)$, as

$$W^{\mathrm{C}}(\tfrac{nT}{2}, \tfrac{k}{2NT}) = \frac{\mathrm{e}^{-\mathrm{j}\pi kn/N}}{4N^2} \sum_{l=0}^{2N-1} Z(\tfrac{l}{2NT}) Z^{*}((2k-l)\tfrac{1}{2NT})\, \mathrm{e}^{\mathrm{j}\pi lk/N}. \tag{3.16}$$

3.5.1 Aliasing in the DWVD

To begin, recall how we quantify aliasing in the discrete-time domain. Consider the signal $y(t)$ which is bandlimited in the frequency-domain to the region $|f| < 1/(2T)$. We sample $y(t)$, with sampling period T, to obtain the discrete-time signal $y(nT)$. This signal $y(nT)$ is alias free because the periodic copies in the frequency domain for $y(nT)$ do not overlap. Now consider another discrete signal $y_1(nT)$, obtained by sampling $y(t)$ with sampling period $T_1 = 2T$. This discrete signal $y_1(nT)$ is aliased because the periodic copies in the frequency-domain do overlap. If we know the spectral content for $y(t)$, then we are able to measure the spectral periodic overlap for $y_1(nT)$, and are therefore able to quantify the aliasing in $y_1(nT)$. Similarly, to evaluate aliasing in the DWVD, we measure spectral content in a specific region of the Doppler–frequency domain.

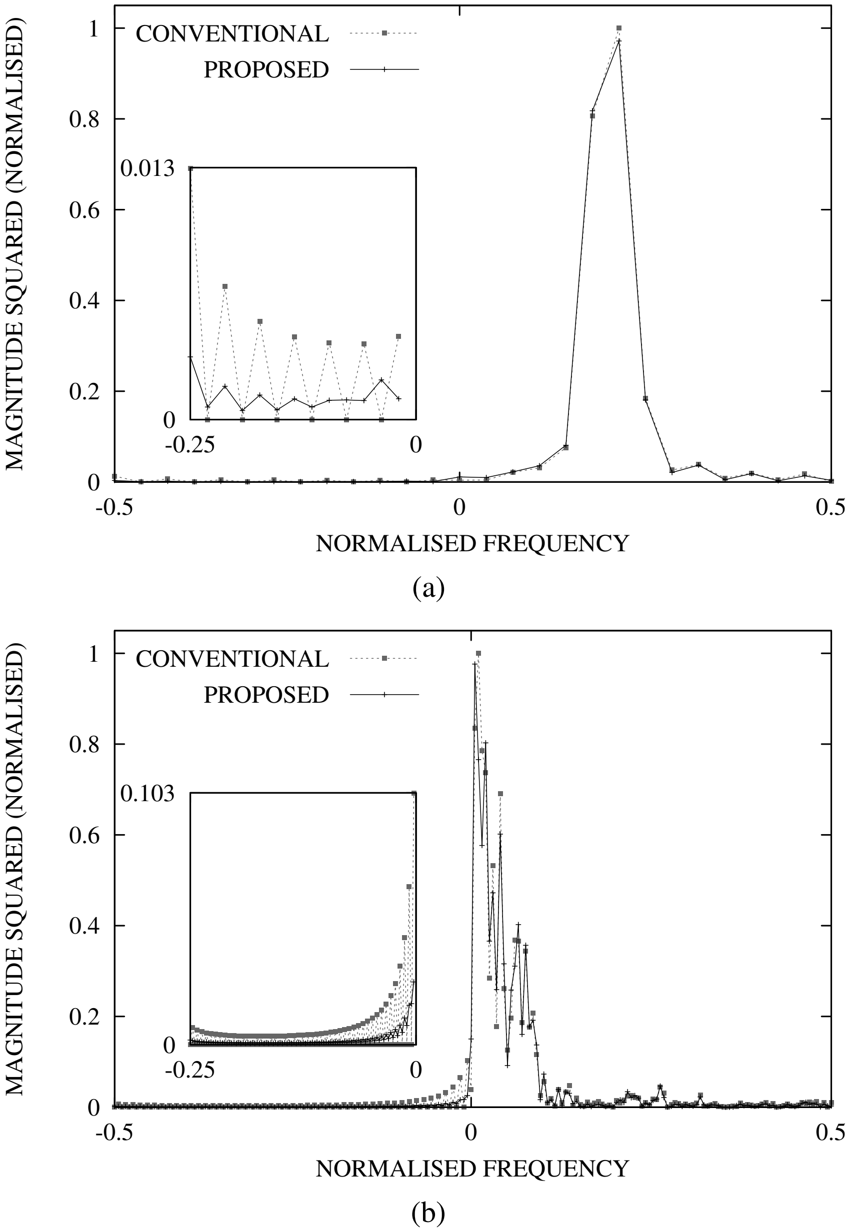

Figure 3.3: Discrete spectra comparing the two analytic signals for two test signals: (a) a sinusoidal signal, and (b) an EEG epoch. The inset plots show a portion of the negative frequency axis with a reduced magnitude range.

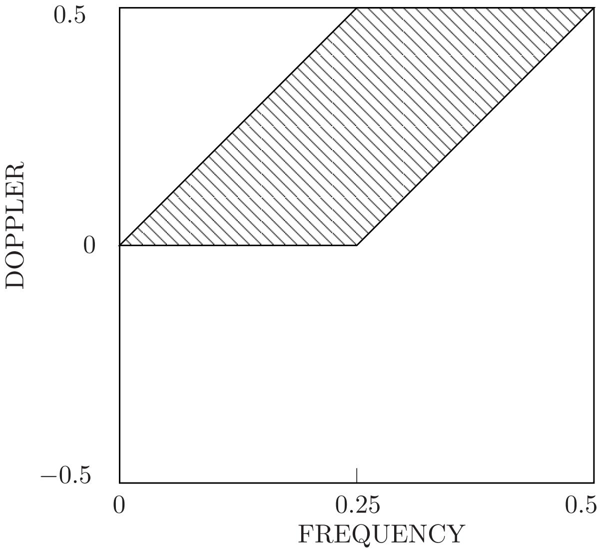

FIGURE 3.4: Asymmetrical SIAF using discrete analytic signal. Area outside shaded region represents the ideally-zero Doppler–frequency region. Doppler and frequency axes are normalised.

The Doppler–frequency function,

$$\mathcal{K}(\tfrac{l}{2NT},\tfrac{k}{2NT}) = Z(\tfrac{l}{2NT})Z^*((2k-l)\tfrac{1}{2NT}) \tag{3.17}$$

from (3.16), is the asymmetrical spectral instantaneous function (SIAF), which differs from the symmetrical SIAF from Chapter 2. I use the asymmetrical, rather than symmetrical, SIAF to simplify calculations.

If we assume that $Z(k/2NT)$ satisfies the frequency-constraint of (3.2), then the nonzero content (or energy) in $\mathcal{K}$ is contained within a specific region in Fig. 3.4. Any energy outside this region results in aliasing in the DWVD. We shall refer to this undesirable phenomenon as *spectral-leakage*.

As $Z_c(k/2NT)$ does not satisfy the frequency-constraint, its asymmetrical SIAF $\mathcal{K}_c$ contains spectral-leakage. This is true also for the Doppler–frequency function of $Z_p(k/2NT)$, $\mathcal{K}_p$. I quantify this spectral-leakage by summing the squared error over this region, where the ideal here is zero. Accordingly, to asses the relative merit of the proposed analytic signal, I use the ratio squared error measure

$$\mu = \frac{\alpha(\mathcal{K}_p)}{\alpha(\mathcal{K}_c)}$$

where $\alpha(\mathcal{K})$ is a measure of the two-dimensional spectral-leakage for $\mathcal{K}$, defined as

$$\alpha(\mathcal{K}) = \sum_{k=0}^{2N-1}\sum_{l=N}^{2N-1}\left|\mathcal{K}(\tfrac{l}{2NT},\tfrac{k}{2NT})\right|^2 + \sum_{k=N}^{2N-1}\sum_{l=0}^{k-N}\left|\mathcal{K}(\tfrac{l}{2NT},\tfrac{k}{2NT})\right|^2 + \sum_{k=0}^{N}\sum_{l=k+1}^{N}\left|\mathcal{K}(\tfrac{l}{2NT},\tfrac{k}{2NT})\right|^2.$$

As the function $\mathcal{K}$ is quadratic in $Z(k/2NT)$, cross-terms between the positive and negatives frequencies will be present in the resultant DWVD. These cross-terms are part of the spectral-leakage in the Doppler–frequency function, and are therefore incorporated into the $\alpha(\mathcal{K})$ measure. We consider these cross-terms as aliasing as they would not be present if the frequency-constraint was satisfied.

Table 3.2: Ratio measure comparing aliasing in the DWVD of the proposed analytic signal with the DWVD of the conventional analytic signal.

Signal Type	μ (N even)	μ (N odd)
Impulse	0.4671	0.4444
Step	0.4465	0.4463
Sinusoid	0.4583	0.5666
NLFM	0.5055	0.4999
WGN[a]	0.5863 (0.0986)	0.5327 (0.0996)
EEG[b]	0.4237 (0.0743)	0.4210 (0.0726)

[a] 1000 realisations used.

[b] 1000 epochs used. [a,b] Values are in the form, mean (standard deviation).

3.5.2 Numerical Examples

I present the results in Table 3.2 for the same set of example signals used in Section 3.4.2. The results for μ are not equal to η because the Doppler–frequency function $\mathcal{K}$ is quadratic in the signal $Z(k/2NT)$. We see from the results, however, that μ approximates η for all test signals apart from the impulse signal, where μ is less than η. From these results we infer that the amount of spectral-leakage for $\mathcal{K}_{\text{p}}$ is approximately half of the spectral-leakage for $\mathcal{K}_{\text{c}}$. Hence, the amount of aliasing present in the DWVD of $z_{\text{p}}(nT)$ is approximately half of the aliasing present in the DWVD of $z_{\text{c}}(nT)$.

To show some examples of this reduced aliasing, I plot the DWVDs of the two analytic signals using two different signals from the test set—namely, the impulse signal and an EEG epoch. Fig. 3.5 shows the two DWVDs of the impulse signal. For this signal, the energy in the DWVD should, ideally, be concentrated around the time sample $n = 0$, as $\delta(nT) = 0$ for $n > 0$. Fig. 3.5 shows that the DWVD of the proposed analytic signal better approximates this ideal compared with the DWVD of the conventional analytic signal.

Fig. 3.6 shows the two DWVDs using the EEG epoch. We previously plotted the spectra of the two analytic signals for this EEG epoch in Fig. 3.3b. From this frequency-domain plot, we can see that very little relative energy is present above the normalised frequency value of 0.25. Thus, we expect little energy in the DWVD above the frequency value 0.25. Accordingly, from Fig. 3.6, we see that the DWVD of the proposed signal has less energy in this region compared with that for the DWVD of the conventional analytic signal.

3.6 Summary and Conclusions

The failure of a discrete analytic signal to satisfy both a finite-time and finite-frequency bandwidth constraint causes aliasing in the DWVD. I presented, in this chapter, a new discrete analytic signal which, compared with the conventional discrete analytic signal, better approximates these constraints and consequently reduces aliasing in the DWVD.

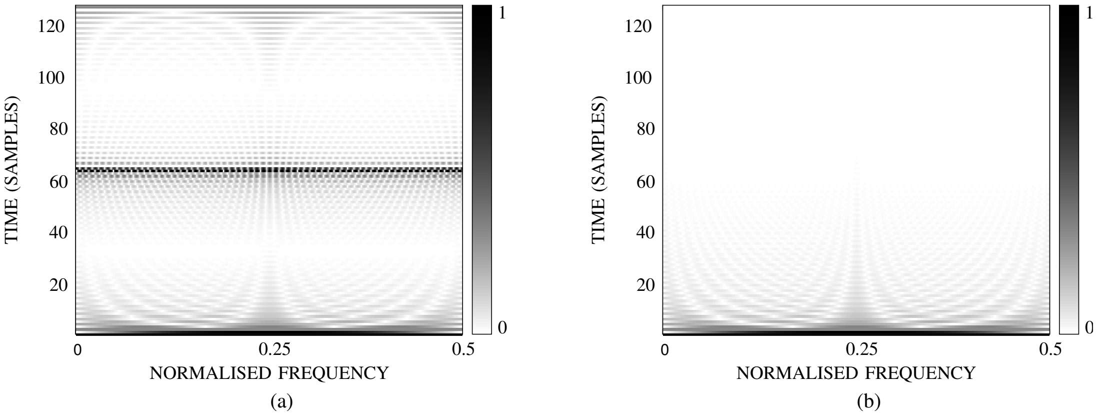

FIGURE 3.5: DWVDs of the two analytic signals using the impulse test signal $\delta(n)$: absolute value of the DWVD for the (a) conventional analytic signal, and (b) proposed analytic signal. Both DWVDs are normalised.

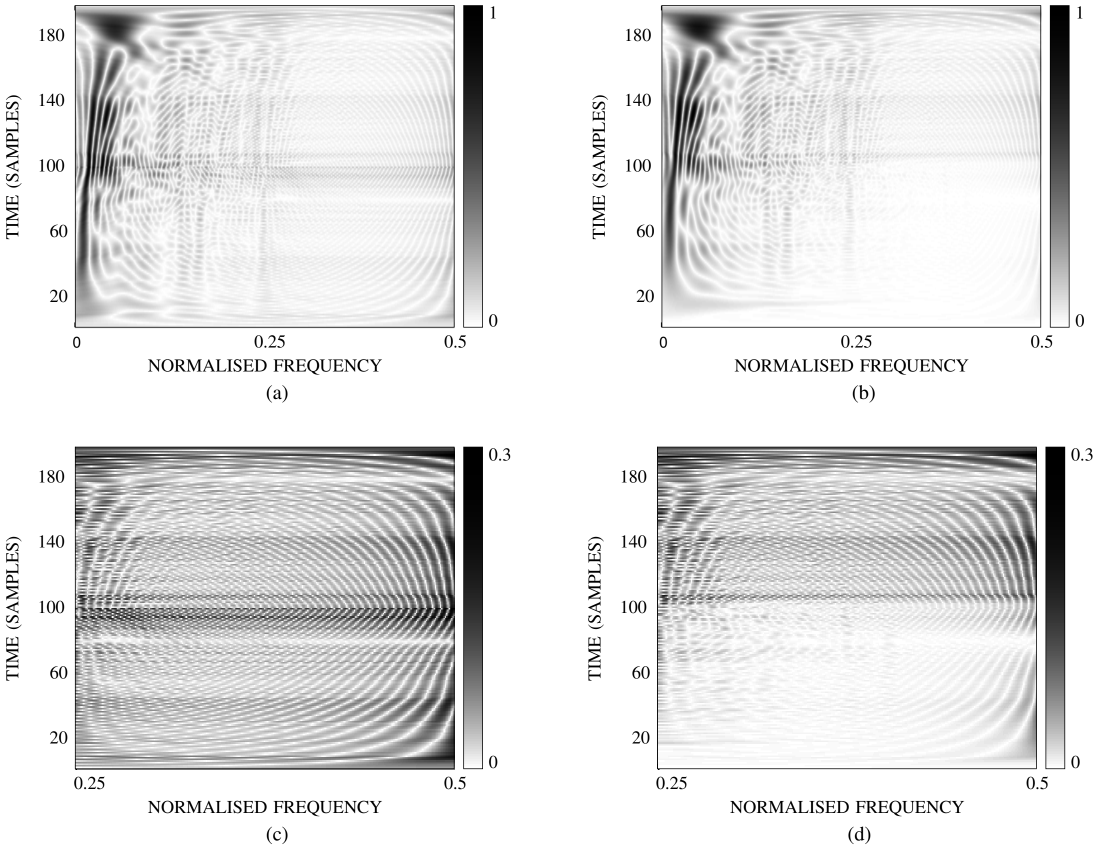

FIGURE 3.6: DWVDs of the two analytic signals using an EEG epoch: absolute value of the DWVD for the (a) conventional analytic signal, and (b) proposed analytic signal. To highlight the differences between the distributions, (c) and (d) display a portion of the distribution where, for this particular signal, we expect little energy. The plot in (c) is one-half of the distribution in (a); likewise, the plot in (d) is one-half of the distribution in (b). Both DWVDs are normalised.

I showed that the DWVD of the proposed analytic signal has approximately 50% less aliasing than that for the DWVD of the conventional analytic signal. The proposed signal retains two useful attributes of the conventional signal: it satisfies the recovery and orthogonality properties and has a simple implementation using DFTs.

Chapter 4

Discrete Time–Frequency Distributions

4.1 Introduction

This chapter proposes a new DTFD definition that incorporates the proposed DWVD-C from Chapter 2 and the proposed discrete analytic signal from Chapter 3. The purpose of the proposed DTFD definition *is to better approximate, relative to existing DTFD definitions, the ideal DTFD.* An ideal DTFD equals samples of the continuous TFD, and is therefore alias free, and satisfies all important mathematical properties that the continuous TFD satisfies.

The continuous TFD of $z(t)$, in terms of the WVD, is

$$\rho_z(t,f) = W_z(t,f) \underset{t}{*} \underset{f}{*} \gamma(t,f) \tag{4.1}$$

where $*_t$ represents the convolution operation in the time direction, and likewise $*_f$ represents convolution in the frequency direction; the $\gamma(t,f)$ function is called the time–frequency kernel and is independent of the signal $z(t)$. The purpose of convolving the WVD with the kernel is to suppress the cross-terms introduced by the WVD [1]. Cross-terms appear in the WVD for particular signal types, such as multicomponent or nonlinear frequency modulated signals, because the WVD is quadratic—rather than linear—in the signal. Possible consequences of convolving the WVD with the time–frequency kernel in (4.1) include a loss of resolution in the distribution, loss of mathematical properties, or both.

To form a DTFD, we need to convolve a DWVD with a discrete time–frequency kernel. Because we define the DTFD solely for the purpose of implementing the continuous TFD on a computer, we would like the DTFD to closely resemble the continuous TFD. The DTFD should therefore be free from aliasing and should satisfy the set of important properties that the TFD satisfies.

The DTFD can have three different types of aliasing: 1) aliasing from the wrap-around artefacts caused by the circular convolution operation of the discrete WVD (DWVD) with the discrete kernel [23], 2) aliasing from the discrete analytic signal's approximation of two mutually exclusive constraints (2.38), and 3) aliasing from the periodic overlap in the DWVD (2.36). We shall ignore the first and second types of aliasing because we can eliminate the first type of aliasing by replacing circular convolution with linear convolution [23] and, although we never completely eliminate the second type of aliasing, we can minimise it by using the discrete analytic signal proposed in the previous chapter. This second type of aliasing is, for most signals, small compared with the aliasing caused by the periodic overlap in the DWVD, the third type of aliasing—the difference between (2.36) and (2.39), (2.40). Thus, we shall use the term *pseudo-alias–free* DTFD to mean that the DTFD is free from periodic overlap caused by the underlying DWVD.

Different methods exist for defining DTFDs. In this chapter, I consider the widely-used definitions; namely, the generalised discrete TFD (GDTFD) [32, 33, 34] and the alias-free GDTFD (AF-GDTFD) [36, 29]. The GDTFD is a pseudo-alias–free DTFD but fails to satisfy all properties listed in Section 2.2.1. The AF-GDTFD satisfies all properties, except the time- and frequency-support properties, but is not always a pseudo-alias–free DTFD [59, 29, 58].

To address the limitations of the GDTFD and AF-GDTFD, I propose a new DTFD definition. This proposed definition is a more general form of the GDTFD, as the GDTFD is a time-decimated version of the proposed definition. The proposed definition satisfies all properties, and like the GDTFD, is a pseudo-alias–free definition.

4.2 Review

We now examine two commonly used DTFD definitions which use the DWVD definitions introduced in Chapter 2. Assume that all definitions use the $2N$-point discrete analytic signal $z(nT)$ proposed in Chapter 3.

The first, known as the generalised DTFD (GDTFD), uses the DWVD-A and is defined as [32, 33, 34, 35]

$$\rho^{\mathrm{A}}(nT, \tfrac{k}{2NT}) = W^{\mathrm{A}}(nT, \tfrac{k}{2NT}) \underset{n}{\circledast} \underset{k}{\circledast} \gamma^{\mathrm{A}}(nT, \tfrac{k}{2NT}) \tag{4.2}$$

for $n, k = 0, 1, \ldots, N-1$, where the symbol $\circledast$ represents the circular convolution operation. The discrete time–frequency kernel γ^{A} is formed in the Doppler–lag domain (ν, τ) by sampling $g(\nu, \tau)$ with the discrete grid $(\nu = l/NT, \tau = 2mT)$ to form $g^{\mathrm{A}}(l/NT, 2mT)$. Mapping $g^{\mathrm{A}}(l/NT, 2mT)$ to time–frequency results in the discrete kernel $\gamma^{\mathrm{A}}(nT, k/2NT)$. As the definition is formed by convolving a pseudo-alias–free DWVD with a time–frequency kernel, the GDTFD is therefore a pseudo-alias–free definition.

Fig. 4.1 shows the convolution process from (4.2) in the time–lag domain. Convolving the TIAF with the time–lag kernel results in the smoothed TIAF R^{A},

$$R^{\mathrm{A}}(nT, 2mT) = K^{\mathrm{A}}(nT, 2mT) \underset{n}{\circledast} G^{\mathrm{A}}(nT, 2mT)$$

where the time–lag kernel G^{A} is the IDFT of the Doppler–lag function g^{A}. Because R^{A} and K^{A} have the same sample grid, $(t = nT, \tau = 2mT)$, the GDTFD has the same periodicity as DWVD-A [34]; that is,

$$\rho^{\mathrm{A}}(nT, \tfrac{k}{2NT}) = \rho^{\mathrm{A}}((n + pN)T, (k + qN)\tfrac{1}{2NT})$$

where p and q are integers. Hence all the signal information is contained within the quarter plane time–frequency region $0 \leq t \leq NT$ and $0 \leq f \leq 1/(2T)$. We shall therefore call the GDTFD a *quarter-plane distribution*.

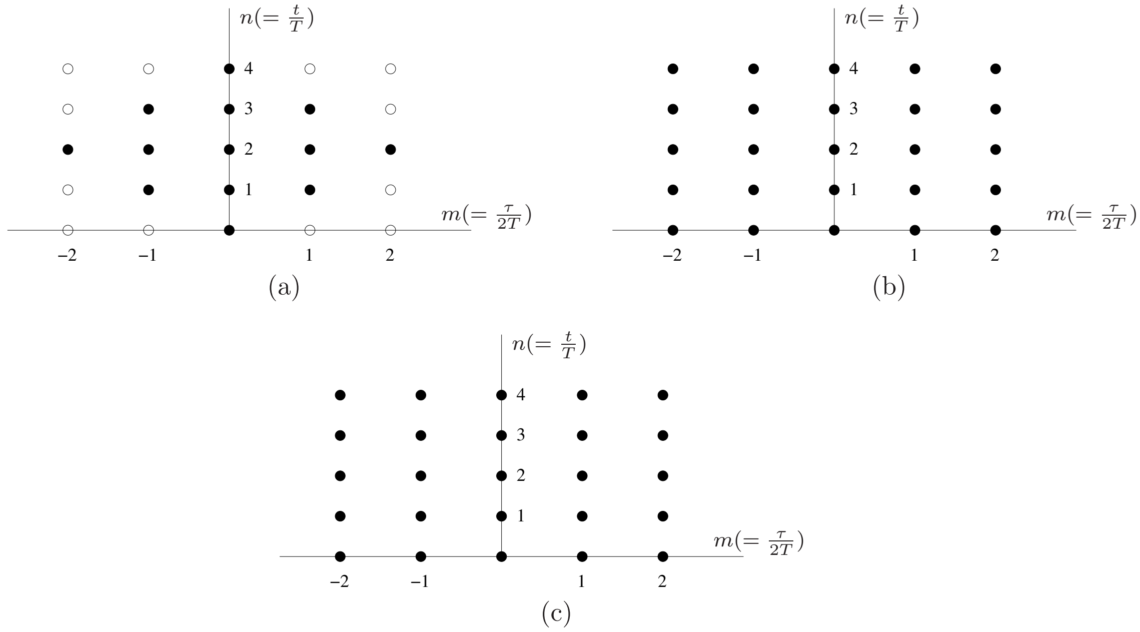

FIGURE 4.1: Forming the GDTFD in the time–lag domain. TIAF $K^{\mathrm{A}}(nT, 2mT)$ in (a) is convolved, in time, with kernel $G^{\mathrm{A}}(nT, 2mT)$ in (b) to produce the smoothed TIAF $R^{\mathrm{A}}(nT, 2mT)$ in (c) for signal of length $2N = 10$. Open circles represent zero values; filled circles represent the sample points of the function.

GDTFD is related to the continuous WVD and continuous kernel as follows:

$$\rho^{\mathrm{A}}(nT, \tfrac{k}{2NT}) \approx W(nT, \tfrac{k}{2NT}) \underset{n}{\circledast} \underset{k}{\circledast} \Big[\gamma(nT, \tfrac{k}{2NT}) + \gamma(nT, \tfrac{k+N}{2NT})\Big] \tag{4.3}$$

for $0 \leq n \leq N-1$ and $0 \leq k \leq N-1$. The approximation in this equation is caused by the approximation in (2.39), which shows that the DWVD-A only approximates samples of the WVD.

We assume that the time–frequency kernel $\gamma(t, f)$ is time and frequency bandlimited to the half-plane region $0 \leq t \leq NT$ and $|f| \leq 1/(2T)$. Because the kernel g^{A} is sampled in the lag direction with a period of $2T$, the kernel in (4.3) is folded in the frequency direction. This folding is necessary to represent the kernel's frequency extent of $|f| \leq 1/(2T)$ in the $0 \leq f \leq 1/(2T)$ convolution region in (4.3). Thus, the GDTFD approximates a WVD convolved with a time–frequency kernel and because we do not consider the potential wrap around effects from the circular convolution operation as aliasing [23], the GDTFD is a pseudo-alias–free definition.

The second definition is known as the alias-free generalised DTFD (AF-GDTFD) [36] and is, despite its name, not always alias free [29, 58]. I present the AF-GDTFD as

$$\rho^{\mathrm{AF}}(nT, \tfrac{k}{2NT}) = F(\tfrac{2nT}{2}, \tfrac{2k}{4NT}) \tag{4.4}$$

for $n, k = 0, 1, \ldots, 2N-1$ where F is defined in terms of DWVD-B as

$$F(\tfrac{nT}{2}, \tfrac{k}{4NT}) = W^{\mathrm{B}}(\tfrac{nT}{2}, \tfrac{k}{4NT}) \underset{n}{\circledast} \underset{k}{\circledast} \gamma^{\mathrm{AF}}(\tfrac{nT}{2}, \tfrac{k}{4NT}) \tag{4.5}$$

for $n, k = 0, 1, \ldots, 4N-1$. The discrete time–frequency kernel γ^{AF} is formed in the time–lag domain by sampling $g(t, \tau)$ with the nonuniform discrete grid $(t = nT, \tau = 2mT)$ and

$(t = (n+1/2)T, \tau = 2(m+1/2)T)$ to form $G^{\mathrm{AF}}(nT/2, mT)$. This time–lag kernel has the same nonuniform sample grid as that for the TIAF K^{B}.

The $4N \times 4N$ DWVD-B in (4.5) encompasses the time–frequency area $0 \leq t \leq 2NT$ and $|f| \leq 1/(2T)$—a larger area than we saw in Section 2.4.5 for the DWVD-B. This extension process is equivalent to inserting zeros into the discrete time–lag grid for K^{B} as shown in Fig. 4.2a. Also, K^{B} is periodically extended from $2N$ to $4N$ in the time direction using the periodic relation in [27]. The AF-GDTFD is not always pseudo-alias free because the $4N \times 4N$ DWVD-B in (4.4) is aliased [27], although the extent of this aliasing is controlled by the convolution operation with the kernel.

Note that we consider only the even values of n and k from F in (4.4) because the odd values of both n and k are zero. The time–lag domain provides insight: the convolution of the two similar shaped sample grids in Fig. 4.2(a) and Fig. 4.2(b) produces a different sample grid in Fig. 4.2(c) which is zero at odd time samples. A similar process occurs in the Doppler–frequency domain, which results in zero values at odd discrete-frequency samples. These two processes combined result in the zero sample points at odd time and frequency samples from the convolution in (4.5).

The AF-GDTFD, unlike the GDTFD, is periodic over the full time–frequency extent of the signal, as

$$\rho^{\mathrm{AF}}(nT, \tfrac{k}{2NT}) = \rho^{\mathrm{AF}}((n-p2N)T, (k-q2N)\tfrac{1}{2NT})$$

where p, q are integers. Thus, the AF-GDTFD requires the full time–frequency region $0 \leq t \leq 2N$ and $|f| \leq 1/2$ to represent all the signal information. Therefore, we refer to the AF-GDTFD as a *full-plane distribution.*

The AF-GDTFD is related to the WVD and continuous kernel as follows:

$$F(\tfrac{n}{2}, \tfrac{k}{4N}) \approx \left[\sum_{m=0}^{1} \sum_{l=0}^{1} (-1)^{nm+lk} W((n-l2N)\tfrac{1}{2}, (k-m2N)\tfrac{1}{4N}) \right] \underset{n}{\circledast} \underset{k}{\circledast} \gamma(\tfrac{n}{2}, \tfrac{k}{4N}) \qquad (4.6)$$

where the AF-GDTFD is related to F in (4.4). This relation is not exact because, as (2.40) shows, DWVD-B only approximates samples of the WVD. Thus, the AF-GDTFD does not approximate samples of the WVD convolved with a kernel but rather approximates samples of the sum of time- and frequency-shifted copies of the WVD convolved with a kernel.

Another notable DTFD definition was proposed by Nuttall [39]. The definition uses an interpolated, zero-padded, real-valued signal. The interpolation rate is determined by the time–frequency bandwidth of the kernel, thus avoiding the wrap around effects from circular convolution. Because we can rewrite Nuttall's original definition as the GDTFD of the interpolated signal, I do not consider it as a separate definition for this chapter.

4.3 Proposed DTFD Definition

The DWVD-C definition from Chapter 2 requires only $2N^2$ sample points and satisfies all important mathematical properties. Inspired by this DWVD definition, I attempted to define an equivalent DTFD definition. The result is a DTFD definition which extends the DWVD-C to the more general DTFD form.

The proposed DTFD definition is formed as follows [49, 51, 50]:

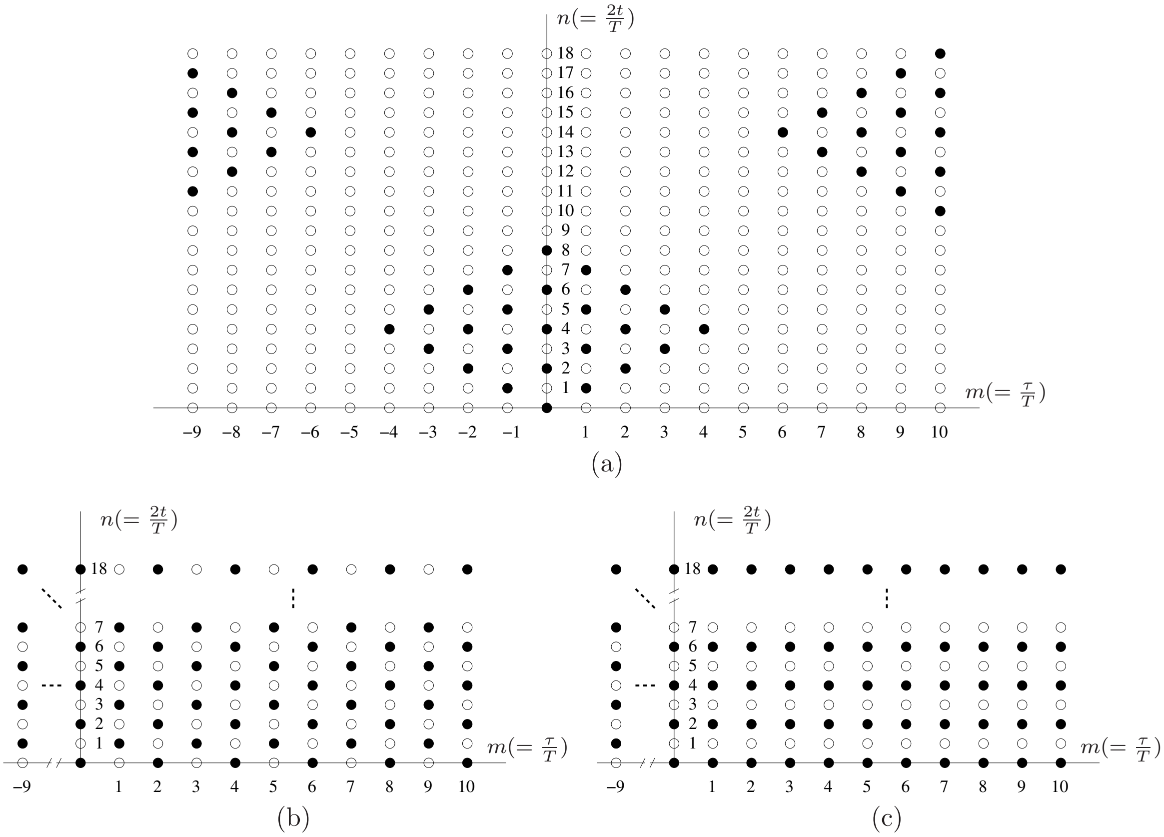

Figure 4.2: Forming the AF-GDTFD in the time–lag domain. TIAF $K_s^{\mathrm{A}}(nT/2, mT)$ in (a) is convolved, in time, with the kernel $G^{\mathrm{AF}}(nT/2, mT)$ in (b) to produce the smoothed TIAF $R_s^{\mathrm{AF}}(nT, mT)$ in (c) for signal of length $2N = 10$. Open circles represent zero values; filled circles represent the sample points of the function.

1. form the DWVD-C $W^{\mathrm{C}}(nT/2, k/2NT)$ for $n, k = 0, 1, \ldots, 2N-1$;
2. form the time–frequency kernel:
    (a) sample the Doppler–lag kernel $g(\nu, \tau)$ with the discrete grid $(\nu = l/NT, \tau = mT)$ for $l = 0, 1, \ldots, N-1$ and $m = 0, 1, \ldots, 2N-1$;
    (b) periodically extend this kernel $g^{\mathrm{C}}(l/NT, mT)$ in the Doppler l direction from N to $2N$;
    (c) and map $g^{\mathrm{C}}(l/NT, mT)$ to the time–frequency domain to obtain the discrete kernel $\gamma^{\mathrm{C}}(nT/2, k/2NT)$;
3. convolve the $2N \times 2N$ DWVD with the $2N \times 2N$ kernel:

$$\rho^{\mathrm{C}}(\tfrac{nT}{2}, \tfrac{k}{2NT}) = \left[W^{\mathrm{C}}(\tfrac{nT}{2}, \tfrac{k}{2NT}) \underset{n}{\circledast} \underset{k}{\circledast} \gamma^{\mathrm{C}}(\tfrac{nT}{2}, \tfrac{k}{2NT}) \right] \Bigg|_{k=0,1,\ldots,N-1} . \qquad (4.7)$$

The DWVD-C and the kernel γ^{C} in (4.7) extend over the negative and positive frequency range, but limiting the frequency axis to $k = 0, 1, \ldots, N-1$ means we take only

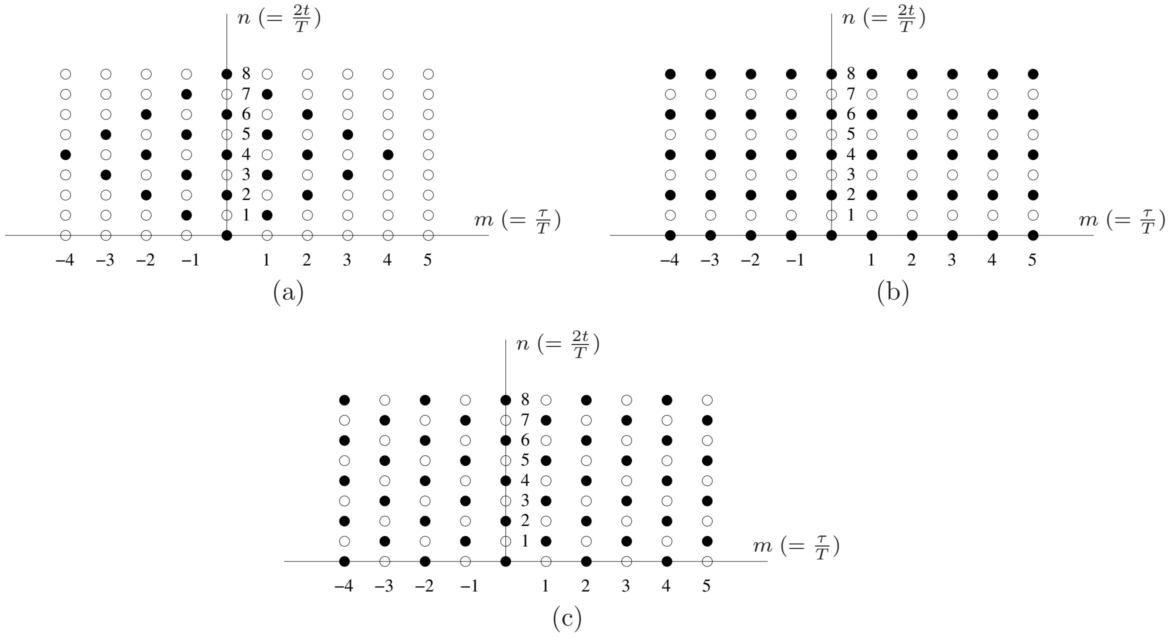

(a) (b) (c)

FIGURE 4.3: Forming the proposed definition in the time–lag domain. Convolving, in time, the TIAF $K^{\mathrm{C}}(nT/2, mT)$ in (a) with the kernel $G^{\mathrm{C}}(nT/2, mT)$ in (b) produces the smoothed TIAF $R^{\mathrm{C}}(nT/2, mT)$ in (c) for signal of length $2N = 10$. The time–lag kernel $G^{\mathrm{C}}(nT/2, mT)$ is the IDFT of the Doppler–lag kernel $g^{\mathrm{C}}(l/NT, mT)$. Open circles represent zero values; filled circles represent the sample points of the function.

the positive frequencies. I do this because the proposed definition is a quarter-plane distribution—that is, the distribution is periodic over the quarter-plane region:

$$\rho^{\mathrm{C}}(\tfrac{nT}{2}, \tfrac{k}{2NT}) = (-1)^{qn} \rho^{\mathrm{C}}((n - p2N)\tfrac{nT}{2}, (k - qN)\tfrac{1}{2NT}) \tag{4.8}$$

where p, q are integers. The definition is a quarter-plane distribution because the smoothed TIAF R^{C} has the same-shaped nonuniform sample grid as the K^{C} function.

We could rewrite (4.7) to equal a pseudo-alias–free DWVD convolved with a kernel, for $n/2$ in terms of n and $n + 1/2$, as

$$\rho^{\mathrm{C}}(nT, \tfrac{k}{2NT}) = W^{\mathrm{C}}(nT, \tfrac{k}{2NT}) \underset{n}{\circledast} \underset{k}{\circledast} \left[\gamma^{\mathrm{C}}(nT, \tfrac{k}{2NT}) + \gamma^{\mathrm{C}}(nT, \tfrac{k+N}{2NT})\right] \tag{4.9}$$

$$\rho^{\mathrm{C}}((n + \tfrac{1}{2})T, \tfrac{k}{2NT}) = W^{\mathrm{C}}((n + \tfrac{1}{2})T, \tfrac{k}{2NT}) \underset{n}{\circledast} \underset{k}{\hat{\circledast}} \left[\gamma^{\mathrm{C}}(nT, \tfrac{k}{2NT}) - \gamma^{\mathrm{C}}(nT, \tfrac{k+N}{2NT})\right]. \tag{4.10}$$

Thus, the proposed definition is a pseudo-alias–free definition. The symbol $\hat{\circledast}$ represents a modified circular convolution operation that differs from the convolution operation $\circledast$ as follows: for an arbitrary length-N function $a(nT)$, the modified convolution operation $a(nT) \hat{\circledast} a(nT)$ assumes that $a(nT)$ has the nonstandard periodic relation $a(nT) = -a((n - N)T)$, rather than the usual periodic relation $a(nT) = a((n - N)T)$.

Using (4.9) and (4.10), the proposed definition in terms of the WVD and the continuous kernel is

$$\begin{aligned} \rho^{\mathrm{C}}(nT, \tfrac{k}{2NT}) &\approx W(nT, \tfrac{k}{2NT}) \underset{n}{\circledast} \underset{k}{\circledast} \left[\gamma(nT, \tfrac{k}{2NT}) + \gamma(nT, \tfrac{k+N}{2NT})\right] \\ \rho^{\mathrm{C}}((n + \tfrac{1}{2})T, \tfrac{k}{2NT}) &\approx W((n + \tfrac{1}{2})T, \tfrac{k}{2NT}) \underset{n}{\circledast} \underset{k}{\hat{\circledast}} \left[\gamma(nT, \tfrac{k}{2NT}) - \gamma(nT, \tfrac{k+N}{2NT})\right]. \end{aligned} \tag{4.11}$$

4.3.1 Properties

Here we examine the set of mathematical properties for the DTFD definitions; these properties were presented in Chapter 2 for the DWVD. Each property requires a different constraint on the kernel, some of which are mutually exclusive which means that no single DTFD is capable of satisfying all properties simultaneously. Therefore, different distributions in the quadratic TFD class satisfy different properties.

I show that the proposed DTFD definition may satisfy all of these discrete properties, provided that the kernel satisfies the particular constraint. A DTFD from the GDTFD or AF-GDTFD, will not, regardless of kernel constraint, satisfy all these properties [35,36,29]. The following lists the properties and the sufficient kernel constraints. Assume that the signals $z(nT)$, $s(nT)$, and $y(nT)$ are $2N$-point discrete analytic signals of the form in (2.38). The proof for these properties is in [70].

- **Quadratic form:** the proposed definition has the form

  $$\rho^{\mathrm{C}}(\tfrac{nT}{2}, \tfrac{k}{2NT}) = \sum_{a=0}^{N-1} \sum_{b=0}^{N-1} z(aT) z^*(bT) H(a, b; n, k)$$

  where the function $H(a, b; n, k)$ is defined as

  $$H(a, b; n, k) = \sum_{p=0}^{2N-1} \mathrm{e}^{-\mathrm{j}\pi p(a-b)/N} \gamma^{\mathrm{C}}((n - b - a)\tfrac{T}{2}, (k - p)\tfrac{1}{2NT}).$$

  Note that the GDTFD does not satisfy this property because it uses the DWVD-A which, as described in Section 2.5.5, does not satisfy the quadratic form property.

- **Real:** The proposed DTFD is real-valued if

  $$G^{\mathrm{C}}(\tfrac{nT}{2}, mT) = \left[G^{\mathrm{C}}(\tfrac{nT}{2}, (2N - m)T)\right]^*.$$

  (I use the notation $[G^{\mathrm{C}}]^*$ to represent the complex conjugate of G^{C}, if indeed G^{C} is complex.)

- **Time–frequency covariance:** A time and frequency shift in the time-domain signal causes the same time and frequency shift in the proposed DTFD. A signal of the form

  $$y(nT) = x((n - n_0)T)\, \mathrm{e}^{\mathrm{j}\pi k_0 n/N}$$

  produces a shift in the DTFD:

  $$\rho_y^{\mathrm{C}}(\tfrac{nT}{2}, \tfrac{k}{2NT}) = \rho_x^{\mathrm{C}}((n - 2n_0)\tfrac{T}{2}, (k - k_0)\tfrac{1}{2NT}).$$

  Note that the proposed definition has nonstandard periodicity in the frequency direction, as we detailed in (4.8). This property, which is a necessary property of the quadratic class [7], is always satisfied.

- **Time marginal:** Summing along the frequency direction of the proposed DTFD yields the instantaneous power of the signal:

  $$2\sum_{k=0}^{N-1} \rho^{\mathrm{C}}(\tfrac{2nT}{2}, \tfrac{k}{2NT}) = \left|z(nT)\right|^2$$

  if

  $$G^{\mathrm{C}}(\tfrac{nT}{2}, 0) = \delta(n).$$

- **Frequency marginal:** Summing along the time direction of the proposed DTFD yields the energy spectrum:

  $$\sum_{n=0}^{2N-1} \rho^{\mathrm{C}}(\tfrac{nT}{2}, \tfrac{k}{2NT}) = \frac{1}{2N}\left|Z(\tfrac{k}{2NT})\right|^2$$

  if

  $$\mathcal{G}^{\mathrm{C}}(\tfrac{0}{NT}, \tfrac{k}{2NT}) = \delta(k).$$

  where $\mathcal{G}^{\mathrm{C}}(l/NT, k/2NT)$ is the Doppler–frequency kernel.

  Note that the GDTFD does not satisfy this property, as

  $$\sum_{n=0}^{2N-1} \rho^{\mathrm{A}}(nT, \tfrac{k}{2NT}) = \frac{1}{4N}\left[\left|Z(\tfrac{k}{2NT})\right|^2 + Z(\tfrac{k+N}{2NT})Z^*(\tfrac{k-N}{2NT})\right].$$

- **Time support:** The time support of $z(nT)$ is reflected in the time–frequency domain; that is, when $z(nT) = 0$ for $n < n_1$ and $n > n_2$, then

  $$\rho^{\mathrm{C}}(\tfrac{nT}{2}, \tfrac{k}{2NT}) = 0, \qquad \text{for } n < 2n_1 \text{ and } n > 2n_2$$

  over the quarter-plane region $n = 0, 1, \ldots, 2N-1$ and $k = 0, 1, \ldots, N-1$, if

  $$G^{\mathrm{C}}(\tfrac{nT}{2}, mT) = 0, \qquad \text{for } |n| > |m|.$$

  Note that the AF-GDTFD does not satisfy this property because it is aliased.

- **Frequency support:** The frequency support of $Z(k/2NT)$ is reflected in the time–frequency domain; that is, when $Z(k/2NT) = 0$ for $k < k_1$ and $k > k_2$, then

  $$\rho^{\mathrm{C}}(\tfrac{nT}{2}, \tfrac{k}{2NT}) = 0, \qquad \text{for } k < k_1 \text{ and } k > k_2$$

  over the quarter-plane region $n = 0, 1, \ldots, 2N-1$ and $k = 0, 1, \ldots, N-1$, if

  $$\mathcal{G}^{\mathrm{C}}(\tfrac{l}{NT}, \tfrac{k}{2NT}) = 0, \qquad \text{for } |k| > |l|.$$

  Note that, again, the AF-GDTFD does not satisfy this property because it is aliased.

- **Instantaneous frequency:** The periodic first moment [41] [66, pp. 463] of the DTFD, with respect to frequency, is equal to the instantaneous frequency $f(nT)$ of the signal:

  $$\frac{1}{4\pi T}\left\{\arg\left[\sum_{k=0}^{N-1}\rho^{\mathrm{C}}\left(\tfrac{2nT}{2},\tfrac{k}{2NT}\right)\mathrm{e}^{\mathrm{j}2\pi k/N}\right] \mod 2\pi\right\} = f(nT)$$

  where instantaneous frequency $f(nT)$, for a signal of the form $z(nT) = A(n)\,\mathrm{e}^{\mathrm{j}\varphi(n)}$, is

  $$f(nT) = \frac{1}{2\pi T}\left[\frac{\varphi(n+1)-\varphi(n-1)}{2} \mod \pi\right].$$

  The property requires that

  $$G^{\mathrm{C}}\left(\tfrac{nT}{2}, 2T\right) = a\delta(n)$$

  where a is a positive constant.

- **Group delay:** The periodic first moment of the DTFD, with respect to time, is equal to the group delay $\tau(k/2NT)$ of the signal:

  $$-\frac{NT}{2\pi}\left\{\arg\left[\sum_{n=0}^{2N-1}\rho^{\mathrm{C}}\left(\tfrac{nT}{2},\tfrac{k}{2NT}\right)\mathrm{e}^{-\mathrm{j}\pi n/N}\right] \mod -2\pi\right\} = \tau\left(\tfrac{k}{2NT}\right)$$

  where the group delay function $\tau(k/2NT)$, for a signal of the form $Z(k/2NT) = a(k)\,\mathrm{e}^{\mathrm{j}\theta(k)}$, is

  $$\tau\left(\tfrac{k}{2NT}\right) = -\frac{NT}{2\pi}\left[\frac{\theta(k+1)-\theta(k-1)}{2} \mod -\pi\right].$$

  The property requires that

  $$\mathcal{G}^{\mathrm{C}}\left(\tfrac{1}{NT},\tfrac{k}{2NT}\right) = a\delta(k)$$

  where a is a positive constant.

  Note that the GDTFD does not satisfy this property, as $\tau(k/2NT)$ equates to

  $$\tau\left(\tfrac{k}{2NT}\right) = -\frac{N}{2\pi}\left\{\arg\left[\; Z\left((k+1)\tfrac{1}{2NT}\right)Z^*\left((k-1)\tfrac{1}{2NT}\right)\right.\right.$$
  $$\left.\left. +\; Z\left((k+1+N)\tfrac{1}{2NT}\right)Z^*\left((k-1-N)\tfrac{1}{2NT}\right)\right] \mod -2\pi\right\}.$$

- **Moyal's formula:** The inner product in the time–frequency domain equates to the magnitude squared of the inner product in the time domain—that is,

  $$4N\sum_{n=0}^{2N-1}\sum_{k=0}^{N-1}\rho_s^{\mathrm{C}}\left(\tfrac{nT}{2},\tfrac{k}{2NT}\right)\rho_y^{\mathrm{C}}\left(\tfrac{nT}{2},\tfrac{k}{2NT}\right) = \left|\sum_{n=0}^{N-1} s(nT)y(nT)\right|^2$$

if

$$\sum_{p=0}^{2N-1} G^{\mathrm{C}}(\tfrac{pT}{2}, mT) G^{*\mathrm{C}}((n-p)\tfrac{T}{2}, mT) = \delta(n).$$

Note that the GDTFD does not satisfy this property, as

$$4N \sum_{n=0}^{N-1} \sum_{k=0}^{N-1} \rho_s^{\mathrm{A}}(nT, \tfrac{k}{2NT}) \rho_y^{\mathrm{A}}(nT, \tfrac{k}{2NT}) \\ = \left| \sum_{n=0}^{N/2-1} s(2nT) y(2nT) \right|^2 + \left| \sum_{n=0}^{N/2-1} s((2n+1)T) y((2n+1)T) \right|^2 .$$

- **Signal recovery:** We can recover the time-domain signal, up to a constant phase, from the DTFD:

$$2 \sum_{k=0}^{N-1} \rho^{\mathrm{C}}(\tfrac{nT}{2}, \tfrac{k}{4NT}) \, \mathrm{e}^{\mathrm{j}\pi kn/N} = z(nT) z^*(0)$$

if $G^{\mathrm{C}}(nT/2, mT) = \delta(n)$ for all values of m.

Note that the GDTFD does not satisfy this property, as

$$2 \sum_{k=0}^{N-1} \rho^{\mathrm{A}}(nT, \tfrac{k}{2NT}) \, \mathrm{e}^{\mathrm{j}\pi kn/N} = z(2nT) z^*(0).$$

Table 4.1 summarises the properties for the three DTFD definitions, assuming that the kernel is appropriately constrained for each property. Neither the GDTFD nor the AF-GDTFD satisfy all properties. Note that the DWVD associated with the AF-GDTFD only exists when the signal length is odd [29], which never happens as $z(nT)$ is length $2N$. The proposed definition, however, satisfies all properties and contains a DWVD definition.

Recall that the DWVD-A does not satisfy all properties whereas the DWVD-C does satisfy all properties, as we saw in Table 4.1. Likewise, the proposed definition, which uses the DWVD-C, satisfies all properties, and the GDTFD, which uses the DWVD-A, does not satisfy all properties. Also, the AF-GDTFD, which uses the DWVD-B, does not satisfy the time- or frequency-support properties because the DWVD-B in (4.4) is defined over the full plane region $0 \leq nT \leq 2NT$ and $|f| \leq 1/(2T)$, whereas the DWVD-B in Chapter 2 is defined over the smaller quarter plane region $0 \leq t \leq NT$ and $0 \leq f \leq 1/(2T)$. The full plane region DWVD-B is aliased and will not, therefore, satisfy the time- or frequency-support properties.

4.3.2 Relation to the GDTFD and AF-GDTFD

The GDTFD is a time-decimated version of the proposed definition,

$$\rho^{\mathrm{C}}(\tfrac{2nT}{2}, \tfrac{k}{2NT}) = \rho^{\mathrm{A}}(nT, \tfrac{k}{2NT}). \tag{4.12}$$

I obtain this results by substituting $\gamma^{\mathrm{A}}(nT, k/2NT) = \gamma^{\mathrm{C}}(nT, k/2NT) + \gamma^{\mathrm{C}}(nT, (k+N)/2NT)$ into (4.9) and comparing with the definition of the GDTFD in (4.2). The

Table 4.1: Discrete properties satisfied by the three DTFD definitions.

properties[1]	GDTFD	AF-GDTFD	proposed
quadratic form		✓	✓
real	✓	✓	✓
time–frequency covariance	✓	✓	✓
time marginal	✓	✓	✓
frequency marginal		✓	✓
time support	✓		✓
frequency support	✓		✓
instantaneous frequency	✓	✓	✓
group delay		✓	✓
Moyal's formula		✓	✓
signal recovery		✓	✓

[1] assuming that the kernel satisfies the appropriate constraint.

kernel $\gamma^{\mathrm{A}}(nT, k/2NT)$ equals a folded, in frequency, version of $\gamma^{\mathrm{C}}(nT, k/2NT)$ because the kernel $G^{\mathrm{A}}(nT, 2mT)$ is a decimated, in lag, version of the kernel $G^{\mathrm{C}}(nT, mT)$.

The proposed DTFD definition is, however, considerably different to the AF-GDTFD because of the following reasons.

- The Doppler–lag region of the AF-GDTFD's kernel is larger than the region of the proposed DTFD's kernel. The AF-GDTFD's kernel extends over the region $|\nu| \leq 1/T$ and $|m| \leq 2NT$ whereas the proposed definition's kernel extends over the smaller region $|\nu| \leq 1/(2T)$ and $|m| \leq NT$.
- The time–lag kernels have different discrete grids: the AF-GDTFD's kernel has a nonuniform discrete grid, illustrated in Fig. 4.2b whereas the DTFD-C's kernel has a uniform discrete gird, illustrated in Fig. 4.3b.
- The AF-GDTFD is a full-plane distribution, periodic over the time–frequency region $0 \leq t \leq 2NT$ and $|f| \leq 1/(2T)$, whereas the proposed DTFD is a quarter-plane distribution, periodic over the smaller region $0 \leq t \leq NT$ and $0 \leq f \leq 1/(2T)$.

4.3.3 Examples

I present two examples to illustrate the difference between the AF-GDTFD and the proposed definition—specifically to show that AF-GDTFD may be aliased whereas the proposed definition is a pseudo-alias–free definition. I do not show the GDTFD here because the GDTFD is a time-decimated version of the proposed definition. Each distribution uses three different Doppler–lag kernel types: a lag-independent kernel, which uses a Hamming window; a Doppler-independent kernel, which uses a Hanning window; and a separable kernel, which combines the Hamming and Hanning windows [8].

I use two test signals, a linear frequency modulated (LFM) signal $x_1(nT)$ and a sinusoidal signal with Gaussian amplitude modulation $x_2(nT)$:

$$\begin{aligned} x_1(nT) &= \cos\left(2\pi(0.1n + 0.3n^2/128)\right) \\ x_2(nT) &= \mathrm{e}^{-(n-32)^2/25}\cos\left(\pi n/3\right) \end{aligned}$$

for $n = 0, 1, \ldots, N-1$, where $N = 64$ and $T = 1$. The DTFDs for $x_1(nT)$, using the three different kernel types, are plotted in Fig. 4.4; likewise, the DTFDs for $x_2(nT)$ are plotted in Fig. 4.5. I transformed the real-valued signals $x_1(nT)$ and $x_2(nT)$ into the $2N$-point complex-valued signals using the proposed method from the previous chapter. Both signal types produce the same following results.

In a full-plane distribution, such as the AF-GDTFD, the signal energy should be contained within the bottom right-hand corner quadrant $0 \leq t \leq NT$ and $0 \leq f \leq 1/(2T)$ because of the zero regions of the analytic signal in (2.38). As the plots show, this is not so; although, depending on the kernel structure these aliased components may be suppressed—for example, when the AF-GDTFD uses the separable kernel the aliasing energy is suppressed. The proposed definition, however, remains alias-free for all kernel types. I provide an analysis, in Appendix E, which explains why and when the AF-GDTFD is aliased.

4.4 Discussion

The proposed definition, and the GDTFD, are pseudo-alias–free definitions; the AF-GDTFD, however, may be aliased. Recall how we define the term *pseudo-alias free* in the introduction: I ignore aliasing from the non-ideal discrete analytic signal and aliasing from the circular convolution operations. As the examples in Section 4.3.3 show, the aliasing in the AF-GDTFD, which is caused by periodic overlap in the underlying DWVD in (4.6), is significant compared with the other two sources of aliasing.

This AF-GDTFD, in this chapter, uses the analytic signal to provide a more equal comparison with the proposed definition, although the authors never specified that the analytic signal was necessary [36, 29]. If we use the real-valued signal with the AF-GDTFD, then the periodic overlap occurs over the quarter-plane region, and the aliased components are within the region of the signal components—I show this aliasing for the two test signals in Fig. 4.6. Thus, using the real-valued signal may distort the signal components in the DTFD to a greater extent compared with the distortion from aliasing when we use the analytic signal. Yet using the real-valued N-point signals results in a $N \times N$ AF-GDTFD, whereas using the analytic signals results in a $2N \times 2N$ AG-GDTFD. Hence there is a computational advantage to using the AF-GDTFD with the N-point signal.

We now examine the merits of the proposed definition comparative to the existing definitions. The advantage of the proposed definition, over the GDTFD, is that the proposed definition satisfies all important properties. The disadvantage is that the proposed definition contains $2N \times N$ sample points whereas the GDTFD contains $N \times N$ sample points; thus, the proposed definition requires twice the computational load compared with that for the GDTFD [52].

The proposed definition also has some advantages over the AF-GDTFD:

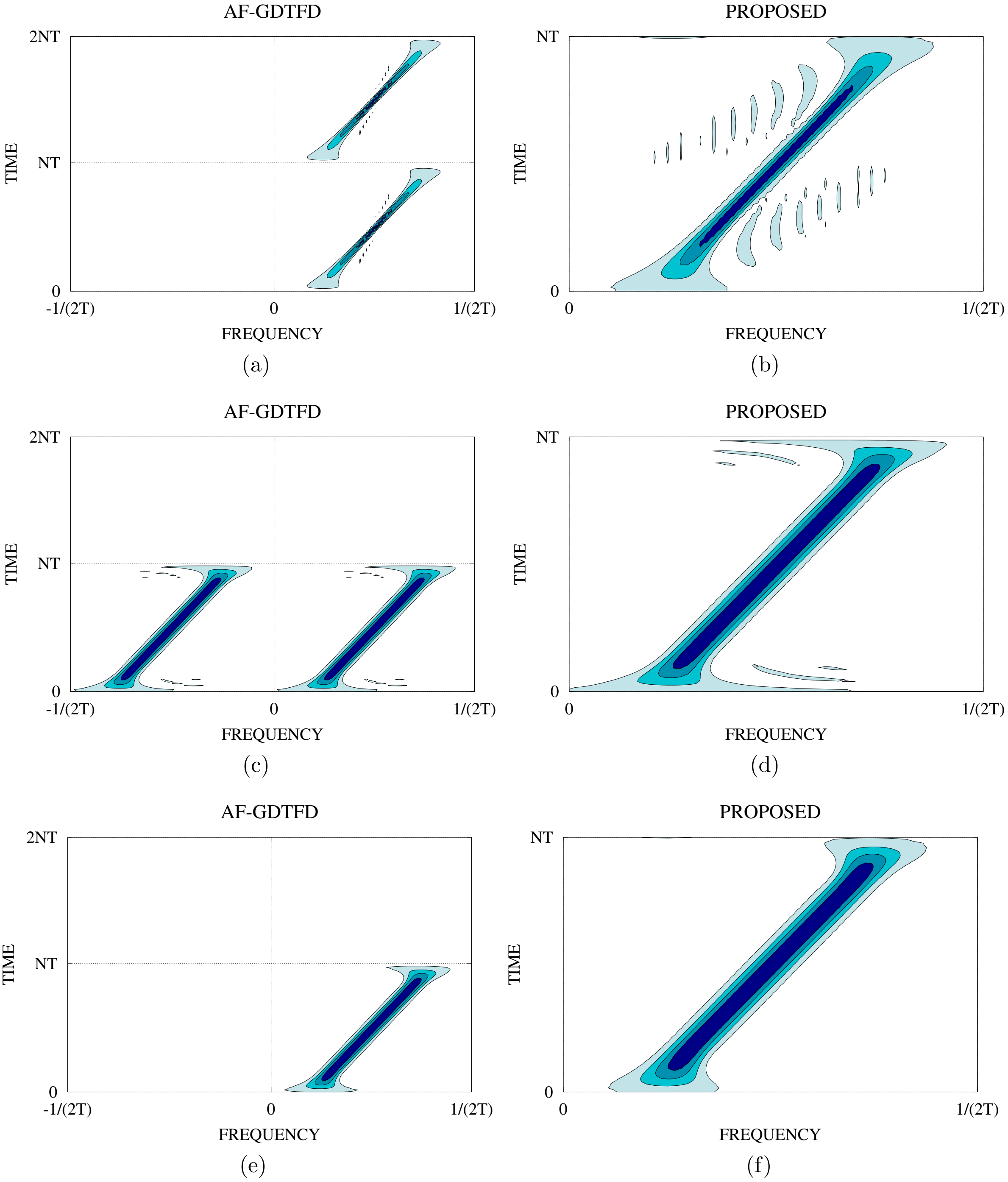

Figure 4.4: Comparison of AF-GDTFD and proposed DTFD definition of a LFM signal $x_1(nT)$: left-hand side column is AF-GDTFD with (a) lag-independent kernel, (c) Doppler-independent kernel, and (e) separable kernel; right-hand side column is proposed definition with (b) lag-independent kernel, (d) Doppler-independent kernel, and (f) separable kernel. In the AF-GDTFD, any energy outside the bottom right quadrant is caused by aliasing.

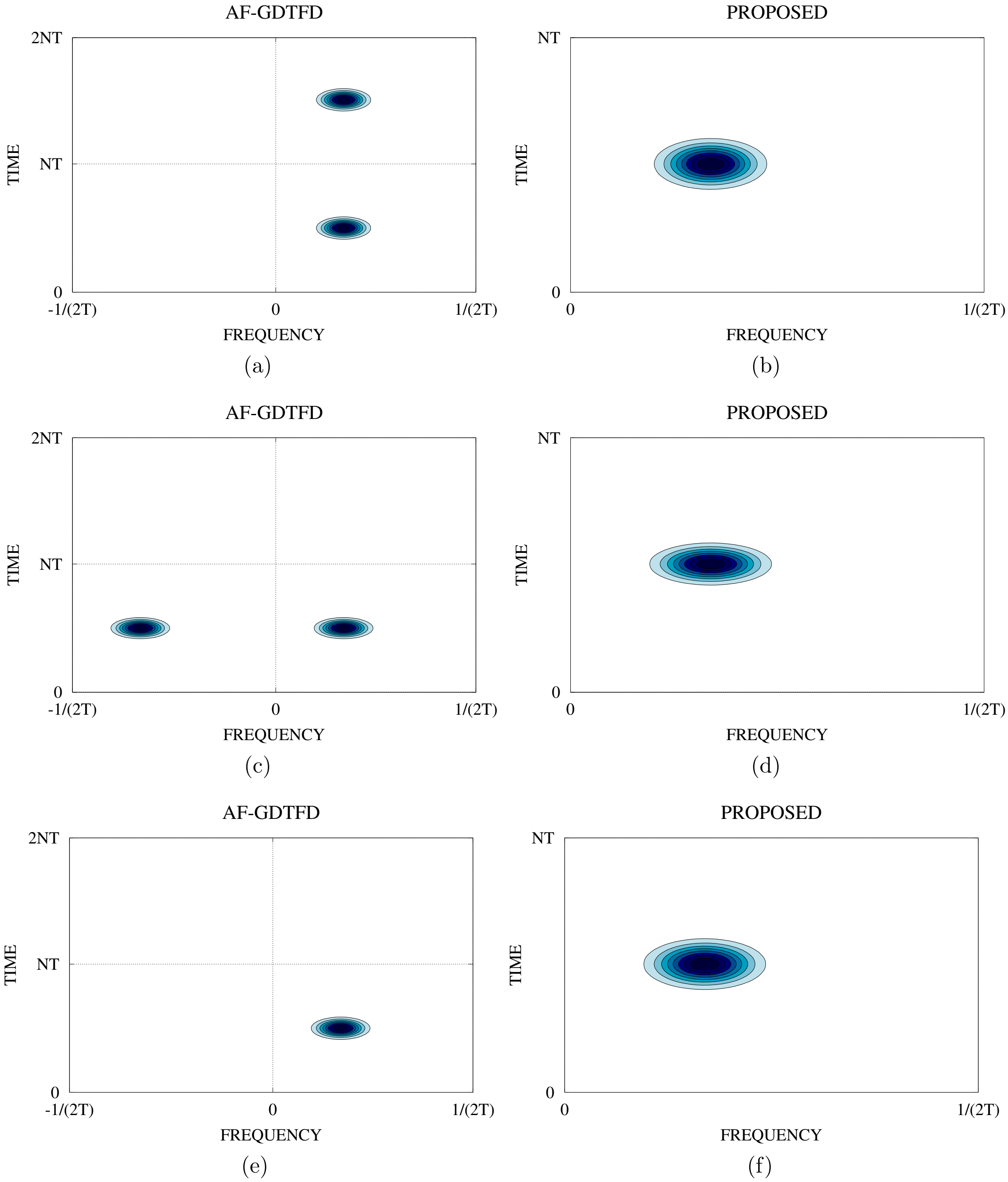

(a) (b)

(c) (d)

(e) (f)

FIGURE 4.5: Comparison of AF-GDTFD and proposed DTFD definition of a Gaussian modulated sinusoidal signal $x_2(nT)$: left-hand side column is AF-GDTFD with (a) lag-independent kernel, (c) Doppler-independent kernel, and (e) separable kernel; right-hand side column is proposed definition with (b) lag-independent kernel, (d) Doppler-independent kernel, and (f) separable kernel. For the AF-GDTFD, any energy outside the bottom right quadrant is caused by aliasing.

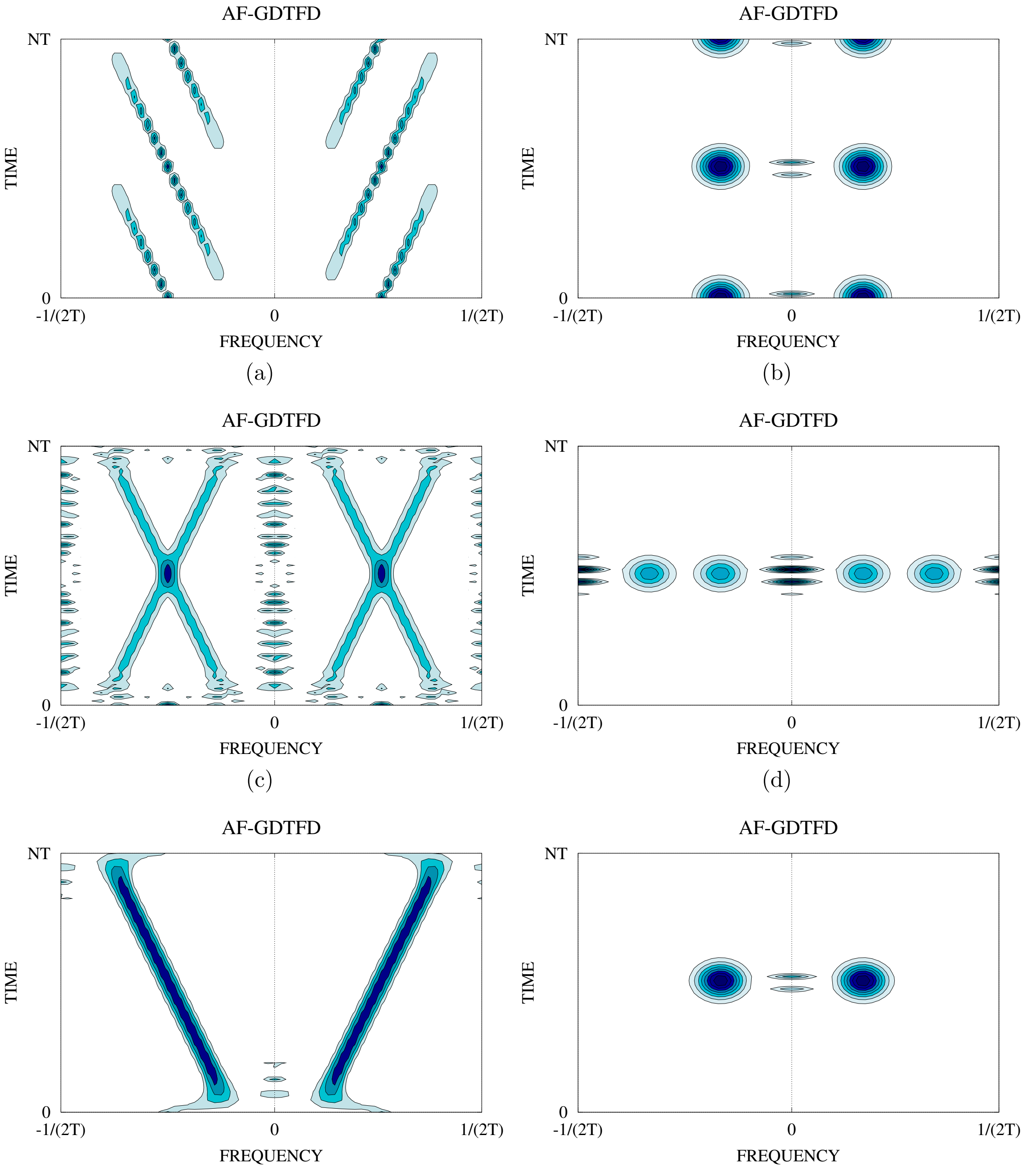

(a) (b) (c) (d) (e) (f)

Figure 4.6: AF-GDTFD using a real-valued signal: left-hand side column is the LFM signal $x_1(nT)$ with (a) lag-independent kernel, (c) Doppler-independent kernel, and (e) separable kernel; right-hand side column is the Gaussian modulated signal $x_2(nT)$ with (b) lag-independent kernel, (d) Doppler-independent kernel, and (f) separable kernel.

- the proposed definition is always pseudo-alias free, regardless of kernel structure;
- the AF-GDTFD contains a DWVD only when the signal length is odd. Thus, because the signal length $2N$ is always even, the AF-GDTFD does not contain a DWVD, although the authors in [29] proposed an approximation to the DWVD. This *pseudo*-DWVD does not satisfy important DWVD properties such as Moyal's formula and signal recovery [29]. The proposed definition, in contrast, contains a DWVD which satisfies these properties, regardless of signal-length parity;
- the proposed definition satisfies the time- and frequency-support properties;
- the AF-GDTFD contains $2N \times 2N$ sample points and thus requires approximately twice the computational load compared with that for the proposed definition, which contains only $2N \times N$ sample points.
- the proposed definition has a direct relation with the continuous WVD—it (approximately) equals a WVD convolved with a kernel.

A disadvantage to the proposed definition, comparative to the AF-GDTFD, is that it does not contain a spectrogram. Although the spectrogram is a member of the (continuous) quadratic TFD class, we would always implement the spectrogram in its original form, as this is the most computational efficient approach [26]. Note that the proposed definition can produce a nonnegative distribution which closely approximates the spectrogram [50]. Also, the proposed definition analyses real-valued signals only; the AF-GDTFD, however, may analyse complex-valued, non-analytic signals. As all measurable real-world signals are real valued we do not consider this a significant limitation.

4.5 Summary and Conclusions

This chapter presented a new discrete definition of the quadratic TFD class. The chapter also reviewed the GDTFD and AF-GDTFD to show their limitations and justify the need for a new definition.

The proposed definition is, comparative to the GDTFD or AF-GDTFD, closer to the ideal DTFD—it satisfies all desirable properties and is (approximately) equal to samples of the continuous WVD convolved with a time–frequency kernel. Neither the GDTFD nor the AF-GDTFD satisfy all desirable properties and only the GDTFD approximates samples of the continuous WVD convolved with a kernel. Also, the proposed definition—unlike either the GDTFD or AF-GDTFD—contains a DWVD definition that satisfies important DWVD properties such as Moyal's formula and signal recovery. The proposed definition, like the existing definitions, may be computed on a computer by a simple and efficient algorithm; the next chapter presents this algorithm.

The proposed DTFD definition should, therefore, appeal to the signal analyst: it reduces, comparative to the GDTFD and AF-GDTFD, the error in going from the design stage in the continuous domain to the implementation stage in the discrete domain.

Chapter 5

Efficient Algorithms for Discrete Time–Frequency Distributions

5.1 Introduction

Computing a DTFD is a large computational task that requires a large amount of computer memory. For example, the DFT algorithm, known as the fast Fourier transform (FFT), requires typically $\mathcal{O}(N \log_2 N)$ multiplications and additions and N sample points of memory to compute for an N-point signal [38], whereas DTFD algorithms typically require $\mathcal{O}(N^2 \log_2 N)$ multiplications and additions and N^2 sample points of memory [34]. To compound this computational problem, the proposed DTFD, from the preceding chapter, requires twice as many sample points as an existing popular DTFD definition: the GDTFD has N^2 sample points whereas the proposed DTFD has $2N^2$ sample points. This chapter presents algorithms that *aim to minimise the computational time and memory* required to compute the proposed DTFD.

The first efficient DTFD algorithms were for the DWVD, or more specifically the DWVD-A [41, 71] and a frequency-decimation version of the DWVD-A [33, 72, 73]. Later came algorithms for the general quadratic DTFD class, including algorithms for the GDTFD [34] and the AF-GDTFD [74]. Other DTFD algorithms include approximations to the DTFD, most notably the *sum-of-spectrograms* approach [53, 54]. The sum-of-spectrograms approach constructs the AF-GDTFD from a weighted sum of spectrograms, and depending on the accuracy required, the computational load can be reduced by approximating the DTFD by a limited number of spectrograms. Similarly, the Zak transform can also produce a band limited version of the DTFD approximation [75].

This chapter presents algorithms for computing the proposed DTFD. These algorithms aim to minimise the computational load and the amount of memory required to compute the proposed DTFD. I define the computational load as the total number of real-valued multiplications and additions that the algorithm requires; I define the memory requirement as the number of real-valued numbers, for each sample point, that the algorithm requires to compute and store the DTFD. Reducing the computational load of an algorithm reduces the time taken for the algorithm to compute. For example, if an algorithm with a computational load of N takes 1 minute to compute, then the same algorithm with a larger computational load of N^2 will take 1 hour to compute. Algorithms also require computer memory to compute and store the DTFD, which is limited by the fixed size of the computer's memory. This may become an issue for DTFDs, which require typically N^2 sample points, because if the memory is not large enough to store N^2 sample points, then the algorithm will not compute. For example, the FFT of a signal of length $N = 16,000$ requires N sample points of memory which equals 65 kilobytes of computer memory, assuming that 4 bytes stores one sample point; a DTFD algorithm that requires N^2 sample points, however, uses 1 gigabyte of computer memory.

I present two approaches for the proposed algorithms. The first approach, computes the proposed DTFD exactly. The aim is to reduce computational load and memory by using kernel specific algorithms. I group the kernels into four different categories—namely, nonseparable, separable, Doppler–independent, and lag–independent kernels—and design an algorithm for each kernel type. The second approach efficiently computes a decimated DTFD. The decimated DTFD requires less memory than the original, non-decimated DTFD. Nonetheless, as the decimated DTFD does not represent the full DTFD, the decimated DTFD may not contain all the signal information.

The algorithms of the first approach compute the exact DTFD efficiently: some DTFD kernel types require significantly less computational load and memory than other kernel types. Also, for all kernel types except the nonseparable-kernel DTFD, the size of the DTFD may be reduced. For example, the nonseparable-kernel DTFD requires $N_{\mathrm{t}} N_{\mathrm{f}}$ sample points, where $N_{\mathrm{t}} \leq 2N$ and $N_{\mathrm{f}} \leq N$; the two values N_{f} and N_{t} depend on the parameters of the kernel. The second set of algorithms compute the decimated DTFD efficiently by using kernel-specific algorithms to minimise the computational load.

The layout of this chapter is as follows. Section 5.2 presents a review of existing DWVD and DTFD algorithms; more specifically, algorithms for the DWVD-A and the GDTFD. These algorithms form the basis for the proposed algorithms. Section 5.3 presents the first set of algorithms that compute the kernel-specific DTFDs. Section 5.4 presents the second set of algorithms that compute the kernel-specific decimated DTFDs.

5.2 Review

Here we look at some of the existing efficient algorithms for computing the DWVD-A and GDTFD [71,34]. To simply notation, I drop the sampling information in the discrete functions and use sequence notation wherever possible. For example, I use the notation $W^{\mathrm{A}}[n,k]$ to represent $W^{\mathrm{A}}(nT/2, k/2NT)$. Sequence notation often appears in digital signal processing literature [23,38,76,24].

5.2.1 DWVD-A Algorithms

We can compute the DWVD-A by first forming the time–lag function K^{A} from the discrete signal $z[n]$ as

$$K^{\mathrm{A}}[n,m] = z[n+m]z^*[n-m] \tag{5.1}$$

for $n, m = 0, 1, \ldots, N-1$ and then take the DFT of the K^{A}; that is,

$$W^{\mathrm{A}}[n,k] = \underset{m \to k}{\mathrm{DFT}} \left(K^{\mathrm{A}}[n,m] \right) \tag{5.2}$$

where the DFT$\{\cdot\}$ function, with $m \to k$, represents the DFT from the lag domain m to the frequency domain k. Fig. 5.1 illustrates this simple algorithm. Recall that $z[n]$ is

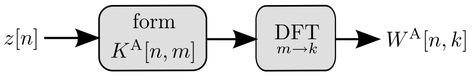

FIGURE 5.1: DWVD-A algorithm.

the discrete analytic signal of the form, $z[n] = 0$ for $N \leq n \leq 2N-1$. We can use the use the fast Fourier transform (FFT) algorithm to implement the DFT operation in the preceding equation [38]. Thus, computing (5.2) requires N FFT$-N$ operations, using the notation FFT$-N$ to represent one FFT operation on a signal of length-N.

Boashash and Black [71] proposed an algorithm, initially suggested by Claasen and Mecklenbräuker [41], for the DWVD-A that requires only $N/2$ FFT$-N$ operations. To do so, the algorithm uses one FFT operation to simultaneously compute two DFTs for two different values of n, which is possible because the DWVD is a real-valued function. The algorithm works as follows. Let

$$K^{\mathrm{A}}_{\text{combined}}[n',m] = K^{\mathrm{A}}[n_1,m] + \mathrm{j}K^{\mathrm{A}}[n_2,m] \tag{5.3}$$

where n_1 and n_2 are two successive values in the sequence $0,1,\ldots,N-1$. The DFT of $K^{\mathrm{A}}_{\text{combined}}[n,m]$ yields both the DFT of $K^{\mathrm{A}}[n_1,m]$ and $K^{\mathrm{A}}[n_2,m]$ as

$$\begin{aligned}\underset{m\to k}{\mathrm{DFT}}\left(K^{\mathrm{A}}[n_1,m]\right) &= \Re\left\{\underset{m\to k}{\mathrm{DFT}}\left(K^{\mathrm{A}}_{\text{combined}}[n',m]\right)\right\}\\ \underset{m\to k}{\mathrm{DFT}}\left(K^{\mathrm{A}}[n_2,m]\right) &= \Im\left\{\underset{m\to k}{\mathrm{DFT}}\left(K^{\mathrm{A}}_{\text{combined}}[n',m]\right)\right\}.\end{aligned}$$

Thus, we may recover the values for $W^{\mathrm{A}}[n_1,k]$ and $W^{\mathrm{A}}[n_2,k]$ from the one FFT operation on $K^{\mathrm{A}}_{\text{combined}}[n,m]$. Iterating this process on all values of n' results in an algorithm that requires only $N/2$ FFT$-N$ operations.

The FFT operation on $K^{\mathrm{A}}_{\text{combined}}$ requires a complex-valued FFT algorithm. An alternative to the Boashash–Black algorithm is to use an inverse real-valued FFT algorithm for each time value of n to implement the N length-N DFT operations in (5.2). The inverse real-valued FFT algorithm requires just less than half of the computational load of the complex-valued FFT algorithm [77]. Thus, using this FFT algorithm has a slight advantage over the Boashash–Black method as it does not require the overhead in (5.3). The disadvantage to using the inverse real-valued FFT algorithm is that the algorithm is not, to date, available in the many hardware-optimised FFT libraries used by popular signal processing software packages such as Matlab and Octave [78].

I proposed an alternative to these two methods that uses a forward real-valued FFT algorithm [43]. The advantage of the method, over the two preceding methods, is that it requires slightly less computational load than the Boashash–Black method and the forward real-valued FFT algorithm is available in the Matlab and Octave packages. The method does, however, require slightly more overhead than the inverse real-valued FFT method.

This new method exploits the fact that the DFT of a real and even function is a real-valued function and the DFT of a real and odd function is an imaginary-valued function. Thus, we let

$$u[n,m] = \Re\Big(K^{\mathrm{A}}[n,m]\Big) + \Im\Big(K^{\mathrm{A}}[n,m]\Big) \tag{5.4}$$

where the real part of K^{A} is an even function in m and imaginary part of K^{A} is an odd function in m because K^{A} is conjugate symmetrical in m [41]. Thus, we retrieve the DWVD from

$$W^{\mathrm{A}}[n,k] = \Re\big(U[n,k]\big) - \Im\big(U[n,k]\big) \tag{5.5}$$

where

$$U[n,k] = \underset{m\to k}{\mathrm{DFT}}\left(u[n,k]\right).$$

We implement this DFT operation with the real-valued FFT algorithm as $u[n,m]$ is real valued. Although (5.4) and (5.5) require some additional overhead, this method has slightly less computational load than the Boashash–Black method because the real-valued FFT algorithm requires slightly less than half of the computational load compared with the load for the complex-valued FFT algorithm [43].

Other DWVD algorithms include those proposed by Martin and Flandrin [33], Sun *et al.* [72], and Chan [73], all of which compute a frequency-decimated version of the DWVD-A, $W^{\mathrm{A}}[n,2k]$. Chan's method simply folds the time–lag function $K^{\mathrm{A}}[n,m]$ in the lag direction to produce the frequency-decimated DWVD [73]. I shall use this concept in the decimated-DTFD algorithms in Section 5.4.

5.2.2 GDTFD Algorithm

Boashash and Reilly proposed an algorithm to efficiently compute the GDTFD [34]. The algorithm exploits the Hermitian property of the K^{A} function. (A Hermitian signal is conjugate symmetrical.) As we saw in (4.2), we form the GDTFD by convolving the DWVD-A with the time–frequency kernel γ^{A}:

$$\rho^{\mathrm{A}}[n,k] = W^{\mathrm{A}}[n,k] \underset{n}{\circledast} \underset{k}{\circledast} \gamma^{\mathrm{A}}[n,k].$$

The algorithm, outlined in Fig. 5.2, uses DFTs to implement the convolution operations as follows:

1. Generate the time–lag function $K^{\mathrm{A}}[n,m]$ from $z[n]$ using (5.1).
2. Obtain the smoothed time–lag function R^{A} as follows:

   $$R^{\mathrm{A}}[n,m] = \underset{l\to n}{\mathrm{IDFT}}\left\{\underset{n\to l}{\mathrm{DFT}}\left(K^{\mathrm{A}}[n,m]\right) g^{\mathrm{A}}[l,m]\right\}, \qquad 0 \le m \le N/2$$

   Because R^{A}, like K^{A}, is Hermitian in the lag direction m, we need only compute the preceding equation for $m = 0, 1, \ldots, N/2$, the positive lag values, rather than the full lag support which consists of positive and negative lag values. This halves the number of FFT operations required.

3. Recover the negative lag values from the positive lag values for the smoothed time–lag function R^{A} from the relation,

   $$R^{\mathrm{A}}[n,m] = \left(R^{\mathrm{A}}[n,N-m]\right)^{*}, \qquad N/2+1 \le m \le N-1.$$

   The function $R^{\mathrm{A}}[n,m]$ is periodic in the lag m direction in N, thus the lag values $N/2+1 \le m \le N-1$ represent the negative values. The operator $(a)^{*}$ represents the complex conjugate operation of a.

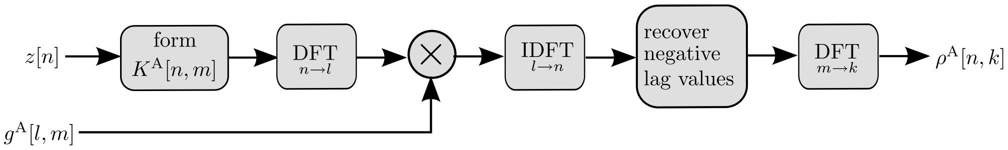

FIGURE 5.2: GDTFD algorithm.

4. DFT to the time–frequency domain:

$$\rho^{\mathrm{A}}[n,k] = \underset{m\to k}{\mathrm{DFT}}\left(R^{\mathrm{A}}[n,m]\right)$$

   using the Boashash–Black method, which we examined in the previous section, by substituting R^{A} for K^{A}.

The method requires $3N/2$ FFT$-N$ operations to compute the $N \times N$ GDTFD. The following proposed algorithms use this GDTFD algorithm as a basis—the algorithms implement the convolution by a multiplication in the Doppler–lag domain and compute only one-half, in the lag direction, of the smoothed time–lag function. The nonuniform time–lag discrete grid for the proposed DTFD, however, complicates the following algorithms somewhat.

5.3 Proposed DTFD Algorithms

The purpose of the following algorithms is to minimise the computational load and memory required to compute the proposed DTFD. I achieve this by exploiting the Hermitian property of the time–lag functions and specifying kernel-specific algorithms for different kernel types.

The following algorithms use two different forms of the discrete time–lag functions K^{C} and R^{C} because the nonuniform sample grid, represented in Fig. 5.3(a), is not a suitable form for storage in an array—the time samples n in $K^{\mathrm{C}}((n/2)T, mT)$ are not integer values. We have two options: either we shift the sample points at $K^{\mathrm{C}}((n+1/2)T, 2(m+1/2)T)$, highlighted as the grey points in Fig. 5.3a, across in the lag direction by T or we shift these sample points down in the time direction by $T/2$. We call the time-shifted function the *shifted-down* array $K_{\mathrm{d}}^{\mathrm{C}}[n,m]$ and the lag-shifted function the *shifted-across* array $K_{\mathrm{a}}^{\mathrm{C}}[n,m]$—Fig. 5.3 illustrates this process. Note that both arrays contain the same sample points but are ordered differently.

5.3.1 DWVD-C Algorithm

The DWVD, as we saw Chapter 2, is an important member of the DTFD class. For this reason, and because the proposed DTFD algorithm is based on the DWVD-C algorithm, I first present a computationally efficient DWVD-C algorithm [43].

The DWVD-C algorithm is similar to the DWVD-A algorithm: we first form the discrete time–lag function, this time the $2N \times N$ shifted-across array $K_{\mathrm{a}}^{\mathrm{C}}[n,m]$, and then DFT this function to obtain the DWVD. A problem arises, however, for $2n+1$ values, as the DFT of $K_{\mathrm{a}}^{\mathrm{C}}[2n+1,m]$ results in a complex valued DWVD—because $K_{\mathrm{a}}^{\mathrm{C}}[2n+1,m] \neq$

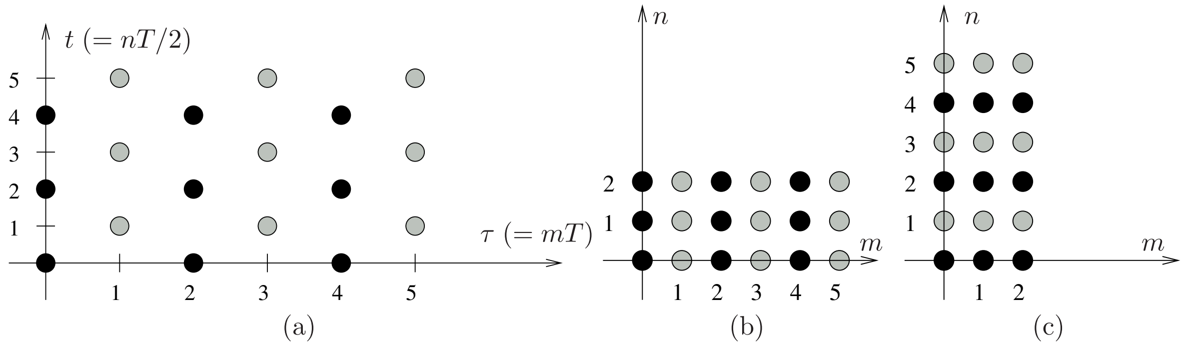

FIGURE 5.3: Two ways to store the time–lag function $K^{\mathrm{C}}(nT/2, mT)$ as an array. (a) $K^{\mathrm{C}}(nT/2, mT)$, (b) the shifted-down array $K^{\mathrm{C}}_{\mathrm{d}}[n,m]$, and (c) the shifted-across array $K^{\mathrm{C}}_{\mathrm{a}}[n,m]$. The grey circles in (a) represent the sample points shifted either *down* in (b) or *across* in (c).

$\Big(K^{\mathrm{C}}_{\mathrm{a}}[2n+1, N-m]\Big)^*$. The output of the DFT is modulated to ensure a real-valued DWVD [27]:

$$W^{\mathrm{C}}[2n+1,k] = \mathrm{e}^{-\mathrm{j}\pi k/N} \underset{m\to k}{\mathrm{DFT}} \Big(K^{\mathrm{C}}_{\mathrm{a}}[2n+1,m]\Big) \tag{5.6}$$

unlike for $2n$, which is similar to (5.2) as

$$W^{\mathrm{C}}[2n,k] = \underset{m\to k}{\mathrm{DFT}} \Big(K^{\mathrm{C}}_{\mathrm{a}}[2n,m]\Big).$$

Thus, we cannot use the methods in Section 5.2.1 because the DFT in (5.6) produces a complex-valued output.

To implement (5.6) efficiently, we can do the following: rewrite (5.6) as

$$W^{\mathrm{C}}[2n+1,k] = \left[\frac{\cos^2(\pi k/N)}{\sin(\pi k/N)} + \sin(\pi k/N)\right] \Im\Big\{\underset{m\to k}{\mathrm{DFT}} \Big(K^{\mathrm{C}}_{\mathrm{a}}[2n+1,m]\Big)\Big\} \tag{5.7}$$

for $k = 1, \ldots, N-1$. Next, define the array $\hat{K}^{\mathrm{C}}_{\mathrm{a}}[n,m]$ so that

$$\underset{m\to k}{\mathrm{DFT}} \Big(\hat{K}^{\mathrm{C}}_{\mathrm{a}}[n,m]\Big) = \Im\Big\{\underset{m\to k}{\mathrm{DFT}} \Big(K^{\mathrm{C}}_{\mathrm{a}}[n,m]\Big)\Big\} \tag{5.8}$$

Thus, because the DFT of $\hat{K}^{\mathrm{C}}_{\mathrm{a}}[n,m]$ is real valued, we can reduce the computational load using the methods discussed in Section 5.2.1.

Note that when $k = 0$, (5.7) is undefined. For this special case, we simply sum along the lag values:

$$W^{\mathrm{C}}[2n+1,0] = \sum_{m=0}^{N-1} K^{\mathrm{C}}_{\mathrm{a}}[2n+1,m].$$

Fig. 5.4 outlines the algorithm, and the following details the complete method.

ALGORITHM-1: DWVD-C

- INPUT: $2N$-point analytic signal $z[n]$

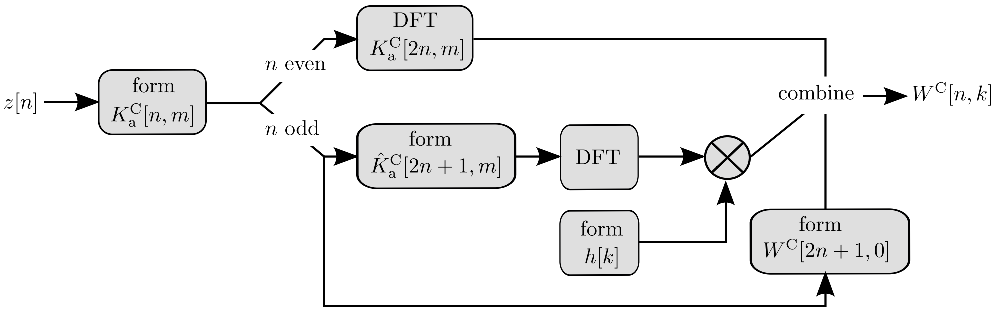

FIGURE 5.4: DWVD-C algorithm.

- OUTPUT: $2N \times N$ DWVD $W^C[n,k]$.

1. Let $N_h = \lceil N/2 \rceil$ and form the time–lag array $K_a^C[n,m]$ from the signal $z[n]$ using the relation in (2.29),

$$K_a^C[2n,m] = z[n+m]z^*[n-m]$$
$$K_a^C[2n+1,m] = z[n+m+1]z^*[n-m]$$

for $n = 0,1,\dots,N-1$ and $m = 0,1,\dots,N_h$. The array $K_a^C[n,m]$ is the shifted-down version of the function $K^C(nT/2,mT)$, as illustrated in Fig. 5.3(c). Next, recover the negative lag values from the positive ones:

$$K_a^C[2n,N-m] = \Big(K_a^C[2n,m]\Big)^*, \qquad m = 1,2,\dots,N_h-1,$$
$$K_a^C[2n+1,N-m-1] = \Big(K_a^C[2n+1,m+1]\Big)^*, \qquad m = 0,1,\dots,N_h-1,$$

over all $n = 0,1,\dots,N-1$.

2. Transform to the time–frequency domain for even–odd values of n :

   (a) For n even, we get

$$W^C[2n,k] = \underset{m\to k}{\mathrm{DFT}}\Big(K_a^C[2n,m]\Big)$$

   (b) (To make this segment more general so that other algorithms in this chapter can refer to it, I use the variable N_f to represent number of discrete-frequency sample points k; that is, $k = 0,1,\dots,N_f-1$. For the DWVD-C, $N_f = N$.) For n odd, we do the following

      i. Let

$$h[k] = \begin{cases} \sin(\pi k/N_f) + \cos^2(\pi k/N_f)/\sin(\pi k/N_f), & 1 \le k \le N_f-1, \\ 0, & k = 0. \end{cases}$$

      ii. Form the function $\hat{K}_a^C$ so that it satisfies (5.8),

$$\hat{K}_a^C[2n+1,0] = \Im\Big(K_a^C[2n+1,0]\Big),$$
$$\hat{K}_a^C[2n+1,m] = \frac{1}{2\mathrm{j}}\left\{K_a^C[2n+1,m] - \Big(K_a^C[2n+1,N_f-m]\Big)^*\right\},$$
$$1 \le m \le N_{fh}$$

where $N_{\mathrm{fh}} = \lceil N_{\mathrm{f}}/2 \rceil$.

iii. Recover the negative lag values from the positive ones:

$$\hat{K}_{\mathrm{a}}^{\mathrm{C}}[2n+1,m] = \left(\hat{K}_{\mathrm{a}}^{\mathrm{C}}[2n+1,N_{\mathrm{f}}-m]\right)^*, \quad N_{\mathrm{fh}}+1 \leq m \leq N_{\mathrm{f}}-1.$$

iv. DFT to the time–frequency domain and multiply by constant $h[k]$

$$W^{\mathrm{C}}[2n+1,k] = \underset{m\to k}{\mathrm{DFT}}\left(\hat{K}_{\mathrm{a}}^{\mathrm{C}}[2n+1,m]\right) h[k].$$

v. Do for frequency sample $k=0$:

$$W^{\mathrm{C}}[2n+1,0] = \sum_{m=0}^{N_{\mathrm{f}}-1} K_{\mathrm{a}}^{\mathrm{C}}[2n+1,m]$$

The algorithm requires $2N$ FFT$-N$ operations to compute the $2N \times N$ DWVD-C. Because these FFT operations results in a real-valued output, we can use one of the methods from Section 5.2.1 to implement this FFT which results in a halving of the computational load. Thus, this algorithm requires only N FFT$-N$ operations. We shall assume that all the following algorithms do the same: N FFT$-N$ operations to compute $2N$ FFT$-N$ that produce a real-valued output.

5.3.2 Kernel-Specific DTFD Algorithms

To minimise the computational load when computing the proposed DTFD, I present four different algorithms for four different Doppler–lag kernel $g^{\mathrm{C}}[l,m]$ types [79], namely

- the nonseparable kernel, $g^{\mathrm{C}}[l,m] = g^{\mathrm{C}}[l,m]$;
- the separable kernel, $g^{\mathrm{C}}[l,m] = G_1[l]g_2[m]$;
- the lag–independent (LI) kernel, $g^{\mathrm{C}}[l,m] = G_1[l]$;
- the Doppler–independent (DI) kernel, $g^{\mathrm{C}}[l,m] = g_2[m]$.

The nonseparable kernel type is the most general form of the kernel, as any kernel can be represented in this form. The algorithm for the nonseparable-kernel DTFD, however, requires a greater computational load than that for the other three kernel types. We can thus reduce the computational load for the separable-, LI-, or DI-kernel DTFD compared with the load for the nonseparable-kernel DTFD.

ALGORITHM-2: Nonseparable-kernel DTFD

We shall start with the nonseparable-kernel DTFD algorithm. This algorithm is based on the GDTFD algorithm in Section 5.2.2; that is, the computational load is minimised by forming the smoothed time–lag function R^{C} for positive values of m only. Also, this algorithm uses the same process as the DWVD-C algorithm in Section 5.3.1 to transform the discrete time–lag function to the time–frequency domain. The algorithm, outlined in Fig. 5.5, is as follows [51, 52].

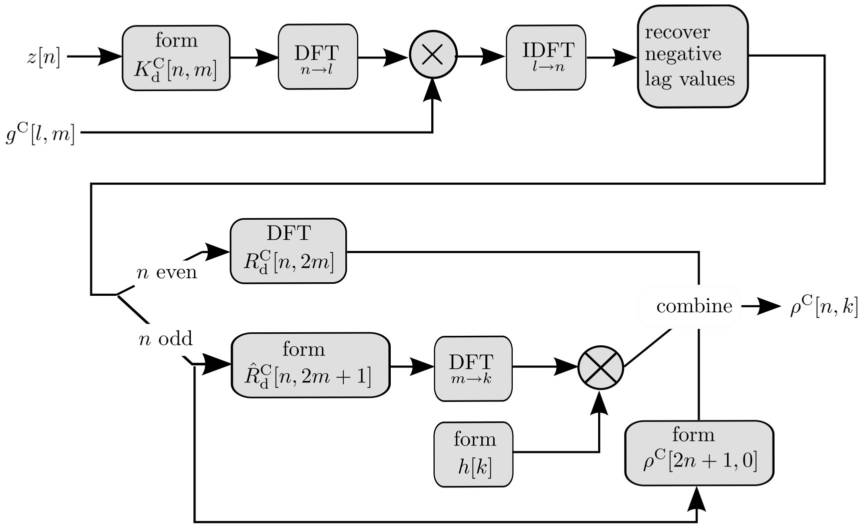

FIGURE 5.5: Algorithm for the nonseparable-kernel DTFD.

- INPUT:
  - $2N$-point analytic signal $z[n]$;
  - and $N \times (N+1)$ Doppler–lag kernel $g^{\mathrm{C}}[l,m]$.
- OUTPUT: $2N \times N$ DTFD $\rho^{\mathrm{C}}[n,k]$.

1. Let $N_{\mathrm{h}} = \lceil N/2 \rceil$ and form the time–lag function $K_{\mathrm{d}}^{\mathrm{C}}[n,m]$ from the signal $z[n]$ for positive lag values only:

$$\begin{aligned} K_{\mathrm{d}}^{\mathrm{C}}[n,2m] &= z[n+m]z^*[n-m] \\ K_{\mathrm{d}}^{\mathrm{C}}[n,2m+1] &= z[n+m+1]z^*[n-m] \end{aligned}$$

   for $n = 0,1,\ldots,N-1$ and $m = 0,1,\ldots,N_{\mathrm{h}}$. The array $K_{\mathrm{d}}^{\mathrm{C}}[n,m]$ is the *shifted-down* version of $K^{\mathrm{C}}(nT/2,mT)$, as illustrated in Fig. 5.3(b).

2. DFT $K_{\mathrm{d}}^{\mathrm{C}}[n,m]$ to the Doppler–lag domain to obtain the DAF $A^{\mathrm{C}}[l,m]$:

$$A^{\mathrm{C}}[l,m] = \underset{n\to l}{\mathrm{DFT}} \left(K_{\mathrm{d}}^{\mathrm{C}}[n,m] \right)$$

   over $0 \le m \le N-1$.

3. Multiple the DAF with the kernel:

$$S^{\mathrm{C}}[l,m] = A^{\mathrm{C}}[l,m] g^{\mathrm{C}}[l,m].$$

4. Go back to the time–lag domain:

$$R_{\mathrm{d}}^{\mathrm{C}}[n,m] = \underset{l\to n}{\mathrm{IDFT}} \left(S^{\mathrm{C}}[l,m] \right)$$

   over $0 \le m \le N-1$.

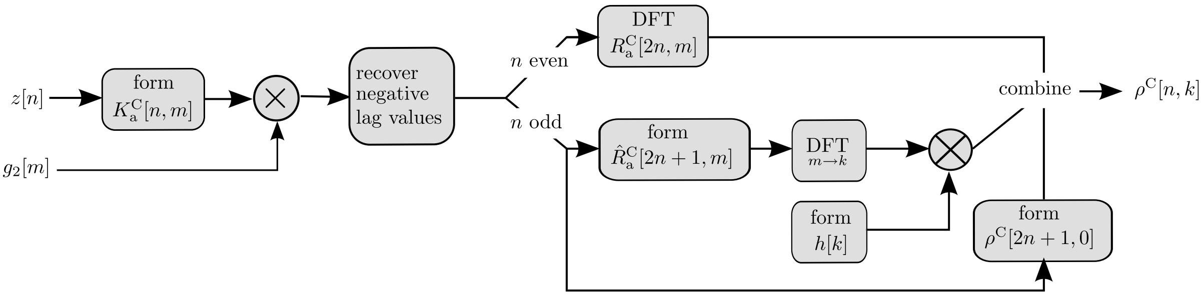

FIGURE 5.6: Algorithm for DI-kernel DTFD.

5. Recover the negative lag values from the positive ones:

$$R_{\mathrm{d}}^{\mathrm{C}}[n,2N-2m] = \left(R_{\mathrm{d}}^{\mathrm{C}}[n,2m]\right)^{*}, \qquad m = 1,2,\ldots,N_{\mathrm{h}}-1,$$

$$R_{\mathrm{d}}^{\mathrm{C}}[n,2N-2m-1] = \left(R_{\mathrm{d}}^{\mathrm{C}}[n,2m+1]\right)^{*}, \qquad m = 0,1,\ldots,N_{\mathrm{h}}-1.$$

6. Transform the time–lag function $R_{\mathrm{d}}^{\mathrm{C}}[n,m]$ to time–frequency domain to obtain the DTFD $\rho^{\mathrm{C}}[n,k]$ using a slightly modified version of the method in Step 2 of ALGORITHM-1. This segment of the algorithm is in Appendix F.1, with N_{f} in this appendix set to $N_{\mathrm{f}} = N$.

The algorithm requires $(3N+1)$ FFT$-N$ operations to compute the $2N \times N$ proposed DTFD.

ALGORITHM-3: DI-kernel DTFD

Next, I present the algorithm when the Doppler–lag kernel has the form $g^{\mathrm{C}}[l,m] = g_2[m]$, known as the Doppler-independent kernel. The function $g_2[m]$ is length P, with $P \leq 2N$. To give the user more control, the algorithm provides an extra parameter, N_{f}, which sets the frequency domain sampling to $k/2N_{\mathrm{f}}T$, with

$$N_{\mathrm{f}} \geq \left\lceil \tfrac{(P+1)}{2} \right\rceil, \qquad \text{when } P < 2N,$$

$$N_{\mathrm{f}} = N, \qquad \text{when } P = 2N.$$

Hence the algorithm results in a $2N \times N_{\mathrm{f}}$ DTFD. Note that no information is lost when $N_{\mathrm{f}} < N$ because the P-point function $g_2[m]$ will zero part of the discrete time–lag function, as $P < 2N$. Thus, N_{f} zero-pads the smoothed time–lag function in the lag direction to obtain oversampling in the frequency domain, a common practice for spectral analysis [23]. Even though the following algorithm is similar to the previous nonseparable-kernel algorithm, we present it here as there are some subtle—but important—differences in defining the discrete time–lag functions. Fig. 5.6 outlines this algorithm.

- INPUT:
  - $2N$-point analytic signal $z[n]$;
  - P-point window function $g_2[m]$, where $P \leq 2N$;

  - and parameter N_{f} where $\lceil (P+1)/2 \rceil \leq N_{\mathrm{f}} \leq N$ when $P < 2N$ or $N_{\mathrm{f}} = N$ when $P = 2N$.

- OUTPUT: $2N \times N_{\mathrm{f}}$ DTFD matrix $\rho^{\mathrm{C}}[n,k]$.

1. Let $P_{\mathrm{h}} = \lfloor P/2 \rfloor$, $P_{\mathrm{q}} = \lceil P_{\mathrm{h}}/2 \rceil$, and $N_{\mathrm{fh}} = \lceil N_{\mathrm{f}}/2 \rceil$. Also, let $i = o(P_{\mathrm{h}})$, where the function $o(\cdot)$ is
$$o(N) = \begin{cases} -1, & N \text{ is even,} \\ 0, & N \text{ is odd.} \end{cases} \tag{5.9}$$

2. Form the smoothed time–lag function $K_{\mathrm{a}}^{\mathrm{C}}[n,m]$ from the signal $z[n]$ and function $g_2[m]$:
$$\begin{aligned} R_{\mathrm{a}}^{\mathrm{C}}[2n,m] &= z[n+m]z^*[n-m]g_2[2m], && 0 \leq m \leq P_{\mathrm{q}} - 1 - i \\ R_{\mathrm{a}}^{\mathrm{C}}[2n+1,m] &= z[n+m+1]z^*[n-m]g_2[2m+1], && 0 \leq m \leq P_{\mathrm{q}} - 1 \end{aligned}$$
and if zero-padding, which occurs when $N_{\mathrm{f}} \geq \lceil (P+1)/2 \rceil$, then
$$\begin{aligned} R_{\mathrm{a}}^{\mathrm{C}}[2n,m] &= 0, && (P_{\mathrm{q}} - i) \leq m \leq (N_{\mathrm{f}} - N_{\mathrm{fh}}) \\ R_{\mathrm{a}}^{\mathrm{C}}[2n+1,m] &= 0, && P_{\mathrm{q}} \leq m \leq (N_{\mathrm{f}} - N_{\mathrm{fh}} - 1) \end{aligned}$$
over all the time values $0 \leq n \leq N-1$.

3. Then, recover the negative lag values from the positive ones:
$$\begin{aligned} R_{\mathrm{a}}^{\mathrm{C}}[2n, N_{\mathrm{f}} - m] &= \left(R_{\mathrm{a}}^{\mathrm{C}}[2n,m] \right)^*, && 1 \leq m \leq N_{\mathrm{fh}} - 1 \\ R_{\mathrm{a}}^{\mathrm{C}}[2n+1, N_{\mathrm{f}} - m - 1] &= \left(R_{\mathrm{a}}^{\mathrm{C}}[n, m+1] \right)^*, && 0 \leq m \leq N_{\mathrm{fh}} - 1. \end{aligned}$$

4. Transform the time–lag function $R_{\mathrm{a}}^{\mathrm{C}}[n,m]$ to time–frequency domain to obtain the DTFD $\rho^{\mathrm{C}}[n,k]$ using the method in Step 2 of ALGORITHM-1.

The algorithm requires N FFT$-N_{\mathrm{f}}$ operations to compute the $2N \times N_{\mathrm{f}}$ DTFD, where $N_{\mathrm{f}} \leq N$.

ALGORITHM-4: LI-kernel DTFD

The next algorithm is for the lag-independent kernel DTFD, where the Doppler–lag kernel has the form $g^{\mathrm{C}}[l,m] = G_1[l]$. Like the DI-kernel DTFD algorithm, we need only compute the $N_{\mathrm{t}} \times N$ DTFD, where N_{t} is a parameter, specified by the user, to change the time-domain sample rate. Note that this time-decimation process is not linear in time—Appendix F explains why. The parameter must satisfy the inequality $N_{\mathrm{t}} \geq 2Q$, where Q is the length of the function $G_1[l]$. Thus, oversampling occurs in the time-direction when $N_{\mathrm{t}} > 2Q$.

To form the LI-kernel DTFD, the algorithm simply forms the windowed SIAF in Doppler–frequency domain and then maps this function to the time–frequency domain. (The SIAF is the spectral instantaneous autocorrelation function, see Chapter 2 for more

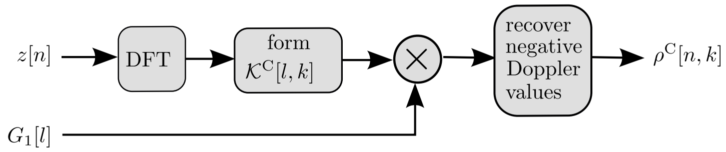

FIGURE 5.7: Algorithm for the LI-kernel DTFD.

details.) The general form of the SIAF for the proposed DTFD has, unlike the SIAF of DWVD-B in Chapter 2, a uniform discrete grid,

$$\mathcal{K}^{\mathrm{C}}[l,k] = Z[k+l]Z^*[k-l], \qquad 0 \le l \le N$$

and is conjugate symmetrical in the Doppler direction about the frequency axis:

$$\mathcal{K}^{\mathrm{C}}[2N-l,k] = \left(\mathcal{K}^{\mathrm{C}}[l,k]\right)^*, \qquad 1 \le l \le N-1.$$

The LI kernel $g_1[n]$ is length Q, where $Q \le N$. Thus, to multiply the SIAF by the LI kernel we need to periodically extend the kernel from Q to $2Q$. For example, if $Q = N$, then

$$\begin{aligned} \mathcal{R}^{\mathrm{C}}[l,k] &= \mathcal{K}^{\mathrm{C}}[l,k]G_1[l], && 0 \le l \le N-1,\\ \mathcal{R}^{\mathrm{C}}[l+N,k] &= \mathcal{K}^{\mathrm{C}}[l+N,k]G_1[l], && 0 \le l \le N-1. \end{aligned}$$

The LI kernel is periodically extended from Q to $2Q$ because, in the time–lag domain, the kernel $G^{\mathrm{C}}(nT/2, mT)$ is zero at odd-value time samples $G^{\mathrm{C}}((2n+1)T/2, mT)$, as Fig. 4.3(b) shows, which results in a periodic Doppler–frequency function $g^{\mathrm{C}}(l/NT, k/2NT) = g^{\mathrm{C}}((l+N)/NT, k/2NT)$. Fig. 5.7 outlines the following algorithm.

- INPUT:
  - $2N$-point analytic signal $z[n]$;
  - Q-point window function $G_1[l]$, where $Q \le N$;
  - and parameter N_{t} where $2Q \le N_{\mathrm{t}} \le 2N$.
- OUTPUT: $N_{\mathrm{t}} \times N$ DTFD matrix $\rho^{\mathrm{C}}[n,k]$.

1. Let $Q_{\mathrm{h}} = \lfloor Q/2 \rfloor$, $N_{\mathrm{th}} = \lfloor N_{\mathrm{t}}/2 \rfloor$, and
$$Z[k] = \underset{n \to k}{\mathrm{DFT}}\left(z[n]\right).$$
Also, let $f = o(N_{\mathrm{t}})$ and $g = o(Q)$, where the function $o(\cdot)$ is defined in (5.9).

2. Form the windowed Doppler–frequency function $\mathcal{R}^{\mathrm{C}}[l,k]$ for the positive Doppler values $0 \le l \le N_{\mathrm{th}}$ and zero pad as necessary:
$$\begin{aligned} \mathcal{R}^{\mathrm{C}}[l,k] &= Z[k+l]Z^*[k-l]G_1[l], && 0 \le l \le Q_{\mathrm{h}},\\ \mathcal{R}^{\mathrm{C}}[l,k] &= 0,\\ &\qquad (Q_{\mathrm{h}}+1) \le l \le (N_{\mathrm{th}} - Q_{\mathrm{h}} - g - 1)\\ \mathcal{R}^{\mathrm{C}}[N_{\mathrm{th}}-l,k] &= Z[k+N-l]Z^*[k-N+l]G_1[Q-l], && 1 \le l \le Q_{\mathrm{h}} + g\\ \mathcal{R}^{\mathrm{C}}[l,k] &= Z[k+N]Z^*[k-N]G_1[0], && l = N_{\mathrm{th}} \end{aligned}$$
over $0 \le k \le N-1$.

3. Recover the negative Doppler values from the positive ones:

$$\mathcal{R}^{\mathrm{C}}[N_{\mathrm{t}} - l, k] = \left(\mathcal{R}^{\mathrm{C}}[l, k]\right)^*, \quad 1 \leq l \leq N_{\mathrm{th}} + f$$

   for $0 \leq k \leq N - 1$.

4. Transform the Doppler–frequency function $\mathcal{R}^{\mathrm{C}}[l, k]$ to time–frequency domain to obtain the DTFD $\rho^{\mathrm{C}}[n, k]$:

$$\rho^{\mathrm{C}}[n, k] = \underset{l \to n}{\mathrm{IDFT}} \left(\mathcal{R}^{\mathrm{C}}[l, k]\right)$$

The algorithm requires $N/2$ FFT$-N_{\mathrm{t}}$ operations to compute the $N_{\mathrm{t}} \times N$ DTFD, where $N_{\mathrm{t}} \leq 2N$.

ALGORITHM-5: Separable-kernel DTFD

The last algorithm combines the previous two algorithms for the separable Doppler–lag kernel $g^{\mathrm{C}}[l, m] = G_1[l]g_2[m]$. For this algorithm the user can specify two parameters N_{t} and N_{f} to compute the $N_{\mathrm{t}} \times N_{\mathrm{f}}$ DTFD. For the Q-point function $G_1[l]$ and P-point function $g_2[m]$, when $N_{\mathrm{t}} > 2Q$, the DTFD is oversampled in the time direction; and when $N_{\mathrm{f}} > \lceil (P + 1)/2 \rceil$, the DTFD is oversampled in the frequency direction.

The outline of the algorithm is as follows:

1. Form the time–lag function $K_{\mathrm{d}}^{\mathrm{C}}[n, m]g_2[m]$;
2. DFT to the Doppler–lag to get $A^{\mathrm{C}}[l, m]$;
3. modulate for odd m values: $A^{\mathrm{C}}[l, 2m + 1] = A^{\mathrm{C}}[l, 2m + 1]\,\mathrm{e}^{\mathrm{j}\pi l/N}$;
4. window in the Doppler direction: $S^{\mathrm{C}}[l, m] = A^{\mathrm{C}}[l, m]G_1[l]$;
5. resize the array $S^{\mathrm{C}}[l, m]$ from $N \times 2N_{\mathrm{f}}$ to $N_{\mathrm{th}} \times 2N_{\mathrm{f}}$; we can do this because of the windowing of the DAF by the Q-point $G_1[l]$ in the previous step, where $N_{\mathrm{th}} = N_{\mathrm{t}}/2$ and $N_{\mathrm{th}} \geq Q$;
6. modulate for odd m values: $S^{\mathrm{C}}[l, 2m + 1] = S^{\mathrm{C}}[l, 2m + 1]\,\mathrm{e}^{-\mathrm{j}\pi l/N_{\mathrm{th}}}$;
7. DFT back to the time–lag domain to get $R_{\mathrm{d}}^{\mathrm{C}}[n, m]$;
8. finally, transform to the time–frequency domain.

The modulation terms in steps 3 and 6 correct for the nonuniform discrete grid of the TIAF, as discussed in Chapter 2 and 4. When $N_{\mathrm{t}} = 2N$ and thus $N_{\mathrm{th}} = N$, the modulation terms in step 3 and 6 cancel and are therefore not needed, which is why they are not present in the nonseparable-kernel DTFD algorithm. When $N_{\mathrm{th}} < N$, we therefore need these modulation terms. In the following nonseparable-kernel DTFD algorithm, I add these modulation terms in the Doppler function $G_1[l]$ so we do not need to modulate and demodulate for each odd m value, thus saving some computation. Fig. 5.8 outlines the following algorithm.

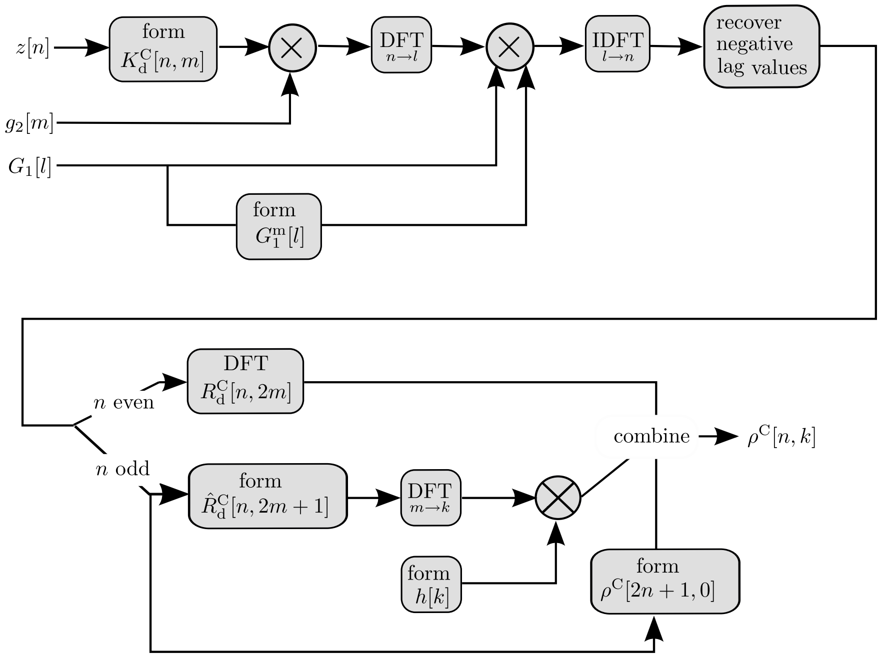

Figure 5.8: Algorithm for seperable-kernel DTFD.

- INPUT:
  - $2N$-point analytic signal $z[n]$;
  - P-point window function $g_2[m]$, where $P \leq 2N$;
  - Q-point window function $G_1[l]$, where $Q \leq N$;
  - parameter N_{t}, where $Q \leq N_{\mathrm{t}} \leq 2N$ and N_{t} is even;
  - and parameter N_{f}, where $\lceil (P+1)/2 \rceil \leq N_{\mathrm{f}} \leq N$ when $P < 2N$ or $N_{\mathrm{f}} = N$ when $P = 2N$.
- OUTPUT: $N_{\mathrm{t}} \times N_{\mathrm{f}}$ DTFD matrix $\rho^{\mathrm{C}}[n,k]$.

1. Let $Q_{\mathrm{h}} = \lfloor Q/2 \rfloor$, $P_{\mathrm{h}} = \lfloor P/2 \rfloor$, $P_{\mathrm{q}} = \lceil P_{\mathrm{h}}/2 \rceil$ $N_{\mathrm{th}} = \lfloor N_{\mathrm{t}}/2 \rfloor$, and $N_{\mathrm{fh}} = \lceil N_{\mathrm{f}}/2 \rceil$. Also, let $i = o(P_{\mathrm{h}})$ and $g = o(Q)$, where the function $o(\cdot)$ is defined in (5.5).
2. Modulate $G_1[l]$ as follows:

$$\begin{aligned} G_1^{\mathrm{m}}[l] &= G_1[l]\,\mathrm{e}^{-\mathrm{j}\pi l/N}\,\mathrm{e}^{\mathrm{j}\pi l/N_{\mathrm{th}}}, && 0 \leq l \leq Q_{\mathrm{h}}, \\ G_1^{\mathrm{m}}[Q-l] &= G_1[Q-l]\,\mathrm{e}^{-\mathrm{j}\pi(N-l)/N}\,\mathrm{e}^{\mathrm{j}\pi(N_{\mathrm{th}}-l)/N_{\mathrm{th}}}, && 1 \leq l \leq (Q_{\mathrm{h}}+g), \end{aligned}$$

3. Form the windowed time–lag function $R_{\mathrm{d}}^{\mathrm{C}}[n,m]$ for the positive lag values:

$$\begin{aligned} R_{\mathrm{d}}^{\mathrm{C}}[n,2m] &= z[n+m]z^*[n-m]g_2[2m], && 0 \leq m \leq P_{\mathrm{q}}-1-i, \\ R_{\mathrm{d}}^{\mathrm{C}}[n,2m+1] &= z[n+m+1]z^*[n-m]g_2[2m+1], && 0 \leq m \leq P_{\mathrm{q}}-1, \end{aligned}$$

over $0 \leq n \leq N-1$.

4. Transform to the Doppler–lag domain:

$$A^{\mathrm{C}}[l,m] = \underset{n\to l}{\mathrm{DFT}}\left(R_{\mathrm{d}}^{\mathrm{C}}[n,m]\right)$$

for $0 \le m \le P_{\mathrm{h}}$.

5. Multiply by the function $G_1[l]$ in the Doppler direction and zero pad as necessary:

$$\begin{aligned} S^{\mathrm{C}}[l,2m] &= A^{\mathrm{C}}[l,2m]G_1[l], && 0 \le l \le Q_{\mathrm{h}}, \\ S^{\mathrm{C}}[N_{\mathrm{th}}-l,2m] &= A^{\mathrm{C}}[N-l,2m]G_1[Q-l], && 1 \le l \le (Q_{\mathrm{h}}+g), \\ S^{\mathrm{C}}[l,2m] &= 0, && (Q_{\mathrm{h}}+1) \le l \le (N_{\mathrm{th}}-Q_{\mathrm{h}}-g-1) \end{aligned}$$

for m values $0 \le m \le P_{\mathrm{q}}-1-i$ and then

$$\begin{aligned} S^{\mathrm{C}}[l,2m+1] &= A^{\mathrm{C}}[l,2m+1]G_1^{\mathrm{m}}[l], && 0 \le l \le Q_{\mathrm{h}}, \\ S^{\mathrm{C}}[N_{\mathrm{th}}-l,2m+1] &= A^{\mathrm{C}}[N-l,2m+1]G_1^{\mathrm{m}}[Q-l], && 1 \le l \le (Q_{\mathrm{h}}+g), \\ S^{\mathrm{C}}[l,2m+1] &= 0, \\ & (Q_{\mathrm{h}}+1) \le l \le (N_{\mathrm{th}}-Q_{\mathrm{h}}-g-1) \end{aligned}$$

for the m values $0 \le m \le P_{\mathrm{q}}-1$.

6. Transform back to the time–lag domain:

$$R_{\mathrm{d}}^{\mathrm{C}}[n,m] = \underset{l\to n}{\mathrm{IDFT}}\left(S^{\mathrm{C}}[l,m]\right)$$

for $0 \le m \le P_{\mathrm{h}}$.

7. Zero-pad the time–lag function in the lag direction as necessary:

$$\begin{aligned} R_{\mathrm{d}}^{\mathrm{C}}[n,2m] &= 0, && (P_{\mathrm{q}}-i) \le m \le (N_{\mathrm{f}}-N_{\mathrm{fh}}), \\ R_{\mathrm{d}}^{\mathrm{C}}[n,2m+1] &= 0, && P_{\mathrm{q}} \le m \le (N_{\mathrm{f}}-N_{\mathrm{fh}}-1) \end{aligned}$$

over $0 \le n \le N-1$.

8. Recover the negative lag values from the positive ones:

$$\begin{aligned} R_{\mathrm{d}}^{\mathrm{C}}[n,2N_{\mathrm{f}}-2m] &= \left(R_{\mathrm{d}}^{\mathrm{C}}[n,2m]\right)^{*}, && m = 1,2,\ldots,N_{\mathrm{fh}}-1, \\ R_{\mathrm{d}}^{\mathrm{C}}[n,2N_{\mathrm{f}}-2m-1] &= \left(R_{\mathrm{d}}^{\mathrm{C}}[n,2m+1]\right)^{*}, && m = 0,1,\ldots,N_{\mathrm{fh}}-1. \end{aligned}$$

9. Transform the time–lag function $R_{\mathrm{d}}^{\mathrm{C}}[n,m]$ to time–frequency domain to obtain the DTFD $\rho^{\mathrm{C}}[n,k]$ using the method in Appendix F.1.

The algorithm requires $(P_{\mathrm{h}}+1)$ FFT$-N$ plus $(P_{\mathrm{h}}+1)$ FFT$-N_{\mathrm{th}}$ plus $N_{\mathrm{t}}/2$ FFT$-N_{\mathrm{f}}$ operations to compute the $N_{\mathrm{t}} \times N_{\mathrm{f}}$ DTFD. When all parameter are at their largest values–that is, when $P = 2N$, $N_{\mathrm{f}} = N$, and $N_{\mathrm{th}} = N$—then the maximum computational load for this algorithm is $(3N+2)$ FFT$-N$ operations, which approximately equals the computational load for the nonseparable kernel.

The preceding algorithms computes the DTFD by moving through the following domains: time–lag to Doppler–lag to time–lag to time–frequency. We could also compute the DTFD for this algorithm by moving through the following domains: Doppler–frequency to Doppler–lag to Doppler–frequency to time–frequency; the algorithm for this procedure is in Appendix F.4. There may be an advantage to having both algorithms for the separable-kernel DTFD as they both have different computational loads depending on the values of the Q and P parameters—the next section details why.

5.3.3 Computational Load

Here I compare the computational load for the algorithms. I assess the computational load as the number of DFT operations that the algorithm requires, as the DFT operations account for most of computational complexity of the algorithm [34,45]. I assume that the FFT implements the DFT operations and requires $\mathcal{O}(cN\log_2 N)$ real multiplications and real additions to compute a length-N DFT, where the constant c is a constant specific to the FFT algorithm and the symbol $\mathcal{O}()$ represents the order of computational complexity [38]. Also, I assume that the variables N, N_f and N_t are of the form 2^a, where a is an integer.

Table 5.1 shows the computational load for each algorithm; here I include the algorithm for the DWVD-C from Section 5.3.1 to compare with the DTFD algorithms. The LI- and DI-kernel DTFD algorithms require a smaller computational load compared with the load for the nonseparable- and separable-kernel DTFD. This difference in load is because we form the LI- and DI-kernel DTFD from convolving the DWVD with a function in either time or frequency directions only, whereas for the nonseparable- and separable-kernel DTFD algorithms we convolve the DWVD with a function in both the time and frequency directions. Hence although the separable-kernel DTFD algorithm computes the smallest array DTFD, the $N_\mathrm{t} \times N_\mathrm{f}$ DTFD, its computational load is greater than the LI- and DI-kernel DTFD algorithms because of the two dimensional convolution.

Note that the computational load for the proposed DTFD for the nonseparable-kernel case is twice the load for GDTFD. This is expected as the proposed DTFD contains twice as many samples points as the GDTFD. The advantage of the proposed kernel-specific algorithms is that they may, depending on the values of N_t and N_f, have a computational load and memory requirement less than the load for the general GDTFD algorithm.

Also, I present, in Appendix F.2, an efficient algorithm for the AF-GDTFD to provide a comparison with the proposed DTFD algorithms. The AF-GDTFD algorithm improves on the existing AF-GDTFD algorithm [74], see Appendix F.2 for more details. The computational load for the AF-GDTFD is more than double the load for the proposed DTFD.

For the separable kernel, the algorithm is this chapter requires the following computational load:

$$\mathcal{O}(cP_\mathrm{h}N\log_2 N + cP_\mathrm{h}N_\mathrm{th}\log_2 N_\mathrm{th} + cN_\mathrm{th}N_\mathrm{f}\log_2 N_\mathrm{f})$$

which is dependant on the value of parameter P, but independent of the parameter Q. The alternative algorithm for the separable-kernel DTFD in Appendix F.4 requires the

Existing DTFD definitions:	Computational load	DTFD array size
GDTFD	$\mathcal{O}(c3N^2/2\log_2 N)$	$N \times N$
AF-GDTFD	$\mathcal{O}(c8N^2\log_2 2N)$	$2N \times 2N$
Proposed DTFD:		
DWVD-C	$\mathcal{O}(cN^2\log_2 N)$	$2N \times N$
Nonseparable-kernel DTFD	$\mathcal{O}(c3N^2\log_2 N)$	$2N \times N$
LI-kernel DTFD	$\mathcal{O}[c(N/2)N_{\mathrm{t}}\log_2 N_{\mathrm{t}}]$	$N_{\mathrm{t}} \times N$
DI-kernel DTFD	$\mathcal{O}(cNN_{\mathrm{f}}\log_2 N_{\mathrm{f}})$	$2N \times N_{\mathrm{f}}$
Separable-kernel DTFD	$\mathcal{O}(cP_{\mathrm{h}}N\log_2 N + cP_{\mathrm{h}}N_{\mathrm{th}}\log_2 N_{\mathrm{th}}$ $+cN_{\mathrm{th}}N_{\mathrm{f}}\log_2 N_{\mathrm{f}})$	$N_{\mathrm{t}} \times N_{\mathrm{f}}$

TABLE 5.1: Computational load for the kernel-specific algorithms for the GDTFD, AF-GDTFD, proposed DTFD, and the DWVD-C all using the $2N$-point analytic signal. The algorithms for the GDTFD and AF-GDTFD assume that the kernel is the general nonseparable kernel. The user-selected parameter $N_{\mathrm{t}} \leq 2N$ controls the oversampling in the time direction; likewise $N_{\mathrm{f}} \leq N$ controls the oversampling in the frequency direction.

following computational load:

$$\mathcal{O}[cQN\log_2 2N + cQN_{\mathrm{f}}\log_2 2N_{\mathrm{f}} + c(N_{\mathrm{t}}N_{\mathrm{f}}/2)\log_2 N_{\mathrm{t}}].$$

where I have assumed that $2Q_{\mathrm{h}} = Q$. This computational load is dependent on the parameter Q but independent of the value P. Thus, there may be a way to determine which of these two algorithms is the most the computational efficient depending on the values of P and Q; I leave this to future work.

5.4 Decimated Proposed DTFD Algorithms

The algorithms in the previous section minimise the computational load and, when possible, the memory required to compute the DTFD. These algorithms compute the DTFD exactly. The emphasis on the next set of algorithms is to reduce the memory required to compute and store the DTFD, while also minimising the computational load. Unlike the previous set of algorithms, these new algorithms do not compute the DTFD exactly; rather, they compute a time- and frequency-decimated version of the DTFD.

To compute a DTFD, using the nonseparable kernel for example, requires an array containing $2N^2$ real-valued numbers. For most personal computers, this may present a problem as N becomes large. The computer may not have the random-access memory (RAM) required to store $2N^2$ real-valued points. When there is insufficient RAM, the algorithms will simply not compute. This differs from an algorithm with a large computational load, which will always compute even if it takes days, months, or even years. The following algorithms present an alternative for large N values as the algorithms require only $2N^2/(ab)$ real-valued numbers, where a and b are integers selected by the user. I achieve this memory reduction by computing decimated DTFDs.

The algorithms achieve the decimation in the time–frequency domain by folding in the Doppler–lag domain. This also reduces the computational load. The following example explains why. If we wish to compute the N-point spectral signal $X[k]$, from the signal $x[n]$, at a intervals only—that is, compute the L-point signal $X[ak]$, where $L = N/a$—we can fold $x[n]$ as follows:

$$x_{\text{fold}}[n] = \sum_{p=0}^{a-1} x[pL + n], \qquad 0 \le n \le L - 1$$

and then take the DFT of this L-point signal

$$X[ak] = \underset{n \to k}{\text{DFT}} \left(x_{\text{fold}}[n] \right) .$$

Thus, we use a FFT$-L$ to compute the $X[ak]$, rather than the FFT$-N$ required to compute $X[k]$. This is the decimation-in-frequency technique used by some FFT algorithms [23]. I apply this basic technique to computing the decimated DTFDs. Thus, the decimated DTFD will be of the form $\rho^{\text{C}}[an, bk]$, where a, b are the positive integer decimation factors, which produces the $2N/a \times N/b$ DTFD array. When possible, the algorithms will present a less restricted decimated grid than the $[an, bk]$ form. For example, the DWVD-C algorithm presents a decimated DWVD with a grid $[an, k_i]$, where a is the decimation factor and $\{k_i\} = k_1, k_2, \dots, k_J$ is a user-select subset of discrete-frequency samples points. The following algorithms explain in more details.

5.4.1 Decimated DWVD-C Algorithm

The following algorithm computes the DWVD $W^{\text{C}}[an, k_i]$, where a is an integer and $\{k_i\} = k_1, k_2, \dots, k_J$ is arbitrary subset of samples points from the set $k = 0, 1, \dots, N-1$. Fig. 5.9(a) shows an example of this type of decimation grid. Thus, the user has completely freedom to select the subset of frequency slices from the DWVD $W^{\text{C}}[n, k]$ but is somewhat more restricted in selecting the time slices from the DWVD $W^{\text{C}}[n, k]$.

ALGORITHM-6: Decimated DWVD-C

- INPUT:
  - $2N$-point analytic signal $z[n]$;
  - time-decimation factor a, where a is an integer, $a \ge 1$, and $L = 2N/a$ is also an integer;
  - and set of J frequency sample points $\{k_i\} = k_1, k_2, \dots, k_J$, where $J \le N$ and each frequency sample k_i from the set satisfies the inequality $0 \le k_i \le N - 1$.
- OUTPUT: $L \times J$ DWVD $W^{\text{C}}[an, k_i]$.

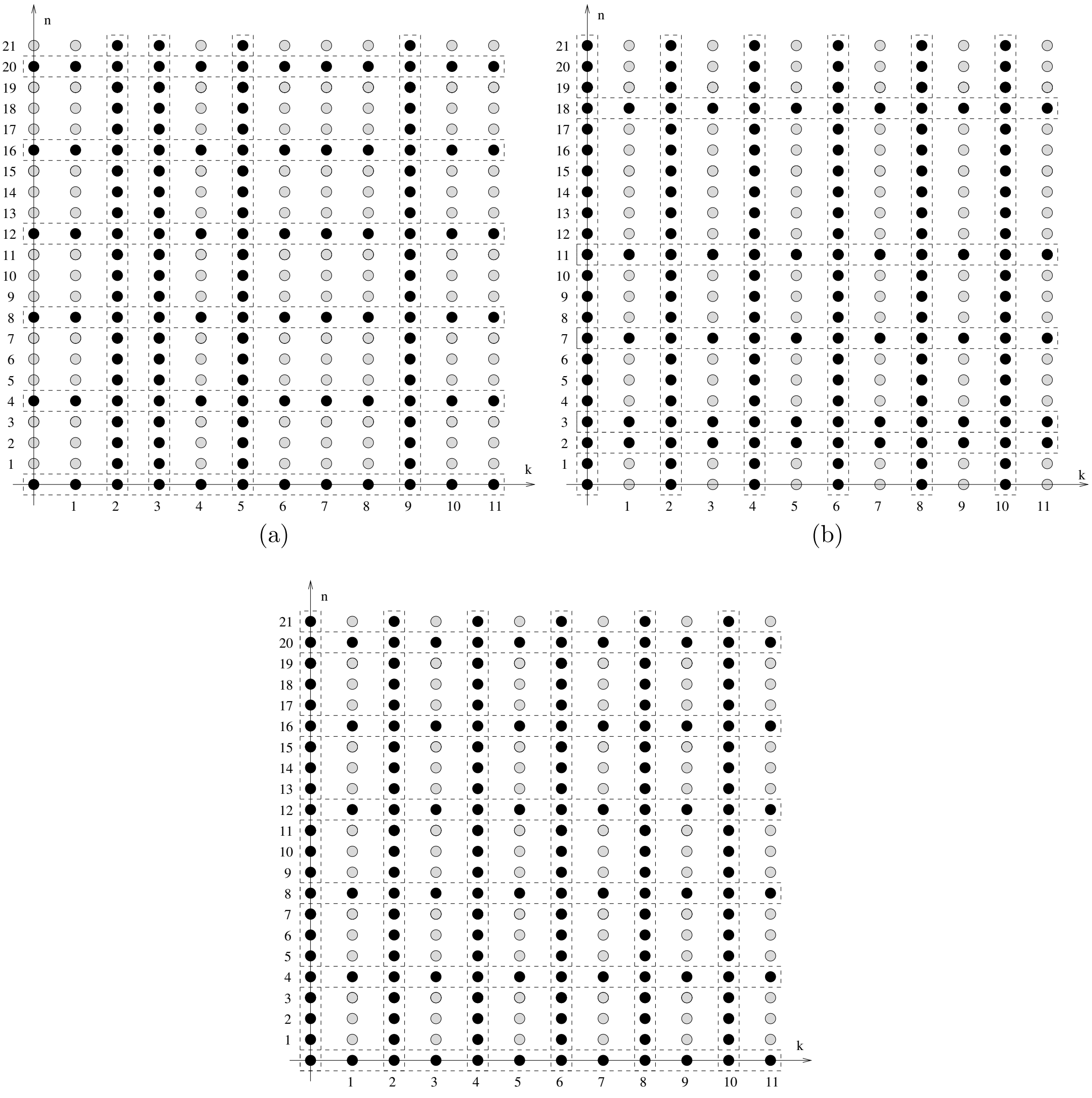

(a)

(b)

(c)

Figure 5.9: Examples of the different decimation grids for the DWVD. The circles, both grey and black, represent sample locations from the $2N \times N$ DTFD or DWVD, where $N = 12$; the black-filled circles represent the sample locations of the decimated DTFD. (a) Decimation grid $[an, k_i]$, where $a = 4$ and k_i is from the set $\{2, 3, 5, 9\}$, (b) the decimation grid $[n_i, bk]$, where $b = 2$ and n_i is from the set $\{1, 2, 9, 10, 11, 18\}$, and (c) decimation grid $[an, bk]$, where $a = 4$ and $b = 2$.

1. Let $L_{\mathrm{h}} = \lceil L/2 \rceil$, and
$$Z[k] = \underset{n \to k}{\mathrm{DFT}} \left(z[n] \right).$$
2. Form the Doppler–frequency function for frequency sample point k_i
$$\mathcal{K}_{\mathrm{tmp}}[l] = Z[k_i + l] Z^*[k_i - l], \qquad 0 \leq l \leq N,$$
and then recover the negative Doppler values from the positive ones
$$\mathcal{K}_{\mathrm{tmp}}[2N - l] = \left(\mathcal{K}_{\mathrm{tmp}}[l+1] \right)^*, \qquad 1 \leq l \leq N - 1.$$
3. For the same frequency sample point k_i fold the $\mathcal{K}_{\mathrm{tmp}}$
$$\mathcal{K}^{\mathrm{C}}[l, k_i] = \frac{1}{a} \sum_{p=0}^{a-1} \mathcal{K}_{\mathrm{tmp}}[pL + l], \qquad 0 \leq l \leq L_{\mathrm{h}}$$
and then recover the negative Doppler values from the positive ones
$$\mathcal{K}^{\mathrm{C}}[L - l, k_i] = \Big(\mathcal{K}^{\mathrm{C}}[l+1] \Big)^*, \qquad 1 \leq l \leq L_{\mathrm{h}} - 1.$$
4. Iterate the two previous steps over all values in the set $\{k_i\}$ to produce the $L \times J$ Doppler–frequency function $\mathcal{K}^{\mathrm{C}}$.
5. Transform the Doppler–frequency function to the time–frequency domain
$$W^{\mathrm{C}}[an, k_i] = \underset{l \to n}{\mathrm{IDFT}} \Big(\mathcal{K}^{\mathrm{C}}[l, k_i] \Big)$$
for all values in the set $\{k_i\}$.

The algorithm requires an $L \times J$ array and $J/2$ FFT$-L$ operations to compute the DWVD. As $L < 2N$ and $J < N$, the algorithm requires less memory and computational load to compute compared with that for the $2N \times N$ DWVD.

ALGORITHM-7: Decimated DWVD-C Again

The next algorithm again computes the decimated DWVD, but this time with a different decimation grid—the algorithm computes the DWVD $W^{\mathrm{C}}[n_i, bk]$, where b is an integer and $\{n_i\}$ is the set $n_1, n_2, \ldots, n_L$ where $0 \leq n_i \leq 2N - 1$. An example of this type of grid is shown in Fig. 5.9(b). Thus, the user has completely freedom to select the subset of time slices from the DWVD $W^{\mathrm{C}}[n, k]$ but is somewhat more restricted in selecting the frequency slices from the DWVD $W^{\mathrm{C}}[n, k]$.

- INPUT:
  - $2N$-point analytic signal $z[n]$;
  - frequency-decimation factor b, where b is an integer, $b \geq 1$, and $J = N/b$ is also an integer;

  - and set of L time sample points $\{n_i\} = n_1, n_2, \ldots, n_L$, where $L \leq 2N$ and each frequency sample n_i from the set satisfies $0 \leq n_i \leq 2N - 1$.

- OUTPUT: $L \times J$ DWVD $W^{\mathrm{C}}[n_i, bk]$.

1. Let $N_{\mathrm{h}} = \lceil N/2 \rceil$, $J_{\mathrm{h}} = \lceil J/2 \rceil$.

2. Separate the time sample points $n_1, n_2, \ldots, n_L$ into two sets: one set for even values of n_i, $\{n_{\mathrm{e}i}\}$ for $0 \leq i \leq L_{\mathrm{e}}$; and one set for odd values of n_i, $\{n_{\mathrm{o}i}\}$ for $0 \leq i \leq L_{\mathrm{o}}$. The value L_{e} is the number of even-valued time sample points and L_{o} is the number of odd-valued time sample points where $L_{\mathrm{e}} + L_{\mathrm{o}} = L$.

3. Form the time–lag function for even–valued samples $n_{\mathrm{e}i}$ and odd-valued samples $n_{\mathrm{o}i}$:

$$K_{\mathrm{etmp}}[m] = z[n_{\mathrm{e}i}/2 + m] z^*[n_{\mathrm{e}i}/2 - m]$$
$$K_{\mathrm{otmp}}[m] = z[(n_{\mathrm{o}i} - 1)/2 + m + 1] z^*[(n_{\mathrm{o}i} - 1)/2 - m]$$

   over $m = 0, 1, \ldots, N_{\mathrm{h}}$ and then recover the negative lag values from the positive ones

$$\begin{aligned} K_{\mathrm{etmp}}[N - m] &= \left(K_{\mathrm{etmp}}[m]\right)^*, && 1 \leq m \leq N_{\mathrm{h}} - 1, \\ K_{\mathrm{otmp}}[N - m - 1] &= \left(K_{\mathrm{otmp}}[m]\right)^*, && 0 \leq m \leq N_{\mathrm{h}} - 1. \end{aligned}$$

4. For the same sample points $n_{\mathrm{e}i}$ and $n_{\mathrm{o}i}$, fold the functions K_{etmp} and K_{otmp}:

$$K_{\mathrm{a}}^{\mathrm{C}}[n_{\mathrm{e}i}, m] = \sum_{p=0}^{b-1} K_{\mathrm{etmp}}[pJ + m]$$
$$K_{\mathrm{a}}^{\mathrm{C}}[n_{\mathrm{o}i}, m] = \sum_{p=0}^{b-1} K_{\mathrm{otmp}}[pJ + m]$$

   over values $m = 0, 1, \ldots, J_{\mathrm{h}}$ and then recover the negative lag values from the positive ones

$$\begin{aligned} K_{\mathrm{a}}^{\mathrm{C}}[n_{\mathrm{e}i}, J - m] &= \left(K_{\mathrm{a}}^{\mathrm{C}}[n_{\mathrm{e}i}, m]\right)^*, && 1 \leq m \leq J_{\mathrm{h}} - 1, \\ K_{\mathrm{a}}^{\mathrm{C}}[n_{\mathrm{o}i}, J - 1 - m] &= \left(K_{\mathrm{a}}^{\mathrm{C}}[n_{\mathrm{o}i}, m]\right)^*, && 0 \leq m \leq J_{\mathrm{h}} - 1. \end{aligned}$$

5. Iterate the two previous steps over all values in the sets $\{n_{\mathrm{e}i}\}$ and $\{n_{\mathrm{o}i}\}$ to produce the $L \times J$ time–lag function $K_{\mathrm{a}}^{\mathrm{C}}$.

6. Transform the time–lag function to the time–frequency domain for even–odd values of n_i:

   (a) for even n_i values $\{n_{\mathrm{e}i}\} = n_{\mathrm{e}1}, n_{\mathrm{e}2}, \ldots, n_{\mathrm{e}L_{\mathrm{e}}}$:

$$W^{\mathrm{C}}[n_{\mathrm{e}i}, bk] = \underset{k \to m}{\mathrm{DFT}} \left(K_{\mathrm{a}}^{\mathrm{C}}[n_{\mathrm{e}i}, m]\right)$$

(b) and odd n_i values $\{n_{\mathrm{o}i}\} = n_{\mathrm{o}1}, n_{\mathrm{o}2}, \ldots, n_{\mathrm{o}L_{\mathrm{o}}}$:

  i. Let

$$h[bk] = \begin{cases} \sin(\pi bk/N_{\mathrm{f}}) + \cos^2(\pi bk/N_{\mathrm{f}})/\sin(\pi bk/N_{\mathrm{f}}), & 1 \leq k \leq J-1, \\ 0, & k = 0. \end{cases}$$

  ii. Let

$$\hat{K}_{\mathrm{a}}^{\mathrm{C}}[n_{\mathrm{o}i}, 0] = \Im\Big(K_{\mathrm{a}}^{\mathrm{C}}[n_{\mathrm{o}i}, 0]\Big)$$

$$\hat{K}_{\mathrm{a}}^{\mathrm{C}}[n_{\mathrm{o}i}, m] = \frac{1}{2\mathrm{j}}\left\{K_{\mathrm{a}}^{\mathrm{C}}[n_{\mathrm{o}i}, m] - \Big(K_{\mathrm{a}}^{\mathrm{C}}[n_{\mathrm{o}i}, J-m]\Big)^*\right\}, \quad 1 \leq m \leq J_{\mathrm{h}}.$$

  iii. Recover the negative lag values from the positive ones:

$$\hat{K}_{\mathrm{a}}^{\mathrm{C}}[n_{\mathrm{o}i}, m] = \Big(\hat{K}_{\mathrm{a}}^{\mathrm{C}}[n_{\mathrm{o}i}, J-m]\Big)^*, \qquad J_{\mathrm{h}} + 1 \leq m \leq J-1.$$

  iv. DFT to the time–frequency domain and multiply by constant $h[bk]$

$$W^{\mathrm{C}}[n_{\mathrm{o}i}, bk] = \underset{m \to k}{\mathrm{DFT}}\Big(\hat{K}_{\mathrm{a}}^{\mathrm{C}}[n_{\mathrm{o}i}, m]\Big)\, h[bk].$$

  v. Finally, do for frequency sample $k = 0$:

$$W^{\mathrm{C}}[n_{\mathrm{o}i}, 0] = \sum_{m=0}^{J-1} K_{\mathrm{a}}^{\mathrm{C}}[n_{\mathrm{o}i}, m].$$

The algorithm requires an $L \times J$ array and $L/2$ FFT$-J$ operations to compute the DWVD.

5.4.2 Decimated Kernel-Specific DTFD Algorithms

ALGORITHM-8: Decimated Nonseparable-kernel DTFD

The first algorithm is for the general nonseparable-kernel DTFD algorithm. The algorithm produces a decimated DTFD using grid shown in Fig. 5.9(c); that is, a $L \times J$ DTFD $\rho^{\mathrm{C}}[an, bk]$, where a and b are integers. To produce this decimated DTFD, the algorithm folds the Doppler–lag function after the DAF is multiplied by the kernel. Even though the algorithm folds the $N \times 2N$ smoothed DAF, it requires only a $L \times J$ array by folding one lag slice of the smoothed DAF at a time and then iterating over all lag values.

Note that when a is odd, the time–lag function $R_{\mathrm{d}}^{\mathrm{C}}[n, 2m+1]$ will have a time offset of $(a-1)/2$ because $R_{\mathrm{d}}^{\mathrm{C}}[n, 2m]$ comes, in time, before $R_{\mathrm{d}}^{\mathrm{C}}[n, 2m+1]$. Thus, the temporal order for the array $R_{\mathrm{d}}^{\mathrm{C}}[n, m]$ is $R_{\mathrm{d}}^{\mathrm{C}}[an, 2m]$ followed by $R_{\mathrm{d}}^{\mathrm{C}}[an + (a-1)/2, 2m+1]$. To enable the decimation with a nonzero offset for $R_{\mathrm{d}}^{\mathrm{C}}[an + (a-1)/2, 2m+1]$, the algorithm requires a modulation of the folded function with a complex exponential, which is done in step 3(d) of the algorithm; this is a more general form of the decimation-in-frequency technique [38].

- INPUT:

  - $2N$-point analytic signal $z[n]$;
  - $N \times 2N$ Doppler–lag kernel $g^{\mathrm{C}}[l, m]$;
  - time-decimation factor a; $a \geq 1$ and both a and $L = 2N/a$ are integers;
  - and frequency-decimation factor b; $b \geq 1$ and both b and $J = N/b$ are integers.

- OUTPUT: $L \times J$ DTFD matrix $\rho^{\mathrm{C}}[an, bk]$.

1. Let $N_{\mathrm{h}} = \lceil N/2 \rceil$, $L_{\mathrm{h}} = \lceil L/2 \rceil$, and $J_{\mathrm{h}} = \lceil J/2 \rceil$.

2. Separate the time sample points $\{0, a, 2a, \ldots, (L-1)a\}$ into two sets: one set for even values of n_i, $\{n_{\mathrm{e}i}\}$ for $0 \leq i \leq L_{\mathrm{e}} - 1$; and one set for odd values of n_i, $\{n_{\mathrm{o}i}\}$ for $0 \leq i \leq L_{\mathrm{o}} - 1$. The value L_{e} is the number of even-valued time sample points and L_{o} is the number of odd-valued time sample points where $L_{\mathrm{e}} + L_{\mathrm{o}} = L$. Note that if a is even, $L_{\mathrm{o}} = 0$ as odd values do not exist in the set $\{0, a, 2a, \ldots, (L-1)a\}$ for a even.

3. Iterate the following over $m_0 = 0, 1, \ldots, J_{\mathrm{h}}$:

   (a) Fold the Doppler–lag function in the lag direction:

   $$S_{\mathrm{etmp}}[l] = \sum_{p=0}^{b-1} A_{\mathrm{etmp}}[l, pJ + m_0] g^{\mathrm{C}}[l, 2(pJ + m_0)], \quad 0 \leq l \leq N - 1,$$

   where A_{etmp} is

   $$A_{\mathrm{etmp}}[l, m_o] = \underset{n \to l}{\mathrm{DFT}} \left(z[n + m_0] z^*[n - m_0] \right)$$

   for positive lag values $m_0 < N_{\mathrm{h}}$ and

   $$A_{\mathrm{etmp}}[l, m_o] = \underset{n \to l}{\mathrm{DFT}} \left(z^*[n + N - m_0] z[n - N + m_0] \right)$$

   for negative lag values $m_0 \geq N_{\mathrm{h}}$. Splitting A_{etmp} up into positive and negative lag values ensures that the A_{etmp} is conjugate symmetrical in the lag direction.

   (b) If a is odd, then do similar to previous step:

   $$S_{\mathrm{otmp}}[l] = \sum_{p=0}^{b-1} A_{\mathrm{otmp}}[l, pJ + m_0] g^{\mathrm{C}}[l, 2(pJ + m_0) + 1], \quad 0 \leq l \leq N - 1,$$

   where A_{otmp} is

   $$A_{\mathrm{otmp}}[l, m_o] = \underset{n \to l}{\mathrm{DFT}} \left(z[n + m_0 + 1] z^*[n - m_0] \right)$$

   for positive lag values $m_0 < N_{\mathrm{h}}$ and

   $$A_{\mathrm{otmp}}[l, m_o] = \underset{n \to l}{\mathrm{DFT}} \left(z^*[n + N - m_0] z[n - N + m_0 + 1] \right)$$

   for negative lag values $m_0 \geq N_{\mathrm{h}}$. These two steps fold the Doppler–lag function in the lag direction.

(c) Fold the Doppler–lag function in the Doppler direction:

$$S_{\mathrm{etmp}}[l] = \sum_{q=0}^{a'-1} S_{\mathrm{etmp}}[qL_{\mathrm{e}} + l], \quad 0 \le l \le L_{\mathrm{e}} - 1.$$

where $a' = a/2$ if a is even and $a' = a$ if a is odd.

(d) If a is odd, then do similar to previous step:

$$S_{\mathrm{otmp}}[l] = \sum_{q=0}^{a-1} S_{\mathrm{otmp}}[qL_{\mathrm{o}} + l]\, \mathrm{e}^{\mathrm{j}[2\pi(pL_{\mathrm{o}}+l)(a-1)/2]/N}, \quad 0 \le l \le L_{\mathrm{o}} - 1.$$

The exponential is this equation is nonzero when $a \ge 3$; this is the offset for folding process—for example, if $a = 5$ then we need to decimate the time–lag function starting at $R_{\mathrm{d}}^{\mathrm{C}}[n+2, 2m+1]$ for $n = 0, 1, \ldots, L_{\mathrm{o}} - 1$.

(e) Then, transform to the time–lag domain:

$$R_{\mathrm{a}}^{\mathrm{C}}[n_{\mathrm{e}i}, m_0] = \underset{l \to n}{\mathrm{IDFT}} \left(S_{\mathrm{etmp}}[l] \right)$$

and if a is odd

$$R_{\mathrm{a}}^{\mathrm{C}}[n_{\mathrm{o}i}, m_0] = \underset{l \to n}{\mathrm{IDFT}} \left(S_{\mathrm{otmp}}[l] \right).$$

4. Recover the negative lag values from the positive lag values:

$$R_{\mathrm{a}}^{\mathrm{C}}[n_{\mathrm{e}i}, J - m] = \left(R_{\mathrm{a}}^{\mathrm{C}}[n_{\mathrm{e}i}, m] \right)^{*}, \quad 1 \le m \le J_{\mathrm{h}} - 1$$

and if a is odd

$$R_{\mathrm{a}}^{\mathrm{C}}[n_{\mathrm{o}i}, J - m - 1] = \left(R_{\mathrm{a}}^{\mathrm{C}}[n_{\mathrm{o}i}, m] \right)^{*}, \quad 0 \le m \le J_{\mathrm{h}} - 1.$$

5. Iterate the two previous steps over all values of $\{n_{\mathrm{e}i}\} = n_{\mathrm{e}1}, n_{\mathrm{e}2}, \ldots, n_{\mathrm{e}L_{\mathrm{e}}}$ and $\{n_{\mathrm{o}i}\} = n_{\mathrm{o}1}, n_{\mathrm{o}2}, \ldots, n_{\mathrm{o}L_{\mathrm{o}}}$ to produce the $L \times J$ time–lag function $R_{\mathrm{a}}^{\mathrm{C}}$.

6. Transform $R_{\mathrm{a}}^{\mathrm{C}}$ to the time–frequency domain for even–odd values of n_i, using the method in Step 6 of ALGORITHM-7 by replacing $K_{\mathrm{a}}^{\mathrm{C}}[n, m]$ with $R_{\mathrm{a}}^{\mathrm{C}}[n, m]$ and $W^{\mathrm{C}}[n, k]$ with $\rho^{\mathrm{C}}[n, k]$.

The algorithm requires N FFT$-N$ plus J_{h} FFT$-L$ plus $J/2$ FFT$-J$ operations to compute the $L \times J$ DTFD.

ALGORITHM-9 for the decimated DI-kernel DTFD and ALGORITHM-10 for the decimated LI-kernel DTFD are in Appendix F.5. I relegate these algorithms to the appendix because there is significant overlap with the decimated DWVD-C algorithms ALGORITHM-6 and ALGORITHM-7, and the following separable-kernel DTFD algorithm.

ALGORITHM-11: Decimated separable-kernel DTFD

- INPUT:
  - $2N$-point analytic signal $z[n]$;
  - Q-point window function $G_1[l]$, with $Q \leq N$;
  - parameter N_t, with $2Q \leq N_\mathrm{t} \leq 2N$ and N_t is even;
  - P-point window function $g_2[m]$, where $P \leq 2N$;
  - parameter N_f, where $\lceil (P+1)/2 \rceil \leq N_\mathrm{f} \leq N$ when $P < 2N$ or $N_\mathrm{f} = N$ when $P = 2N$.
  - time-decimation factor a; $a \geq 1$ and both a and $L = N_\mathrm{t}/a$ are integers;
  - and frequency-decimation factor b; $b \geq 1$ and both b and $J = N_\mathrm{f}/b$ are integers.
- OUTPUT: $L \times J$ DTFD matrix $\rho^\mathrm{C}[an, bk]$.

1. Let $N_\mathrm{h} = \lceil N/2 \rceil$, $L_\mathrm{h} = \lceil L/2 \rceil$, $J_\mathrm{h} = \lceil J/2 \rceil$, $Q_\mathrm{h} = \lfloor Q/2 \rfloor$, $N_\mathrm{th} = \lfloor N_\mathrm{t}/2 \rfloor$, $P_\mathrm{h} = \lfloor P/2 \rfloor$, $P_\mathrm{q} = \lceil P_\mathrm{h}/2 \rceil$, $N_\mathrm{fh} = \lceil N_\mathrm{f}/2 \rceil$, $g = o(Q)$, and $i = o(P_\mathrm{h})$.
2. Separate the time sample points $\{0, a, 2a, \dots, (L-1)a\}$ into two sets: one set for even values of n_i, $\{n_{\mathrm{e}i}\}$ for $0 \leq i \leq L_\mathrm{e} - 1$; and one set for odd values of n_i, $\{n_{\mathrm{o}i}\}$ for $0 \leq i \leq L_\mathrm{o} - 1$. The value L_e is the number of even-valued time sample points and L_o is the number of odd-valued time sample points where $L_\mathrm{e} + L_\mathrm{o} = L$. Note that if a is even $L_\mathrm{o} = 0$ as odd values do not exist in the set $\{0, a, 2a, \dots, (L-1)a\}$ when a is even.
3. Modulate $G_1[l]$ as follows:
$$\begin{aligned} G_1^\mathrm{m}[l] &= G_1[l]\, \mathrm{e}^{-\mathrm{j}\pi l/N}\, \mathrm{e}^{\mathrm{j}\pi l/N_\mathrm{th}}, && 0 \leq l \leq Q_\mathrm{h}, \\ G_1^\mathrm{m}[Q-l] &= G_1[Q-l]\, \mathrm{e}^{-\mathrm{j}\pi(N-l)/N}\, \mathrm{e}^{\mathrm{j}\pi(N_\mathrm{th}-l)/N_\mathrm{th}}, && 1 \leq l \leq (Q_\mathrm{h} + g). \end{aligned}$$
4. Iterate the following over of $m_0 = 0, 1, \dots, J_\mathrm{h}$:
   (a) Fold the Doppler–lag function in the lag direction:
$$R_\mathrm{etmp}[n] = \sum_{p=0}^{b-1} K_\mathrm{etmp}[n, pJ + m_o] g_2[2(pJ + m_0)]$$
   for $0 \leq n \leq N-1$, where $K_\mathrm{etmp}[n]$ is defined as
$$\begin{aligned} K_\mathrm{etmp}[n, m_0] &= z[n + m_0 + 1] z^*[n - m_0], && \text{if } m_0 < N_\mathrm{h}, \\ K_\mathrm{etmp}[n, m_0] &= z^*[n + N - m_0] z[n - N + m_0 + 1], && \text{if } m_0 \geq N_\mathrm{h}; \end{aligned}$$
   then DFT to the Doppler–lag domain:
$$A_\mathrm{etmp}[l] = \underset{n \to l}{\mathrm{DFT}} \left(R_\mathrm{etmp}[n] \right)$$
   and finally multiply by the function $G_1[l]$:
$$\begin{aligned} S_\mathrm{etmp}[l] &= A_\mathrm{etmp}[l] G_1[l], && 0 \leq l \leq Q_\mathrm{h} \\ S_\mathrm{etmp}[N_\mathrm{th} - l] &= A_\mathrm{etmp}[N - l] G_1[Q - l], && 0 \leq l \leq Q_\mathrm{h} + g. \end{aligned}$$

(b) If a is odd, then do similar to the previous step: fold the Doppler–lag function in the lag direction:

$$R_{\text{otmp}}[n] = \sum_{p=0}^{b-1} K_{\text{otmp}}[n, pJ + m_0] g_2[2(pJ + m_0) + 1]$$

where $K_{\text{etmp}}[n]$ is defined as

$$\begin{aligned} K_{\text{otmp}}[n, m_0] &= z[n + m_0 + 1] z^*[n - m_0], && \text{if } m_0 < N_{\text{h}}, \\ K_{\text{otmp}}[n, m_0] &= z^*[n + N - m_0] z[n - N + m_0 + 1], && \text{if } m_0 \geq N_{\text{h}}; \end{aligned}$$

for $0 \leq n \leq N - 1$; then DFT to the Doppler–lag domain:

$$A_{\text{otmp}}[l] = \underset{n \to l}{\text{DFT}} \left(R_{\text{otmp}}[n] \right) .$$

Finally, multiply by the function $G_1^{\text{m}}[l]$:

$$\begin{aligned} S_{\text{otmp}}[l] &= A_{\text{otmp}}[l] G_1^{\text{m}}[l], && 0 \leq l \leq Q_{\text{h}} \\ S_{\text{otmp}}[N_{\text{th}} - l] &= A_{\text{otmp}}[N - l] G_1^{\text{m}}[Q - l], && 0 \leq l \leq Q_{\text{h}} + g. \end{aligned}$$

(c) Fold the Doppler–lag function in the Doppler direction:

$$S_{\text{etmp}}[l] = \sum_{q=0}^{a'-1} S_{\text{etmp}}[qL_{\text{e}} + l], \quad 0 \leq l \leq L_{\text{e}} - 1,$$

where $a' = a/2$ if a is even and $a' = a$ if a is odd; then IDFT back to the time–lag domain:

$$R_{\text{a}}^{\text{C}}[n_{\text{e}i}, m_0] = \underset{l \to n}{\text{IDFT}} \left(S_{\text{etmp}}[l] \right) .$$

(d) If a is odd, then again do similar to the previous step: fold the Doppler–lag function in the Doppler direction:

$$S_{\text{otmp}}[l] = \sum_{q=0}^{a-1} S_{\text{otmp}}[qL_{\text{o}} + l] \, \mathrm{e}^{\mathrm{j}[2\pi(pL_{\text{o}} + l)(a-1)/2]/N}, \quad 0 \leq l \leq L_{\text{o}} - 1,$$

then IDFT back to the time–lag domain:

$$R_{\text{a}}^{\text{C}}[n_{\text{o}i}, m_0] = \underset{l \to n}{\text{IDFT}} \left(S_{\text{otmp}}[l] \right) .$$

5. Recover the negative lag values from the positive lag values:

$$R^{\text{C}}[n_{\text{e}i}, J - m] = \left(R^{\text{C}}[n_{\text{e}i}, m] \right)^*, \quad 1 \leq m \leq J_{\text{h}} - 1$$

and if a is odd

$$R^{\text{C}}[n_{\text{o}i}, J - m - 1] = \left(R^{\text{C}}[n_{\text{o}i}, m] \right)^*, \quad 0 \leq m \leq J_{\text{h}} - 1.$$

6. Iterate the two previous steps over the sets $\{n_{\mathrm{e}i}\}$ and $\{n_{\mathrm{o}i}\}$ to produce the $L \times J$ time–lag function $R_{\mathrm{a}}^{\mathrm{C}}$.

7. Transform $R_{\mathrm{a}}^{\mathrm{C}}$ to the time–frequency domain for even–odd values of n_i, using the method in Step 6 of ALGORITHM-7 by replacing $K_{\mathrm{a}}^{\mathrm{C}}[n,m]$ with $R_{\mathrm{a}}^{\mathrm{C}}[n,m]$ and $W^{\mathrm{C}}[n,k]$ with $\rho^{\mathrm{C}}[n,k]$.

The algorithm requires $2J_{\mathrm{h}}$ FFT$-N$ plus $2J_{\mathrm{h}}$ FFT$-L$ plus $(LJ/2)$ FFT$-J$ operations to compute the $L \times J$ DTFD.

5.4.3 Computational Load and Memory

As with the algorithms in Section 5.3, this part concludes with a summary of the computational load for the decimated DTFD algorithms. Table 5.2 contains the computational load for each $L \times J$ DTFD. Because the dimensions L and J differ for each algorithm, the table details the algorithm-specific definition of these parameters. Also, the table shows the different decimation grids for the each algorithm.

All these algorithms, expect the nonseparable-kernel DTFD algorithm, compute the decimated DTFD efficiently as the computational load is independent of the $N^2 \log_2 N$ term. The computational load for the nonseparable-kernel DTFD algorithm contains this term because we must compute the entire DAF, which requires a computational load of $N^2 \log_2 N$, before we begin the folding process. All is not lost however, as the nonseparable-kernel DTFD, like the other algorithms in this section, computes a decimated DTFD and therefore should not cause memory problems.

The LI-kernel DTFD computes a decimated version of the $N_{\mathrm{t}} \times N$ DTFD; the DI-kernel DTFD computes a decimated version of the $N \times N_{\mathrm{f}}$ DTFD; and the separable-kernel DTFD computes a decimated version of the $N_{\mathrm{t}} \times N_{\mathrm{f}}$ DTFD. In contrast, the algorithms for the DWVD and nonseparable-kernel DTFD compute a decimated version of the $2N \times N$ DTFD. Thus, the computational load and memory required to compute the LI-, DI-, and separable-kernel DTFD decrease as $N_{\mathrm{t}} \leq 2N$ and $N_{\mathrm{f}} \leq N$ decrease.

5.5 Summary and Conclusions

This chapter addressed one of the major limitations of the DTFD as a signal analysis tool: a large computational load and memory is required to compute the DTFD. I presented two approaches for efficiently computing the proposed DTFD from Chapter 4. Both approaches included a set of kernel-specific DTFD algorithms for the DWVD, the nonseparable-kernel DTFD, the separable-kernel DTFD, the LI-kernel DTFD, and the DI-kernel DTFD.

The first approach computes the DTFD exactly. For this set of algorithms, the nonseparable-kernel DTFD and DWVD algorithms require a fixed computational load, depending only on signal length N. The three other algorithms—the LI-, DI- and separable-kernel DTFD algorithms—may have a variable computational load as they are dependent on the user-selected variables N_{t} and N_{f}, where $N_{\mathrm{t}} \leq 2N$ and $N_{\mathrm{f}} \leq N$. The variable N_{t} sets the amount of oversampling in the time direction of the DTFD. As $N_{\mathrm{t}} \geq 2Q$, where Q is the length of the time smoothing kernel $g_1[n]$, no signal information or properties

	Computational complexity	Decimation Grid
DWVD[a]	$\mathcal{O}(cLJ_{\mathrm{h}}\log_2 J)$	$W^{\mathrm{C}}[n_i, bk]$
DWVD[b]	$\mathcal{O}(cLJ_{\mathrm{h}}\log_2 L)$	$W^{\mathrm{C}}[an, k_i]$
Nonsep.-kernel DTFD[c]	$\mathcal{O}(c\ N^2\log_2 N + cJ_{\mathrm{h}}L\log_2 L + cJ_{\mathrm{h}}L\log_2 J)$	$\rho^{\mathrm{C}}[an, bk]$
LI-kernel DTFD[d]	$\mathcal{O}(cLJ_{\mathrm{h}}\log_2 L)$	$\rho^{\mathrm{C}}[an, k_i]$
DI-kernel DTFD[e]	$\mathcal{O}(cLJ_{\mathrm{h}}\log_2 J)$	$\rho^{\mathrm{C}}[n_i, bk]$
Sep.-kernel DTFD[f]	$\mathcal{O}(cJN\log_2 N + cJ_{\mathrm{h}}L\log_2 L + cJ_{\mathrm{h}}L\log_2 J)$	$\rho^{\mathrm{C}}[an, bk]$

TABLE 5.2: Computational load to compute the decimated $L \times J$ DTFD and DWVD-C. The different algorithms have different decimation grids for the DTFD. These results assume that $J_{\mathrm{h}} = J/2$.

[a] $J = N/b$, where a is the decimation integer; L is the number of elements in the set $\{n_i\}$;

[b] $L = 2N/a$, where a is the decimation integer; J is the number of elements in the set $\{k_i\}$;

[c] $L = 2N/a$ and $J = N/b$, where a, b are the decimation integers;

[d] $L = N_{\mathrm{t}}/a$, where a is the decimation integer; J is the number of elements in the set $\{k_i\}$;

[e] $J = N_{\mathrm{f}}/b$, where b is the decimation integer; L is the number of elements in the set $\{n_i\}$;

[f] $L = N_{\mathrm{t}}/a$ and $J = N_{\mathrm{f}}/b$, where a, b are the decimation integers.

of the DTFD is lost for the $N_{\mathrm{t}} \times N$ DTFD. The same is true for N_{f}, where N_{f} sets the amount of oversampling in the frequency direction of the DTFD. Thus, the memory for computing and storing the DTFD for these three algorithms may be reduced from $2N^2$ sample points to either $N_{\mathrm{t}}N$, $2NN_{\mathrm{f}}$, or $N_{\mathrm{t}}N_{\mathrm{f}}$ sample points, depending on the kernel type.

The second set of algorithms compute the DTFD efficiently with a restricted memory size. This set of algorithms computes, with a minimal computational load, a time- and frequency-decimated version of the DTFD; thus, these methods do not compute the DTFD exactly and signal information or properties of the DTFD may be lost. We can use these algorithms to compute the DTFD when N is large, as the algorithms compute an $L \times J$ DTFD, where $L < 2N$ and $J < N$, thus requiring less memory than the $2N \times N$ DTFD.

Chapter 6

Neonatal EEG Seizure Detection

6.1 Introduction

This chapter gives an example of how we may use the DTFD methods from previous chapters to solve a real-life problem. The problem is how to effectively detect seizure events in newborn electroencephalographic data. Approximately one in every 200 newborn babies have some form of seizure episodes [80]. Seizures are the most common indication of neurological disease for the newborn. Rapid diagnosis is therefore important so that the clinician may treat the neurological problem causing the seizure activity promptly and properly [81].

Monitoring newborn brain activity through the electroencephalogram (EEG)—a measurement of the electrical activity of the brain—is the most common approach for identifying seizure activity and is sometimes the only method of identification available to the clinician [82, 83, 84, 85]. Detecting seizure activity in adult EEG involves identifying spikes and repetitive sharp waveforms [86]. These seizure signals are prominently displayed against a background of low amplitude random activity, thus a distinct separation exists between the seizure and nonseizure signal morphology.

Identifying seizure in the newborn is, however, more complicated than in adults due to a number of factors. First, because the newborn's immature brain continues to form, healthy newborn EEG displays extra electrical activity, which can mimic seizure activity [87, 88]. Second, visual symptoms that clearly characterise seizure for the adult—such as muscle spasms, rapid eye movement, and drooling—are much more subtle in newborns due to the underdeveloped central nervous system. Also, some of these indicators are natural behaviour traits common to all newborns [82]. And lastly, the physical activity of newborns in the intensive care environment is often subdued by medication [89, 90]. Hence detecting seizure from either clinical or EEG indicators is a difficult task and may lead to misdiagnosis, which can have acute physical repercussions for the patient.

The current practice of identifying electrical seizures in the neonatal EEG is based on the electroencephalographer's interpretation of the time-domain EEG signal. Clinicians and researchers have described various types of EEG seizure morphologies [81, 91, 86, 87, 88, 82, 83, 84, 89, 85]. The clinician visually searches the EEG for these seizure waveforms. In an effort to eliminate this time consuming and subjective process [92], researchers have proposed signal processing methods to automate the EEG seizure detection process [93, 94, 95, 96, 97, 98, 55, 99, 56].

Existing automated seizure detection methods, however, are not suitable for use in the clinical environment because of their poor performance [100,101]. Thus, there is a need to improve on the existing methods. Most methods assume that the EEG signal is stationary or locally stationary [93,94,95,96,102] even though there is evidence that the EEG signal is nonstationary [103,104]. Of the methods that account for the nonstationarity of EEG, the time–frequency matched filter method [103] and the method by Navakatikyan [99] showed the most promise. I present a new method based on these two existing methods. The existing time–frequency matched filter detects seizure with a large probability of error because the method requires a large predefined template set [56]; the Navakatikyan method requires over 40 parameters. The proposed method, conversely, does not require a predefined template set, nor does it require an excessive amount of parameters.

The chapter layout is as follows. Section 6.2 presents a literature review on automated newborn EEG seizure detection methods. Section 6.3 presents a detailed review of the existing time–frequency matched filter method and then presents the proposed method. I test the proposed method using simulated and real EEG data. The initial results are promising, although the method needs to be compared with other existing detection methods. The proposed method is an example of how DTFDs are used in real-world problems; more specifically, the proposed method is an example of how the proposed analytic signal in Chapter 3, the proposed DTFD in Chapter 4, and the proposed algorithms in Chapter 5 may be used to solve a real-world problem.

6.2 Review

Most of the work on automating the process of newborn EEG seizure detection has been based on identifying some form of periodicity in the EEG that is distinguishable from the background EEG [82,83]. (Background is any EEG event that is not seizure.) Other methods assume that the seizure event is a deterministic signal whereas the background is a stochastic one. These methods try to detect a deterministic signal from the random signal.

The following is a summary of some automatic seizure detection techniques. I group the methods into two groups—namely, stationary and nonstationary methods. Throughout the chapter I use two values to assess the performance of the detection methods: the true detection rate (TDR)—the number of true detections divided by the number of EEG seizure epochs—and the false detection rate (FDR)—the number of incorrect detections divided by the total number of EEG nonseizure epochs.

6.2.1 Stationary Methods

We can subdivide the stationary seizure detection methods into two categories: nonparametric and parametric. Roessgen *et al.* [95] proposed a linear parametric model of background and seizure EEG. This parametric method estimates eleven model parameters from the EEG and then produces a test statistic to classify the EEG epoch as either a seizure or nonseizure event. The method is limited—parameter estimation is computationally expense, there is no guarantee of convergence to a global minimum, and results indicate poor performance [105]. The rest of the methods reviewed here are non-parametric methods.

Gotman [90] proposed a method that uses spectral analysis to detect seizure by detecting periodicity in the EEG. The method compares the spectrum of a 10-second epoch of EEG with a 20-second epoch that occurred at a lag of 60 seconds. The method measures and compares the power in the band around the spectral peak for the two segments of EEG and thus makes a decision about the periodicity of the EEG signal to classify seizure or nonseizure events.

Liu *et al.* [94] proposed a time domain approach which measures the degree of periodicity in the EEG by taking the autocorrelations of 5 segments in a 30-second duration epoch. Each segment receives a periodicity score from the autocorrelation functions and the scores are then combined for the epoch. The epoch score is then compared to a threshold to declare seizure or nonseizure.

Celka *et al.* [96] proposed a method that uses a singular spectrum approach. The method first preprocesses the data using a nonlinear whitening filter that spreads the spectrum of the background activity while retaining the periodic features of the seizure. The singular spectrum approach projects the EEG into signal subspaces which can determine whether seizure is present or not. Celka *et al.* acknowledged that the performance of their method is limited by the degree of nonstationarity of the newborn EEG.

Faul *et al.* [100] assessed the three preceding methods—the Gotman, Liu, and Celka methods—and concluded that all three methods perform poorly and should not be used in a clinical setting.

Karayiannis *et al.* proposed an EEG seizure detection method [102] based on detecting pseudo-sinusoidal EEG activity. The method uses the spectral rule based approach proposed by Gotman *et al.* [90] in which the thresholds are decreased to increase the TDR. This also has the unwanted side effect of increasing the FDR. The authors then used neural networks for classification to reduce the FDR, although the published results still have a high FDR [102].

6.2.2 Nonstationary Methods

Nonstationary detection methods use nonstationary signal processing techniques such as time-scale and time-frequency techniques to detect seizure. Time-scale methods include the model proposed by Nagasubramanin [106], which suffers from a very high FDR [106], and the model proposed by Zarjam *et al.* [107], which uses a neural network classification scheme to improve the FDR.

Time-frequency newborn seizure detection methods include the matching pursuit algorithm proposed by Rankine *et al.* [108, 109], which was based on the adult EEG detection model by Franaszczuk *et al.* [110]. The matching pursuit (MP) algorithm uses an over-complete dictionary of basis functions, which are called atoms, to represent or approximate a signal by a linear superposition of these atoms. The atomic dictionary in Rankine's method uses time-frequency atoms. The authors showed that the number of atoms required to represent the EEG drops as the signal changes from a background to seizure event. The method preforms poorly in the presence of artifacts [108].

Hassanpour *et al.* [111, 112, 113, 98] proposed a method to detect seizure by detecting spikes in the TFD of the EEG. The method [113] first preprocesses the TFD of EEG data in an effort to isolate the spikes. Then two high frequency slices of the filtered TFD are obtained to which a nonlinear energy operator is applied to amplify the spike signatures. The method assumes that the spikes in the time-domain EEG are represented as high-frequency localised energy in the TFD. The method measures the interval between successive spikes and produces a histogram of these intervals. By comparing the histograms to a predefined reference histogram, the method classifies the epoch as seizure or nonseizure. Analysis of the methods shows a low TDR [114].

Boashash and Mesbah [103] proposed a method using a time-frequency matched detector; Schiff *et al.* [115] also applied this method to adult EEG. The method extends the existing theory for the time-domain matched filter to the time–frequency domain. The method constructs a filter based on features of EEG seizure in the time–frequency domain. Different types of EEG seizure require different filters; thus, the time–frequency matched filter uses a set of filters, known as templates. Each template is correlated with the EEG TFD to produce a test statistic. By comparing this test statistic to a threshold, we may classify the epoch as a seizure or nonseizure event.

More recently, Navakatikyan *et al.* [99] proposed a method which uses a series of ad-hoc techniques to manipulate, in the time domain, short-time segments from an epoch of EEG. At its core, the method correlates these short-time segments with neighbouring segments to determine whether seizure is present or not. Although the model estimates over 40 parameters from the EEG, the results on the large database are promising.

6.2.3 New Method

The stationary detection methods, which assume that the EEG is stationary or at least quasi-stationary, have poor performance because newborn EEG is a nonstationary signal [104]. Of the nonstationary methods, the time–frequency matched filter detector and the Navakatikyan method display the most promise; I base the new detection method in this chapter on both these existing methods.

6.3 Time–Frequency Matched Filter

I start with a detailed review of the time–frequency matched filter, as this forms the basis for the new method.

6.3.1 Theory

We may reduce the problem of detecting an EEG seizure event from the EEG background to the classic detection problem of detecting a known signal in noise. For a signal $x(t)$ there are two possibilities:

$$\begin{aligned} &H_0: \ x(t) = n(t), && \text{signal absent,} \\ &H_1: \ x(t) = s(t) + n(t), && \text{signal present.} \end{aligned}$$

where $s(t)$, of duration T, represents the signal to detect and $n(t)$ represents the noise. The detection problem is how to select the correct hypothesis, H_0 or H_1. Thus, if we assume H_1 and $s(t)$ is present, then this is a true detection; if we assume H_1 and $s(t)$ is not present, then this is a false detection.

The matched filter is a time-domain detection method that linearly filters $x(t)$ [116]. The method maximises the signal to noise ratio (SNR) of $s(t)$ and $n(t)$. The method requires that the signal $s(t)$ is a known signal and $n(t)$ is a Gaussian noise process, assuming here that the noise is white Gaussian with a constant power spectral density. To make the decision as to whether $s(t)$ is present or not, we form a test statistic as follows:

$$\eta_{\mathrm{t}} = \int_{(T)} x(t)s^*(t)\,\mathrm{d}t \tag{6.1}$$

and then compare this test statistic with a predefined threshold value ζ to determine hypothesis. Thus,

$$\begin{aligned} H_0 &: \eta_{\mathrm{t}} < \zeta, \\ H_1 &: \eta_{\mathrm{t}} > \zeta. \end{aligned}$$

The matched filter is known as an optimum detector because it maximise the SNR and therefore maximises the probability of a true detection [117].

We can extend the matched filter method, which uses time-domain signal in (6.1), to use time–frequency representations. The inner-product of the WVDs for the signals $x(t)$ and $s(t)$,

$$\eta_{\mathrm{tf}} = \int\int_{(T)} W_x(t,f)W_s(t,f)\,\mathrm{d}t\,\mathrm{d}f \tag{6.2}$$

is simply related to the matched filter in (6.1) as [118, 119]

$$\eta_{\mathrm{tf}} = |\eta_{\mathrm{t}}|^2. \tag{6.3}$$

The test statistic η_{tf} is also know as a locally optimal detector [118, 119] and because of its direct relation with η_{t} provides no advantage over the conventional matched filter.

If we replace the WVD with the more general TFD representation,

$$\eta_{\mathrm{tf}} = \int\int_{(T)} \rho_x(t,f)\rho_s(t,f)\,\mathrm{d}t\,\mathrm{d}f \tag{6.4}$$

then this test statistic η_{tf} is only related to the η_{t} in (6.3) if the Doppler–lag kernels for ρ_x and ρ_s satisfies the condition $|g(\nu,\tau)| = 1$ [118]. This condition severely constrains the type of TFDs as most useful TFDs have non-unity, real-valued kernels. The notably exception is, of course, the WVD.

The time–frequency matched filter, using the test statistic in (6.4), is known as a sub-optimum detector [118, 14] because the filter does not maximise the SNR ratio. The method, however, may prove useful for an application when the constraints on the matched filter do not hold. That is, if the signal $s(t)$ is not exactly known, or if $s(t)$ is randomly perturbed in some way, or if the noise $n(t)$ is not white Gaussian noise then the sub-optimum method may prove useful [118, 120, 14, 103, 56].

Before applying the matched filter to newborn EEG seizure detection, I present an analysis on selecting a suitable TFD for newborn EEG signals.

6.4 Selecting a Time–Frequency Distribution

The TFD should represent the important characteristics of both seizure and nonseizure events and represent the events in a discriminatory way. In this section, I discuss the important time–frequency characteristics of the seizure and nonseizure events and present an analysis on selecting a TFD that best represents both seizure and nonseizure. The conclusion is that the separable-kernel TFD, with a medium-sized Doppler and lag smoothing windows, is a suitable TFD for newborn EEG seizure detection.

6.4.1 Quadratic Time-Frequency Distributions

There are many different types of TFDs in the quadratic TFD class, as the type of TFD depends on the structure of the kernel $\gamma(t, f)$. Recall how the quadratic class is defined,

$$\rho(t, f) = W(t, f) \underset{t}{*} \underset{f}{*} \gamma(t, f) \tag{6.5}$$

where $W(t, f)$ represents the WVD. As we saw in Chapter 2, the WVD is unique in that it satisfies a certain set of mathematical properties [1] whereas all other TFDs only satisfy a subset of these properties. These properties are useful for understanding the theoretical characteristics of the particular TFD. They may not, however, be needed for some practical problems.

In order to address this problem, Boashash and Sucic [1, pp. 72] [121] presented a general framework of desirable features for TFDs more in accordance with practical rather than theoretical requirements. The properties are

P1. *Concentration of local energy:* The TFD should be real and adhere to the notion of local energy concentration. That is, the energy E_R in a time–frequency region R should equal the time and frequency integral of the TFD over this region:

$$\int_{\Delta f} \int_{\Delta t} \rho(t, f) \, \mathrm{d}t \, \mathrm{d}f = E_R.$$

where R is the region within the time interval Δt and frequency bandwidth Δt. (Assuming that Δt and Δf satisfy the uncertainty principal [1].)

P2. *Instantaneous frequency (IF) visualisation:* The peak of the TFD of a monocomponent signal, with respect to frequency, should equal, or approximate, the IF $f_i(t)$ law of the signal; that is,

$$\max_f \rho(t, f) = f_i(t).$$

With multicomponent signals, the same property should apply to the individual components.

P3. *Reduced interference:* The TFD should attenuate or suppress cross-terms.

These properties are different from the set of precise mathematical properties in Chapter 2. Unlike mathematical properties, we can not easily quantify whether a TFD satisfies these properties or not. But these properties can be taken as general features that a TFD should, in most cases, adhere to. For example, an ideal TFD of multicomponent signal that satisfies these three properties, is a flat two-dimensional area consisting of delta-like functions centred around the IF laws of the signal's components. See [1] for a more thorough discussion on these properties.

The properties P1-P3 are general desirable TFD properties regardless of the application. Some applications, however, require further TFD properties. Hence I now present a discussion on the specific requirements for the two important EEG events—seizure and nonseizure.

TFD Performance for Seizure Events

The seizure event is a slowly-evolving periodic signal [87, 88], often described as a quasi-linear frequency modulated signal [103,122]. I therefore propose that the TFD of a seizure event should

- satisfy properties P1, P2 and P3;
- and be invariant to time, frequency, and scale shifts.

The class of quadratic TFDs are inherently time–frequency covariant, although not necessarily scale covariant. The scale covariance property requires a product kernel [123], which may prove to be too restrictive.

TFD Performance for Background Events

A background event has been described in the literature as a stochastic nonstationary process [104, 122], distinguishable from the more deterministic seizure event. Because background has a time-varying spectral power law [122] and is high-pass filtered at approximately 0.5Hz, the TFD of background may look like a short-time linear frequency modulated (LFM) component. It is therefore crucial that these components are not confused with seizure components. Thus the criteria for the ideal background TFD is to

- satisfy property P1;
- and highlight the stochastic nature of the event by not excessively smoothing in the time–frequency domain.

An ideal TFD for background would be the WVD, as the smoothing introduced by the time–frequency kernel will only smear energy over the time–frequency plane. For the seizure event, however, we require some sort of smoothing to suppress the cross-terms. Thus it would appear that there is a conflict between the needs of the two different events.

6.4.2 Design of Newborn EEG Quadratic TFD

The design of a TFD will now be examined for each separate event with the goal of approximating, as closely as possible, the desirable properties discussed in the previous section.

Seizure Events

Based on time–frequency observations, seizure has been modelled as a summation of LFM and piecewise-LFM signals [124, 104, 125, 122]. The model is consistent with the clinical EEG literature which describes seizure as an evolving periodic pattern [88]. Boashash *et al.* observed these LFM-type characteristics with and without additional harmonics [104, 125, 103]. Schiff *et al.* also reported these LFM-type signals in adult EEG. I use this LFM-type model in the following analysis.

Analysis of LFM-Type Signals

Lets define the LFM signal as

$$x(t) = \sum_{i=1}^{K+1} \mathrm{e}^{\mathrm{j}2\pi(if_0 t + \frac{\alpha}{2}t^2)} \tag{6.6}$$

with starting frequency f_0, slope α, and K harmonic components. We assume the signal is of infinite length. The WVD of $x(t)$ is [126]

$$W_x(t,f) = \sum_{i=1}^{K+1} \delta(f - (if_0 + \alpha t))) + 2\sum_{i=0}^{K-1}\sum_{q=i+1}^{K} \delta(f - ((\tfrac{i+q}{2} + 1)f_0 + \alpha t)) \cos\left(2\pi(i-q)f_0 t\right) \tag{6.7}$$

where the first summation in the right hand side (RHS) of the equation represents the auto-terms and the second set of summations in the RHS represents the cross-terms. The ambiguity function (AF) of $x(t)$ is

$$A_x(\nu,\tau) = \delta(\nu - \alpha\tau)\sum_{i=1}^{K+1} \mathrm{e}^{\mathrm{j}2\pi i f_0 \tau} + \sum_{i=0}^{K}\sum_{\substack{q=0\\ q\neq i}}^{K} \delta(\nu - (i-q)f_0 - \alpha\tau)\, \mathrm{e}^{\mathrm{j}2\pi(\frac{i+q}{2}+1)f_0\tau} \tag{6.8}$$

where, similar to (6.7), the first summation in the RHS of the equation represents the auto-terms and the second set of summations in the RHS represents the cross-terms.

Because the EEG is not an infinite length signal, this previous assumption needs refining. Lets define $x(t)$ over a time period T as $x_T(t) = x(t)\mathrm{rect}_T\big(t - T/2\big)$, where the rectangular window function is defined as

$$\mathrm{rect}_T\,(t) = \begin{cases} 1, & |t| < \frac{T}{2}, \\ 0, & |t| > \frac{T}{2}. \end{cases}$$

The WVD in (6.7) can be rewritten for finite signal $x_T(t)$ as

$$\begin{aligned} W_{x_T}(t,f) &= \mathrm{rect}_T\left(t - \tfrac{T}{2}\right) W_x(t,f) \underset{f}{*} \frac{\sin\left(4\pi(T - |t - \frac{T}{2}|)f\right)}{\pi f} \\ &= \mathrm{rect}_T\left(t - \tfrac{T}{2}\right) 4B_T(t - \tfrac{T}{2}) W_x(t,f) \underset{f}{*} \mathrm{sinc}(4\pi(T - |t - \tfrac{T}{2}|)f) \end{aligned} \tag{6.9}$$

where the Bartlett function $B_T(t)$, which is a scaled triangular function, is defined as

$$B_T(t) = 1 - \frac{|t|}{T}.$$

Two important modifications to the WVD of $x(t)$ take place due to the time-limiting process in (6.9). First, the WVD of the infinite signal $x(t)$ is spread or smeared in the frequency direction due to the convolution with the time-dependent sinc function. Thus the δ functions in (6.7) are replaced with a time dependent sinc function centred around the trajectory of the δ functions in the time–frequency plane. As the dimension of T decreases the spread or width of the main lobe of the sinc function will increase. Second, the WVD of the infinite signal $x(t)$ is multiplied with the Bartlett function centred around $t = T/2$ which results in a linear tapering in the time direction of the energy away from the centre of the WVD.

The effect of the finite windowing in the Doppler–lag domain in relation to the AF A_x is

$$\begin{aligned} A_{x_T}(\nu,\tau) &= \mathrm{rect}_{2T}\,(\tau)\, A_x(\nu,\tau) \underset{\nu}{*} \frac{\sin\left(\pi\nu(2T-|\tau|)\right)}{\pi\nu}\, \mathrm{e}^{-\mathrm{j}\pi T\nu} \\ &= \mathrm{rect}_{2T}\,(\tau)\, B_{2T}(\tau) A_x(\nu,\tau) \underset{\nu}{*} \mathrm{sinc}(\pi\nu(2T-|\tau|))\, \mathrm{e}^{-\mathrm{j}\pi T\nu} \qquad (6.10) \end{aligned}$$

Similar to the time–frequency domain, the AF of $x(t)$ is smeared in the Doppler direction by the (modulated by an exponential term) lag-dependent sinc function. Also, the spread of energy in the lag direction is scaled by a Bartlett function centred at $\tau = 0$. Thus, the energy in the AF decreases away from the origin in the lag direction. Combining (6.10) with (6.8),

$$\begin{aligned} A_{x_T}(\nu,\tau) = \mathrm{rect}_{2T}\,(\tau)\, B_{2T}(\tau) \Bigg(& \mathrm{sinc}(\pi(\nu-\alpha\tau)(2T-|\tau|)) \sum_{i=1}^{K+1} \mathrm{e}^{\mathrm{j}2\pi i f_0 \tau} \\ & + \sum_{i=0}^{K} \sum_{\substack{q=0 \\ q\neq i}}^{K} \mathrm{sinc}(\pi(\nu-(i-q)f_0-\alpha\tau)(2T-|\tau|))\, \mathrm{e}^{\mathrm{j}2\pi(\frac{i+q}{2}+1)f_0\tau} \Bigg). \qquad (6.11) \end{aligned}$$

Kernel Design

It is evident from (6.7) that many cross-term components are present in the WVD. Thus, probably the biggest challenge here is to satisfy property P3, which is to reduce these cross-terms. However, this should not be at the expense of sacrificing TFD's ability to resolve the components—and hence satisfy property P1.

The design of the TFD is aided by examining the kernel in both the time–frequency domain and Doppler–lag domain. The kernel in the Doppler–lag domain can be thought of as a two-dimensional filter which aims to suppress the cross-terms whilst preserving the auto-terms.

The cross-terms in the time–frequency domain, as described in (6.7), not only exist in between the auto-terms but also sit *on top* all components except the fundamental and K^{th} harmonic component. The cross-terms in the Doppler–lag domain, as described in (6.8), are placed $\pm f_0$ in the Doppler direction away from the auto-terms. The nearest cross-terms to the auto-terms at $\delta(\nu-\alpha\tau)$ are located along $\delta(\nu \pm f_0 - \alpha\tau)$. Assuming a finite duration of T for the signal then (6.8) is replaced by (6.11). The main difference here is that the aforementioned δ functions are now replaced with sinc functions, the width of which is dependent on T and the lag value. Also, these components are multiplied by the Bartlett function $B_{2T}(\tau)$, which results in a tapering of the energy of the components away from the origin in the lag direction. I assume that T is large enough that most of the significant energy for the auto-terms is contained within the bandwidth $\pm T\alpha$ in the Doppler direction of the AF, see Fig. 6.1a for an example.

If we assume that T is constant, then the ease at which the cross-terms can be eliminated, whilst preserving the auto-terms, is dependent on the values of f_0 and α. To design the Doppler–lag filter, lets consider three different scenarios which depend on the value of α, the rate of change of the IF.

- **Scenario 1: slowly varying IF law**

  If we assume that $\alpha < f_0/(2T)$, then the goal of eliminating the cross-terms is achievable by placing a window function, centred on $\nu = 0$, along the τ axis. This Doppler–lag domain kernel is known as the lag-independent (LI) kernel and is represented as $g(\nu, \tau) = G_1(\nu)$, where $G_1(\nu)$ for this case is an even window function of width $2\alpha T$. This is illustrated in Fig. 6.1a for the Doppler–lag domain, where a clear separation can be seen between auto and cross-terms. In the time–frequency domain, the cross-terms will oscillate along the $\delta(f - (3/2)f_0 - \alpha t)$ trajectory with frequency $\cos(2\pi f_0 t)$, as expressed in (6.7). Thus convolving in the time direction with $g_1(t)$ should suppress this cross-term energy. For this particular case, there is a clear separation, in frequency, between cross-terms and auto-terms, as highlighted in Fig. 6.1b. Thus no cross-term energy will be displaced onto the auto-terms from the convolution process.

- **Scenario 2: moderately varying IF law**

  If we assume that $f_0/(2T) < \alpha < f_0/T$, as displayed in Fig. 6.1c and Fig. 6.1d, then using the LI kernel here may not sufficiently suppress the cross terms. As $G_1(\nu)$ is a window-type function of width $2\alpha T$, then the extremities (in the lag direction) of the cross-terms will be within the pass region of the $G_1(\nu)$ function, which is best illustrated in Fig. 6.1c. Not only will some of the cross-terms be present, but the auto-terms will be altered by this kernel. This effect is best assessed in the time–frequency domain, where the convolution of $g_1(t)$ in the time direction will result in some of the cross-term energy being distributed to the auto-term. This can be seen in Fig. 6.1d, where it is clear that there is an overlap, in the frequency direction, between the auto- and cross-terms.

  A solution to this problem involves a compromise. The cross-terms within the $-\alpha T < \nu < \alpha T$ range can be filtered out by placing a windowing type function $g_2(\tau)$ along the ν axis, centred on $\tau = 0$. Thus towards the extremities in the lag direction this energy would be suppressed, which should encompass the cross-terms. This would also suppress some of the auto-term energy as well, hence the compromise. This windowing, of course, would be needed in conjunction with the LI kernel. This resultant kernel would be a separable kernel, of the form $g(\nu, \tau) = G_1(\nu)g_2(\tau)$. It is worth noting that a nonseparable kernel, of the form $g(\nu, \tau) = g_n(\nu, \tau)$, could also approximate this shape of kernel. In the time–frequency domain the convolution in

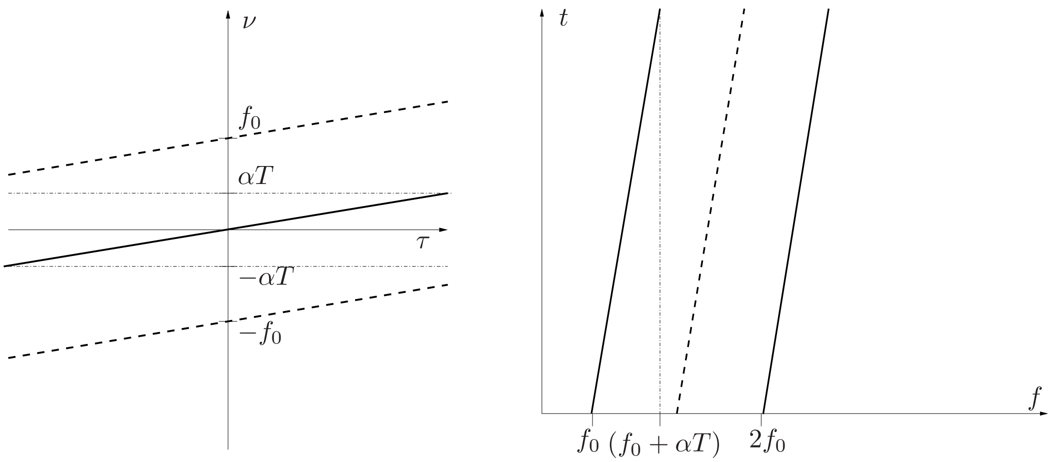

(a) AF with $\alpha < f_0/(2T)$ (b) TFD with $\alpha < f_0/(2T)$

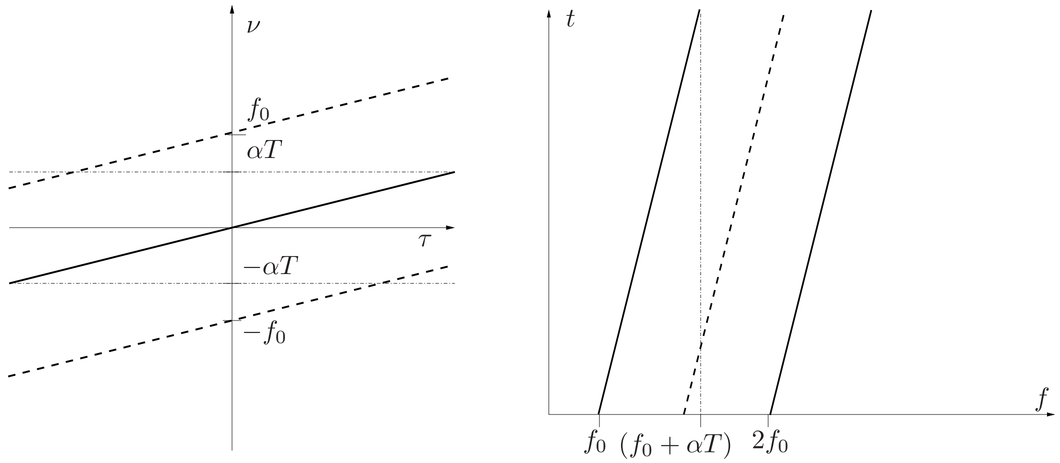

(c) AF with $f_0/(2T) < \alpha < f_0/2$ (d) TFD with $f_0/(2T) < \alpha < f_0/T$

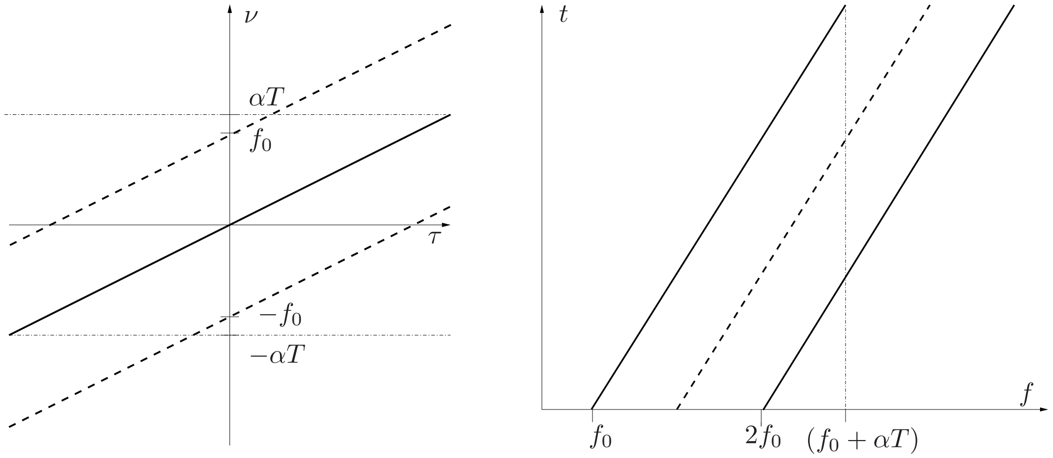

(e) AF with $\alpha > f_0/T$ (f) TFD with $\alpha > f_0/T$

FIGURE 6.1: Doppler–lag and time–frequency representations for an LFM-type signal of slope α with one harmonic. The main component has a starting frequency f_0 and the harmonic has a starting frequency of $2f_0$. In the Doppler–lag domain, the main and harmonic components are both located along the same trajectory $\delta(\nu - \alpha\tau)$. The auto-terms are represented by the bold lines and the cross-terms are represented by the dashed bold lines.

the frequency direction with $G_2(f)$ will smooth or spread the auto-term components about their centre.

- **Scenario 3: quickly varying IF law**

  The third scenario, when $\alpha > f_0/T$ as illustrated in Fig. 6.1e and Fig. 6.1f, is the most difficult to deal with it. For this case, most of the cross-term energy is located inside the bandwidth $-\alpha T < \nu < \alpha T$. Without knowledge of α, the previously suggested nonseparable or separable kernels types may not preform well in terms of cross-term suppression.

Of course for the last two scenarios when $-f_0/T < \alpha < f_0/T$ and $\alpha > f_0/T$ an improved solution exists. This involves applying a windowing function $g_0(\cdot)$ along the auto-term location of $\delta(\nu - \alpha\tau)$ in the Doppler–lag domain. This would result in a nonseparable kernel, of the form $g(\nu, \tau) = g_0(\nu - \alpha\tau)$. This kernel, however, requires knowledge of α which can vary considerably for different EEG seizure events [104]. Although adaptive kernels, such as [127] or [55], may be able to determine the value for α and thus yield high resolution TFDs, they are not quadratic TFDs and will not be considered here.

Based on this analysis either a nonseparable- or separable-kernel TFD seems like a suitable choice of TFD to analyse EEG seizure events. The separable-kernel has the advantage over the nonseparable kernel because the amount of smoothing in the Doppler and lag direction can be controlled independently by $g_1(\nu)$ and $g_2(\tau)$.

6.4.3 Background Events

As I defined the EEG background event as any type of event other than seizure, it is a little more difficult to analyse. To start, the signal characteristics of these events are highly dependent on the conceptional age of the newborn [87, 88]. Second, normal infant behaviour—such as muscle movement and sucking—along with a range of external sources—such as electrical noise and electrodes falling—introduce artefacts into the EEG. Third, for the sick neonate there is yet another set of signal characteristics classified as abnormal EEG which may be present [87, 128]. These three different types of background events leads to a nonseizure signal which is highly variable in nature—that is, varying in amplitude, frequency, and morphology. Because of the variability in signal structure, the characteristics of the background events can sometimes mimic the characteristics of the seizure events.

The most significant difference between the two events is time duration. For example, the power-law spectrum of the background may be stationary for a short period of time, say T_b seconds, thus creating what appears like an LFM component in the TFD. Conversely, a seizure event is defined as a continuous, evolving periodic event for at least T_s seconds. To date there is no agreed definition of what T_s should be, although it is commonly taken as $T_s = 10$ seconds [88, 104]. It is therefore implied that $T_s > T_b$, although T_b may be close to T_s.

Herein lies the major challenge in designing a seizure detection method, one that is able to precisely discern between background and seizure events. As discussed in Section 6.4.1, the main time–frequency characteristic of seizure contains quasi-LFM components, with or without harmonics. Thus it is desirable not to enhance any quasi-LFM like components for the background events, which is in direct conflict with the desired seizure event TFD. A compromise has to be made, although where exactly to draw the line remains unclear. With this in mind, I examine some of the issues involved in designing a suitable TFD for background EEG.

Kernel Design

Unlike the kernel design for the seizure events, which are modelled as deterministic signals, it is harder to assess the ability of the TFD to represent, what is in essence, a stochastic event. The most applicable approach to analyse this nonstationary stochastic process [104] is the Wigner-Ville spectrum [1, pp. 37]. As only one realisation of the stochastic process is available, this Wigner-Ville spectrum reduces to the WVD. But the kernel is required for the seizure events and thus we cannot use the WVD.

In terms of the properties discussed in Section 6.4.1, only property P1 is relevant for a stochastic signal. In order to maximise the separation between TFDs for the two events, however, I now examine some undesirable features for the background event with the view to minimising them.

- **Time Support:**

  First, we assume that the kernel designed for the seizure events, discussed in Section 6.4.2, contains some significant smoothing in the time direction in the time–frequency domain. The danger here, however, is that as this low pass filter decreases in bandwidth to create more resolved distributions, the smearing in the time direction will increase. This may not pose a problem for the seizure event as the LFM-type component may appear well resolved through the TFD. For the background events this time-directional smearing may extend the LFM-like component of length T_b to be of length $\geq T_s$, and thus may appear similar to a seizure event. To improve the distinction between TFDs of the two events, we could add the time-support property to the distributions [129]. This involves restricting the kernel in the time–lag domain $G(t,\tau)$ to

  $$G(t,\tau) = 0, \qquad \text{if } |\tau| < 2|t|. \tag{6.12}$$

  I present an example to help clarify the issue. Boashash and Sucic [121] proposed that a TFD using a particular LI kernel, called the modified-B (MB) [130] distribution, produces highly resolved TFDs for LFM-type signals. The LI kernel can be described as

  $$g(\nu,\tau) = g_1(\nu) = \frac{|\Gamma(\beta + \mathrm{j}\pi\nu)|}{\Gamma^2(\beta)}$$

  where β is a real positive number that controls the spread of the LI filter in the Doppler–lag domain. The authors in [121] proposed an optimal parameter value of $\beta = 0.002$ for a multicomponent LFM signal. Also, the closely related B-distribution [131] with a parameter value of $\beta = 0.01$ was used as a suitable TFD for newborn EEG seizure events in [104] and [103]. A low value for β was also reported in the original articles [130] and [131] to produce high resolution TFDs. The effects of this will be examined in the time–frequency domain.

If the bandwidth of the LI filter is small in the Doppler–lag domain, which is the case when $\beta = 0.01$ for a typical signal length of $N = 128$, then the bandwidth of the kernel in the time–frequency domain will be large. Thus convolving the WVD with $G_1(t)$ will result in a large spread or smearing of the signal energy about the components in the time direction. To illustrate this effect, I use a test signal

$$z_a(nT) = \mathrm{rect}_{N/2}\left(n - \tfrac{N}{4}\right)\, \mathrm{e}^{\mathrm{j}2\pi 0.2nT} + \mathrm{rect}_{N/2}\left(n - \tfrac{3N}{4}\right)\, \mathrm{e}^{\mathrm{j}2\pi 0.3nT}.$$

This test signal consists of two sinusoidal components, as shown in Fig. 6.2a. The MB distribution for $\beta = 0.01$ in Fig. 6.2b, spreads the energy for both components beyond the bounds of the signal. The MB distribution's kernel can be changed to accommodate the time-support property by applying the constraint specified in (6.12). This modified MB distribution, now having a nonseparable kernel rather than a LI kernel, restricts the smearing of the component energy in the time direction, as illustrated in Fig. 6.2c. The disadvantage of enforcing the time-support property is an increase in the sidelobe magnitude, as highlighted for a time slice in Fig. 6.3. This effect was also observed in [129]. A compromise to these scenarios would be to enforce a lower limit on the bandwidth of the Doppler filter $g_1(\nu)$, thus reducing the spread in the time–frequency domain. The effect of this is shown in Fig. 6.2d where the MB distribution without the time support property is used with $\beta = 0.1$. As shown in Fig. 6.3 shows, the magnitude of the sidelobe, compared with the MB distribution with the time-support property enforced, is reduced. The same process applies to any kernel that has a significant low pass filtering operation in the Doppler direction.

- **Smoothing in the Frequency Direction:**

  More than one short-time LFM-like "component" previously discussed will produce cross-terms between these components in the TFD. This may not pose a problem when the components exist at the same time and are separated in frequency, but may pose a problem when they are separated in time, particular if they approximately have the same frequency. For these signals types, cross-terms will appear in between, in time, two components separated in time and may appear as one longer component. Although the cross-terms will oscillate in the frequency direction with a frequency related to the separation distance and thus have a different structure to the LFM-like components, they may cause confusion for the detection method and will certainly undermine property P1.

  We can eliminated these cross-terms by smoothing in the frequency direction, which is equivalent to low-pass filtering along the Doppler axis in the Doppler–lag domain. Again, lets use a test signal to illustrate the point. The signal,

$$z_b(nT) = \mathrm{rect}_{N/4}\left(n - \tfrac{N}{8}\right)\, \mathrm{e}^{\mathrm{j}2\pi 0.15nT} + \mathrm{rect}_{3N/4}\left(n - \tfrac{7N}{8}\right)\, \mathrm{e}^{\mathrm{j}2\pi 0.15nT}$$

  plotted in Fig. 6.4a shows this effect. When an LI kernel is employed, no smoothing takes place in the frequency direction. Thus the cross-terms are not suppressed for the MB distribution, as Fig. 6.4b shows. An example of a nonseparable kernel, the Choi–Williams distribution [132], contains limited smoothing in the frequency

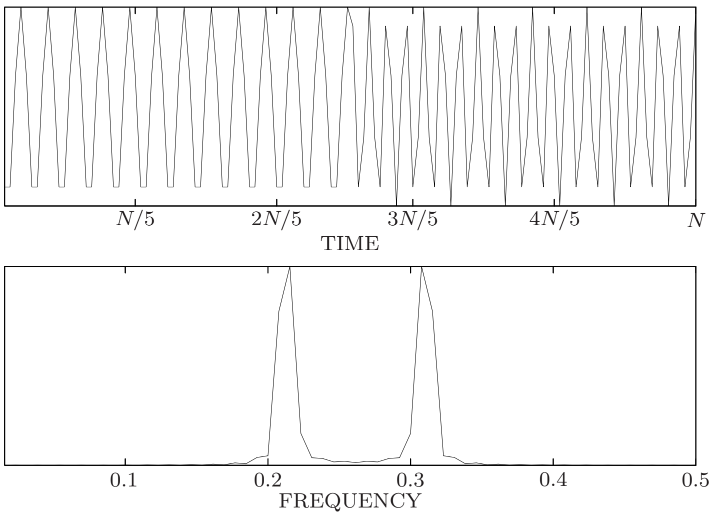

(a) Time and frequency plots for $z_a(nT)$

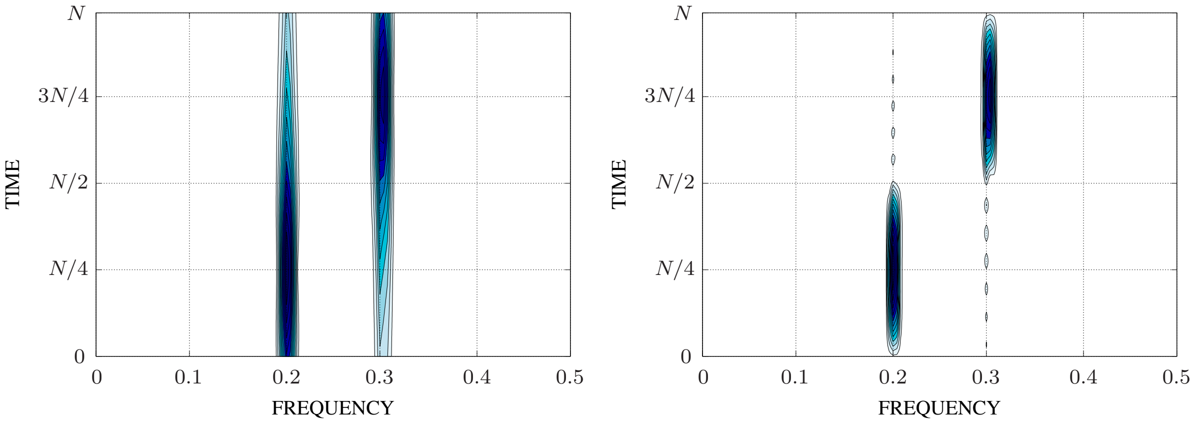

(b) MB distribution of $z_a(nT)$ with $\beta = 0.01$

(c) MB distribution of $z_a(nT)$ with $\beta = 0.01$ with time-support enforced on the kernel

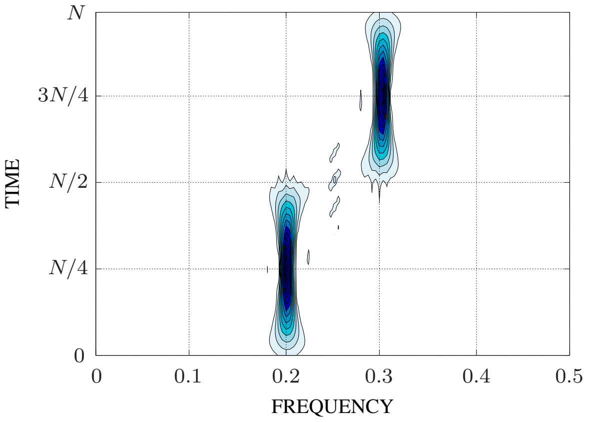

(d) MB distribution of $z_a(nT)$ with $\beta = 0.1$

FIGURE 6.2: Effects of convolving, in the time direction, with an LI kernel. The test signal used is $z_a(nT)$, with sampling period $T = 1$.

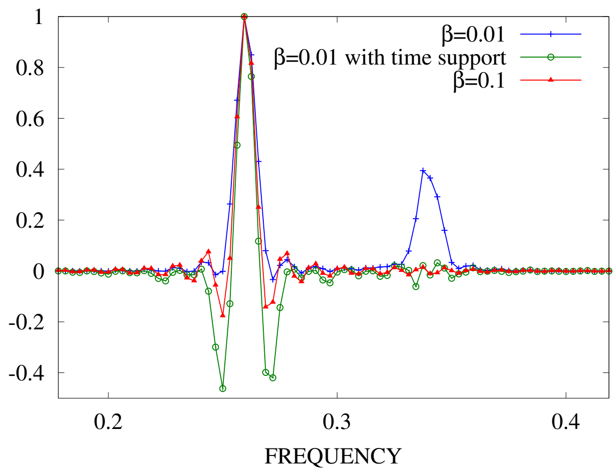

FIGURE 6.3: Time slice at $n = 30$ for the three distributions, MB with $\beta = 0.01$, MB with enforced time-support and with $\beta = 0.01$, and MB with $\beta = 0.1$.

direction, as the kernel's shape in the Doppler–lag domain is like a two-dimensional Gaussian centred at the origin. Fig. 6.4c illustrates this limited suppression of cross-terms. The non-separable kernel provides more flexibility in terms of frequency direction smoothing, as this is controlled by the lag part of kernel $g_2(\tau)$. Thus high attenuation of these cross-terms is achieved by decreasing the bandwidth of $g_2(\tau)$, as shown in Fig. 6.4d.

For the EEG background, if using the separable-kernel TFD then care should be taken on setting the parameters for $g_1(\nu)$ and $g_2(\tau)$. The Doppler window $g_1(\nu)$ should be large enough to ensure that excessive smoothing does not take place in the time direction in the time–frequency domain. Also, the lag window $g_2(\tau)$ should be small enough to ensure that some smoothing does take place in the frequency direction in the time–frequency domain.

In conclusion, both seizure and background events are best represented by different TFDs. A separable-kernel TFD with a small Doppler window and a large lag window to smooth cross-terms whilst preserving the resolution of the auto-terms would suit seizure events. Conversely, a Wigner–Ville spectrum to emphasis the stochastic nature of the background would suit background events. As a comprise, I propose using a separable-kernel TFD with medium sized Doppler and lag windows. The separable-kernel TFD is more flexible than the nonseparable-kernel as it can smooth in both the time and frequency directions independently. The following seizure detection method uses the separable-kernel TFD.

6.5 Newborn EEG Time–Frequency Matched Filter Method

Boashash and Mesbah [103] proposed using the time–frequency matched filter method to detect seizure in newborn EEG. The method correlates a template set, a collection of seizure-like events, with the EEG signal in time–frequency as follows:

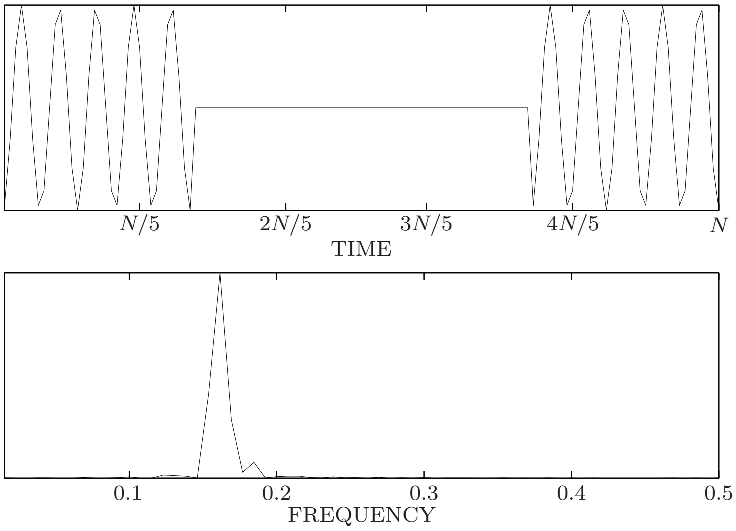

(a) Time and frequency plots for $z(n)$.

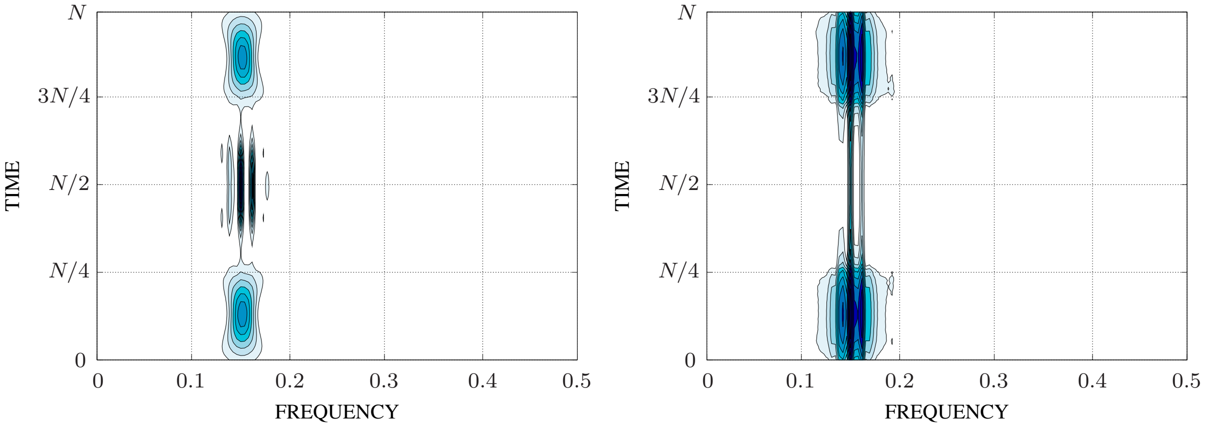

(b) MB distribution, $\beta = 0.1$.

(c) CW distribution, $\sigma = 1$.

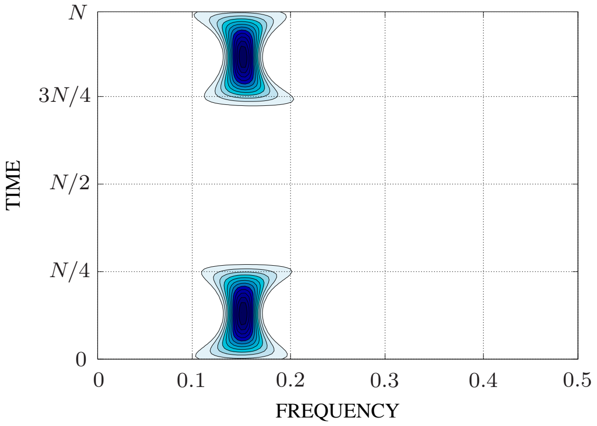

(d) Separable kernel distribution, $g_1(t)$ is a Hanning window of length 15 and $g_2(\tau)$ is a Barttlett window of length 43

Figure 6.4: Comparison of three distributions and their cross-terms. The test signal used is $z_b(nT)$, with sampling period $T = 1$.

1. form the TFD ρ_{eeg} for EEG signal $\text{eeg}(t)$ for an epoch of length T;
2. form the TFD ρ_r for reference signal $r(t)$ from the template set;
3. produce the time–frequency matched filter test statistic, shifting over time and frequency:
$$\eta_{\text{tf}}(t,f) = \int\int_{(T)} \rho_{\text{eeg}}(t',f')\rho_r(t'-t,f'-f)\,\mathrm{d}t'\,\mathrm{d}f'$$
4. threshold $\eta_{\text{tf}}(t,f)$ to a predefined constant c; that is, if $\eta_{\text{tf}}(t_0,f_0) < c$ at the point (t_0,f_0) then let $\eta_{\text{tf}}(t_0,f_0) = 0$;
5. extract the instantaneous frequency (IF) from $\eta_{\text{tf}}(t,f)$;
6. if the IF is continuous for more than 20 seconds then declare seizure for the epoch.
7. iterate over all the reference signals in the template set;
8. iterate over all epochs for the EEG signal.

The authors in [103] use the piecewise LFM signal model to characterise EEG seizure. Hence the template set is a collection of piecewise linear frequency modulated (LFM) signals with different LFM slope parameters.

The method produced excellent results for simulated EEG data [103] but poor results, with high false detection rates, for real EEG data [133, 55]. Defining the template set is a major problem for the method. Although the piecewise LFM model, or piecewise LFM model with harmonic components [122], can accurately model seizure events [122], the parameters in these models vary from newborn to newborn, or even from EEG channel to channel in the same patient [133]. Thus the method requires a large template set to represent patient or channel specific seizures. The size of the template set is, however, proportional to the probability of error—as the template set size increases so does the false alarm rate [14, 55].

6.5.1 Modified Method

To try and address this problem, I proposed a modified time–frequency matched filter method to reduce the template set size by one-half [55]. This method reduces the false detection rate of the Boashash–Mesbah method without reducing the true detection rate. The size of the template set is reduced by defining the templates as a real-valued functions in the Doppler–lag domain. For the Boashash–Mesbah method, the piecewise LFM signal has $2L$ parameters, where L is the number of pieces. For example, a 2-piece LFM signal requires $[T_1, T_2, \alpha_1, \alpha_2]$, where T_i is the time duration and α_i is the slope of the i-th piece, to uniquely define the signal. The modified method in [55] requires only the slope α_i parameter; thus for our 2-piece LFM example this modified method requires only the parameters $[\alpha_1, \alpha_2]$.

To explain how this modified method works, lets start with the test statistic $\eta_{\text{tf}}(t,f)$, which equates to
$$\eta_{\text{tf}}(t,f) = \underset{\nu\to t}{\mathcal{F}^{-1}}\left\{\underset{\tau\to f}{\mathcal{F}}\left\{A_{\text{eeg}}(\nu,\tau)\hat{A}_r(\nu,\tau)\right\}\right\}$$

where $\mathcal{F}$ represents the Fourier transform and $\hat{A}_r$ is two-dimensional Fourier transform of the time- and frequency-reversed reference TFD:

$$\hat{A}_r(\nu,\tau) = \underset{t\to\nu}{\mathcal{F}^{-1}} \left\{ \underset{f\to\tau}{\mathcal{F}} \left\{ \rho_r(-t,-f) \right\} \right\}.$$

Because the reference signal is a piecewise LFM signal it will contain both auto- and cross-terms. Thus, for the Boashash–Mesbah method the reference TFD contains both the auto- and cross-terms. With the modified method, the AF $\hat{A}_r$ of the reference signal models the auto-terms only. The AF $\hat{A}_r$ is a sum of window functions $h(t)$ located along the $(\nu - \alpha_i\tau)$ axis, as this is where the auto-terms reside [126]. The AF $\hat{A}_r$ is therefore given as

$$\hat{A}_r(\nu,\tau) = \sum_{i=0}^{L-1} h(\nu - \alpha_i\tau).$$

Thus, the AF of the reference signal is independent of T_i, the length of the pieces in piecewise LFM model.

There are three advantages, comparative to the Boashash–Mesbah method, of this modified method: 1) the template set may be reduced by one-half which reduces the probability of error in the method [14]; 2) by defining the AF as a sum of smoothing functions located on the auto-terms of the piecewise LFM model, the modified method is more robust to differences between the template and EEG seizure epoch because the method needs only match the auto-terms and not the cross-terms; and 3) the computational load is reduced by one-half because of the smaller template set size. These first two advantages are reflected by the results in [55] which show how the modified method outperforms the Boashash–Mesbah method. Although these results reflect an improvement, the main problem still exists—how best to predefine the template set?

6.5.2 Proposed Method

I present a new EEG seizure detection method [56] which does not require a predefined template set. The method uses the time–frequency matched filter and, as described in Section 6.3.1, produces the hypothesis by comparing the test statistic to a predefined threshold. This approach differs to the Boashash–Mesbah and modified Boashash–Mesbah methods, which use the test statistic as a time–frequency representation to extract an IF law.

The proposed method uses the principal that, because the seizure event is repetitive in nature, a short-time segment of the seizure should correlate well with an adjacent short-time segment. That is the principal that Navakatikyan [99] bases his method on. The proposed method uses additional prior information however. We know, from time–frequency analysis, that a seizure signal is best represented by a piecewise LFM with or without additional harmonics [125, 122]. The proposed method correlates time-adjacent, short-time segments in the time–frequency domain to match a slowly varying IF law with or without harmonic components. This method correlates two TFDs, not WVDs, in the time–frequency domain and therefore differs from the time-domain matched filter.

The outline of the method is as follows. First, define an epoch of length T_e seconds. Then, spilt this epoch up into 4 segments each of length $T_s = T_e/4$. The method assumes

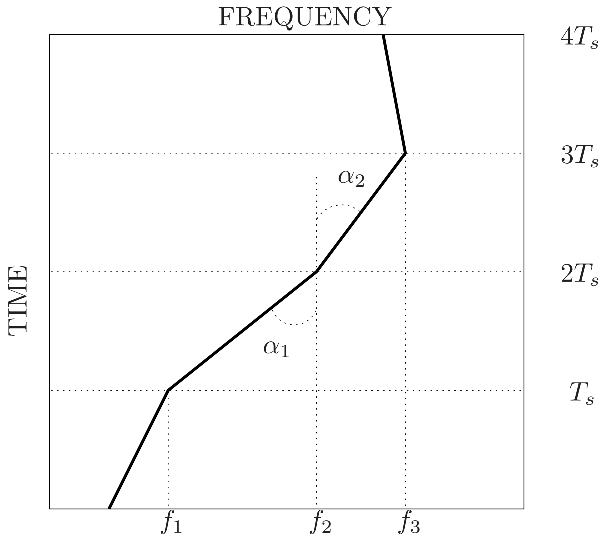

FIGURE 6.5: The epoch TFD split into 4 segments of length T_s. The bold line represents the IF law of the signal.

that the IF laws in each segment is linear, although these IF segments can have different slope values. Next, correlate segment one with segment two, rotating segment one to allow for a difference in slopes between the two segments. Continue this procedure for all the segments; that is, segment 2 correlated with segment 3, and segment 3 correlated with segment 4. Finally, find the minimum test statistic from these correlations and compare this with a threshold to produce the hypothesis.

The advantage of this method over the previous two methods is that the method does not require a predefined template set. I now present the details of the method.

The detection process is as follows.

1. Split the EEG data up into epochs $\text{eeg}_j(t)$ of length T_e.

2. Form the TFD for $\text{eeg}_j(t)$ as $\rho_{\text{eeg}}(t,f)$.

3. Divide this TFD, in time, into four segments of length $T_s = T_e/4$, known as $\rho_i(t,f)$ for $i = 0, 1, 2, 3$. This segmentation process is illustrated in Fig. 6.5.

4. iterate the following over $i = 1, 2, 3$:

   (a) Define the template TFD $\hat{\rho}$ for the i-th segment as a time inverted TFD $(i-1)$ segment; that is, let

   $$\hat{\rho}_{(i-1)}(t,f) = \rho_{(i-1)}(iT_s - t, f).$$

   Thus, the time inverting process for $\rho_{(i-1)}(t,f)$ is equivalent to turning the TFD segment upside down in time.

   (b) Rotate the template TFD $\hat{\rho}_{(i-1)}$ over a set of discrete angles $\Theta = \{\theta_1, \theta_2, \ldots, \theta_K\}$; let

   $$\rho_i^{\mathrm{T}}(t,f;\theta_k) = \hat{\rho}_{(i-1)}(t,f) \underset{f}{*} W_{m_k}(t,f), \tag{6.13}$$

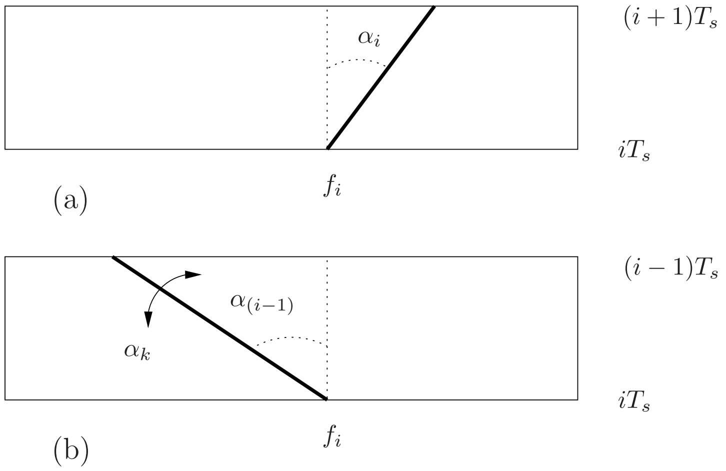

FIGURE 6.6: The i-th TFD segment (a) $\rho_i(t,f)$ and (b) template TFD $\rho_i^{\mathrm{T}}(t,f;\theta_k)$. Note that the template TFD is a time-reversed version of the $(i-1)$ TFD segment. The template TFD is rotated about a set of angles to attempt a match with the i-th TFD segment. This example is taken from Fig. 6.5 for $i=2$.

where $m_k(t) = \mathrm{e}^{\mathrm{j}2\pi(\theta_k/2)t^2}$ and θ_k is from the set Θ. This results in a set of rotated TFD templates.

(c) Correlate the template set with the i-th segment TFD,

$$\eta(\theta_k) = \int\int_{(T_s)} \rho_i(t,f)\rho_i^{\mathrm{T}}(t,f;\theta_k)\,\mathrm{d}t\,\mathrm{d}f$$

and then take the maximum test statistic,

$$\eta_i = \max_{\theta_k \in \Theta} \eta_i(\theta_k).$$

Fig. 6.6 illustrates this process.

Why is this rotation process necessary? Recall that we have assumed a piecewise LFM-type signal is present in $\rho_{\mathrm{eeg}}(t,f)$ and that the turning points of the IF in the TFD segments are located at $t = t_s + iT_s$. Because the IF law for the continuous component passes through the time–frequency point $(t_s + iT_s, f_i)$, then $\bar{\rho}_{(i-1)}(t,f)$ and $\rho_i(t,f)$ will be equal around $t=0$, as Fig. 6.5 illustrates. If the slope of the LFM in the $(i-1)$ segment, $\alpha_{(i-1)}$, does not equal the slope, α_i, in LFM of the i-th segment, then the correlation between the $(i-1)$ and i segments will be small. Thus, if we rotate the template TFD $\bar{\rho}_{(i-1)}(t,f)$ about the point $(0,f_i)$ to the angle $\alpha_k = \alpha_{(i-1)} + \alpha_i$, then the two TFD segments would match and produce a large correlation. Fig. 6.6 illustrates this process.

5. The test statistic for the epoch is

$$\eta = \min_{i \in \{1,2,3\}} \eta_i$$

The rationale for this is that if the LFM component is continuous and present throughout the four segments, then each η_i will remain relatively large; likewise, if the LFM component is not present over all segments then η will be reduced. Thus, the size of the epoch T_e should reflect some lower limit on the duration of the EEG seizure.

6. Although the seizure LFM-type components can have slope values as large as ±0.1Hz per second, the rate of slope change is rather small over an epoch of less than 20 seconds [103, 122]. Therefore, the method has a penalisation measure to prevent false detections of components that do not conform to this signal type. This is achieved by first specifying the rotation angles selected from $\eta_i(\theta_k)$,

   $$\tilde{\theta}_i = \arg\max_{\theta_k \in \Theta} \eta_i(\theta_k).$$

   and then defining the penalisation function as

   $$c(\sigma) = \left(1 - \frac{\sigma}{w}\right) \tag{6.14}$$

   where σ is the variance of $\tilde{\theta}_i$ over $i = 1, 2, 3$. The value w in (6.14) is a predefined weighting parameter in the range $\sigma < w < \infty$. Limiting w ensures that $0 < c(\sigma) < 1$. Within the range $\sigma < w < \infty$, as $w \to \infty$ then $c(\sigma) \to 0$ and as $w \to \sigma$ then $c(\sigma) \to 1$.

   We then use the function $c(\sigma)$ to weight the epoch's test statistic η; that is, let

   $$\eta \leftarrow c(\sigma)\eta.$$

   If the variance of the slope values σ is large, then $c(\sigma)$ will be small and thus reduce the value of η. Simply put, a large value for σ will penalise the test statistic. This is desirable as a large σ value indicates a signal type that is not slowly varying, and therefore not a seizure signal [103, 122]. Conversely, when σ is small then $c(\sigma)$ will be small and the test statistic η will not be heavily penalised. A small σ value is indicative of a signal with a slowly varying IF, such as a seizure signal.

7. Is seizure present?

   $$\begin{aligned} &\eta < \zeta, && \text{no seizure,} \\ &\eta > \zeta, && \text{seizure present,} \end{aligned}$$

   where ζ is the predefined detection threshold.

8. Iterate this whole process over the different EEG epochs with an overlap window.

Limitations and Assumptions for Method

The method assumes that the EEG signal is a piecewise LFM signal where the end time points of the pieces, known as turning points, are located at the end of the TFD segments $t = iT_s$. The turning points for the EEG will not be an abrupt or sudden change in the IF law because, as others have observed [103,109], EEG seizure typically has a continuous IF law that varies slowly and smoothly over time [103] and because the TFD provides some time–frequency smoothing of the components. Hence the method should be able to cope with the situation when the turning points are not located at values of iT_s. The results in the next section support this statement.

EEG background may have discontinuous LFM-like components, which could results in a false detection for the method. Two scenarios could cause this: if the discontinuous components are centred in time around iT_s, or if the discontinuous components are equidistant in time from iT_s, for $i = 1, 2, 3$. To ensure that these scenarios do not produce a large η value, the method uses a sliding window on the data with a significant overlap, larger than 75% of T_e. Thus, by shifting the EEG by a fraction of T_s, the LFM-like components will no longer be centred around the turning points or equidistant from the turning points and therefore the method should not produce a large ζ value. Again, the results in the next section support this statement.

The description of the method shows, in Fig. 6.5 and Fig. 6.6, a piecewise LFM signal model without harmonic components. Whether the piecewise LFM model has harmonic components or not, the method will produce a large test statistic for both these signal types. This is because the harmonic components have IF laws that are parallel to the main component's IF law. Therefore, when the main component's IF laws are matched in the correlation process the harmonic components will also match and the method will produce a large ζ value. Note that most of EEG seizure signals from the next section are signals with harmonic components.

Results

The method uses a quadratic TFD, but which type of TFD to use and why? Appendix 6.4 presents a discussion on the merits of using different TFDs for newborn EEG seizure detection. Based on this analysis, the method uses the separable-kernel TFD. The time–frequency kernel is represented as $\gamma(t, f) = g_1(t)G_2(f)$, where $g_1(t)$ is a Hamming window of length $T_e/12$ and $g_2(\tau)$, the Fourier transform of $G_2(f)$, is a Hanning window of length $T_e/3$.

The TFD epoch length was set at $T_e = 11.4$ seconds with an epoch overlap over of 10 seconds. A vector of slopes of length $K = 8$ was used, ranging linearly from -1 to 1 Hz/sec. The penalisation function $c(\sigma)$, defined in (6.14), used a weight value of $w = 0.08$.

To implement the method on a computer, we must first define a discrete version of the method. Thus, the TFD requires a discrete definition. For this, I used the DTFD definition proposed in Chapter 4 with the discrete analytic signal proposed in Chapter 3. The method used the separable-kernel DTFD algorithm proposed in Chapter 5 to compute the DTFD.

I tested the method on real and simulated data, which was segmented into 12.8 second epochs. The simulated data, using the method proposed by Rankine *et al.* [122], contained 400 epochs of background and 400 epochs of seizure. This data models seizure events as piecewise LFM signals with harmonic components and models background events as nonlinear, nonstationary stochastic signals. For the real data, I used a set of 100 epochs taken from 6 different babies. I filtered the data in the range from 0.5 to 10Hz and down sampled to 20Hz. To assess the performance of the method, I used receiver operator characteristic (ROC) plots to show true detection and false detection rates over a range of different threshold values ζ. Also, to compare different results, I used the area under curve (AUC) measure as a single measure of overall performance.

Test 1: Simulated Data The purpose of the first test is to show why using the time–frequency matched filter outperforms using the time-domain matched filter in this application. To do so, the method uses the DWVD, because of the relation in (6.3), to represent the time-domain matched filter approach.

The simulated EEG data consists of two data sets: one set of seizure epochs and background epochs and another set of seizure epochs combined with background epochs, at signal to background ratio (SBR) of 5dB, and background epochs. As real EEG seizure events evolve over time from the background, combining the seizure epochs with the background epochs may give a more accurate representation of EEG seizure [134].

- **Test 1a. DWVD-A versus DWVD-C**

  The test also shows how the performance of different DWVD definitions compare. For the test, which uses simulated data, I compare the difference between two DWVD definitions: DWVD-A and DWVD-C. The DWVD-A does not satisfy Moyal's formula, a requirement for the optimum time–frequency matched filter as mentioned previously. The DWVD-C does satisfy this property, and this is reflected in the results: the AUC for the DWVD-A is less than the AUC for the DWVD-C as Fig. 6.7 shows. Richard [14] and Yasotharan and Thayaparan [135] reported similar results—they showed that the DWVD-B, which also satisfies Moyal's formula, outperforms the DWVD-A in the detection problem.

- **Test 1b: GDTFD versus Proposed DTFD**

  Next, I compare two DTFD definitions for the separable-kernel DTFD. The results in Fig. 6.8 produces another interesting results: although Moyal's formula is not satisfied by the separable-kernel DTFD, the proposed DTFD, from Chapter 4, outperforms the GDTFD for the data set with the 5dB SBR. For the other data set, both DTFD definitions perform well with an AUC value close to one.

Comparing the results from test 1a, in Fig. 6.7, and test 1b, in Fig. 6.8, we see that the method gives better performance when the DTFD, rather than the DWVD, is used in the method. This result justifies using the time–frequency matched filter in (6.4) rather the using the conventional time-domain matched filter method in (6.1). Although the time-domain matched filter is an optimum detector, the conditions which the optimum detector requires are violated in this data: the simulated data consists of nonlinear, nonstationary components for seizure and background data [122]. Richard noted similar results when comparing the DWVD-B with a DTFD for a sub-optimum detection problem [14].

Test 2: Real EEG Data For the real EEG data, I again use the GDTFD and proposed DTFD to compare performance. Similar to the simulated data results, the method using the proposed DTFD outperforms the method using the GDTFD, as Fig. 6.9 shows. The method performs well for this data set with an AUC value of 0.94. By selecting a point from the ROC plots, the method produces a 90% true detection rate with a false detection rate of 10%.

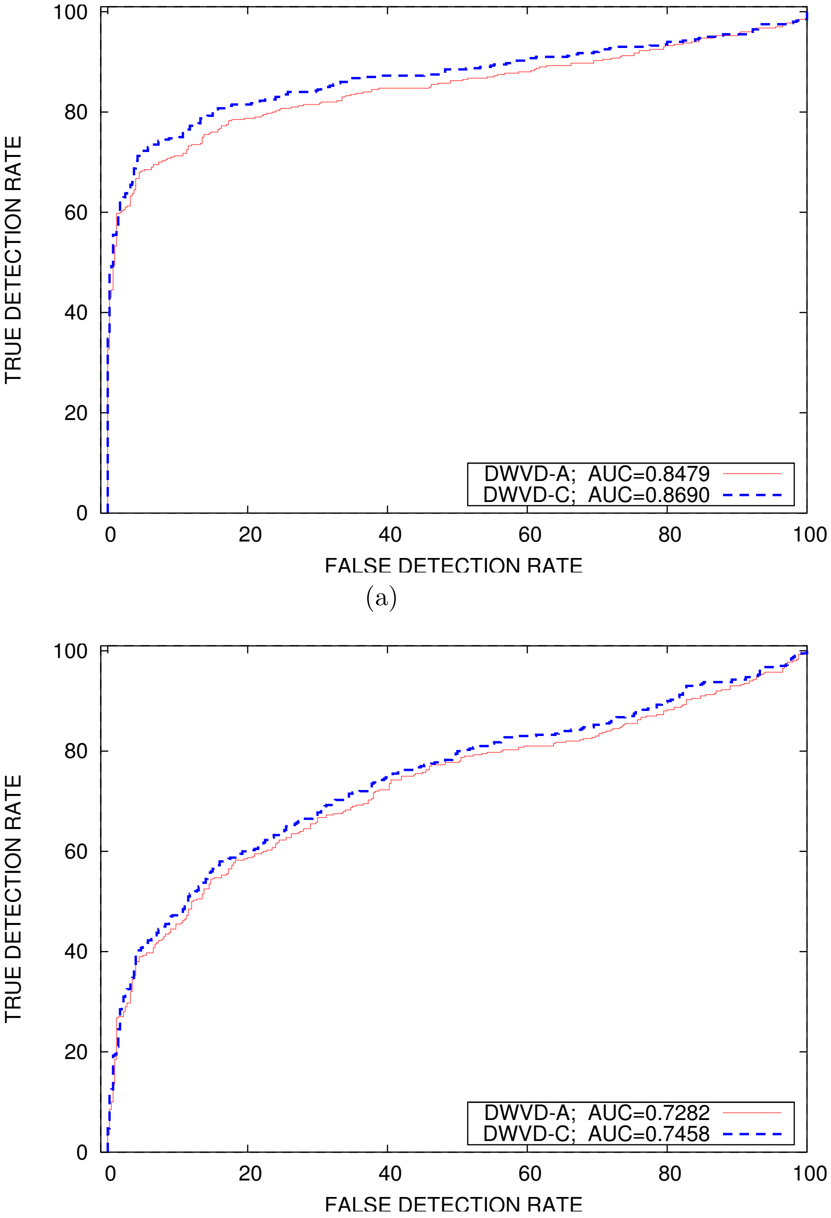

(a)

(b)

Figure 6.7: EEG seizure detection method using simulated data, 400 epochs background and 400 epochs of seizure. The method uses both the DWVD-A and the DWVD-C. (a) Seizure epochs with no noise, and (b) seizure epochs with 5dB of background added to it. Area under the curve (AUC) is in the label tag.

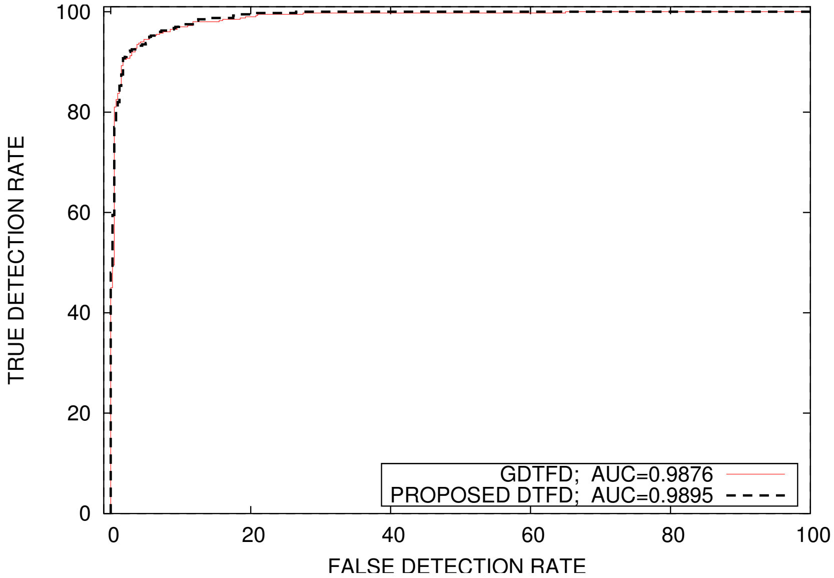

(a)

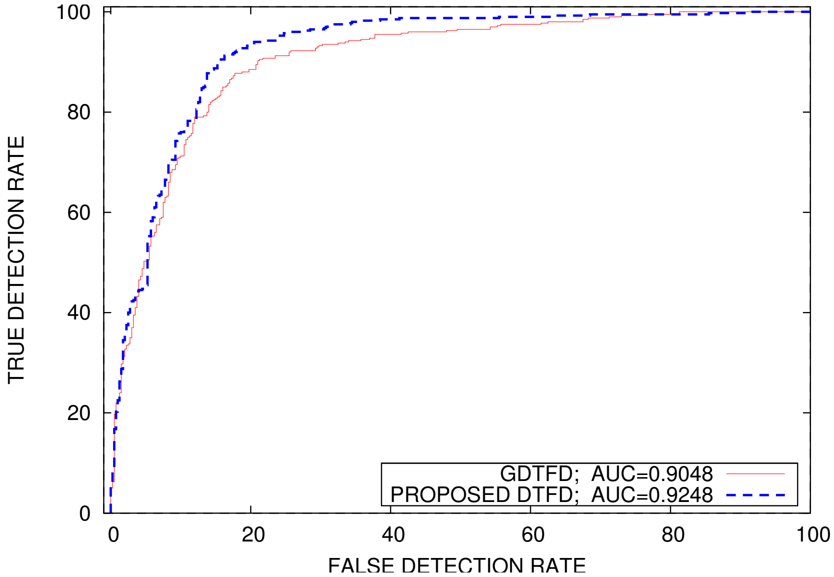

(b)

FIGURE 6.8: EEG seizure detection method using simulated data, 400 epochs background and 400 epochs of seizure. The method uses both the GDTFD and the proposed DTFD. (a) Seizure epochs with no noise, and (b) seizure epochs with 5dB of background added to it. Area under the curve (AUC) is in the label tag.

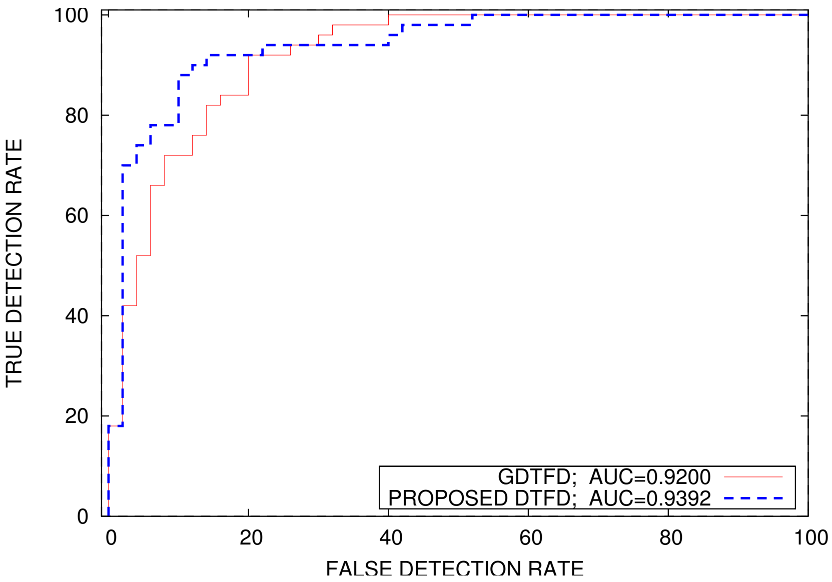

Figure 6.9: EEG seizure detection method using real EEG data, 50 epochs of background and 50 epochs of seizure. The method compares using the GDTFD and the proposed DTFD.

The method, however, needs further testing. The proposed method needs to be tested on a continuous recording of EEG, rather than the short epoch segments used in the previous results section. Also, the proposed method could benefit from optimising some model parameters, in particular the set of slopes Θ and the weighting parameter w for the penalisation function $c(\sigma)$. Finally, this method should be compared with other existing methods, such as existing time–frequency matched filter methods [55] and the Navakatikyan method [99], using a common data set to assess its relative performance.

6.6 Summary and Conclusions

The chapter presented a newborn EEG seizure detection method. The purpose of this chapter was to provide an application for the previous work: the detection method uses the discrete analytic signal from Chapter 3, the proposed DTFD from Chapter 4, and the proposed algorithms from Chapter 5. The proposed detection method is based on the existing Bosashash–Mesbah time–frequency matched filter method and the Navakatikyan method. The method—which correlates time-adjacent, short-time EEG segments in the time–frequency domain—assumes that the seizure is represented in the time–frequency domain by a series of slowly evolving LFM signals. This assumption is consistent with the clinician's definition of a slowly evolving periodic signal [88] and engineer's description of the nonlinear, nonstationary signal [122].

The results for the method are promising, although further testing is needed. The method needs testing on a large EEG database and compared with other existing methods. The results also show the usefulness of the proposed DTFD—the method with the proposed DTFD outperforms the method with GDTFD.

Chapter 7

Conclusion

7.1 Introduction

The purpose of signal processing is to extract useful information from signals. There can be two parts to this process: the analysis of signals, which describes or characterises the signal; and the processing of signals, which modifies or transforms the signal. Both the analysis and processing of signals can be done in a joint time–frequency domain. This two-dimensional domain is particularly useful for analysing or processing *nonstationary* signals, as these signals have frequency content that changes over time.

There are many different ways to represent the time–frequency domain. In this dissertation, I considered only the most commonly-used type of time–frequency representation—the quadratic time–frequency distribution class. The broad goal of this work was *to make the quadratic class of time–frequency distributions a more effective signal processing tool.*

My contribution to this goal was to improve the implementation of time–frequency distributions (TFDs) on a digital device, such as a computer. To compute a TFD, we need a discrete version of the TFD. The work, which focused on discrete TFDs (DTFDs), had three broad themes:

1. *theory:* improved, comparative to existing methods, the definition of DTFDs;
2. *computation:* designed algorithms to efficiently compute the DTFD;
3. *application:* showed how DTFDs can be used to solve practical signal processing problems.

I now present some conclusions from this work.

7.2 Conclusions

- Chapter 2 presented a new discrete WVD definition, the DWVD-C, which, similar to the existing DWVD-B definition, satisfies all important mathematical properties inherent to the continuous WVD.

    - The proposed DWVD-C and DWVD-B are closely related—DWVD-C is a frequency-decimated version of DWVD-B.

  - Because of this decimation relation, DWVD-C, comparative to DWVD-B, requires only one-half of the computational load and memory required to compute and store the DWVD.

- Chapter 3 presents a new discrete analytic signal. By using this proposed signal, compared with using the conventional signal, we can reduce aliasing in the DWVD by approximately 50%. The amount of aliasing in the discrete WVD is dependent on two things:

  - *signal length N:* as N increases, aliasing decreases. This is because as N goes to infinity, we move away from the finite-time, finite-frequency bandwidth constraint.
  - *signal type:* I found, experimently, that signals with more energy near the DC and Nyquist frequencies produced more aliasing in the DWVD. This is probably because the energy leaks into the nearby negative-frequency region. (Because the discrete signal is periodic, the region near the Nyquist frequency is nearby the negative frequency region.)

  In addition, the proposed discrete analytic signal retains the two useful attributes of the conventional discrete analytic signal: the signal recovery and orthogonality properties and an efficient, simple implementation.

- Chapter 4 presents a new DTFD definition. The proposed DTFD definition improves on the two popular DTFD definitions—it is pseudo-alias free and satisfies all important TFD properties. In contrast, the GDTFD definition does not satisfy all these properties and the AF-GDTFD is not always pseudo-alias free.

  - I defined the term pseudo-alias free to refer to a DTFD that contains minimal aliasing—aliasing only from the discrete analytic signal's approximation of the finite-time, finite-frequency bandwidth constraint. Otherwise, a distribution using the discrete real-valued signal will contain aliasing caused by the periodic overlap of the signal's components in time and frequency. The type of aliasing caused by the real-valued signal is significantly greater than the aliasing caused by the discrete analytic signal.
  - The proposed DTFD definition is based on the *smoothed DWVD* form; that is, I define the DTFD as a DWVD (circularly) convolved with a discrete kernel. This differs from the AF-GDTFD definition, which is based on sampling the TFD. Consequentially, some types of distributions, which do not fit well into the smoothed DWVD form, may not be contained in the proposed DTFD. For example, the proposed DTFD does not contain a spectrogram, although it does contain a positive distribution that closely approximates a spectrogram. I designed the proposed DTFD as a smoothed DWVD as this is the most common quadratic TFD form.

- Chapter 5 presents algorithms to minimise the computational load and memory needed to compute the proposed DTFD. These algorithms can be categorised into two groups: one group computes the DTFD exactly; the other group, in an effort to save memory, computes a decimated version of the DTFD. Both groups consist of four kernel-specific algorithms.

The two groups of algorithms are designed to minimise computational load—this makes the algorithms execute faster. Yet probably the most limiting factor for the DTFD algorithms is the signal's length, N, as the algorithm requires an array of $2N^2$ points. Thus, the computer must be able to store $2N^2$ real-valued numbers. This memory limit is different to the computational load: the computer must have this memory to compute the DTFD, whereas computational load is proportional to processing time and does not have a similar hard limit. For example, an algorithm requiring a large computational load may require hours, days, or even months to compute; an algorithm requiring more memory than available will simply not compute.

  - The first group of DTFD algorithms address this limitation to a certain degree. Depending on the kernel type and the region of nonzero support for the kernel, these algorithms produce DTFDs with a reduced number of sample points—thus reducing the memory required. Note that this is not the same as decimating the DTFD as no signal information is lost in the DTFD; rather the time or frequency resolution is adjusted in accordance with the kernel's time–frequency bandwidth. This process is common in discrete spectral analysis.
  - The second group of DTFD algorithms, however, produce decimated DTFDs—that is, DTFDs requiring $2N^2/(ab)$ real-valued numbers, where a, b are integers. Of course, because this group of algorithms do not compute the full DTFD array, its not a *proper* representation of the DTFD, rather an approximation which does not provide all the sample points of the DTFD. Yet these algorithms allow the user to adjust this memory hard-limit by choosing suitable values for a and b.

- Chapter 6 presents a newborn EEG seizure detection method. Of note:
  - The detection of newborn EEG seizures require nonstationary signal processing techniques.
  - The time–frequency matched filter, using TFDs, gives better performance compared with the performance of the time-domain matched filter.
  - The proposed time–frequency matched filter, which does not require a predefined template set, outperforms the existing time–frequency matched filter, which does require a predefined template set, because of the newborn's variability of EEG seizure characteristics.
  - The proposed time–frequency matched filter using the proposed DTFD produces better detection results comparative to same method using the GDTFD. This is expected as the GDTFD is a frequency-decimated version of the proposed DTFD and does not satisfies Moyal's formula—a important property for the time–frequency matched filter [118, 14].

7.3 Future work

There is no end-point to exploratory science. Methods in science should be constantly challenged, questioned, and then, if possible, updated. With this in mind, I point to a few areas where the methods in this dissertation may be extended. Undoubtedly, there is much work to be done.

1. Does the proposed discrete analytic signal have applications in other areas of signal processing? Will this signal improve the instantaneous frequency estimate of the analytic signal [61]? Would it be useful in reducing aliasing in the discrete wavelet transform [69]?

2. The proposed discrete analytic signal satisfies the frequency constraint but not the time constraint. The time constraint is satisfied by appling a rectangular window to the signal. It may be possible to achieve better performance by applying a smooth tapered window rather than the rectangular window. Even though the resultant signal would satisfy neither the frequency nor time constraint, this approach may reduce the total energy in the ideally-zero regions comparative to that for the proposed analytic signal. Additionally, an optimisation process applied to the parameters of the tapered windows may further minimise the energy in the ideally-zero regions for both domains.

3. The discrete analytic signal produces aliasing in the DWVD because it does not satisfy both the time and frequency constraints. To form the DTFD we convolve the DWVD with a kernel—does the convolution with this kernel effect aliasing? And if so, why? If we could answer these questions then we might be able to design a kernel to eliminate or better suppress the aliasing.

4. The algorithms in chapter 5 compute the DTFD using circular convolution between the DWVD and the kernel. This circular convolution operation may produce undesirable wrap-around effects [23]. To eliminate these wrap around effects, we could use linear convolution instead. These algorithms could be easily extended to use linear convolution as well as circular convolution.

5. The EEG seizure detection method needs to be compared with other detection methods using a full EEG database.

Appendix A

Discrete Fourier Transform

A.1 Sampling Time-Domain Signals

To sample the time-domain $x(t)$ we take discrete points at intervals of T. This discrete signal $x(nT)$ is illustrated in Fig. A.1a. Another sampling approach is to multiply $x(t)$ by an infinite sequence of delta functions, known as an impulse train [23], as follows:

$$\begin{aligned} x_{\mathrm{i}}(t) &= x(t)\sum_{n}\delta(t-nT) \\ &= \sum_{n} x(nT)\delta(t-nT). \end{aligned}$$

This operation results in the continuous time-domain signal $x_{\mathrm{i}}(t)$, illustrated in Fig. A.1b. The signal $x_{\mathrm{i}}(t)$ is zero everywhere except at $t = nT$, where n is an integer. For $t = nT$, this signal is not defined, although the area under this impulse is equal to $x(nT)$. This signal $x_{\mathrm{i}}(t)$ is used to develop discrete signal processing theory.

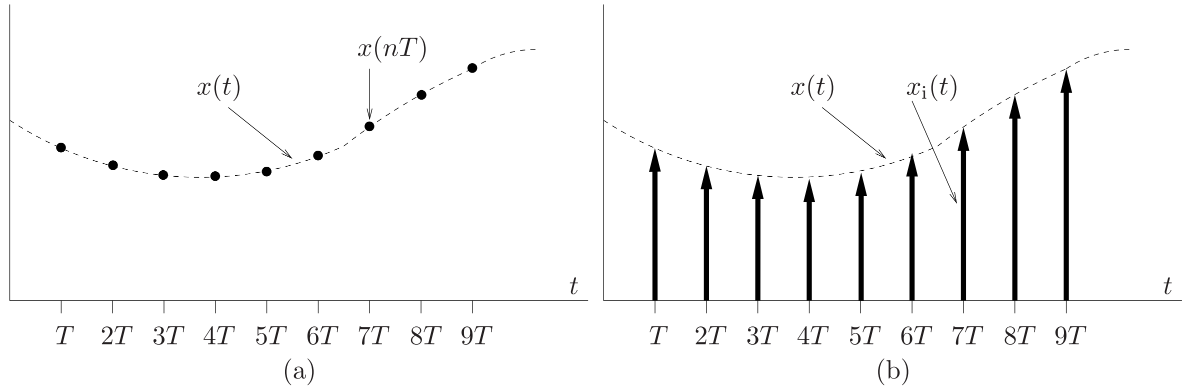

(a) (b)

FIGURE A.1: Two types of sampled signals: (a) the discrete-time signal $x(nT)$ represented by the black dots and (b) continuous sampled signal $x_{\mathrm{i}}(t)$, represented by the vertical arrows.

A.2 Discrete-Time Fourier Transform

The discrete-time Fourier transform [136],

$$\tilde{X}(f) = \sum_n x(nT)\, \mathrm{e}^{-\mathrm{j}2\pi nTf}$$

maps the discrete-time signal to the frequency domain and the inverse discrete-time Fourier transform,

$$x(nT) = \int_{-\frac{1}{2T}}^{\frac{1}{2T}} \tilde{X}(f)\, \mathrm{e}^{\mathrm{j}2\pi fnT}\, \mathrm{d}f \tag{A.1}$$

maps the continuous-frequency signal $\tilde{X}(f)$ to the discrete-time domain. These two transforms are the discrete-time version of the continuous Fourier transform pair in (2.8) and (2.9).

The following relates $\tilde{X}(f)$ to $X(f)$. The Fourier transform of the sampled signal $x_{\mathrm{i}}(t)$ is also equal to $\tilde{X}(f)$:

$$\begin{aligned}\mathcal{F}\left[x_{\mathrm{i}}(t)\right] &= \int \sum_n x(nT)\delta(t-nT)\, \mathrm{e}^{-\mathrm{j}2\pi tf}\, \mathrm{d}t \\ &= \sum_n x(nT)\, \mathrm{e}^{-\mathrm{j}2\pi nTf} = \tilde{X}(f)\end{aligned}$$

where $\mathcal{F}\left[\cdot\right]$ denotes the Fourier transform. Again take the Fourier transform of $x_{\mathrm{i}}(t)$ but this time write the expression as

$$\begin{aligned}\tilde{X}(f) &= \int x(t) \sum_n \delta(t-nT)\, \mathrm{e}^{-\mathrm{j}2\pi tf}\, \mathrm{d}t \\ &= \int x(t)\, \mathrm{e}^{-\mathrm{j}2\pi tf}\, \mathrm{d}t \underset{f}{*} \int \sum_n \delta(t-nT)\, \mathrm{e}^{-\mathrm{j}2\pi tf}\, \mathrm{d}t \\ &= X(f) \underset{f}{*} \frac{1}{T} \sum_n \delta(f - \tfrac{n}{T}) \\ &= \frac{1}{T} \sum_n X(f - \tfrac{n}{T})\end{aligned} \tag{A.2}$$

where $*_f$ denotes the convolution operation in the frequency direction. Thus, $\tilde{X}(f)$ is equal to an infinite sum of shifted and scaled copies of $X(f)$; the period for these frequency shifted copies is $1/T$. Fig. 2.1 in Chapter 2 illustrates this relation between $X(f)$ and $\tilde{X}(f)$.

A.3 Discrete-Frequency Fourier Transform

Sampling the frequency-domain signal with sample frequency $1/\Lambda$ results in the discrete-frequency signal $X(k\Lambda)$. To transform this signal to the continuous time-domain, we use the inverse discrete-frequency Fourier transform, defined as

$$\tilde{x}(t) = \sum_k X(k\Lambda)\, \mathrm{e}^{\mathrm{j}2\pi k\Lambda t}.$$

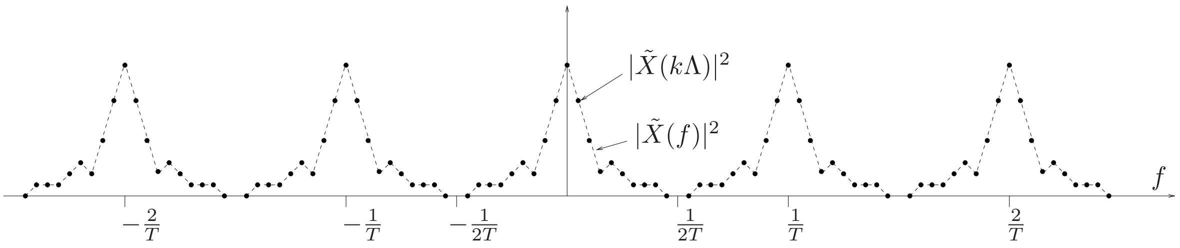

FIGURE A.2: Discrete, periodic frequency-domain signal $\tilde{X}(k\Lambda)$. Each dot represents a k separated by Λ in frequency.

and the discrete-frequency Fourier transform, defined as

$$X(k\Lambda) = \int_{-\frac{1}{2\Lambda}}^{\frac{1}{2\Lambda}} \tilde{x}(t)\, \mathrm{e}^{-\mathrm{j}2\pi t k\Lambda}\, \mathrm{d}t, \tag{A.3}$$

to map the continuous-time signal to the discrete-frequency signal.

The relation between continuous signal $\tilde{x}(t)$ and discrete signal $X(k\Lambda)$ is

$$\tilde{x}(t) = \frac{1}{\Lambda} \sum_k x(t - \tfrac{k}{\Lambda}).$$

This relation is derived using a method similar to that for the discrete-time Fourier transform from the previous section. The continuous signal $\tilde{x}(t)$ consists of periodically shifted copies of the scaled signal $x(t)$, with a period of $1/\Lambda$.

A.4 Discrete-Time, Discrete-Frequency Fourier Transform

To create a signal that is both discrete in the time and frequency domains, we need to sample both periodic continuous signals $\tilde{x}(t)$ and $\tilde{X}(f)$. We can start with either signal; lets start with $\tilde{X}(f)$,

$$\begin{aligned} \tilde{X}_{\mathrm{i}}(f) &= \tilde{X}(f) \sum_k \delta(f - k\Lambda) \\ &= \sum_k \tilde{X}(k\Lambda)\delta(f - k\Lambda). \end{aligned}$$

The signal $\tilde{X}(k\Lambda)$ is both discrete and periodic, as Fig. A.2 shows.

The following relates $\tilde{x}(nT)$ to $x(t)$. Taking the inverse discrete-time Fourier transform, in (A.1), of $\tilde{X}_{\mathrm{i}}(f)$ results in the following:

$$\begin{aligned} \int_{-\frac{1}{2T}}^{\frac{1}{2T}} \tilde{X}_{\mathrm{i}}(f)\, \mathrm{e}^{\mathrm{j}2\pi f nT}\, \mathrm{d}f &= \int_{-\frac{1}{2T}}^{\frac{1}{2T}} \sum_k \tilde{X}(k\Lambda)\delta(f - k\Lambda)\, \mathrm{e}^{\mathrm{j}2\pi f nT}\, \mathrm{d}f \\ &= \sum_k \tilde{X}(k\Lambda)\, \mathrm{e}^{\mathrm{j}2\pi k\Lambda nT} = N\tilde{x}(nT) \end{aligned}$$

and therefore

$$\begin{aligned}
\tilde{x}(nT) &= \frac{1}{N}\int_{-\frac{1}{2T}}^{\frac{1}{2T}} \tilde{X}(f)\sum_k \delta(f-k\Lambda)\,\mathrm{e}^{\mathrm{j}2\pi fnT}\,\mathrm{d}f \\
&= \frac{1}{N}\int_{-\frac{1}{2T}}^{\frac{1}{2T}} \tilde{X}(f)\,\mathrm{e}^{\mathrm{j}2\pi tnT}\,\mathrm{d}f \underset{n}{*} \int_{-\frac{1}{2T}}^{\frac{1}{2T}} \sum_k \delta(f-k\Lambda)\,\mathrm{e}^{\mathrm{j}2\pi fnT}\,\mathrm{d}f \\
&= \frac{1}{N}\int_{-\frac{1}{2T}}^{\frac{1}{2T}} \tilde{X}(f)\,\mathrm{e}^{\mathrm{j}2\pi tnT}\,\mathrm{d}f \underset{n}{*} \frac{1}{\Lambda}\sum_k \int_{-\frac{1}{2T}}^{\frac{1}{2T}} \mathrm{e}^{\mathrm{j}2\pi f(nT-\frac{k}{\Lambda})}\,\mathrm{d}f \\
&= x(nT) \underset{n}{*} \frac{1}{T\Lambda}\sum_k \delta(n-\tfrac{k}{T\Lambda}) \\
&= \frac{1}{T\Lambda}\sum_k x(nT-\tfrac{k}{\Lambda}) \qquad \text{(A.4)}
\end{aligned}$$

assuming $1/(T\Lambda)$ is an integer. That is, the discrete-time signal is now periodic with period $1/\Lambda$.

Next, we sample the periodic, continuous signal $\tilde{x}(nT)$:

$$\begin{aligned}
\tilde{x}_{\mathrm{i}}(t) &= \tilde{x}(nT)\sum_n \delta(t-nT) \\
&= \sum_n \tilde{x}(nT)\delta(t-nT)
\end{aligned}$$

and then take the discrete-frequency FT, in (A.3), of $\tilde{x}_{\mathrm{i}}(t)$,

$$\begin{aligned}
\int_{-\frac{1}{2\Lambda}}^{\frac{1}{2\Lambda}} \tilde{x}_{\mathrm{i}}(t)\,\mathrm{e}^{-\mathrm{j}2\pi tk\Lambda}\,\mathrm{d}t &= \int_{-\frac{1}{2\Lambda}}^{\frac{1}{2\Lambda}} \sum_n \tilde{x}(nT)\delta(t-nT)\,\mathrm{e}^{-\mathrm{j}2\pi tk\Lambda}\,\mathrm{d}t \\
&= \sum_n \tilde{x}(nT)\,\mathrm{e}^{-\mathrm{j}2\pi nTk\Lambda} = \tilde{X}(k\Lambda)
\end{aligned}$$

which we can also express as

$$\begin{aligned}
\tilde{X}(k\Lambda) &= \int_{-\frac{1}{2\Lambda}}^{\frac{1}{2\Lambda}} \tilde{x}(t)\sum_n \delta(t-nT)\,\mathrm{e}^{-\mathrm{j}2\pi tk\Lambda}\,\mathrm{d}t \\
&= \int_{-\frac{1}{2\Lambda}}^{\frac{1}{2\Lambda}} \tilde{x}(t)\,\mathrm{e}^{-\mathrm{j}2\pi tk\Lambda}\,\mathrm{d}t \underset{k}{*} \int_{-\frac{1}{2\Lambda}}^{\frac{1}{2\Lambda}} \sum_n \delta(t-nT)\,\mathrm{e}^{-\mathrm{j}2\pi tk\Lambda}\,\mathrm{d}f \\
&= X(k\Lambda) \underset{k}{*} \frac{1}{\Lambda T}\sum_n \delta(k-\tfrac{n}{T\Lambda}) \\
&= \frac{1}{\Lambda T}\sum_n X(k\Lambda-\tfrac{n}{T}) \qquad \text{(A.5)}
\end{aligned}$$

assuming $1/(T\Lambda)$ is an integer.

Sampling in both the time-domain and the frequency-domain results in a discrete and periodic time-domain signal and a discrete and periodic frequency-domain signal. If $x(t)$ and $X(f)$ are not appropriately band limited, then periodic overlap will distort the discrete signals. This periodic distortion is known as aliasing.

The discrete-time, discrete-frequency Fourier transform, known as the discrete Fourier transform, is defined as:

$$\begin{aligned}\tilde{X}(\tfrac{k}{NT}) &= \sum_{n=0}^{N-1} \tilde{x}(nT)\, \mathrm{e}^{-\mathrm{j}2\pi nk/N} \\ \tilde{x}(nT) &= \sum_{k=0}^{N-1} \tilde{X}(\tfrac{k}{NT})\, \mathrm{e}^{\mathrm{j}2\pi kn/N}.\end{aligned}$$

A.4.1 Avoiding Aliasing

Lets assume that $x(t)$ has a bandwidth, or time duration, of B_t; that is, $x(t) = 0$ for $t < 0$ and $t > B_t$. Also, lets assume that $X(f)$ has a bandwidth, or frequency extent, of B_f; that is, $X(f) = 0$ for $|f| > B_f/2$. For the discrete-time domain signal $x(nT)$, let $NT = B_t$, and for the discrete-frequency signal let $M\Lambda = B_f$.

Thus, from (A.4) and (A.5), we avoid aliasing if T and Λ satisfy the two following constraints:

$$\begin{aligned}\frac{1}{T} &\geq B_f \\ \frac{1}{\Lambda} &\geq B_t.\end{aligned}$$

If we assume that both sampling frequencies $1/\Lambda$ and $1/T$ satisfy these conditions, then taking the lower limit—that is, $T = 1/(M\Lambda)$ and $T = 1/(N\Lambda)$—gives the equality $N = M$. Thus , when $1/T \geq B_f$ and $NT \geq B_t$, the discrete signals $\tilde{x}(nT)$ and $\tilde{X}(k/NT)$, as $\Lambda = 1/NT$, are alias free.

For these alias free signals the discrete periodic signals equal samples of the continuous signals, as the relation (2.11) shows. As I mentioned in Chapter 2, the assumption that both the time- and frequency-domain signals are band limited is not valid. Hence the discrete-time or discrete-frequency signal can only approximate samples of the continuous signals.

Note that although we may never completely eliminate aliasing from the discrete signals we can minimise it by increasing the sampling frequency $1/T$. In most applications this aliasing is negligible and is ignored. Thus, we call the discrete signal $\tilde{x}(nT)$ alias free, assuming that the condition $1/T \geq B_f$ is meet.

Appendix B

Derivations for Discrete Wigner–Ville Distributions

The following chapter contains derivations, used in Chapter 2, to define the DWVD. I start with the discrete-time WVD, followed by the discrete-frequency WVD, before presenting the discrete-time, discrete-frequency WVD, known as the DWVD.

B.1 Discrete-Time WVD

Here I use two different approaches to sample the continuous TIAF $K(t,\tau)$ and then form the discrete-time WVD by using the discrete-time Fourier transform of the discrete TIAF.

B.1.1 TIAF Sampling Approach A

Applying sampling approach A, illustrated in Fig. 2.3b, to the TIAF $K(t,\tau)$ results in the sampled continuous TIAF $K_{\mathrm{i}}^{\mathrm{A}}(t,\tau)$; that is

$$K_{\mathrm{i}}^{\mathrm{A}}(t,\tau) = K(t,\tau)\sum_{n}\delta(t-nT)\sum_{m}\delta(\tfrac{\tau}{2}-mT). \tag{B.1}$$

The discrete TIAF $K^{\mathrm{A}}(nT,2mT)$ in terms of the discrete-time signal is

$$K^{\mathrm{A}}(nT,2mT) = x((n+m)T)x^{*}((n-m)T).$$

The following derivation, based on the derivation for the discrete-time Fourier transform in Appendix A.2, relates the discrete-time WVD to the continuous WVD. First, take the discrete-time Fourier transform of the TIAF $K_{\mathrm{i}}^{\mathrm{A}}(t,\tau)$,

$$\begin{aligned} W_{\mathrm{i}}^{\mathrm{A}}(t,f) &= \int K(t,\tau)\sum_{n}\delta(t-nT)\sum_{m}\delta(\tfrac{\tau}{2}-mT)\,\mathrm{e}^{-\mathrm{j}2\pi f\tau}\,\mathrm{d}\tau \\ &= \sum_{n}\sum_{m}K^{\mathrm{A}}(nT,2mT)\,\mathrm{e}^{-\mathrm{j}4\pi mTf}\delta(t-nT) \\ &= \frac{1}{2T}\sum_{n}\widetilde{W}^{\mathrm{A}}(nT,f)\delta(t-nT). \end{aligned} \tag{B.2}$$

Lets take the discrete-time Fourier transform of the TIAF $K_{\mathrm{i}}^{\mathrm{A}}(t,\tau)$ once more, but this time we obtain a different result:

$$\begin{aligned}
W_{\mathrm{i}}^{\mathrm{A}}(t,f) &= \int K(t,\tau)\sum_{n}\delta(t-nT)\sum_{m}\delta(\tfrac{\tau}{2}-mT)\,\mathrm{e}^{-\mathrm{j}2\pi f\tau}\,\mathrm{d}\tau \\
&= \sum_{n}\delta(t-nT)\left[W(t,f)\underset{f}{*}\frac{1}{2T}\sum_{m}\delta(f-\tfrac{m}{2T})\right] \\
&= \frac{1}{2T}\sum_{m}\sum_{n}W(t,f-\tfrac{m}{2T})\delta(t-nT).
\end{aligned}$$

Comparing (B.2) with the preceding expression results in the relation

$$\widetilde{W}^{\mathrm{A}}(nT,f)=\sum_{m}W(nT,f-\tfrac{m}{2T}).$$

Thus, $\widetilde{W}^{\mathrm{A}}(nT,f)$ is periodic in f with period $1/(2T)$.

B.1.2 TIAF Sampling Approach B

The method uses a nonuniform sampling grid, illustrated in Fig. 2.3c. The resultant continuous sampled TIAF $K_{\mathrm{i}}^{\mathrm{B}}(nT/2,mT)$, for n and $n+1/2$ values of n, is

$$\begin{aligned}
K_{\mathrm{i}}^{\mathrm{B}}(t,\tau) =& K(t,\tau)\left[\sum_{n}\delta(t-nT)\sum_{m}\delta(\tau-2mT)\right. \\
&\left. + \sum_{n}\delta(t-(n+\tfrac{1}{2})T)\sum_{m}\delta(\tau-(2m+1)T)\right] \\
=& K(t,\tau)\sum_{\substack{n \\ n+m}}\sum_{\substack{m \\ \text{even}}}\delta(t-\tfrac{nT}{2})\delta(\tau-mT).
\end{aligned} \tag{B.3}$$

Thus, the discrete TIAF, as a function of $x(nT)$, is

$$\begin{aligned}
K^{\mathrm{B}}(nT,2mT) &= x((n+m)T)x^{*}((n-m)T) \\
K^{\mathrm{B}}((n+\tfrac{1}{2})T,2(m+\tfrac{1}{2})T) &= x((n+m+1)T)x^{*}((n-m)T).
\end{aligned}$$

The discrete-time WVD is the discrete-time Fourier transform of $K^{\mathrm{B}}(nT,mT)$, as defined in (2.17).

To relate the discrete-time WVD to the continuous WVD, we do as follows. The WVD of the sampled TIAF $K_{\mathrm{i}}^{\mathrm{B}}$ results in

$$\begin{aligned}
W_{\mathrm{i}}^{\mathrm{B}}(t,f) &= \int K(t,\tau) \sum_{\substack{n \quad m \\ n+m \text{ even}}} \sum \delta(t - \tfrac{nT}{2}) \delta(\tau - mT)\,\mathrm{e}^{-\mathrm{j}2\pi f\tau}\,\mathrm{d}\tau \\
&= \int K(t,\tau) \sum_{n} \delta(t - nT) \sum_{m} \delta(\tau - 2mT)\,\mathrm{e}^{-\mathrm{j}2\pi f\tau}\,\mathrm{d}\tau \\
&\quad + \int K(t,\tau) \sum_{n} \delta(t - (n+\tfrac{1}{2})T) \sum_{m} \delta(\tau - 2(m+\tfrac{1}{2})T)\,\mathrm{e}^{-\mathrm{j}2\pi f\tau}\,\mathrm{d}\tau \\
&= \sum_{n}\sum_{m} K^{\mathrm{B}}(nT, 2mT)\,\mathrm{e}^{-\mathrm{j}4\pi mTf} \delta(t - nT) \\
&\quad + \sum_{n}\sum_{m} K^{\mathrm{B}}((n+\tfrac{1}{2})T, 2(m+\tfrac{1}{2})T)\,\mathrm{e}^{-\mathrm{j}4\pi mTf}\,\mathrm{e}^{-\mathrm{j}2\pi Tf} \delta(t - (n+\tfrac{1}{2})T) \\
&= \frac{1}{2T} \sum_{n} \widetilde{W}^{\mathrm{B}}(nT, f) \delta(t - nT) + \frac{1}{2T} \sum_{n} \widetilde{W}^{\mathrm{B}}((n+\tfrac{1}{2})T, f) \delta(t - (n+\tfrac{1}{2})T) \\
&= \frac{1}{2T} \sum_{n} \widetilde{W}^{\mathrm{B}}(\tfrac{nT}{2}, f) \delta(t - \tfrac{nT}{2}). \qquad \text{(B.4)}
\end{aligned}$$

using the substitution of the $\widetilde{W}^{\mathrm{B}}$ as defined in (2.17). Also, $W_{\mathrm{i}}^{\mathrm{B}}$ can be related to periodic copies in f of W as

$$\begin{aligned}
W_{\mathrm{i}}^{\mathrm{B}}(t,f) &= \int K(t,\tau) \sum_{\substack{n \quad m \\ n+m \text{ even}}} \sum \delta(t - \tfrac{nT}{2}) \delta(\tau - mT)\,\mathrm{e}^{-\mathrm{j}2\pi f\tau}\,\mathrm{d}\tau \\
&= W(t,f) \underset{f}{*} \Bigg[\int \sum_{n} \delta(t - nT) \sum_{m} \delta(\tau - 2mT)\,\mathrm{e}^{-\mathrm{j}2\pi f\tau}\,\mathrm{d}\tau \\
&\qquad + \int \sum_{n} \delta(t - (n+\tfrac{1}{2})T) \sum_{m} \delta(\tau - 2(m+\tfrac{1}{2})T)\,\mathrm{e}^{-\mathrm{j}2\pi f\tau}\,\mathrm{d}\tau \Bigg] \\
&= W(t,f) \underset{f}{*} \Bigg[\frac{1}{2T} \sum_{n} \delta(t - nT) \sum_{m} \delta(f - \tfrac{m}{2T}) \\
&\qquad + \frac{1}{2T} \sum_{n} \delta(t - (n+\tfrac{1}{2})T)\,\mathrm{e}^{-\mathrm{j}2\pi fT} \sum_{m} \delta(f - \tfrac{m}{2T}) \Bigg] \\
&= \frac{1}{2T} \sum_{n}\sum_{m} W(nT, f - \tfrac{m}{2T}) \delta(t - nT) \\
&\quad + \frac{1}{2T} \sum_{n}\sum_{m} (-1)^m W((n+\tfrac{1}{2})T, f - \tfrac{m}{2T}) \delta(t - (n+\tfrac{1}{2})T).
\end{aligned}$$

For n and $n+1/2$ values of $n/2$, this equates to

$$\begin{aligned}&\frac{1}{2T}\sum_n\sum_m W(nT, f-\tfrac{m}{2T})\delta(t-nT),\\&\frac{1}{2T}\sum_n\sum_m(-1)^m W((n+\tfrac{1}{2})T, f-\tfrac{m}{2T})\delta(t-(n+\tfrac{1}{2})T),\end{aligned}$$

or combined to represent

$$\frac{1}{2T}\sum_n\sum_m(-1)^{nm}W(\tfrac{nT}{2}, f-\tfrac{m}{2T})\delta(t-\tfrac{nT}{2}).$$

Combining this expression with (B.4) gives the relation between discrete-time and continuous WVD as

$$\widetilde{W}^{\mathrm{B}}(\tfrac{nT}{2}, f)=\sum_m(-1)^{nm}W(\tfrac{nT}{2}, f-\tfrac{m}{2T}).$$

B.2 Periodic Doppler–Frequency Domains

Sampling the TIAF results in a periodic SIAF. Here I look at this Doppler–frequency periodicity for the two TIAF sampling approaches.

B.2.1 Periodic SIAF for TIAF Sampling Approach A

The periodic SIAF as a function of K^{A} can be written as

$$\begin{aligned}\widetilde{\mathcal{K}}^{\mathrm{A}}(\nu, f)&=\sum_n\widetilde{W}^{\mathrm{A}}(nT, f)\,\mathrm{e}^{-\mathrm{j}2\pi\nu nT}\\&=2T\sum_n\sum_m K^{\mathrm{A}}(nT, 2mT)\,\mathrm{e}^{-\mathrm{j}4\pi mTf}\,\mathrm{e}^{-\mathrm{j}2\pi\nu nT}.\end{aligned}$$

Next, I define the function $\mathcal{K}_1(\nu,\tau)$ as the Fourier transform of the WVD of $K_{\mathrm{i}}^{\mathrm{A}}$, denoted as $W_{\mathrm{i}}^{\mathrm{A}}(t,f)$; that is,

$$\mathcal{K}_1(\nu, f)=\int W_{\mathrm{i}}^{\mathrm{A}}(t,f)\,\mathrm{e}^{-\mathrm{j}2\pi t\nu}\,\mathrm{d}t.$$

which can be rewritten as

$$\begin{aligned}\mathcal{K}_1(\nu, f)&=\iint K(t,\tau)\sum_n\delta(t-nT)\sum_m\delta(\tfrac{\tau}{2}-mT)\,\mathrm{e}^{-\mathrm{j}2\pi f\tau}\,\mathrm{e}^{-\mathrm{j}2\pi t\nu}\,\mathrm{d}\tau\,\mathrm{d}t\\&=\sum_n\sum_m K^{\mathrm{A}}(nT, 2mT)\,\mathrm{e}^{-\mathrm{j}4\pi mTf}\,\mathrm{e}^{-\mathrm{j}2\pi\nu nT}\\&=\frac{1}{2T}\widetilde{\mathcal{K}}^{\mathrm{A}}(\nu, f).\end{aligned}$$

I then use this result to relate $\widetilde{\mathcal{K}}^{\mathrm{A}}(\nu,f)$ to $\mathcal{K}(\nu,f)$ as

$$\begin{aligned}
\widetilde{\mathcal{K}}^{\mathrm{A}}(\nu,f) &= 2T\int\!\!\int K(t,\tau)\sum_n \delta(t-nT)\sum_m \delta(\tfrac{\tau}{2}-mT)\,\mathrm{e}^{-\mathrm{j}2\pi(f\tau+t\nu)}\,\mathrm{d}\tau\,\mathrm{d}t \\
&= 2T\mathcal{K}(\nu,f)\underset{\nu}{*}\underset{f}{*}\left[\frac{1}{2T^2}\sum_m \delta(f-\tfrac{m}{2T})\sum_n \delta(\nu-\tfrac{n}{T})\right] \\
&= \frac{1}{T}\sum_n\sum_m \mathcal{K}(\nu-\tfrac{n}{T}, f-\tfrac{m}{2T}).
\end{aligned}$$

B.2.2 Periodic SIAF for TIAF Sampling Approach B

The periodic SIAF as a function of K^{B} can be written as

$$\begin{aligned}
\widetilde{\mathcal{K}}^{\mathrm{B}}(\nu,f) &= \sum_n \widetilde{W}^{\mathrm{B}}(\tfrac{nT}{2},f)\,\mathrm{e}^{-\mathrm{j}\pi\nu nT} \\
&= 2T\sum_{\substack{n\\ n+m}}\sum_{\substack{m\\ \text{even}}} K^{\mathrm{B}}(\tfrac{nT}{2},mT)\,\mathrm{e}^{-\mathrm{j}2\pi mTf}\,\mathrm{e}^{-\mathrm{j}\pi\nu nT}.
\end{aligned}$$

Next, I define the function $\mathcal{K}_2(\nu,\tau)$ as the Fourier transform of the WVD of $K_{\mathrm{i}}^{\mathrm{B}}$, denoted as $W_{\mathrm{i}}^{\mathrm{B}}(t,f)$; that is,

$$\begin{aligned}
\mathcal{K}_2(\nu,f) &= \int W_{\mathrm{i}}^{\mathrm{B}}(t,f)\,\mathrm{e}^{-\mathrm{j}2\pi t\nu}\,\mathrm{d}t \\
&= \int\!\!\int K(t,\tau)\sum_{\substack{n\\ n+m}}\sum_{\substack{m\\ \text{even}}}\delta(t-\tfrac{nT}{2})\delta(\tau-mT)\,\mathrm{e}^{-\mathrm{j}2\pi(f\tau+t\nu)}\,\mathrm{d}\tau\,\mathrm{d}t \\
&= \sum_{\substack{n\\ n+m}}\sum_{\substack{m\\ \text{even}}} K^{\mathrm{B}}(\tfrac{nT}{2},mT)\,\mathrm{e}^{-\mathrm{j}2\pi mTf}\,\mathrm{e}^{-\mathrm{j}\pi\nu nT} \\
&= \frac{1}{2T}\widetilde{\mathcal{K}}^{\mathrm{B}}(\nu,f).
\end{aligned}$$

and then obtain the SIAF periodicity as follows:

$$
\begin{aligned}
\widetilde{\mathcal{K}}^{\mathrm{B}}(\nu, f) &= 2T \int\!\!\int K(t,\tau) \Bigg[\sum_n \delta(t - nT) \sum_m \delta(\tau - 2mT) \\
&\qquad + \sum_n \delta(t - (n + \tfrac{1}{2})T) \sum_m \delta(\tau - 2(m + \tfrac{1}{2})T) \Bigg] \, \mathrm{e}^{-\mathrm{j}2\pi(f\tau + t\nu)} \, \mathrm{d}\tau \, \mathrm{d}t \\
&= 2T\mathcal{K}(\nu, f) \underset{\nu}{*} \underset{f}{*} \Bigg[\frac{1}{2T^2} \sum_m \delta(f - \tfrac{m}{2T}) \sum_n \delta(\nu - \tfrac{n}{T}) \\
&\qquad + \frac{1}{2T^2} \sum_m (-1)^m \delta(f - \tfrac{m}{2T}) \sum_n (-1)^n \delta(\nu - \tfrac{n}{T}) \Bigg] \\
&= 2T\mathcal{K}(\nu, f) \underset{\nu}{*} \underset{f}{*} \Bigg[\frac{1}{T^2} \sum_{\substack{n \\ n+m \text{ even}}} \sum_{m} \delta(f - \tfrac{m}{2T}) \delta(\nu - \tfrac{n}{T}) \Bigg] \\
&= \frac{2}{T} \sum_{\substack{n \\ n+m \text{ even}}} \sum_{m} \mathcal{K}(\nu - \tfrac{n}{T}, f - \tfrac{m}{2T}).
\end{aligned}
$$

B.3 Discrete-Frequency WVD

Sampling the SIAF and then using the inverse discrete-frequency Fourier transform on this discrete SIAF results in the discrete-frequency WVD. Here, I use two SIAF sampling approaches to define two discrete-frequency WVDs.

B.3.1 SIAF Sampling Approach A

Sampling the SIAF in f and $\nu/2$ with sampling frequency $1/\Lambda$ results in the sampled continuous SIAF $\mathcal{K}_{\mathrm{i}}^{\mathrm{A}}$

$$
\mathcal{K}_{\mathrm{i}}^{\mathrm{A}}(\nu, f) = \mathcal{K}(\nu, f) \sum_k \delta(f - k\Lambda) \sum_l \delta(\tfrac{\nu}{2} - l\Lambda).
$$

The discrete SIAF $\mathcal{K}^{\mathrm{A}}$, in terms of $X(k\Lambda)$, is

$$
\mathcal{K}^{\mathrm{A}}(2l\Lambda, k\Lambda) = X((k + l)\Lambda) X^*((k - l)\Lambda).
$$

The discrete-frequency WVD is the inverse discrete-frequency Fourier transform of $\mathcal{K}^{\mathrm{A}}$, as defined in (2.21).

The following relates the discrete-frequency WVD to the continuous WVD. Using the definition in (2.21), the WVD of $\mathcal{K}_\mathrm{i}^\mathrm{A}$ is

$$\begin{aligned}
\mathcal{W}_\mathrm{i}^\mathrm{A}(t,f) &= \int \mathcal{K}(\nu,f)\sum_k \delta(f-k\Lambda)\sum_l \delta(\tfrac{\nu}{2}-l\Lambda)\,\mathrm{e}^{\mathrm{j}2\pi\nu t}\,\mathrm{d}\nu \\
&= \sum_k\sum_l \mathcal{K}^\mathrm{A}(2l\Lambda,k\Lambda)\,\mathrm{e}^{\mathrm{j}4\pi l\Lambda t}\delta(f-k\Lambda) \\
&= \frac{1}{2\Lambda}\sum_k \widetilde{\mathcal{W}}^\mathrm{A}(t,k\Lambda)\delta(f-k\Lambda)
\end{aligned} \tag{B.5}$$

which can also be expressed as

$$\begin{aligned}
\mathcal{W}_\mathrm{i}^\mathrm{A}(t,f) &= \int \mathcal{K}(\nu,f)\sum_k \delta(f-k\Lambda)\sum_l \delta(\tfrac{\nu}{2}-l\Lambda)\,\mathrm{e}^{\mathrm{j}2\pi\nu t}\,\mathrm{d}\nu \\
&= \sum_k \delta(f-k\Lambda)\left[\mathcal{W}(t,f) \underset{t}{*} \frac{1}{2\Lambda}\sum_m \delta(t-\tfrac{l}{2\Lambda})\right] \\
&= \frac{1}{2\Lambda}\sum_k\sum_l \mathcal{W}(t-\tfrac{l}{2\Lambda},k\Lambda)\delta(f-k\Lambda).
\end{aligned}$$

Substituting (B.5) into the above expression yields the periodic nature of the DFWD $\mathcal{W}^\mathrm{A}$ as

$$\widetilde{\mathcal{W}}^\mathrm{A}(t,k\Lambda) = \sum_l \mathcal{W}(t-\tfrac{l}{2\Lambda},k\Lambda).$$

B.3.2 SIAF Sampling Approach B

The sampled continuous SIAF $\mathcal{K}_\mathrm{i}^\mathrm{B}$, using sampling approach B, is

$$\begin{aligned}
\mathcal{K}_\mathrm{i}^\mathrm{B}(\nu,f) &= \mathcal{K}(\nu,f)\left[\sum_k \delta(f-k\Lambda)\sum_l \delta(\nu-2l\Lambda)\right. \\
&\qquad \left. + \sum_k \delta(f-(k+\tfrac{1}{2})\Lambda)\sum_l \delta(\nu-(2l+1)\Lambda)\right] \qquad \text{(B.6)} \\
&= \mathcal{K}(\nu,f)\sum_{\substack{k \\ k+l \text{ even}}}\sum_l \delta(f-\tfrac{k\Lambda}{2})\delta(\nu-l\Lambda).
\end{aligned}$$

The discrete SIAF $\mathcal{K}^\mathrm{B}(2l\Lambda,k\Lambda)$, in terms of $X(k\Lambda)$, is

$$\begin{aligned}
\mathcal{K}^\mathrm{B}(2l\Lambda,k\Lambda) &= X((k+l)\Lambda)X^*((k-l)\Lambda) \\
\mathcal{K}^\mathrm{B}((2l+1)\Lambda,(k+\tfrac{1}{2})\Lambda) &= X((k+l+1)\Lambda)X^*((k-l)\Lambda)
\end{aligned}$$

The inverse discrete-frequency Fourier transform of this discrete SIAF $\mathcal{K}^\mathrm{B}$ is the discrete-frequency WVD in (2.23).

Here I derive the relation between the discrete-frequency WVD and the continuous WVD. The WVD, using the definition in (2.23), of $\mathcal{K}_{\mathrm{i}}^{\mathrm{B}}$ is

$$\begin{aligned}
\mathcal{W}_{\mathrm{i}}^{\mathrm{B}}(t,f) &= \int \mathcal{K}(\nu,f) \sum_{\substack{k \quad l \\ k+l \text{ even}}} \sum \delta(f-\tfrac{k\Lambda}{2})\delta(\nu-l\Lambda)\,\mathrm{e}^{\mathrm{j}2\pi\nu t}\,\mathrm{d}\nu \\
&= \int \mathcal{K}(\nu,f) \sum_{k} \delta(f-k\Lambda) \sum_{l} \delta(\nu-2l\Lambda)\,\mathrm{e}^{\mathrm{j}2\pi\nu t}\,\mathrm{d}\nu \\
&\quad + \int \mathcal{K}(\nu,f) \sum_{k} \delta(f-(k+\tfrac{1}{2})\Lambda) \sum_{l} \delta(\nu-(2l+1)\Lambda)\,\mathrm{e}^{\mathrm{j}2\pi\nu t}\,\mathrm{d}\nu \\
&= \sum_{k}\sum_{l} \mathcal{K}^{\mathrm{B}}(2l\Lambda,k\Lambda)\,\mathrm{e}^{\mathrm{j}4\pi l\Lambda t}\delta(f-k\Lambda) \\
&\quad + \sum_{k}\sum_{l} \mathcal{K}^{\mathrm{B}}(2(m+\tfrac{1}{2})\Lambda,(k+\tfrac{1}{2})\Lambda)\,\mathrm{e}^{\mathrm{j}4\pi l\Lambda t}\,\mathrm{e}^{\mathrm{j}2\pi\Lambda t}\delta(f-(k+\tfrac{1}{2})\Lambda) \\
&= \frac{1}{2\Lambda}\sum_{k} \widetilde{\mathcal{W}}^{\mathrm{B}}(t,k\Lambda)\delta(f-k\Lambda) + \frac{1}{2\Lambda}\sum_{k} \widetilde{\mathcal{W}}^{\mathrm{B}}(t,(k+\tfrac{1}{2})\Lambda)\delta(f-(k+\tfrac{1}{2})\Lambda) \\
&= \frac{1}{2\Lambda}\sum_{n} \widetilde{\mathcal{W}}^{\mathrm{B}}(t,\tfrac{k\Lambda}{2})\delta(f-\tfrac{k\Lambda}{2}).
\end{aligned} \tag{B.7}$$

using the definition of $\widetilde{\mathcal{W}}^{\mathrm{B}}$ in (2.23). Also, $\mathcal{W}_{\mathrm{i}}^{\mathrm{B}}$, the WVD of $\mathcal{K}_{\mathrm{i}}^{\mathrm{B}}$, is related to $\mathcal{W}$, the WVD of $\mathcal{K}(\nu,f)$, as follows:

$$\begin{aligned}
\mathcal{W}_{\mathrm{i}}^{\mathrm{B}}(t,f) &= \int \mathcal{K}(\nu,f) \sum_{\substack{k \quad l \\ k+l \text{ even}}} \sum \delta(f-\tfrac{k\Lambda}{2})\delta(\nu-l\Lambda)\,\mathrm{e}^{\mathrm{j}2\pi\nu t}\,\mathrm{d}\nu \\
&= \mathcal{W}(t,f) \underset{t}{*} \Bigg[\int \sum_{k} \delta(f-k\Lambda) \sum_{l} \delta(\nu-2l\Lambda)\,\mathrm{e}^{\mathrm{j}2\pi\nu t}\,\mathrm{d}\nu \\
&\qquad + \int \sum_{k} \delta(f-(k+\tfrac{1}{2})\Lambda) \sum_{l} \delta(\nu-(2l+1)\Lambda)\,\mathrm{e}^{\mathrm{j}2\pi\nu t}\,\mathrm{d}\nu\Bigg] \\
&= \mathcal{W}(t,f) \underset{t}{*} \Bigg[\frac{1}{2\Lambda}\sum_{k} \delta(f-k\Lambda) \sum_{l} \delta(t-\tfrac{l}{2\Lambda}) \\
&\qquad + \frac{1}{2\Lambda}\sum_{k} \delta(f-(k+\tfrac{1}{2})\Lambda)\,\mathrm{e}^{\mathrm{j}2\pi\Lambda t} \sum_{l} \delta(t-\tfrac{l}{2\Lambda})\Bigg] \\
&= \frac{1}{2\Lambda}\sum_{k}\sum_{l} \mathcal{W}(t-\tfrac{l}{2\Lambda},k\Lambda)\delta(f-k\Lambda) \\
&\qquad + \frac{1}{2\Lambda}\sum_{k}\sum_{l} (-1)^{l}\mathcal{W}(t-\tfrac{l}{2\Lambda},(k+\tfrac{1}{2})\Lambda)\delta(f-(k+\tfrac{1}{2})\Lambda) \\
&= \frac{1}{2\Lambda}\sum_{k}\sum_{l} (-1)^{kl}\mathcal{W}(t-\tfrac{l}{2\Lambda},\tfrac{k\Lambda}{2})\delta(f-\tfrac{k\Lambda}{2}).
\end{aligned}$$

This result, combined with (B.7), gives the periodic relation

$$\widetilde{\mathcal{W}}^{\mathrm{B}}(t, \tfrac{k\Lambda}{2}) = \sum_{l} (-1)^{kl} \mathcal{W}(t - \tfrac{l}{2\Lambda}, \tfrac{k\Lambda}{2}).$$

B.4 Periodic Time–Lag Domain

Here I look at the time–lag periodicity, a result of sampling the SIAF, for the two SIAF sampling approaches.

B.4.1 Periodic TIAF for SIAF Sampling Approach A

To start, the periodic TIAF is related to the discrete SIAF as follows:

$$\begin{aligned}\widetilde{K}^{\mathrm{A}}(t,\tau) &= \sum_{k} \mathcal{W}^{\mathrm{A}}(t, k\Lambda)\, \mathrm{e}^{\mathrm{j}2\pi k\Lambda\tau} \\ &= 2\Lambda \sum_{k}\sum_{l} \mathcal{K}^{\mathrm{A}}(2l\Lambda, k\Lambda)\, \mathrm{e}^{\mathrm{j}2\pi(k\Lambda\tau + 2l\Lambda t)}.\end{aligned}$$

Next, define the TIAF $K_1(t,\tau)$ as the inverse Fourier transform of $\mathcal{W}_{\mathrm{i}}^{\mathrm{A}}$ as

$$\begin{aligned}K_1(t,\tau) &= \int \mathcal{W}_{\mathrm{i}}^{\mathrm{A}}(t,f)\, \mathrm{e}^{\mathrm{j}2\pi f\tau}\, \mathrm{d}f \\ &= \int\int \mathcal{K}(\nu,f) \sum_{k} \delta(f - k\Lambda) \sum_{l} \delta(\nu - 2l\Lambda)\, \mathrm{e}^{\mathrm{j}2\pi(\nu t + f\tau)}\, \mathrm{d}f\, \mathrm{d}\nu \\ &= \sum_{k}\sum_{l} \mathcal{K}^{\mathrm{A}}(2l\Lambda, k\Lambda)\, \mathrm{e}^{\mathrm{j}2\pi(k\Lambda\tau + 2l\Lambda t)} \\ &= \frac{1}{2\Lambda} \widetilde{K}^{\mathrm{A}}(t,\tau).\end{aligned}$$

Using this result, the periodicity in $\widetilde{K}^{\mathrm{A}}(t,\tau)$ is

$$\begin{aligned}\widetilde{K}^{\mathrm{A}}(t,\tau) &= 2\Lambda \int\int \mathcal{K}(\nu,f) \sum_{k} \delta(f - k\Lambda) \sum_{l} \delta(\nu - 2l\Lambda)\, \mathrm{e}^{\mathrm{j}2\pi(\nu t + f\tau)}\, \mathrm{d}f\, \mathrm{d}\nu \\ &= 2\Lambda K(t,\tau) \underset{t}{*} \underset{\tau}{*} \left[\int\int \sum_{k} \delta(f - k\Lambda) \sum_{l} \delta(\nu - 2l\Lambda)\, \mathrm{e}^{\mathrm{j}2\pi(\nu t + f\tau)}\, \mathrm{d}f\, \mathrm{d}\nu \right] \\ &= 2\Lambda K(t,\tau) \underset{t}{*} \underset{\tau}{*} \left[\frac{1}{2\Lambda^2} \sum_{k} \delta(\tau - \tfrac{k}{\Lambda}) \sum_{l} \delta(t - \tfrac{l}{2\Lambda}) \right] \\ &= \frac{1}{\Lambda} \sum_{k}\sum_{l} K(t - \tfrac{l}{2\Lambda}, \tau - \tfrac{k}{\Lambda}).\end{aligned}$$

B.4.2 Periodic TIAF for SIAF Sampling Approach B

First, define the periodic TIAF as

$$\begin{aligned}\widetilde{K}^{\mathrm{B}}(t,\tau) &= \sum_{k} \mathcal{W}^{\mathrm{B}}(t, \tfrac{k\Lambda}{2})\, \mathrm{e}^{\mathrm{j}\pi k\Lambda\tau} \\ &= 2\Lambda \underset{k+l\ \text{even}}{\sum_{k}\sum_{l}} \mathcal{K}^{\mathrm{B}}(l\Lambda, \tfrac{k\Lambda}{2})\, \mathrm{e}^{\mathrm{j}\pi(k\Lambda\tau+2l\Lambda t)}.\end{aligned}$$

Second, define the TIAF $K_2(t,\tau)$ as the inverse Fourier transform of $\mathcal{W}_{\mathrm{i}}^{\mathrm{B}}$ to give the following:

$$\begin{aligned}K_2(t,\tau) &= \int \mathcal{W}_{\mathrm{i}}^{\mathrm{B}}(t,f)\, \mathrm{e}^{\mathrm{j}2\pi f\tau}\, \mathrm{d}f \\ &= \int\int \mathcal{K}(\nu,f) \underset{k+l\ \text{even}}{\sum_{k}\sum_{l}} \delta(f - \tfrac{k\Lambda}{2})\delta(\nu - l\Lambda)\, \mathrm{e}^{\mathrm{j}2\pi(\nu t+f\tau)}\, \mathrm{d}f\, \mathrm{d}\nu \\ &= \underset{k+l\ \text{even}}{\sum_{k}\sum_{l}} \mathcal{K}^{\mathrm{B}}(l\Lambda, \tfrac{k\Lambda}{2})\, \mathrm{e}^{\mathrm{j}\pi(k\Lambda\tau+2l\Lambda t)} \\ &= \frac{1}{2\Lambda}\widetilde{K}^{\mathrm{B}}(t,\tau).\end{aligned}$$

Third, use this result to obtain the periodicity of $\widetilde{K}^{\mathrm{B}}(t,\tau)$ as

$$\begin{aligned}\widetilde{K}^{\mathrm{B}}(t,\tau) = 2\Lambda \int\int \mathcal{K}(\nu,f) &\left[\sum_{k} \delta(f - k\Lambda) \sum_{l} \delta(\nu - 2l\Lambda) \right. \\ &\left. + \sum_{k} \delta(f - (k+\tfrac{1}{2})\Lambda) \sum_{l} \delta(\nu - (2l+1)\Lambda) \right] \mathrm{e}^{\mathrm{j}2\pi(f\tau+\nu t)}\, \mathrm{d}f\, \mathrm{d}\nu \\ = 2\Lambda K(t,\tau) \underset{t}{*} \underset{\tau}{*} &\left[\frac{1}{2\Lambda^2} \sum_{k} \delta(\tau - \tfrac{m}{2T}) \sum_{l} \delta(t - \tfrac{l}{2\Lambda}) \right. \\ &\left. + \frac{1}{2\Lambda^2} \sum_{k} (-1)^k \delta(\tau - \tfrac{k}{\Lambda}) \sum_{l} (-1)^l \delta(t - \tfrac{l}{2\Lambda}) \right] \\ = 2\Lambda K(t,\tau) \underset{t}{*} \underset{\tau}{*} &\left[\frac{1}{\Lambda^2} \underset{k+l\ \text{even}}{\sum_{k}\sum_{l}} \delta(\tau - \tfrac{k}{2\Lambda})\delta(t - \tfrac{l}{\Lambda}) \right] \\ = \frac{2}{\Lambda} \underset{k+l\ \text{even}}{\sum_{k}\sum_{l}} K(t - \tfrac{l}{2\Lambda}, \tau - \tfrac{k}{\Lambda}).&\end{aligned}$$

B.5 Discrete-Time, Discrete-Frequency WVD

To form the DWVD—a discrete-time, discrete-frequency WVD—we sample either the periodic TIAF or the periodic SIAF. Here I start with the TIAF, applying the two sampling approaches from the Appendix B.1.

B.5.1 TIAF Sampling Approach A

Sample the periodic TIAF, from (2.25), with sample approach A to obtain the following:

$$\widetilde{K}_{\mathrm{i}}^{\mathrm{A}}(t,\tau) = \widetilde{K}^{\mathrm{A}}(t,\tau) \sum_n \sum_m \delta(t-nT)\delta(\tfrac{\tau}{2}-mT).$$

Using (2.25) and the relation $\Lambda = 1/NT$ from Section 2.4.5, the discrete TIAF $\widetilde{K}^{\mathrm{A}}(nT, 2mT)$ is related to the continuous TIAF as follows:

$$\widetilde{K}^{\mathrm{A}}(nT,2mT) = NT \sum_k \sum_l K((n-\tfrac{lN}{2})T, (2m-kN)T). \tag{B.8}$$

Thus, one period in the TIAF is bounded by the region $|n| < N/4$ and $|2m| < N/2$ and therefore (B.8) for one period is

$$\widetilde{K}^{\mathrm{A}}(nT,2mT) = \sum_{k=-1}^{1} \sum_{l=-1}^{1} K^{\mathrm{A}}((n-\tfrac{lN}{2})T, (2m-kN)T), \quad \text{for } |n| < \tfrac{N}{4}, |m| < \tfrac{N}{4}.$$

The discrete, periodic TIAF in terms of the discrete, periodic signal $\tilde{x}(nT)$ is

$$\widetilde{K}^{\mathrm{A}}(nT,2mT) = \tilde{x}((n+m)T)\tilde{x}((n-m)T) + \tilde{x}((n+m+\tfrac{N}{2})T)\tilde{x}((n-m-\tfrac{N}{2})T)$$

and the DWVD is the DFT of $\widetilde{K}^{\mathrm{A}}(nT,2mT)$, as defined in (2.27).

The following relates the DWVD W^{A} to the continuous WVD. First, taking the inverse discrete-frequency Fourier transform of $\widetilde{K}_{\mathrm{i}}^{\mathrm{A}}$ results in

$$\begin{aligned}
W_{\mathrm{i}}^{\mathrm{A}}(t,\tfrac{k}{NT}) &= \int_{(NT)} \widetilde{K}_{\mathrm{i}}^{\mathrm{A}}(t,\tau)\,\mathrm{e}^{-\mathrm{j}2\pi\tau k/(NT)}\,\mathrm{d}\tau \\
&= \int_{(NT)} \widetilde{K}^{\mathrm{A}}(t,\tau) \sum_{|n|<N/4} \sum_{|m|<N/4} \delta(t-nT)\delta(\tau-2mT)\,\mathrm{e}^{-\mathrm{j}2\pi\tau k/(NT)}\,\mathrm{d}\tau \\
&= \sum_{|n|<N/4} \sum_{|m|<N/4} \widetilde{K}^{\mathrm{A}}(nT,2mT)\,\mathrm{e}^{-\mathrm{j}(4\pi/N)mk}\delta(t-nT) \\
&= \frac{N}{2} \sum_{|n|<N/4} W^{\mathrm{A}}(nT,\tfrac{k}{NT})\delta(t-nT)
\end{aligned} \tag{B.9}$$

which can also be expressed as

$$
\begin{aligned}
W_{\mathrm{i}}^{\mathrm{A}}(t, \tfrac{k}{NT}) &= \int_{(NT)} \widetilde{K}^{\mathrm{A}}(t,\tau) \sum_{|n|<N/4} \sum_{|m|<N/4} \delta(t-nT)\delta(\tau-2mT)\, \mathrm{e}^{-\mathrm{j}2\pi\tau k/(NT)}\, \mathrm{d}\tau \\
&= \int_{(NT)} \widetilde{K}^{\mathrm{A}}(t,\tau)\, \mathrm{e}^{-\mathrm{j}2\pi\tau k/(NT)}\, \mathrm{d}\tau \\
&\quad \underset{k}{*} \left[\sum_{|n|<N/4} \delta(t-nT) \int_{(NT)} \sum_{|m|<N/4} \delta(\tau-2mT)\, \mathrm{e}^{-\mathrm{j}2\pi\tau k/(NT)}\, \mathrm{d}\tau \right] \\
&= \widetilde{W}_{\mathcal{K}^{\mathrm{A}}}(t, \tfrac{k}{NT}) \underset{k}{*} \left[\sum_{|n|<N/4} \delta(t-nT) \frac{N}{2} \sum_{m} \delta(k-\tfrac{mN}{2}) \right] \\
&= \frac{N}{2} \sum_{|n|<N/4} \sum_{m} \widetilde{\mathcal{W}}^{\mathrm{A}}(t, (k-\tfrac{mN}{2})\tfrac{1}{NT})\delta(t-nT).
\end{aligned}
$$

Comparing (B.9) with the above expression yields

$$
W^{\mathrm{A}}(nT, \tfrac{k}{NT}) = \sum_{m} \widetilde{\mathcal{W}}^{\mathrm{A}}(nT, (k-\tfrac{mN}{2})\tfrac{1}{NT}).
$$

Substituting (2.22) into this expression relates the DWVD W^{A} to the WVD, namely

$$
W^{\mathrm{A}}(nT, \tfrac{k}{NT}) = \sum_{l} \sum_{k} \mathcal{W}((n-\tfrac{lN}{2})T, (k-\tfrac{mN}{2})\tfrac{1}{NT}).
$$

B.5.2 TIAF Sampling Approach B

Sample the periodic TIAF $\widetilde{K}^{\mathrm{B}}(t,\tau)$, from (2.26), with sampling approach B to obtain the following:

$$
\widetilde{K}_{\mathrm{i}}^{\mathrm{B}}(t,\tau) = \widetilde{K}^{\mathrm{B}}(t,\tau) \sum_{\substack{|n|<N \\ n+m \text{ even}}} \sum_{|m|<N} \delta(t-\tfrac{nT}{2})\delta(\tau-mT).
$$

Substituting $\Lambda = 1/NT$ into (2.26) gives the relation between the discrete TIAF $\widetilde{K}^{\mathrm{B}}(nT/2, mT)$ and the continuous TIAF $K(t,\tau)$, as

$$
\widetilde{K}^{\mathrm{B}}(\tfrac{nT}{2}, mT) = 2NT \sum_{\substack{k \\ k+l \text{ even}}} \sum_{l} K((n-lN)\tfrac{T}{2}, (m-kN)T).
$$

Thus, one period in this discrete TIAF is bounded by the rectangular region $|n| < N$, $|m| < N$, and therefore (B.5.2) over one period is

$$
\begin{aligned}
\widetilde{K}^{\mathrm{B}}(\tfrac{nT}{2}, mT) =& K^{\mathrm{B}}(\tfrac{nT}{2}, mT) + K^{\mathrm{B}}((n-N)\tfrac{T}{2}, (m-N)T) + K^{\mathrm{B}}((n+N)\tfrac{T}{2}, (m-N)T) \\
&+ K^{\mathrm{B}}((n-N)\tfrac{T}{2}, (m+N)T) + K^{\mathrm{B}}((n+N)\tfrac{T}{2}, (m+N)T),
\end{aligned}
$$

for $|n| < N$ $|m| < N$. In terms of $\tilde{x}(nT)$,

$$
\begin{aligned}
\widetilde{K}^{\mathrm{B}}(nT, 2mT) &= \tilde{x}((n+m)T)\tilde{x}((n-m)T) \\
\widetilde{K}^{\mathrm{B}}((n+\tfrac{1}{2})T, 2(m+\tfrac{1}{2})T) &= \tilde{x}((n+m+1)T)\tilde{x}((n-m)T)
\end{aligned}
$$

The DWVD is the DFT transform of the discrete TIAF $\widetilde{K}^{\mathrm{B}}(nT/2, mT)$, as defined in (2.30).

The following relates the DWVD to the WVD. The inverse discrete-frequency Fourier transform of $\widetilde{K}_{\mathrm{i}}^{\mathrm{B}}$ results in

$$\begin{aligned}
W_{\mathrm{i}}^{\mathrm{B}}(t, \tfrac{k}{2NT}) &= \int_{(2NT)} \widetilde{K}_{\mathrm{i}}^{\mathrm{B}}(t,\tau)\, \mathrm{e}^{-\mathrm{j}\pi\tau k/(NT)}\, \mathrm{d}\tau \\
&= \int_{(2NT)} \widetilde{K}^{\mathrm{B}}(t,\tau) \sum_{|n|<N/2} \sum_{|m|<N/2} \delta(t-nT)\delta(\tau-2mT)\, \mathrm{e}^{-\mathrm{j}\pi\tau k/(NT)}\, \mathrm{d}\tau \\
&\quad + \int_{(2NT)} \widetilde{K}^{\mathrm{B}}(t,\tau) \sum_{|n|<N/2} \sum_{|m|<N/2} \delta(t-(n+\tfrac{1}{2})T)\delta(\tau-2(m+\tfrac{1}{2})T) \\
&\quad .\, \mathrm{e}^{-\mathrm{j}\pi\tau k/(NT)}\, \mathrm{d}\tau \\
&= \sum_{|n|<N/2} \sum_{|m|<N/2} \widetilde{K}^{\mathrm{B}}(nT, 2mT)\, \mathrm{e}^{-\mathrm{j}(2\pi/N)mk} \delta(t-nT) \\
&\quad + \sum_{|n|<N/2} \sum_{|m|<N/2} \widetilde{K}^{\mathrm{B}}((n+\tfrac{1}{2})T, 2(m+\tfrac{1}{2})T)\, \mathrm{e}^{-\mathrm{j}(\pi/N)(2m+1)k} \delta(t-(n+\tfrac{1}{2})T) \\
&= N \sum_{|n|<N/2} W^{\mathrm{B}}(nT, \tfrac{k}{2NT})\delta(t-nT) \\
&\quad + N \sum_{|n|<N/2} W^{\mathrm{B}}((n+\tfrac{1}{2})T, \tfrac{k}{2NT})\delta(t-(n+\tfrac{1}{2})T) \\
&= N \sum_{|n|<N} W^{\mathrm{B}}(\tfrac{nT}{2}, \tfrac{k}{2NT})\delta(t-\tfrac{nT}{2})
\end{aligned} \tag{B.10}$$

This can also be expressed as

$$\begin{aligned}
W_{\mathrm{i}}^{\mathrm{B}}(t, \tfrac{k}{2NT}) &= \int_{(2NT)} \widetilde{K}^{\mathrm{B}}(t,\tau) \sum_{\substack{|n|<N \\ n+m \text{ even}}} \sum_{|m|<N} \delta(t-\tfrac{nT}{2})\delta(\tau-mT)\, \mathrm{e}^{-\mathrm{j}\pi\tau k/(NT)}\, \mathrm{d}\tau \\
&= \int_{(2NT)} \widetilde{K}^{\mathrm{B}}(t,\tau)\, \mathrm{e}^{-\mathrm{j}\pi\tau k/(NT)}\, \mathrm{d}\tau \\
&\quad \mathop{*}_{k} \Bigg[\int_{(2NT)} \sum_{|n|<N/2} \sum_{|m|<N/2} \delta(t-nT)\delta(\tau-2mT)\, \mathrm{e}^{-\mathrm{j}\pi\tau k/(NT)}\, \mathrm{d}\tau \\
&\quad + \int_{(2NT)} \sum_{|n|<N/2} \sum_{|m|<N/2} \delta(t-(n+\tfrac{1}{2})T)\delta(\tau-2(m+\tfrac{1}{2})T)\, \mathrm{e}^{-\mathrm{j}\pi\tau k/(NT)}\, \mathrm{d}\tau \Bigg] \\
&= \widetilde{\mathcal{W}}^{\mathrm{B}}(t, \tfrac{k}{2NT}) \mathop{*}_{k} \Bigg[\sum_{|n|<N/2} \delta(t-nT) N \sum_{m} \delta(k-mN) \\
&\quad + \sum_{|n|<N/2} \delta(t-(n+\tfrac{1}{2})T) N \sum_{m} \delta(k-mN)(-1)^m \Bigg]
\end{aligned}$$

$$\begin{aligned}
&= N\sum_{m}\sum_{|n|<N/2} \widetilde{\mathcal{W}}^{\mathrm{B}}(nT,(k-mN)\tfrac{1}{2NT})\delta(t-nT)\\
&\quad + N\sum_{m}\sum_{|n|<N/2} \widetilde{\mathcal{W}}^{\mathrm{B}}((n+\tfrac{1}{2})T,(k-mN)\tfrac{1}{2NT})\delta(t-(n+\tfrac{1}{2})T)(-1)^{m}\\
&= N\sum_{m}\sum_{|n|<N} (-1)^{mn}\widetilde{\mathcal{W}}^{\mathrm{B}}(\tfrac{nT}{2},(k-mN)\tfrac{1}{2NT})\delta(t-\tfrac{nT}{2})
\end{aligned}$$

Comparing (B.10) with the above expression yields

$$W^{\mathrm{B}}(\tfrac{nT}{2},\tfrac{k}{2NT}) = \sum_{m}(-1)^{mn}\widetilde{\mathcal{W}}^{\mathrm{B}}(\tfrac{nT}{2},(k-mN)\tfrac{1}{2NT})$$

Substituting (2.24) into this expressions relates the DWVD and WVD, as

$$W^{\mathrm{B}}(\tfrac{nT}{2},\tfrac{k}{2NT}) = \sum_{l}\sum_{m}(-1)^{nm+lk-lmN}\mathcal{W}((n-lN)\tfrac{T}{2},(k-mN)\tfrac{1}{2NT}).$$

Next, I present an alternative method for defining the DWVD by sampling the periodic SIAF. This method is similar to the previous method of sampling the TIAF.

B.5.3 SIAF Sampling Approach A

Sampling the periodic SIAF $\widetilde{\mathcal{K}}^{\mathrm{A}}(\nu,f)$, from (2.19), with sampling approach A, where $\Lambda = 1/NT$, results in

$$\widetilde{\mathcal{K}}^{\mathrm{A}}_{\mathrm{i}}(\nu,f) = \widetilde{\mathcal{K}}^{\mathrm{A}}(\nu,f)\sum_{k=0}^{N/2-1}\sum_{|l|<N/4}\delta(\nu-\tfrac{2l}{NT})\delta(f-\tfrac{k}{NT}).$$

From (2.19),

$$\widetilde{\mathcal{K}}^{\mathrm{A}}(\tfrac{2l}{NT},\tfrac{k}{NT}) = \frac{1}{T}\sum_{n}\sum_{m}\mathcal{K}((2l-nN)\tfrac{1}{NT},(k-\tfrac{mN}{2})\tfrac{1}{NT}).$$

For one period in the SIAF, within the rectangular region $0 \le k < N/2$, $|l| < N/4$, this discrete SIAF is

$$\widetilde{\mathcal{K}}^{\mathrm{A}}(\tfrac{2l}{NT},\tfrac{k}{NT}) = \sum_{n=-1}^{1}\sum_{m=-1}^{1}\mathcal{K}^{\mathrm{A}}((2l-nN)\tfrac{1}{NT},(k-\tfrac{mN}{2})\tfrac{1}{NT}).$$

In terms of the periodic discrete-frequency signal $\tilde{X}(k/NT)$, the discrete SIAF equals

$$\widetilde{\mathcal{K}}^{\mathrm{A}}(\tfrac{2l}{NT},\tfrac{k}{NT}) = \tilde{X}((k+l)\tfrac{1}{NT})\tilde{X}^{*}((k-l)\tfrac{1}{NT})+\tilde{X}((k+l+\tfrac{N}{2})\tfrac{1}{NT})\tilde{X}^{*}((k-l-\tfrac{N}{2})\tfrac{1}{NT}) \quad \text{(B.11)}$$

within the range $0 \le k < N/2$, $|l| < N/4$. The DWVD is the inverse DFT, scaled by $2/N$, of the discrete and periodic $\widetilde{\mathcal{K}}^{\mathrm{A}}$,

$$\mathcal{W}^{\mathrm{A}}(nT,\tfrac{k}{NT}) = \frac{2}{N}\sum_{|l|<N/4}\widetilde{\mathcal{K}}^{\mathrm{A}}(\tfrac{2l}{NT},\tfrac{k}{NT})\,\mathrm{e}^{\mathrm{j}4\pi ln/N}. \quad \text{(B.12)}$$

The DWVD $\mathcal{W}^{\mathrm{A}}$ is related to the continuous WVD as follows:

$$\mathcal{W}^{\mathrm{A}}(nT, \tfrac{k}{NT}) = \sum_m \sum_l W((n - \tfrac{lN}{2})T, (k - \tfrac{mN}{2})\tfrac{1}{NT}). \tag{B.13}$$

(The derivation follows a similar approach to that in Appendix B.5.1.) Comparing this with (2.28) shows that the DWVD $\mathcal{W}^{\mathrm{A}}$ is equal to W^{A},

$$\mathcal{W}^{\mathrm{A}}(nT, \tfrac{k}{NT}) = W^{\mathrm{A}}(nT, \tfrac{k}{NT}).$$

B.5.4 SIAF Sampling Approach B

Sampling the periodic SIAF $\widetilde{\mathcal{K}}^{\mathrm{B}}(\nu, f)$, from (2.20), with sampling approach B, results in

$$\widetilde{\mathcal{K}}^{\mathrm{B}}_{\mathrm{i}}(\nu, f) = \widetilde{\mathcal{K}}^{\mathrm{B}}(\nu, f) \mathop{\sum_{k=0}^{N-1} \sum_{|l|<N}}_{l+k \text{ even}} \delta(\nu - \tfrac{l}{NT})\delta(f - \tfrac{k}{2NT}).$$

The periodicity of the discrete SIAF $\widetilde{\mathcal{K}}^{\mathrm{B}}(\frac{l}{NT}, \frac{k}{2NT})$ is

$$\widetilde{\mathcal{K}}^{\mathrm{B}}(\tfrac{l}{NT}, \tfrac{k}{2NT}) = \frac{2}{T} \mathop{\sum_n \sum_m}_{n+m \text{ even}} \mathcal{K}((l - nN)\tfrac{1}{NT}, (k - mN)\tfrac{1}{2NT}).$$

For one period in the SIAF, within the rectangular region $|n| < N$, $0 \leq k < N$,

$$\begin{aligned} \widetilde{\mathcal{K}}^{\mathrm{B}}(\tfrac{2l}{NT}, \tfrac{k}{NT}) &= \tilde{X}((k + l)\tfrac{1}{NT})\tilde{X}^*((k - l)\tfrac{1}{NT}) \\ \widetilde{\mathcal{K}}^{\mathrm{B}}((2l + 1)\tfrac{1}{NT}, (k + \tfrac{1}{2})\tfrac{1}{NT}) &= \tilde{X}((k + l + 1)\tfrac{1}{NT})\tilde{X}^*((k - l)\tfrac{1}{NT}). \end{aligned}$$

The DWVD is the inverse DFT, scaled by $1/N$, of the discrete and periodic $\widetilde{K}^{\mathrm{A}}$,

$$\mathcal{W}^{\mathrm{B}}(\tfrac{nT}{2}, \tfrac{k}{2NT}) = \frac{1}{N} \sum_{|l|<N} \widetilde{\mathcal{K}}^{\mathrm{B}}(\tfrac{l}{NT}, \tfrac{k}{2NT})\, \mathrm{e}^{\mathrm{j}\pi ln/N}. \tag{B.14}$$

Using an approach similar to that in Appendix B.5.2, we can show that the DWVD is related to the WVD as follows:

$$\mathcal{W}^{\mathrm{B}}(\tfrac{nT}{2}, \tfrac{k}{2NT}) = \sum_l \sum_m (-1)^{nm + lk - lmN} W((n - lN)\tfrac{T}{2}, (k - mN)\tfrac{1}{2NT}). \tag{B.15}$$

From (2.31),

$$\mathcal{W}^{\mathrm{B}}(\tfrac{nT}{2}, \tfrac{k}{2NT}) = W^{\mathrm{B}}(\tfrac{nT}{2}, \tfrac{k}{2NT}).$$

B.5.5 Relation Between DWVD-A and DWVD-B

We can write the DWVD-B, which uses a $2N$-point signal, for even values of n and even values of k as

$$
\begin{aligned}
W^{\mathrm{B}}\left(\tfrac{2nT}{2}, \tfrac{2k}{4NT}\right) &= \frac{1}{2N} \sum_{|m|<N} \widetilde{K}^{\mathrm{B}}(nT, 2mT)\, \mathrm{e}^{-\mathrm{j}(2\pi/N)mk} \\
&= \frac{1}{2N} \left[\sum_{m=0}^{N-1} \widetilde{K}^{\mathrm{B}}(nT, 2mT)\, \mathrm{e}^{-\mathrm{j}(2\pi/N)mk} + \sum_{m=N}^{2N-1} \widetilde{K}^{\mathrm{B}}(nT, 2mT)\, \mathrm{e}^{-\mathrm{j}(2\pi/N)mk} \right] \\
&= \frac{1}{2N} \left[\sum_{m=0}^{N-1} \widetilde{K}^{\mathrm{B}}(nT, 2mT)\, \mathrm{e}^{-\mathrm{j}(2\pi/N)mk} \right. \\
&\qquad \left. + \sum_{m=0}^{N-1} \widetilde{K}^{\mathrm{B}}(nT, (2m+N)T)\, \mathrm{e}^{-\mathrm{j}(2\pi/N)(m+N)k} \right] \\
&= \frac{1}{2N} \sum_{m=0}^{N-1} \left[\widetilde{K}^{\mathrm{B}}(nT, 2mT) + \widetilde{K}^{\mathrm{B}}(nT, (2m+N)T) \right] \mathrm{e}^{-\mathrm{j}(2\pi/N)mk}.
\end{aligned}
$$

Comparing the definition of $\widetilde{K}^{\mathrm{B}}$ in (2.29) with the definition of $\widetilde{K}^{\mathrm{A}}$ in (2.4.5), and substituting N for $2N$ in these equations, results in

$$
\begin{aligned}
W^{\mathrm{B}}\left(\tfrac{2nT}{2}, \tfrac{2k}{4NT}\right) &= \frac{1}{2N} \sum_{m=0}^{N-1} \widetilde{K}^{\mathrm{A}}(nT, 2mT)\, \mathrm{e}^{-\mathrm{j}(2\pi/N)mk} \\
&= \frac{1}{2} W^{\mathrm{A}}\left(nT, \tfrac{k}{2NT}\right)
\end{aligned}
$$

An expected result from the frequency decimation is a folding of the TIAF in the lag direction, that is,

$$
\widetilde{K}^{\mathrm{A}}(nT, 2mT) = \widetilde{K}^{\mathrm{B}}(nT, 2mT) + \widetilde{K}^{\mathrm{B}}(nT, (2m+2N)T) \tag{B.16}
$$

which is equal to definition of $\widetilde{K}^{\mathrm{A}}$ in (2.4.5).

Appendix C

Derivations for Discrete Ambiguity Functions

The appendix presents two methods for deriving a discrete-lag, discrete-Doppler ambiguity function (AF), or discrete AF (DAF) for short. The methods are taken from the DWVD definition, explained in more detail in Section 2.4.

C.1 Discrete-Lag Ambiguity Function

The discrete TIAFs K^{A} and K^{B} are used to form a discrete-lag AF, each yielding a different discrete-lag AF. We examine both here.

C.1.1 TIAF Sampling Approach A

We define the first discrete-lag AF by applying the discrete-time FT on the discrete TIAF $K^{\mathrm{A}}(nT, 2mT)$, with respect to time nT, to get

$$\widetilde{\mathcal{A}}^{\mathrm{A}}(\nu, 2mT) = T \sum_{n} K^{\mathrm{A}}(nT, 2mT)\,\mathrm{e}^{-\mathrm{j}2\pi nT\nu}. \tag{C.1}$$

Relation to Continuous AF As with the discrete-time WVD, the AF of the sampled TIAF in (B.1) can be used to relate the discrete-lag AF to the continuous AF. Therefore

$$\begin{aligned} A_{\mathrm{i}}^{\mathrm{A}}(\nu,\tau) &= \int K(t,\tau) \sum_{n} \delta(t-nT) \sum_{m} \delta(\tfrac{\tau}{2} - mT)\,\mathrm{e}^{\mathrm{j}2\pi t\nu}\,\mathrm{d}t \\ &= \sum_{m}\sum_{n} K^{\mathrm{A}}(nT, 2mT)\,\mathrm{e}^{-\mathrm{j}2\pi nT\nu}\delta(\tau - 2mT) \\ &= \frac{1}{T}\sum_{m} A^{\mathrm{A}}(\nu, 2mT)\delta(\tau - 2mT) \end{aligned} \tag{C.2}$$

where the definition of A^{B} in (C.1) was substituted in the last line. $A_{\mathrm{i}}^{\mathrm{A}}$ can also be expressed in terms of $A(\nu,\tau)$ as

$$\begin{aligned}
A_{\mathrm{i}}^{\mathrm{A}}(\nu,\tau) &= \int K(t,\tau)\sum_n \delta(t-nT)\sum_m \delta(\tfrac{\tau}{2}-mT)\,\mathrm{e}^{\mathrm{j}2\pi t\nu}\,\mathrm{d}t \\
&= \sum_m \delta(\tau-2mT)\left(A(\nu,\tau)\underset{\nu}{*}\frac{1}{T}\sum_n \delta(\nu-\tfrac{n}{T})\right) \\
&= \frac{1}{T}\sum_m\sum_n A(\nu-\tfrac{n}{T},2mT)\delta(\tau-2mT)
\end{aligned}$$

which combined with (C.2) results in

$$\widetilde{A}^{\mathrm{B}}(\nu,2mT) = \sum_n A(\nu-\tfrac{n}{T},2mT).$$

C.1.2 TIAF Sampling Approach B

We define the second discrete-lag AF, using K^{B}, as

$$\widetilde{\mathcal{A}}^{\mathrm{B}}(\nu,mT) = T\sum_n K^{\mathrm{B}}(\tfrac{nT}{2},mT)\,\mathrm{e}^{-\mathrm{j}\pi nT\nu}$$

which, for even–odd values of m, is

$$\begin{aligned}
\widetilde{\mathcal{A}}^{\mathrm{B}}(\nu,2mT) &= T\sum_n K^{\mathrm{B}}(nT,2mT)\,\mathrm{e}^{-\mathrm{j}2\pi nT\nu} \\
\widetilde{\mathcal{A}}^{\mathrm{B}}(\nu,(2m+1)T) &= T\sum_n K^{\mathrm{B}}((n+\tfrac{1}{2})T,(2m+1)T)\,\mathrm{e}^{-\mathrm{j}2\pi(n+1/2)T\nu}.
\end{aligned}\tag{C.3}$$

Relation to Continuous AF The AF of $K_{\mathrm{i}}^{\mathrm{B}}$, defined in (B.3), is

$$\begin{aligned}
A_{\mathrm{i}}^{\mathrm{B}}(\nu,\tau) &= \int K(t,\tau)\sum_n \delta(t-nT)\sum_m \delta(\tau-2mT)\,\mathrm{e}^{-\mathrm{j}2\pi t\nu}\,\mathrm{d}t \\
&\quad + \int K(t,\tau)\sum_n \delta(t-(n+\tfrac{1}{2})T)\sum_m \delta(\tau-(2m+1)T)\,\mathrm{e}^{-\mathrm{j}2\pi t\nu}\,\mathrm{d}t \\
&= \sum_m\sum_n K^{\mathrm{B}}(nT,2mT)\,\mathrm{e}^{-\mathrm{j}2\pi nT\nu}\delta(\tau-2mT) \\
&\quad + \sum_m\sum_n K^{\mathrm{B}}((n+\tfrac{1}{2})T,(2m+1)T)\,\mathrm{e}^{-\mathrm{j}2\pi(n+\frac{1}{2})T\nu}\delta(\tau-(2m+1)T) \\
&= \frac{1}{T}\sum_m A^{\mathrm{B}}(\nu,mT)\delta(\tau-mT)
\end{aligned}\tag{C.4}$$

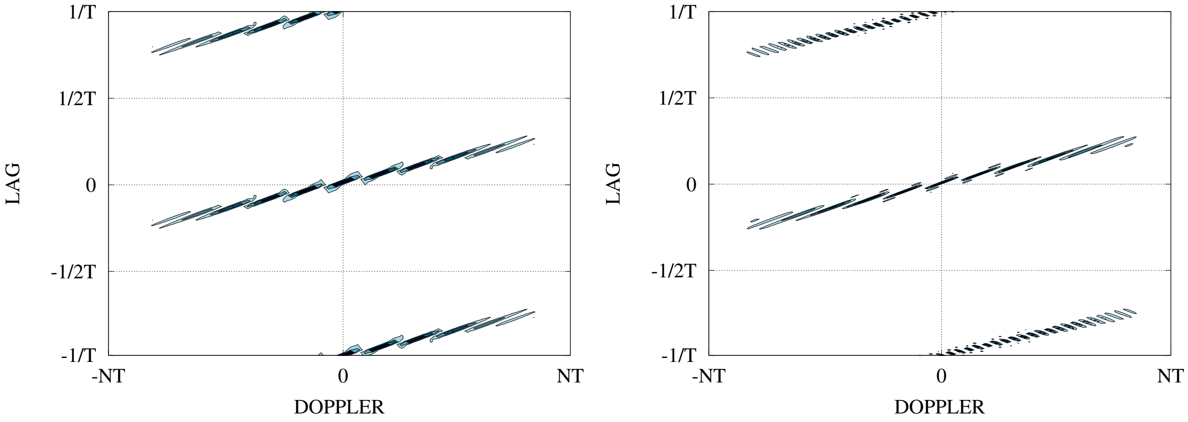

(a) (b)

FIGURE C.1: Discrete-lag AF of analytic LFM signal. (a) Real part of discrete-lag AF produced using sampling approach A, and (b) real part of discrete-lag AF produced using sampling approach B.

using the definition of the discrete-lag AF in (C.3). This also equals

$$
\begin{aligned}
A_{\mathrm{i}}^{\mathrm{B}}(\nu,\tau) &= A(\nu,\tau) \underset{\nu}{*} \Bigg(\int \sum_n \delta(t-nT) \sum_m \delta(\tau-2mT)\, \mathrm{e}^{-\mathrm{j}2\pi t\nu}\, \mathrm{d}t \\
&\qquad + \int \sum_n \delta(t-(n+\tfrac{1}{2})T) \sum_m \delta(\tau-(2m+1)T)\, \mathrm{e}^{-\mathrm{j}2\pi t\nu}\, \mathrm{d}t \Bigg) \\
&= A(\nu,\tau) \underset{\nu}{*} \Bigg(\frac{1}{T} \sum_m \delta(\tau-2mT) \sum_n \delta(\nu-\tfrac{n}{T}) \\
&\qquad + \frac{1}{T} \sum_m \delta(\tau-(2m+1)T) \sum_n (-1)^n \delta(\nu-\tfrac{n}{T}) \Bigg) \\
&= \frac{1}{T} \sum_m \sum_n (-1)^{nm} A(\nu-\tfrac{n}{T}, mT)\, \delta(\tau-mT)
\end{aligned}
$$

which when combined with (C.4) results in

$$
\widetilde{A}^{\mathrm{B}}(\nu, mT) = \sum_n (-1)^{nm} A(\nu-\tfrac{n}{T}, mT).
$$

Fig. C.1 shows the two discrete-lag AFs $\widetilde{\mathcal{A}}^{\mathrm{A}}$ and $\widetilde{\mathcal{A}}^{\mathrm{B}}$ using the same LFM analytic signal used in Section 2.4.3. We see that both discrete-lag AFs contain periodic copies outside the region $|\nu| < 1/2T$. Like the discrete-time WVD $\widetilde{W}^{\mathrm{B}}$, the discrete-lag AF $\widetilde{\mathcal{A}}^{\mathrm{B}}$ has periodic copies that oscillate between positive and negative values, depending in the parity of m. This oscillation is caused by the $(-1)^{nm}$ term in (6.4).

C.2 Discrete-Doppler Ambiguity Function

We use the two discrete SIAFs $\mathcal{K}^{\mathrm{A}}$ and $\mathcal{K}^{\mathrm{B}}$, from Section 2.4.3, to form two discrete-Doppler AFs.

C.2.1 SIAF Sampling Approach A

Apply the inverse discrete-frequency FT to the SIAF $\mathcal{K}^{\mathrm{A}}(2l\Lambda, k\Lambda)$ to obtain

$$\widetilde{\mathcal{A}}^{\mathrm{A}}(2l\Lambda, \tau) = \Lambda \sum_k \mathcal{K}^{\mathrm{A}}(2l\Lambda, k\Lambda)\, \mathrm{e}^{\mathrm{j}2\pi k\Lambda\tau}. \tag{C.5}$$

Relation to Continuous AF As with the discrete-time WVD, we can use the AF of the sampled SIAF defined in (B.1) to relate the discrete-lag AF to the continuous AF:

$$\begin{aligned}
\mathcal{A}_{\mathrm{i}}^{\mathrm{A}}(\nu, \tau) &= \int \mathcal{K}(\nu, f) \sum_l \delta(\nu - 2l\Lambda) \sum_k \delta(f - k\Lambda)\, \mathrm{e}^{\mathrm{j}2\pi f\tau}\, \mathrm{d}f \\
&= \sum_l \sum_k \mathcal{K}^{\mathrm{A}}(2l\Lambda, k\Lambda)\, \mathrm{e}^{\mathrm{j}2\pi k\Lambda\tau} \delta(\nu - 2l\Lambda) \\
&= \frac{1}{\Lambda} \sum_l \mathcal{A}^{\mathrm{A}}(2l\Lambda, \tau) \delta(\nu - 2l\Lambda)
\end{aligned} \tag{C.6}$$

where the definition of $\mathcal{A}^{\mathrm{A}}$ in (C.5) was substituted in the last line. We can rewrite the previous expression in terms of $\mathcal{A}$ as

$$\begin{aligned}
\mathcal{A}_{\mathrm{i}}^{\mathrm{A}}(\nu, \tau) &= \int \mathcal{K}(\nu, f) \sum_l \delta(\nu - 2l\Lambda) \sum_k \delta(f - k\Lambda)\, \mathrm{e}^{\mathrm{j}2\pi f\tau}\, \mathrm{d}f \\
&= \sum_k \delta(\nu - 2l\Lambda) \left(\mathcal{A}(\nu, \tau) \underset{\tau}{*} \frac{1}{\Lambda} \sum_k \delta(\tau - \tfrac{k}{\Lambda}) \right) \\
&= \frac{1}{\Lambda} \sum_l \sum_k \mathcal{A}(2l\Lambda, \tau - \tfrac{k}{\Lambda}) \delta(\nu - 2l\Lambda)
\end{aligned}$$

which when combined with (C.6) results in

$$\widetilde{\mathcal{A}}^{\mathrm{A}}(2l\Lambda, \tau) = \sum_l \mathcal{A}(2l\Lambda, \tau - \tfrac{k}{\Lambda}).$$

C.2.2 SIAF Sampling Approach B

Apply the inverse discrete-frequency FT to the SIAF $\mathcal{K}^{\mathrm{B}}(l\Lambda, k\Lambda/2)$ to obtain

$$\widetilde{\mathcal{A}}^{\mathrm{B}}(l\Lambda, \tau) = \Lambda \sum_k \mathcal{K}^{\mathrm{B}}(l\Lambda, \tfrac{k\Lambda}{2})\, \mathrm{e}^{\mathrm{j}\pi k\Lambda\tau}.$$

For even–odd values of m the preceding expression is

$$\begin{aligned}
\widetilde{\mathcal{A}}^{\mathrm{B}}(2l\Lambda, \tau) &= \Lambda \sum_k \mathcal{K}^{\mathrm{B}}(2l\Lambda, k\Lambda)\, \mathrm{e}^{\mathrm{j}2\pi k\Lambda\tau} \\
\widetilde{\mathcal{A}}^{\mathrm{B}}((2l+1)\Lambda, \tau) &= \Lambda \sum_k \mathcal{K}^{\mathrm{B}}((2l+1)\Lambda, (k + \tfrac{1}{2})\Lambda)\, \mathrm{e}^{\mathrm{j}2\pi(k+1/2)\Lambda\tau}.
\end{aligned} \tag{C.7}$$

Relation to Continuous AF The following derives the relation between the continuous and discrete-Doppler AF:

$$\begin{aligned}
\mathcal{A}_{\mathrm{i}}^{\mathrm{B}}(\nu,\tau) &= \int \mathcal{K}(\nu,f)\sum_k \delta(f-k\Lambda)\sum_l \delta(\nu-2l\Lambda)\,\mathrm{e}^{\mathrm{j}2\pi f\tau}\,\mathrm{d}f \\
&\quad + \int \mathcal{K}(\nu,f)\sum_k \delta(f-(k+\tfrac{1}{2})\Lambda)\sum_l \delta(\nu-(2l+1)\Lambda)\,\mathrm{e}^{\mathrm{j}2\pi f\tau}\,\mathrm{d}f \\
&= \sum_k\sum_l \mathcal{K}^{\mathrm{B}}(2l\Lambda,k\Lambda)\,\mathrm{e}^{\mathrm{j}2\pi k\Lambda\tau}\delta(\nu-2l\Lambda) \\
&\quad + \sum_k\sum_l \mathcal{K}^{\mathrm{B}}((2l+1)\Lambda,(k+\tfrac{1}{2})\Lambda)\,\mathrm{e}^{\mathrm{j}2\pi(k+\frac{1}{2})\Lambda\tau}\delta(\nu-(2l+1)\Lambda) \\
&= \frac{1}{\Lambda}\sum_m \mathcal{A}^{\mathrm{B}}(l\Lambda,\tau)\delta(\nu-l\Lambda)
\end{aligned} \tag{C.8}$$

using the definition of the discrete-Doppler AF in (C.7). We can rewrite the previous expression as

$$\begin{aligned}
\mathcal{A}_{\mathrm{i}}^{\mathrm{B}}(\nu,\tau) &= \mathcal{A}(\nu,\tau) \underset{\tau}{*} \Bigg(\int \sum_k \delta(f-k\Lambda)\sum_l \delta(\nu-2l\Lambda)\,\mathrm{e}^{\mathrm{j}2\pi f\tau}\,\mathrm{d}f \\
&\qquad + \int \sum_k \delta(f-(k+\tfrac{1}{2})\Lambda)\sum_l \delta(\nu-(2l+1)\Lambda)\,\mathrm{e}^{\mathrm{j}2\pi f\tau}\,\mathrm{d}f \Bigg) \\
&= \mathcal{A}(\nu,\tau) \underset{\tau}{*} \Bigg(\frac{1}{\Lambda}\sum_k \delta(\tau-\tfrac{k}{\Lambda})\sum_l \delta(\nu-2l\Lambda) \\
&\qquad + \frac{1}{\Lambda}\sum_k (-1)^k \delta(\tau-\tfrac{k}{\Lambda})\sum_l \delta(\nu-(2l+1)\Lambda) \Bigg) \\
&= \frac{1}{\Lambda}\sum_k\sum_l (-1)^{kl}\mathcal{A}(l\Lambda,\tau-\tfrac{k}{\Lambda})\delta(\nu-l\Lambda)
\end{aligned}$$

which when combined with (C.8) results in

$$\widetilde{\mathcal{A}}^{\mathrm{B}}(l\Lambda,\tau) = \sum_k (-1)^{kl}\mathcal{A}(l\Lambda,\tau-\tfrac{k}{\Lambda}).$$

We show an example of the two discrete-Doppler AFs $\widetilde{\mathcal{A}}^{\mathrm{A}}$ and $\widetilde{\mathcal{A}}^{\mathrm{B}}$ in Fig. C.2, using the LFM analytic signal. These plots show the periodic components, caused by the sampling in the frequency-direction, for the two discrete-Doppler AFs.

C.3 Discrete-Doppler, Discrete-Lag Ambiguity Function

We use the two discrete periodic TIAFs $\widetilde{K}^{\mathrm{A}}$ and $\widetilde{K}^{\mathrm{B}}$, from Section B.5.1 and Section B.5.2, to form two discrete-Doppler, discrete-lag AFs, or the discrete AF (DAF) for short.

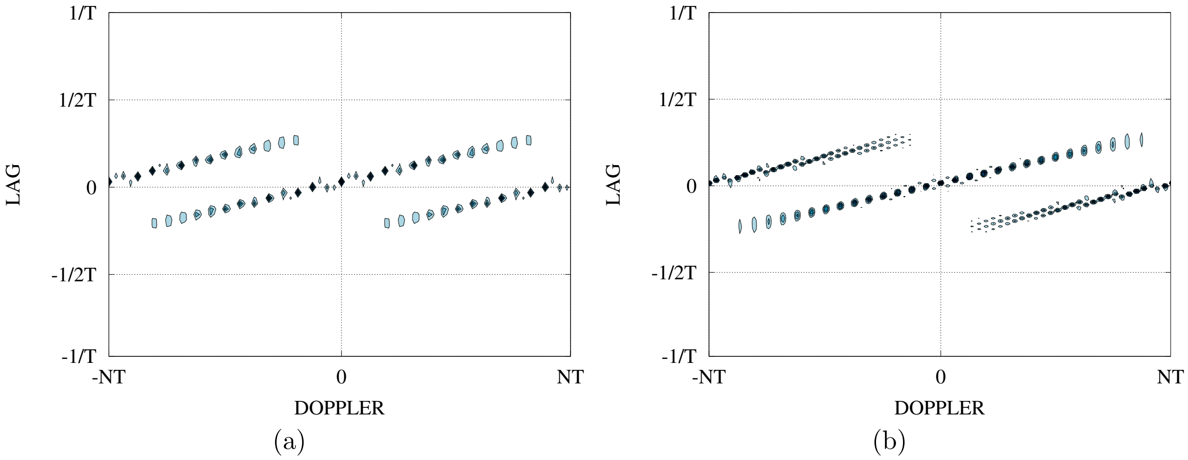

FIGURE C.2: Discrete-Doppler AF of analytic LFM signal. (a) Real part of discrete-Doppler AF produced using sampling approach A, and (b) real part of discrete-Doppler AF produced using sampling approach B.

For the first DAF definition, we use $\widetilde{K}^{\mathrm{A}}$:

$$A^{\mathrm{A}}(\tfrac{2l}{NT}, 2mT) = \frac{2}{N} \sum_{|n|<N/4} \widetilde{K}^{\mathrm{A}}(nT, 2mT)\, \mathrm{e}^{-\mathrm{j}(4\pi/N)nl}. \tag{C.9}$$

Applying the same approach as for the DWVD in Section 2.4.5 the relation between the DAF and AF is

$$A^{\mathrm{A}}(\tfrac{2l}{NT}, 2mT) = \sum_{n}\sum_{k} \mathcal{A}((2l-nN)\tfrac{1}{NT}, (2m-kN)T). \tag{C.10}$$

For the second DAF definition, we use $\widetilde{K}^{\mathrm{B}}$:

$$A^{\mathrm{B}}(\tfrac{l}{NT}, mT) = \frac{1}{N} \sum_{|n|<N} \widetilde{K}^{\mathrm{B}}(\tfrac{nT}{2}, mT)\, \mathrm{e}^{-\mathrm{j}(\pi/N)nl} \tag{C.11}$$

which is related to the continuous AF as follows:

$$A^{\mathrm{B}}(\tfrac{l}{NT}, mT) = \sum_{n}\sum_{k} (-1)^{nm+lk-knN} \mathcal{A}((l-nN)\tfrac{1}{NT}, (m-kN)T). \tag{C.12}$$

We could have also derived the same two DAF definitions by using the discrete periodic SIAFs rather than the discrete periodic TIAFs.

C.3.1 Aliasing and Periodicity in the Doppler–Lag Domain

The DAF is periodic in both Doppler and lag, as shown in (C.10) and (C.12). We now look at why the DAF is aliased using both the real and analytic signal for the two sampling approaches. First, if $x(t)$ is the real-valued signal, band limited as detailed by Section 2.4.6, then the continuous AF is

$$A(\nu, \tau) \approx 0 \quad \text{for } |\nu| > \frac{1}{T} \text{ or } |\tau| > NT.$$

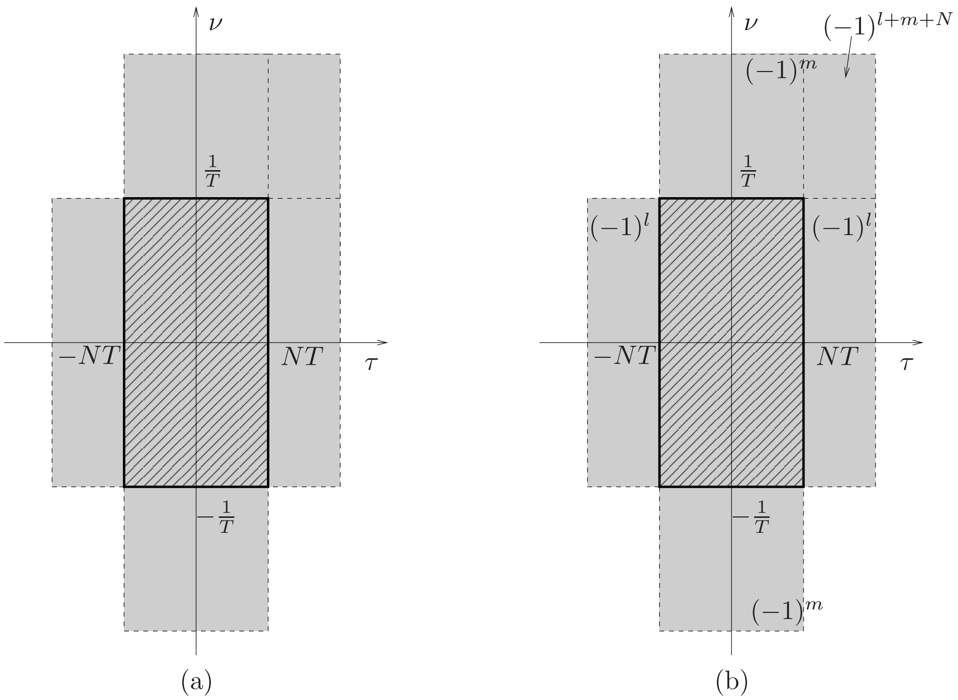

Figure C.3: The DAF (a) A^{A} and (b) A^{B} represented as a sum of Doppler and lag shifted AF copies using a real signal. For clarity, I show only a subset of the terms in the summations in (C.13) and (C.14). The terms $(-1)^l$, $(-1)^m$ and $(-1)^{l+m+N}$ in (b) is a multiplicative factor for the shifted AF copies.

(See Section 2.4.6 for a discussion on why the AF is not exactly zero for this region.)

Within the signal's Doppler–lag region—that is, within the region $|\nu| \leq 1/T$ and $|\tau| \leq NT$—the two DAFs are thus related to the continuous AF

$$A^{\mathrm{A}}(\tfrac{2l}{NT}, 2mT) \approx \sum_{n=-1}^{1} \sum_{k=-1}^{1} A((2l - nN)\tfrac{1}{NT}, (2m - kN)T) \tag{C.13}$$

$$A^{\mathrm{B}}(\tfrac{l}{NT}, mT) \approx \sum_{n=-1}^{1} \sum_{k=-1}^{1} (-1)^{nm+lk-knN} A((l - nN)\tfrac{1}{NT}, (m - kN)T) \tag{C.14}$$

Therefore, both DAFs are aliased—Fig. C.3 illustrates. Both DAFs are aliased to the same extent, the only difference is the addition of the multiplicative factor $(-1)^{nm+lk-knN}$ for the DAF A^{B}, as shown in (C.14).

Second, if we use the band-limited analytic signal $z(t)$, defined in Section 2.4.6, the continuous AF of this signal is

$$A(\nu, \tau) \approx 0 \quad \text{for } |\nu| > \frac{1}{2T} \text{ or } |\tau| > NT$$

which has half the Doppler–lag bandwidth of the AF of real signal $x(t)$.

The two DAFs definitions within the signal's Doppler–lag region—that is, within the

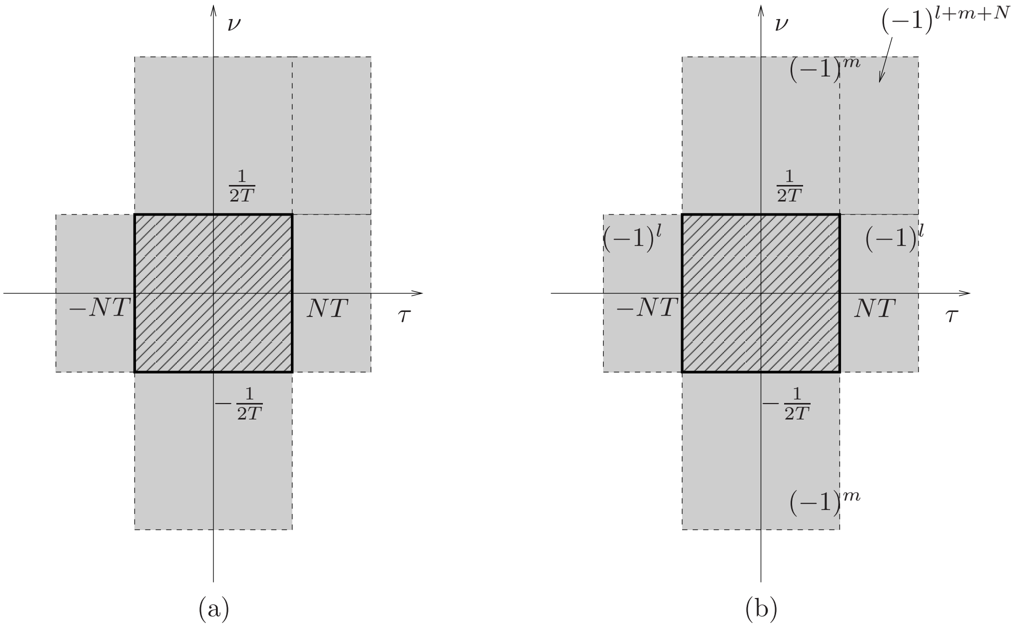

FIGURE C.4: The DAF (a) A^{A} and (b) A^{B} represented as a sum of Doppler and lag shifted AF copies using an analytic signal. For clarity I show only a subset of the terms in the summations in (C.15) and (C.16). The terms $(-1)^l$, $(-1)^m$ and $(-1)^{l+m+N}$ in (b) is a multiplicative factor for the shifted AF copies.

region $|\nu| \leq 1/(2T)$ and $|\tau| \leq NT$—are thus related to the continuous AF

$$A^{\mathrm{A}}(\tfrac{2l}{NT}, 2mT) = \sum_{k=-1}^{1} A(\tfrac{2l}{NT}, (2m - kN)T) \tag{C.15}$$

$$A^{\mathrm{B}}(\tfrac{l}{NT}, mT) = \sum_{k=-1}^{1} (-1)^{nm+lk-knN} A(\tfrac{l}{NT}, (m - kN)T) \tag{C.16}$$

Fig. C.4 illustrates these relations. Even though the Doppler–lag region of extent for the DAF of the analytic signal is smaller than that for the DAF of real-valued signal, the DAF of the analytic signal is still aliased.

To conclude I present an example for the DAFs A^{A} and A^{B} in Fig. C.5.

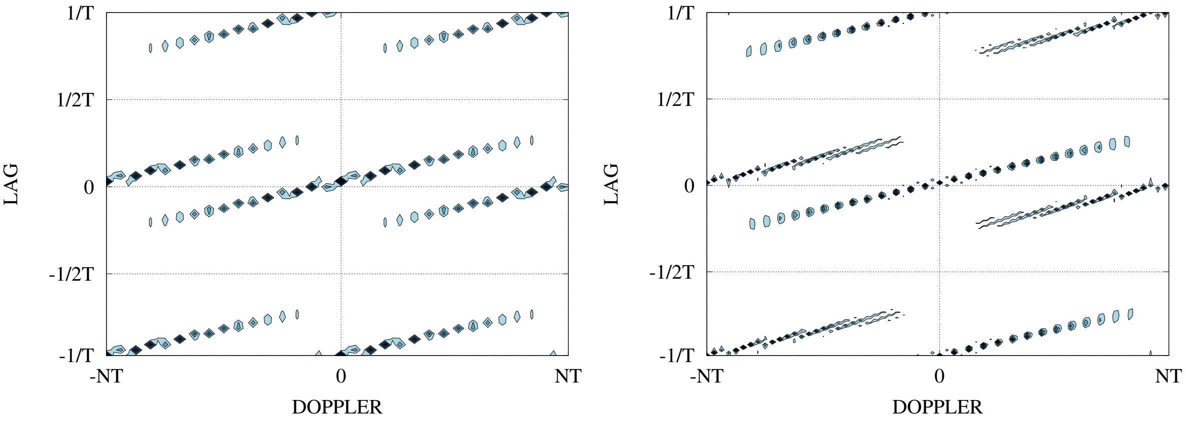

(a) (b)

FIGURE C.5: DAF of analytic LFM signal. (a) Real part of DAF produced using sampling approach A, and (b) real part of DAF produced using sampling approach B.

C.3.2 Relation Between DAF-A and DAF-B

We can write DAF-B, of a $2N$-point signal, for even values of l and m as

$$\begin{aligned}
\mathcal{A}^{\mathrm{B}}(\tfrac{2l}{2NT}, 2mT) &= \frac{1}{2N}\sum_{|k|<N} \widetilde{\mathcal{K}}^{\mathrm{B}}(\tfrac{2l}{2NT}, \tfrac{2k}{4NT})\,\mathrm{e}^{\mathrm{j}(2\pi/N)km} \\
&= \frac{1}{2N}\left(\sum_{k=0}^{N-1} \widetilde{\mathcal{K}}^{\mathrm{B}}(\tfrac{2l}{2NT}, \tfrac{2k}{4NT})\,\mathrm{e}^{\mathrm{j}(2\pi/N)km} + \sum_{k=N}^{2N-1} \widetilde{\mathcal{K}}^{\mathrm{B}}(\tfrac{2l}{2NT}, \tfrac{2k}{4NT})\,\mathrm{e}^{\mathrm{j}(2\pi/N)km}\right) \\
&= \frac{1}{2N}\left(\sum_{k=0}^{N-1} \widetilde{\mathcal{K}}^{\mathrm{B}}(\tfrac{2l}{2NT}, \tfrac{2k}{4NT})\,\mathrm{e}^{\mathrm{j}(2\pi/N)km}\right. \\
&\qquad \left. + \sum_{k=0}^{N-1} \widetilde{\mathcal{K}}^{\mathrm{B}}(\tfrac{2l}{2NT}, (2k+2N)\tfrac{1}{4NT})\,\mathrm{e}^{\mathrm{j}(2\pi/N)km}\right)
\end{aligned}$$

and substituting in the definition of $\widetilde{\mathcal{K}}^{\mathrm{A}}$ from (B.11), now with $2N$ rather than N, results in

$$\begin{aligned}
\mathcal{A}^{\mathrm{B}}(\tfrac{2l}{2NT}, 2mT) &= \frac{1}{2N}\sum_{k=0}^{N-1} \widetilde{\mathcal{K}}^{\mathrm{A}}(\tfrac{2l}{2NT}, \tfrac{2k}{4NT})\,\mathrm{e}^{-\mathrm{j}(2\pi/N)nl} \\
&= \frac{1}{2}\mathcal{A}^{\mathrm{A}}(\tfrac{2l}{2NT}, 2mT).
\end{aligned}$$

An expected result from the lag decimation is a folding of the SIAF in the frequency direction, that is,

$$\widetilde{\mathcal{K}}^{\mathrm{A}}(\tfrac{l}{NT}, \tfrac{k}{NT}) = \widetilde{\mathcal{K}}^{\mathrm{B}}(\tfrac{2l}{2NT}, \tfrac{2k}{4NT}) + \widetilde{\mathcal{K}}^{\mathrm{B}}(\tfrac{2l}{2NT}, \tfrac{(2k+2N)}{4NT}) \tag{C.17}$$

which is consistent with the definition of $\widetilde{\mathcal{K}}^{\mathrm{A}}$ in (B.11).

Appendix D

Proof of Spectral Energy Relation for the Discrete Analytic Signals

I derive the relation, for the negative spectral energy, between the proposed and conventional analytic signals. To do so, I decompose the energy of $Z_\mathrm{p}(k/2NT)$ for $N \leq k \leq 2N-1$ as follows:

$$\sum_{k=N}^{2N-1} \left|Z_\mathrm{p}(\tfrac{k}{2NT})\right|^2 = \left|Z_\mathrm{p}(\tfrac{N}{2NT})\right|^2 + \sum_{k=\lfloor \frac{N}{2} \rfloor+1}^{N-1} \left|Z_\mathrm{p}(\tfrac{2k}{2NT})\right|^2 + \sum_{k=\lceil \frac{N}{2} \rceil}^{N-1} \left|Z_\mathrm{p}(\tfrac{2k+1}{2NT})\right|^2$$

where the function $\lfloor x \rfloor$ returns an integer smaller than or equal to x, and the function $\lceil x \rceil$ returns an integer larger than or equal to x. We examine each part of the preceding decomposition separately.

D.1 Case for k odd

First, write $U_\mathrm{t}(k/2NT)$, which is the DFT of $u_\mathrm{t}(nT)$, as

$$U_\mathrm{t}(\tfrac{k}{2NT}) = \begin{cases} N\delta[k], & k \text{ even,} \\ 1 - \mathrm{j}\cot(\tfrac{\pi k}{2N}), & k \text{ odd.} \end{cases} \tag{D.1}$$

Next, consider the energy at negative frequencies for $Z_\mathrm{c}(k/2NT)$. From (3.11) and (3.13), we express $Z_\mathrm{c}(k/2NT)$ as

$$Z_\mathrm{c}(\tfrac{k}{2NT}) = \frac{1}{N} \sum_{l=0}^{N-1} S_\mathrm{a}(\tfrac{2l}{2NT}) H_\mathrm{a}(\tfrac{2l}{2NT}) U_\mathrm{t}(\tfrac{k-2l}{2NT}).$$

If we use (D.1) in the preceding equation, then we can write $Z_\mathrm{c}(k/2NT)$ for even–odd k values as

$$Z_\mathrm{c}(\tfrac{2k}{2NT}) = S_\mathrm{a}(\tfrac{2k}{2NT}) H_\mathrm{a}(\tfrac{2k}{2NT}) \tag{D.2}$$

$$Z_\mathrm{c}(\tfrac{2k+1}{2NT}) = \frac{1}{N} \sum_{l=0}^{N-1} S_\mathrm{a}(\tfrac{2l}{2NT}) H_\mathrm{a}(\tfrac{2l}{2NT}) U_\mathrm{t}(\tfrac{2k+1-2l}{2NT}). \tag{D.3}$$

The even k terms for $Z_\mathrm{c}(k/2NT)$ do not contribute to the negative spectral energy because, from (3.6), $H_\mathrm{a}(2k/2NT) = 0$ for $2k > N$. Thus, the energy in the negative spectral region is solely caused by the odd k terms in $Z_\mathrm{c}(k/2NT)$,

$$\sum_{k=N+1}^{2N-1} \left| Z_\mathrm{c}(\tfrac{k}{2NT}) \right|^2 = \sum_{k=\lceil \frac{N}{2} \rceil}^{N-1} \left| Z_\mathrm{c}(\tfrac{2k+1}{2NT}) \right|^2 . \tag{D.4}$$

Lastly, consider the energy at negative frequencies for $Z_\mathrm{p}(k/2NT)$. By combining (3.12) and (D.1), $Z_\mathrm{p}(k/2NT)$ for odd k values is

$$Z_\mathrm{p}(\tfrac{2k+1}{2NT}) = \frac{1}{2} S_\mathrm{a}(\tfrac{2k+1}{2NT}) H_\mathrm{a}(\tfrac{2k+1}{2NT}) + \frac{1}{2N} \sum_{l=0}^{N-1} S_\mathrm{a}(\tfrac{2l}{2NT}) H_\mathrm{a}(\tfrac{2l}{2NT}) U_\mathrm{t}(\tfrac{2k+1-2l}{2NT}). \tag{D.5}$$

Thus, relating (D.5) with (D.3) and (3.5), gives us

$$Z_\mathrm{p}(\tfrac{2k+1}{2NT}) = \frac{1}{2} \left[Z_\mathrm{a}(\tfrac{2k+1}{2NT}) + Z_\mathrm{c}(\tfrac{2k+1}{2NT}) \right] . \tag{D.6}$$

From (3.6), we know that $Z_\mathrm{a}(k/2NT) = 0$ for $k > N$; therefore, (D.6) reduces to $Z_\mathrm{p}((2k+1)/2NT) = Z_\mathrm{c}((2k+1)/2NT)/2$ for $(2k+1) > N$. If we combine this relation with (D.4), then we get the negative spectral energy relation,

$$\sum_{k=\lceil \frac{N}{2} \rceil}^{N-1} \left| Z_\mathrm{p}(\tfrac{2k+1}{2NT}) \right|^2 = \frac{1}{4} \sum_{k=N+1}^{2N-1} \left| Z_\mathrm{c}(\tfrac{k}{2NT}) \right|^2 . \tag{D.7}$$

D.2 Case for k even

We start by introducing a new signal $\hat{z}(nT)$, defined as

$$\hat{z}(nT) = \begin{cases} 0, & 0 \le n \le N-1, \\ z_\mathrm{a}(nT), & N \le n \le 2N-1. \end{cases} \tag{D.8}$$

The signal $\hat{z}(nT)$ is purely imaginary because the real part of $z_\mathrm{a}(nT)$ is zero for $N \le n \le 2N-1$. We can also express $\hat{z}(nT)$ as $\hat{z}(nT) = z_\mathrm{a}(nT) - z_\mathrm{p}(nT)$ for all values of n. In the frequency domain, this equates to

$$\widehat{Z}(\tfrac{k}{2NT}) = Z_\mathrm{a}(\tfrac{k}{2NT}) - Z_\mathrm{p}(\tfrac{k}{2NT}) \tag{D.9}$$

where $\widehat{Z}(k/2NT)$ represents the DFT of $\hat{z}(nT)$. We now introduce some properties of $\widehat{Z}(k/2NT)$.

We can show easily, because of the form of $\hat{z}(nT)$ in (D.8), that

$$\sum_{k=0}^{N-1} \left| \widehat{Z}(\tfrac{2k}{2NT}) \right|^2 = \sum_{k=0}^{N-1} \left| \widehat{Z}(\tfrac{2k+1}{2NT}) \right|^2 . \tag{D.10}$$

Also, because $\hat{z}(nT)$ is purely imaginary then following symmetry holds:

$$\widehat{Z}(\tfrac{2N-k}{2NT}) = -\left[\widehat{Z}(\tfrac{k}{2NT})\right]^{*}. \tag{D.11}$$

We express the spectral energy for $\widehat{Z}(2k/2NT)$, using the symmetrical relation in (D.11), as

$$\sum_{k=0}^{N-1} \left|\widehat{Z}(\tfrac{2k}{2NT})\right|^{2} = \left|\widehat{Z}(\tfrac{0}{2NT})\right|^{2} + 2 \sum_{k=\lfloor \frac{N}{2} \rfloor +1}^{N-1} \left|\widehat{Z}(\tfrac{2k}{2NT})\right|^{2} + A. \tag{D.12}$$

with

$$A = \begin{cases} |\widehat{Z}(\tfrac{N}{2NT})|^{2}, & N \text{ even}, \\ 0, & N \text{ odd}. \end{cases}$$

Similarly, the spectral energy at k odd values of $\widehat{Z}(k/2NT)$ is

$$\sum_{k=0}^{N-1} \left|\widehat{Z}(\tfrac{2k+1}{2NT})\right|^{2} = 2 \sum_{k=\lceil \frac{N}{2} \rceil}^{N-1} \left|\widehat{Z}(\tfrac{2k+1}{2NT})\right|^{2} + B. \tag{D.13}$$

with

$$B = \begin{cases} 0, & N \text{ even}, \\ |\widehat{Z}(\tfrac{N}{2NT})|^{2}, & N \text{ odd}. \end{cases}$$

This concludes the segment on the properties of $\widehat{Z}(k/2NT)$.

If we substitute (D.13) and (D.12) into (D.10), then we obtain:

$$\sum_{k=\lfloor \frac{N}{2} \rfloor +1}^{N-1} \left|\widehat{Z}(\tfrac{2k}{2NT})\right|^{2} = \sum_{k=\lceil \frac{N}{2} \rceil}^{N-1} \left|\widehat{Z}(\tfrac{2k+1}{2NT})\right|^{2} - \frac{1}{2}\left[\left|\widehat{Z}(\tfrac{0}{2NT})\right|^{2} + A - B\right].$$

Then we substitute (D.7), and the relation $\widehat{Z}(k/2NT) = -Z_{\mathrm{p}}(k/2NT)$ for $k > N$, into the preceding equation to obtain:

$$\sum_{k=\lfloor \frac{N}{2} \rfloor +1}^{N-1} \left|Z_{\mathrm{p}}(\tfrac{2k}{2NT})\right|^{2} = \frac{1}{4} \sum_{k=N+1}^{2N-1} \left|Z_{\mathrm{c}}(\tfrac{k}{2NT})\right|^{2} - \frac{1}{2}\left[\left|\widehat{Z}(\tfrac{0}{2NT})\right|^{2} + A - B\right]. \tag{D.14}$$

D.3 Nyquist Frequency Terms

The Nyquist term $Z_{\mathrm{a}}(N/2NT)$ is a real number, because of the definition of $Z_{\mathrm{a}}(k/2NT)$ in (3.5); the Nyquist term $\widehat{Z}(N/2NT)$ is an imaginary number, because $\hat{z}(nT)$ is purely imaginary. Thus, we rewrite (D.9) as

$$\left|Z_{\mathrm{p}}(\tfrac{N}{2NT})\right|^{2} = \left|Z_{\mathrm{a}}(\tfrac{N}{2NT})\right|^{2} + \left|\widehat{Z}(\tfrac{N}{2NT})\right|^{2}. \tag{D.15}$$

The remaining relations depend on the parity of N.

D.3.1 Case for N even

We know, from (D.2) and (3.5), that when N is even, $Z_{\mathrm{c}}(N/2NT) = Z_{\mathrm{a}}(N/2NT)$. When we combine this with (D.15) we get

$$\left|Z_{\mathrm{p}}(\tfrac{N}{2NT})\right|^2 = \left|Z_{\mathrm{c}}(\tfrac{N}{2NT})\right|^2 + \left|\widehat{Z}(\tfrac{N}{2NT})\right|^2. \tag{D.16}$$

D.3.2 Case for N odd

We know, from (D.6), that when N is odd,

$$Z_{\mathrm{c}}(\tfrac{N}{2NT}) = 2Z_{\mathrm{p}}(\tfrac{N}{2NT}) - Z_{\mathrm{a}}(\tfrac{N}{2NT}).$$

When we combine this with (D.9) we get

$$\left|Z_{\mathrm{c}}(\tfrac{N}{2NT})\right|^2 = \left|Z_{\mathrm{a}}(\tfrac{N}{2NT})\right|^2 + 4\left|\widehat{Z}(\tfrac{N}{2NT})\right|^2.$$

If we substitute this equation into (D.15), then we get the relation

$$\left|Z_{\mathrm{p}}[N]\right|^2 = \left|Z_{\mathrm{c}}[N]\right|^2 - 3\left|\widehat{Z}[N]\right|^2. \tag{D.17}$$

Finally, we are able to assemble the three parts of the decomposition in (D.1). If we combine the relation for k even in (D.14) with the relation for k odd in (D.7), and add the Nyquist frequency relations in (D.16) and (D.17), then we get the following:

$$\sum_{k=N}^{2N-1} \left|Z_{\mathrm{p}}(\tfrac{k}{2NT})\right|^2 = \frac{1}{2}\sum_{k=N}^{2N-1} \left|Z_{\mathrm{c}}(\tfrac{k}{2NT})\right|^2 + \frac{1}{2}\left(\left|Z_{\mathrm{p}}[N]\right|^2 - \left|\widehat{Z}[0]\right|^2 - C\right)$$

with

$$C = \begin{cases} 0, & N \text{ even}, \\ 2|\widehat{Z}(\tfrac{N}{2NT})|^2, & N \text{ odd}. \end{cases}$$

This concludes the proof.

Appendix E

Aliasing and the AF-GDTFD

The AF-GDTFD is aliased, but, as this section describes, the quantity of aliasing depends on the structure of the kernel. To begin, lets define an alternative DTFD definition, which we shall call the DTFD-R, as follows:

$$\rho^{\mathrm{R}}(\tfrac{nT}{2}, \tfrac{k}{4NT}) = W^{\mathrm{B}}(\tfrac{nT}{2}, \tfrac{k}{4NT}) \underset{n}{\circledast} \underset{k}{\circledast} \gamma^{\mathrm{R}}(\tfrac{nT}{2}, \tfrac{k}{4NT}). \tag{E.1}$$

for $n, k = 0, 1, \ldots, 4N-1$. The DWVD-B in the preceding equation, which uses the $2N$-point analytic signal $z(nT)$, is a full-plane distribution and extends over the time–frequency region $0 \leq t \leq 2NT$ and $|f| \leq 1/(2T)$. Thus the DTFD-R uses the same DWVD definition as the AF-GDTFD uses in (4.4).

The DTFD-R's kernel, like the AF-GDTFD, extends over the Doppler–lag region $|\nu| \leq 1/T$ and $|\tau| \leq 2NT$; the kernel γ^{R}, however, has a denser time–lag sample grid compared with that for the AF-GDTFD, as we can see by comparing Fig. E.1 and Fig. 4.2(b).

The AF-GDTFD is a time- and frequency-decimated version of the DTFD-R:

$$\rho^{\mathrm{AF}}(nT, \tfrac{k}{2NT}) = \rho^{\mathrm{R}}(\tfrac{2nT}{2}, \tfrac{2k}{4NT}). \tag{E.2}$$

[This relation follows simply from (4.4) and (E.1).] Hence, if the DTFD-R is aliased then the AF-GDTFD will be aliased too, and likewise if the DTFD-R contains only minimal aliasing then the AF-GDTFD will contain also only minimal aliasing.

To understand why the DTFD-R, and therefore the AF-GDTFD, is aliased, we examine the distribution in the Doppler–lag domain. The DTFD in the Doppler–lag domain is

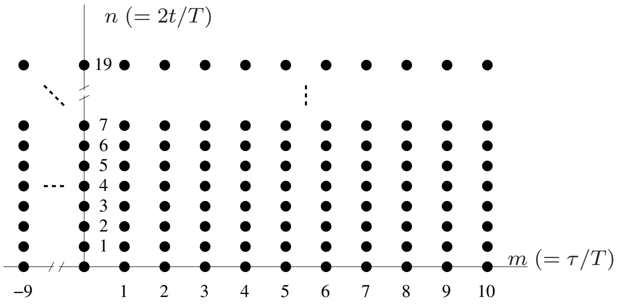

FIGURE E.1: Time–lag (t–τ) sample grid of $G^{\mathrm{R}}(nT/2, mT)$ for length $2N = 10$ signal.

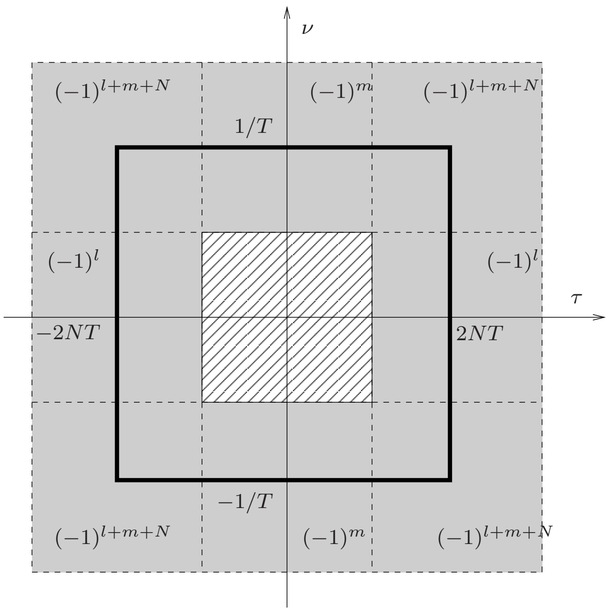

FIGURE E.2: Discrete ambiguity function (DAF) A^{B} of $2N$-point analytic signal. The thick black line denotes the region of extent for $A^{\mathrm{B}}(l/2NT, mT)$. The grey shaded regions represent the periodic shifted copies of the DAF. The terms $(-1)^n$, $(-1)^k$ and $(-1)^{n+k+N}$ are multiplicative factors for the shifted DAF copies.

called the smoothed discrete ambiguity function S^{R}, which is the product of the discrete ambiguity function (DAF) and the Doppler–lag kernel:

$$S^{\mathrm{R}}(\tfrac{l}{2NT}, mT) = A^{\mathrm{B}}(\tfrac{l}{2NT}, mT) g^{\mathrm{R}}(\tfrac{l}{2NT}, mT) \tag{E.3}$$

for $l, m = 0, 1, \ldots, 4N-1$. We know, from (2.41), that the DAF A^{B} is periodic in $2N$; thus, within the region in (E.3), the DAF contains periodic copies, which Fig. E.2 shows. The quantity of aliasing suppressed depends on the structure of Doppler–lag kernel g^{R}. That is, if g^{R} is zero outside the region $|\nu| \leq 1/(2T)$ and $|\tau| \leq NT$, then, from (E.3), the smoothed DAF S^{R} will not contain any periodic copies of the DAF. Conversely, if g^{R} is nonzero outside the region $|\nu| \leq 1/(2T)$ and $|\tau| \leq NT$, then some, or all, of the DAF periodic copies will appear in S^{R}.

To formalise this process, lets define a two-dimensional rectangular function H in the Doppler–lag domain as

$$H(\tfrac{l}{2NT}, mT) = \begin{cases} 1, & \text{if } |l| \leq N \text{ or } |m| \leq N, \\ 0, & \text{otherwise.} \end{cases} \tag{E.4}$$

Fig. E.3 illustrates the function H.

If the Doppler–lag kernel g^{R} satisfies the condition that

$$g^{\mathrm{R}}(\tfrac{l}{2NT}, mT) = g^{\mathrm{R}}(\tfrac{l}{2NT}, mT) H(\tfrac{l}{2NT}, mT) \tag{E.5}$$

then the DTFD-R, and thus the AF-GDTFD, will be a pseudo-alias–free distribution because, from (E.3) and (E.4), the kernel g^{R} will suppress the periodic copies of the DAF

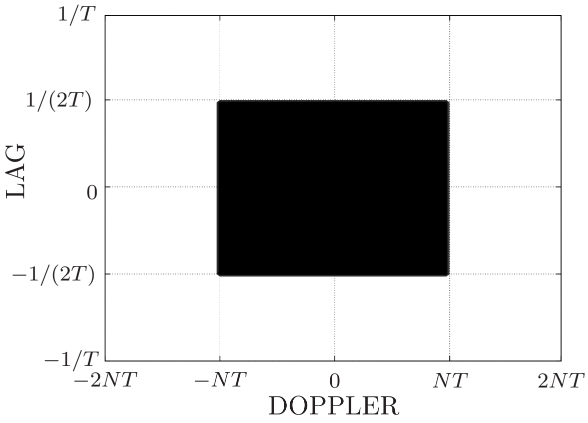

FIGURE E.3: The two-dimensional rectangle-window function H. Black represents one and white represents zero.

in A^{B}. The condition in (E.5) may be true for some kernel types, although certainly not all. For example, Doppler- or lag-independent kernels will not satisfy (E.3), or even most two-dimensional smoothing kernel types, which may tend to—although never reach—zero as they extend out from the Doppler–lag origin [8].

Fig. E.4 shows an example using a LFM signal and a Doppler–independent (DI) kernel of the three functions in (E.3). The DI kernel does not satisfy the relation in (E.5) because it is nonzero for $|\tau| > NT$ as Fig. E.4(b) shows. Fig. E.5 shows a similar example but with a separable, rather than DI, kernel. From Fig. E.5(b) it appears that this kernel satisfies—or at least better approximates—the relation in (E.5). Note, from Fig. E.4(c) and Fig. E.5(c), that the smoothed DAF that uses the separable kernel has less aliasing energy compared with that for the smoothed DAF that uses the DI kernel. This aliasing energy is transformed to the time–frequency domain; Fig. E.6 shows the DTFD-R using the examples in Fig. E.4 and Fig. E.5.

We could, of course, force the DTFD-R to a pseudo-alias–free definition by redefining the DTFD-R as

$$\rho^{\mathrm{R}}(\tfrac{nT}{2}, \tfrac{k}{4NT}) = W^{\mathrm{B}}(\tfrac{nT}{2}, \tfrac{k}{4NT}) \underset{n}{\circledast} \underset{k}{\circledast} \gamma^{\mathrm{R}}(\tfrac{nT}{2}, \tfrac{k}{4NT}) \underset{n}{\circledast} \underset{k}{\circledast} h(\tfrac{nT}{2}, \tfrac{k}{4NT}) \qquad \text{(E.6)}$$

where h is the time–frequency representation for Doppler–lag kernel H. (The multiplication in the Doppler–lag domain equates to a time–frequency convolution in the time–frequency domain.) The consequences of including h in the preceding definition is the modified DTFD-R from (E.6) will not satisfy certain properties, such the time- or frequency-marginal. Thus, forcing the DTFD-R, and therefore the AF-GDTFD, to be a pseudo-alias–free definition, may results in a loss of mathematical properties.

The proposed DTFD definition, from Chapter 4, however, does not require the extra limitation in (E.5) on its kernel—the proposed definition is a pseudo-alias–free definition, regardless of kernel structure and requires only $2N^2$ sample points, unlike the AF-GDTFD which requires $4N^2$ sample points.

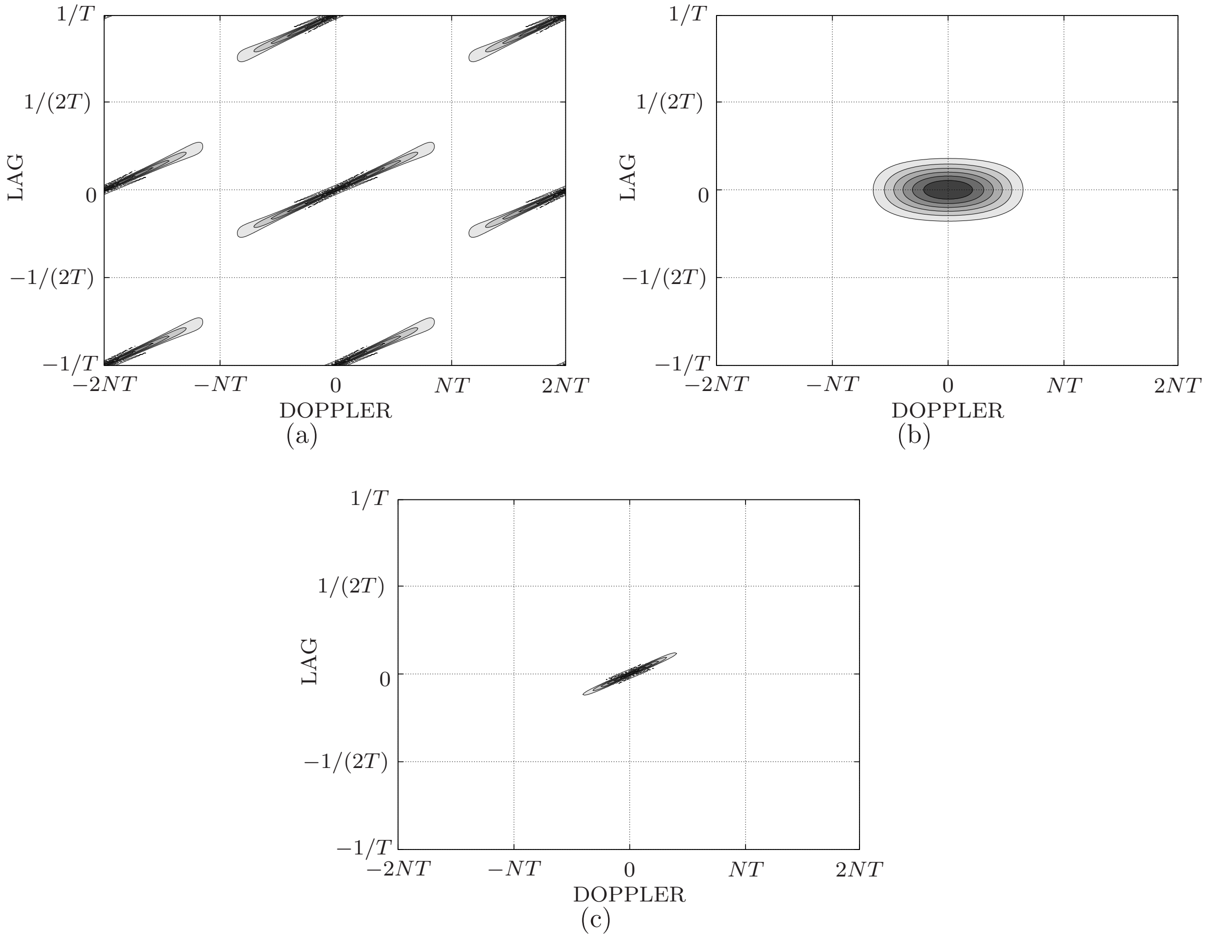

FIGURE E.4: Forming the smoothed DAF, for the DTFD-R, of an LFM signal: multiply DAF in (a) by a Doppler–independent kernel in (b) to produce smoothed DAF in (c).

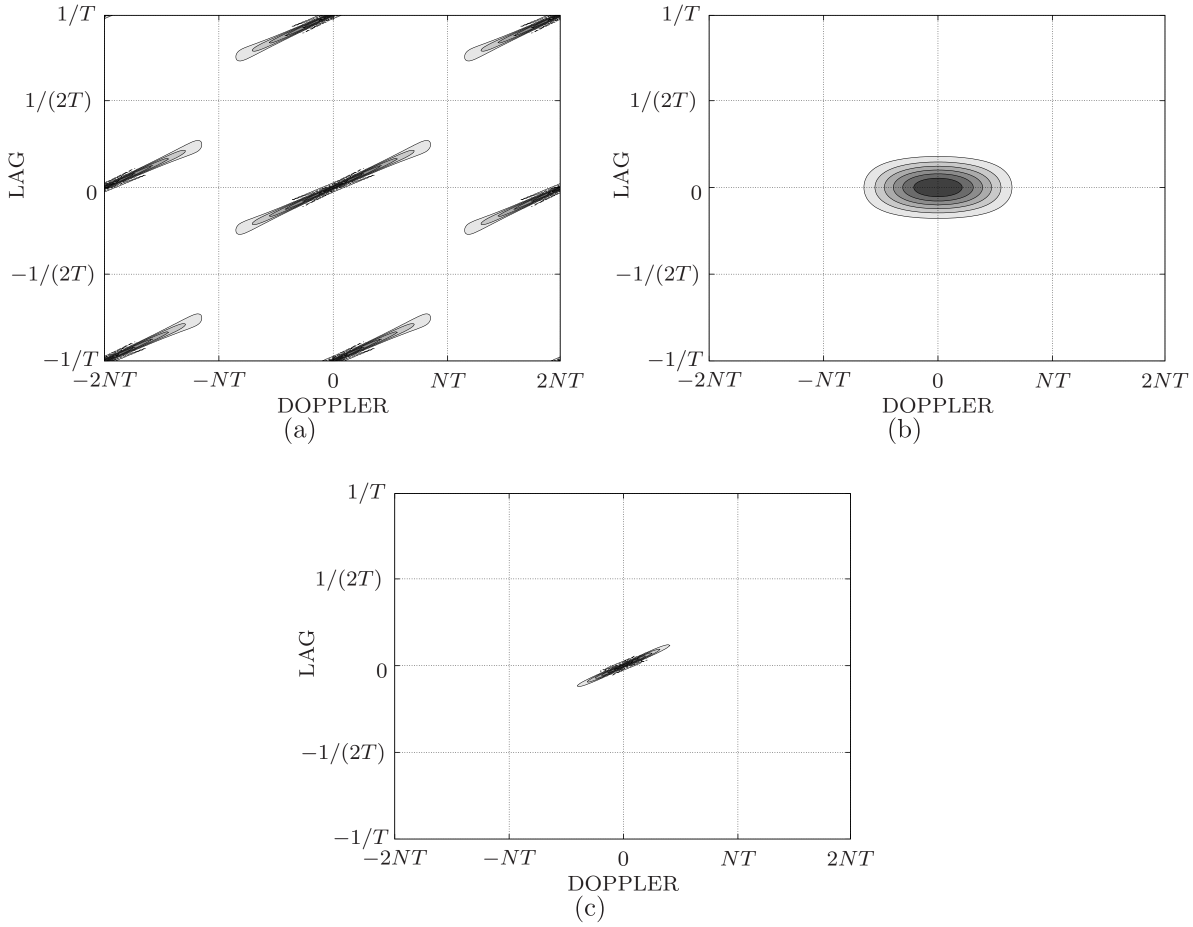

FIGURE E.5: Forming the smoothed DAF, for the DTFD-R, of a LFM signal: multiply DAF in (a) by a separable kernel in (b) to produce smoothed DAF in (c).

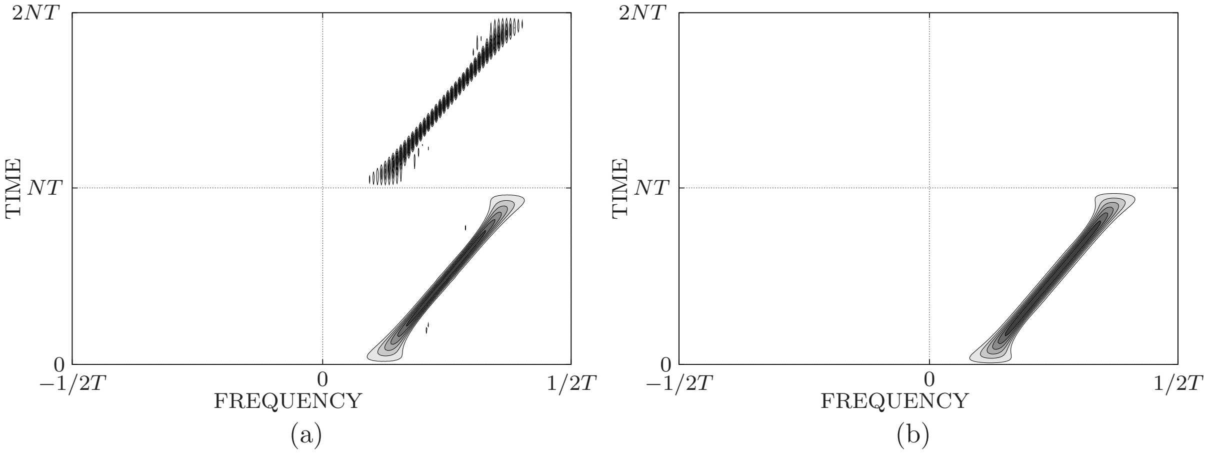

FIGURE E.6: DTFD-R of LFM signal using the (a) Doppler–independent kernel and (b) separable kernel. The AF-GDTFD is a time- and frequency-decimated version of the DTFD-R.

Appendix F

Additional DTFD Algorithms

This chapter provides algorithms and explanations, additional to those in Chapter 5, for efficiently computing the proposed DTFD from Chapter 4.

F.1 Time–Lag to Time–Frequency Algorithm

Transform the time–lag array $R_{\mathrm{d}}^{\mathrm{C}}[n,m]$ to the time–frequency domain to obtain the DTFD.

- INPUT: $N \times 2N_{\mathrm{f}}$ time–lag function $R_{\mathrm{d}}^{\mathrm{C}}[n,m]$;
- OUTPUT: $2N \times N_{\mathrm{f}}$ DTFD $\rho^{\mathrm{C}}[n,k]$.

1. For n even:
$$\rho^{\mathrm{C}}[2n,k] = \underset{m\rightarrow k}{\mathrm{DFT}} \left(R_{\mathrm{d}}^{\mathrm{C}}[n,2m] \right).$$
2. For n odd:
   (a) let
$$\begin{aligned} h[k] &= \frac{\cos^2(\pi k/N_{\mathrm{f}})}{\sin(\pi k/N_{\mathrm{f}})} + \sin(\pi k/N_{\mathrm{f}}), & k &= 1,2,\ldots,N_{\mathrm{f}}-1, \\ h[k] &= 0, & k &= 0. \end{aligned}$$
   (b) and
$$\begin{aligned} \hat{R}_{\mathrm{d}}^{\mathrm{C}}[n,0] &= \Im\Big(R_{\mathrm{d}}^{\mathrm{C}}[n,0] \Big), \\ \hat{R}_{\mathrm{d}}^{\mathrm{C}}[n,m] &= \frac{1}{2\mathrm{j}} \left\{ R_{\mathrm{d}}^{\mathrm{C}}[n,2m+1] - \Big(R_{\mathrm{d}}^{\mathrm{C}}[n,2N_{\mathrm{f}}-2m-1] \Big)^{*} \right\}, \quad 1 \leq m \leq N_{\mathrm{fh}}. \end{aligned}$$
   (c) Recover the negative lag values:
$$\hat{R}_{\mathrm{d}}^{\mathrm{C}}[n,m] = \Big(\hat{R}_{\mathrm{d}}^{\mathrm{C}}[n,2N_{\mathrm{f}}-2m-1] \Big)^{*}, \quad N_{\mathrm{fh}}+1 \leq m \leq N_{\mathrm{f}}-1.$$

(d) DFT to the time–frequency domain and multiply by constant $h[k]$:

$$\rho^{\mathrm{C}}[2n+1,k] = \underset{m\to k}{\mathrm{DFT}}\left(\hat{R}^{\mathrm{C}}_{\mathrm{d}}[n,m]\right) h[k].$$

(e) Do for frequency sample $k=0$,

$$\rho^{\mathrm{C}}[2n+1,0] = \sum_{m=0}^{N_{\mathrm{f}}-1} R^{\mathrm{C}}_{\mathrm{d}}[n,2m+1]$$

F.2 AF-GDTFD Algorithm

Here I present an efficient algorithm to compute the AF-GDTFD for a $2N$-point signal. O' Hair and Suter proposed an algorithm for the AF-GDTFD which does not exploit the conjugate symmetry, in the lag direction, of the time–lag functions [74]. The O' Hair–Suter algorithm requires a $\mathcal{O}(c12N^2\log_2 2N)$ load to compute the AF-GDTFD. The algorithm I propose here requires a smaller $\mathcal{O}(c8N^2\log_2 2N)$ load to compute the AF-GDTFD.

Other AF-GDTFD algorithms include the sum-of-spectrogram approach [53,75] which computes the AF-GDTFD using a weighted sum of spectrograms. The method decomposes the time–lag kernel into a set of $2N$ eigenvalues and eigenvectors and then can approximate the AF-GDTFD with a computational load of $\mathcal{O}(cr2N^2\log_2 2N)$, where r controls the approximation. When $r=2N$, then the method computes the AF-GDTFD exactly. O' Hair and Suter suggested that a value of $r=31$ provided a useful approximation to the AF-GDTFD .

The AF-GDTFD, from Chapter 4, is defined as the time–frequency convolution of the DWVD-B with a kernel:

$$\rho^{\mathrm{AF}}(nT,\tfrac{k}{2NT}) = \left[W^{\mathrm{B}}(\tfrac{n'T}{2},\tfrac{k'}{4NT}) \underset{n'}{\circledast}\underset{k'}{\circledast} \gamma^{\mathrm{AF}}(\tfrac{n'T}{2},\tfrac{k'}{4NT})\right]\Bigg|_{n'=n/2,k'=k/2}$$

which is then decimated in time and frequency. To minimise the computational load, the algorithm implements this decimation process by folding the smoothed DAF in the Doppler and lag direction.

- INPUT:
  - $2N$-point analytic signal $z[n]$;
  - $4N\times(2N+1)$ Doppler–lag kernel $g^{\mathrm{AF}}[l,m]$.
- OUTPUT: $2N\times 2N$ DTFD matrix $\rho^{\mathrm{AF}}[n,k]$.

1. Form the shift-down $2N\times(2N+1)$ matrix $K^{\mathrm{B}}_{\mathrm{d}}[n,m]$ for positive lag values only:

$$\begin{aligned} K^{\mathrm{B}}_{\mathrm{d}}[n,2m] &= z[n+m]z^*[n-m], && 0\le m\le N \\ K^{\mathrm{B}}_{\mathrm{d}}[n,2m+1] &= z[n+m+1]z^*[n-m], && 0\le m\le N-1 \end{aligned}$$

for $0\le n\le 2N-1$.

2. DFT to the Doppler–lag domain :

$$A^{\mathrm{B}}[l,m] = \operatorname*{DFT}_{n\to l}\left(K_{\mathrm{d}}^{\mathrm{B}}[n,m]\right)$$

to get the $2N \times (2N+1)$ DAF A^{AF}.

3. Modulate odd m values to compensate for the nonuniform discrete grid in $K_{\mathrm{d}}^{\mathrm{B}}$:

$$A^{\mathrm{B}}[l,2m+1] = A^{\mathrm{B}}[l,2m+1]\,\mathrm{e}^{-\mathrm{j}\pi l/(2N)}, \quad 0 \leq m \leq N,$$

for $0 \leq l \leq 2N-1$.

4. Periodically extend in the Doppler direction from $2N$ to $4N$:

$$\begin{aligned} A^{\mathrm{B}}[l+2N,2m] &= A^{\mathrm{B}}[l,2m], && 0 \leq m \leq N \\ A^{\mathrm{B}}[l+2N,2m+1] &= -A^{\mathrm{B}}[l,2m+1], && 0 \leq m \leq N-1 \end{aligned}$$

for $0 \leq l \leq 2N-1$. Thus, the DAF is now $4N \times (2N+1)$.

5. Multiply by the kernel:

$$S^{\mathrm{AF}}[l,m] = A^{\mathrm{B}}[l,m]g^{\mathrm{AF}}[l,m]$$

for $0 \leq m \leq 2N$ and $0 \leq l \leq 4N-1$.

6. Then, fold the smoothed DAF S^{AF} in the Doppler and lag directions:

$$\begin{aligned} S_{\mathrm{fold}}^{\mathrm{AF}}[l,m] = S^{\mathrm{AF}}[l,m] + S^{\mathrm{AF}}[l-N2,m] \\ + S^{\mathrm{AF}}[l,m-N2] + S^{\mathrm{AF}}[l-N2,m-N2] \end{aligned}$$

for $0 \leq m \leq N$ and $0 \leq l \leq 2N-1$. Thus, the folded DAF $S_{\mathrm{fold}}^{\mathrm{AF}}$ is $2N \times (N+1)$.

7. IDFT to time–lag domain:

$$R^{\mathrm{AF}}[n,m] = \operatorname*{IDFT}_{l\to n}\left(S_{\mathrm{fold}}^{\mathrm{AF}}[l,m]\right)$$

8. Recover negative lag values from positive ones:

$$R^{\mathrm{AF}}[n,2N-m] = \left(R^{\mathrm{AF}}[n,m]\right)^{*}, \quad 1 \leq m \leq N-1$$

where R^{AF} is now $2N \times 2N$.

9. DFT to get the AF-GDTFD:

$$\rho^{\mathrm{AF}}[n,k] = \operatorname*{DFT}_{m\to k}\left(R^{\mathrm{AF}}[n,m]\right).$$

Thus the method requires $(2N+1)$ FFT$-2N$ plus $(N+1)$ FFT$-2N$ plus N FFT$-2N$ operations.

F.3 Decimation for LI-kernel DTFD Algorithm

The algorithm for the LI-kernel DTFD reduces the size of the DTFD from a $2N \times N$ array to a $N_{\mathrm{t}} \times N$ array, when $(N_{\mathrm{th}} = N_{\mathrm{t}}/2) < N$. For this section we shall call this $N_{\mathrm{t}} \times N$ DTFD the *reduced-size* DTFD which we shall denote by $\bar{\rho}^{\mathrm{C}}$. This reduced-size DTFD is not simply related to the time-decimated DTFD ρ^{C} as

$$\begin{aligned} \bar{\rho}^{\mathrm{C}}[2n,k] &= \rho^{\mathrm{C}}[a2n,k] \\ \bar{\rho}^{\mathrm{C}}[2n+1,k] &\approx \rho^{\mathrm{C}}[a(2n+1)+(1-a),k] \end{aligned} \tag{F.1}$$

where $a = N/N_{\mathrm{th}}$ and $N_{\mathrm{th}} \geq Q$ for $a > 1$. (Note, from Chapter 5, that N_{t} is even.) This sections explains the relation in preceding equation—the reason why the reduced-size DTFD is not decimated linearly in time and why the odd n values of the reduced-size DTFD is not exactly equal to the decimated DTFD.

To help with the interpretation of (F.1), lets examine how to form the LI-kernel DTFD by starting in the time–lag domain:

1. form the shifted-down, $N \times 2N$, time–lag array $K^{\mathrm{C}}_{\mathrm{d}}[n,m]$ from $z[n]$;
2. DFT to the Doppler–lag domain to get $A^{\mathrm{C}}[l,m]$;
3. modulate for odd m values: $A^{\mathrm{C}}[l,2m+1] = A^{\mathrm{C}}[l,2m+1]\,\mathrm{e}^{\mathrm{j}\pi l/N}$;
4. window in the Doppler direction: $S^{\mathrm{C}}[l,m] = A^{\mathrm{C}}[l,m]G_1[l]$;
5. resize the array $S^{\mathrm{C}}[l,m]$ from $N \times 2N$ to $N_{\mathrm{th}} \times 2N$; we can do this because of the windowing of the DAF by Q-point $G_1[l]$ in the previous step, where $Q \leq N_{\mathrm{th}} \leq N$;
6. modulate for odd m values: $S^{\mathrm{C}}[l,2m+1] = S^{\mathrm{C}}[l,2m+1]\,\mathrm{e}^{-\mathrm{j}\pi l/N_{\mathrm{th}}}$;
7. DFT back to the time–lag domain to get $R^{\mathrm{C}}_{\mathrm{d}}[n,m]$;
8. transform the $N_{\mathrm{th}} \times 2N$ shifted-down array $R^{\mathrm{C}}_{\mathrm{d}}[n,m]$ to the $N_{\mathrm{t}} \times N$ shifted-across array $R^{\mathrm{C}}_{\mathrm{a}}[n,m]$; this process is merely a reordering process;
9. DFT $R^{\mathrm{C}}_{\mathrm{a}}[n,m]$ to obtain the DTFD $\rho^{\mathrm{C}}[n,k]$;
10. modulate for odd values of k: $\bar{\rho}^{\mathrm{C}}[n,2k+1] = \bar{\rho}^{\mathrm{C}}[n,2k+1]\,\mathrm{e}^{-\mathrm{j}\pi k/N}$.

This procedure yields the reduced-size DTFD and is an alternative implementation to the LI-kernel algorithm in Section 5.3.2. The modulation terms in step 3 shifts the sample points in the TIAF at $K((n+1/2)T/2,(2m+1)T)$ down to $K(nT,(2m+1)T)$ and then the modulation term in step 6 shifts this back to the now smoothed TIAF $R((n+1/2)T/2,(2m+1)T)$. This shifting process was presented in (2.45). If $N_{\mathrm{th}} = N$, then shifting up and down by 1/2 a sample point cancels, as the two product of the two modulation terms is one. But when $N_{\mathrm{th}} < N$, then the product of these terms does not reduce to one.

There are two aspects to forming this reduced-size $N_{\mathrm{t}} \times N$ DTFD $\bar{\rho}^{\mathrm{C}}[n,k]$. First, the array does not have uniform time sampling. The resizing of $S^{\mathrm{C}}[l,m]$ is equal to folding the $S^{\mathrm{C}}[l,m]$ in the Doppler direction which equates to decimating the shifted-down TIAF

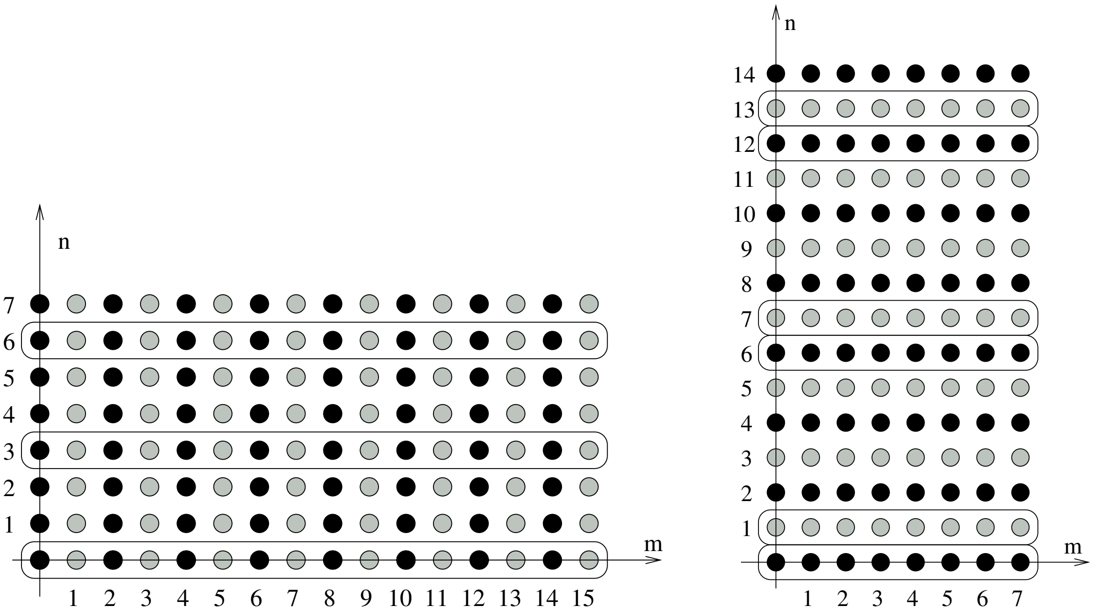

(a) (b)

Figure F.1: Examples of the decimation process in time–lag arrays. (a) Shifted-down array $K_{\mathrm{d}}^{\mathrm{C}}[n,m]$ and (b) shifted-across array $K_{\mathrm{a}}^{\mathrm{C}}[n,m]$. The shifted-down array is decimated in time at $K_{\mathrm{d}}^{\mathrm{C}}[an,m]$, where $a=3$, as shown by the black box around these time slices. Decimating $K_{\mathrm{d}}^{\mathrm{C}}$ results in the decimated shifted-across array $K_{\mathrm{a}}^{\mathrm{C}}[an+y(1-a),m]$, where $y=n \pmod 2$.

$R_{\mathrm{d}}^{\mathrm{C}}[n,m]$. Fig. F.1(a) shows an example of decimating $R_{\mathrm{d}}^{\mathrm{C}}[n,m]$ when $a=N/N_{\mathrm{th}}=3$. But decimating $R_{\mathrm{d}}^{\mathrm{C}}[n,m]$ to $R_{\mathrm{d}}^{\mathrm{C}}[an,m]$ does not equal the decimated shifted-across array $R_{\mathrm{a}}^{\mathrm{C}}[an,m]$; rather $R_{\mathrm{d}}^{\mathrm{C}}[an,m]$ equals $R_{\mathrm{a}}^{\mathrm{C}}[2an,m]$ for even n values and $R_{\mathrm{a}}^{\mathrm{C}}[(2n+1)a+(1-a),m]$ for odd n values; combining the even–odd terms, the decimated function is $R_{\mathrm{a}}^{\mathrm{C}}[an+y(1-a),m]$, where $y=n \pmod 2$. Thus,

$$\begin{aligned} R_{\mathrm{d}}^{\mathrm{C}}[an,2m] &= R_{\mathrm{a}}^{\mathrm{C}}[a2n,m] \\ R_{\mathrm{d}}^{\mathrm{C}}[an,2m+1] &= R_{\mathrm{a}}^{\mathrm{C}}[a(2n+1)+(1-a),m]. \end{aligned}$$

Fig. F.1(b) shows the example of the decimated $R_{\mathrm{a}}^{\mathrm{C}}[an+y(1-a),m]$ for $a=3$. Thus, the decimation in $R_{\mathrm{a}}^{\mathrm{C}}[an+y(1-a),m]$ is not linear in time and, because the DTFD equals the DFT of $R_{\mathrm{a}}^{\mathrm{C}}$, the decimation in the DTFD $\rho^{\mathrm{C}}[an+y(1-a),m]$ is likewise not linear in time.

Second, the reduced-size DTFD $\bar{\rho}^{\mathrm{C}}[2n+1,k]$ is not equal to the corresponding decimated DTFD $\rho^{\mathrm{C}}[a(2n+1)+(1-a),k]$, as indicated in (F.1) with the approximation sign. The odd-valued n sample points in the shifted-across array $R_{\mathrm{a}}^{\mathrm{C}}[2n+1,m]$ correspond to the odd-valued m sample points in the shifted-down array $R_{\mathrm{d}}^{\mathrm{C}}[n,2m+1]$. As I discussed previously, the modulation terms in the DAF and smoothed DAF shift the corresponding n samples points in $R_{\mathrm{d}}^{\mathrm{C}}[n,2m+1]$ up and down by 1/2 a sample. If we decimate the DTFD as $\rho^{\mathrm{C}}[a(2n+1)+(1-a),k]$ for $a>1$, then we fold the smoothed $S^{\mathrm{C}}[l,2m+1]$ in the Doppler direction without this modulation process. But when $a>1$, $N_{\mathrm{th}}<N$ and therefore the modulation terms do not cancel. Hence decimating the DTFD in a to produce $\rho^{\mathrm{C}}[a(2n+1)+(1-a),k]$ does not equal the procedure in the preceding algorithm

for the reduced-size DTFD $\bar{\rho}^{\mathrm{C}}[2n+1,k]$ which removes the zeros from $S^{\mathrm{C}}[l,m]$ and then applies the correct modulation term.

Although the reduced-size DTFD $\bar{\rho}^{\mathrm{C}}[2n+1,k]$ does not equal the decimated DTFD $\rho^{\mathrm{C}}[a(2n+1)+(1-a),k]$, they may be approximately equal. We can incorporate the modulation terms in steps 3 and 6 of the previous algorithm into the function $G_1[l]$ by defining the function $G_1^{\mathrm{m}}[l]$ as

$$\begin{aligned} G_1^{\mathrm{m}}[l] &= G_1[l]\,\mathrm{e}^{-\mathrm{j}\pi l/N}\,\mathrm{e}^{\mathrm{j}\pi l/N_{\mathrm{th}}}, && 0 \le l \le Q_{\mathrm{h}}, \\ G_1^{\mathrm{m}}[Q-l] &= G_1[Q-l]\,\mathrm{e}^{-\mathrm{j}\pi(N-l)/N}\,\mathrm{e}^{\mathrm{j}\pi(N_{\mathrm{th}}-l)/N_{\mathrm{th}}}, && 1 \le l \le (Q_{\mathrm{h}}+g), \end{aligned}$$

where $g=-1$ when Q is even and $g=0$ when Q is odd. Thus, when $G_1^{\mathrm{m}}[l] \approx G_1[l]$ then the reduced-size DTFD $\bar{\rho}^{\mathrm{C}}[2n+1,k]$ will approximate the decimated DTFD $\rho^{\mathrm{C}}[a(2n+1)+(1-a),k]$. The assumption that $G_1^{\mathrm{m}}[l] \approx G_1[l]$ depends on the shape of $G_1[l]$ and the values of N_{th} and Q. I found, experimentally, that for most smoothing-type functions of $G_1[l]$—that is, when $G_1[l]$ tends to zero as $l > 0$ in the $0 < l \le Q_{\mathrm{h}}$ range—the approximation $G_1^{\mathrm{m}}[l] \approx G_1[l]$ is a good one and therefore

$$\bar{\rho}^{\mathrm{C}}[2n+1,k] \approx \rho^{\mathrm{C}}[a(2n+1)+(1-a),k].$$

F.4 Separable-kernel DTFD Algorithm

Here I present another algorithm for the separable-kernel DTFD to the one in Section 5.3.2. The algorithm here forms the DTFD by moving through the following domains: Doppler–frequency to Doppler–lag to Doppler–frequency to, finally, time–frequency.

- INPUT:
    - $2N$-point analytic signal $z[n]$;
    - P-point window function $g_2[m]$, where $P \le 2N$;
    - Q-point window function $G_1[l]$, where $Q \le N$;
    - parameter N_{t}, where $Q \le N_{\mathrm{t}} \le 2N$ and N_{t} is even;
    - parameter N_{f}, where $\lceil (P+1)/2 \rceil \le N_{\mathrm{f}} \le N$ when $P < 2N$ or $N_{\mathrm{f}} = N$ when $P = 2N$.
- OUTPUT: $N_{\mathrm{t}} \times N_{\mathrm{f}}$ DTFD matrix $\rho^{\mathrm{C}}[n,k]$.

1. Let $Q_{\mathrm{h}} = \lfloor Q/2 \rfloor$, $P_{\mathrm{h}} = \lfloor P/2 \rfloor$, $N_{\mathrm{th}} = \lfloor N_{\mathrm{t}}/2 \rfloor$, and
$$Z[k] = \underset{n \to k}{\mathrm{DFT}}\big(z[n]\big).$$
Also, let $f = o(N_{\mathrm{t}})$, $h = o(P)$, and $g = o(Q)$; the function $o(\cdot)$ is defined in (5.5).

2. Form the windowed Doppler–frequency function $\mathcal{R}^{\mathrm{C}}[l,k]$ for the positive Doppler values:
$$\mathcal{R}^{\mathrm{C}}[l,k] = Z[k+l]Z^*[k-l]G_1[l], \quad 0 \le l \le Q_{\mathrm{h}},$$
over the positive and negative frequencies, $0 \le k \le 2N-1$.

3. Transform to the Doppler–lag domain:

$$A^{\mathrm{C}}[l,m] = \underset{k\to m}{\mathrm{IDFT}}\left(\mathcal{R}^{\mathrm{C}}[l,k]\right)$$

This Doppler–lag function includes both positive and negative lag values, $|\tau| \leq NT$, and only positive Doppler values. The DAF array contains $Q_{\mathrm{h}} \times 2N$ sample points.

4. Window the DAF in the lag direction with $g_2[m]$, to create the $Q_{\mathrm{h}} \times 2N_{\mathrm{f}}$ smoothed array S^{C}:

$$\begin{aligned} S^{\mathrm{C}}[l,m] &= A^{\mathrm{C}}[l,m]g_2[m], && 0 \leq m \leq P_{\mathrm{h}} \\ S^{\mathrm{C}}[l,2N_{\mathrm{f}}-m] &= A^{\mathrm{C}}[l,2N-m]g_2[P-m], && 1 \leq m \leq P_{\mathrm{h}}+h. \end{aligned}$$

5. Transform back to the Doppler–frequency domain:

$$\mathcal{R}^{\mathrm{C}}[l,k] = \underset{m\to k}{\mathrm{DFT}}\left(S^{\mathrm{C}}[l,m]\right).$$

6. Taking advantage of the symmetry in the Doppler–frequency, rearrange the $Q_{\mathrm{h}} \times 2N_{\mathrm{f}}$ array $\mathcal{R}^{\mathrm{C}}[l,k]$ to the $N_{\mathrm{th}}+1 \times N_{\mathrm{f}}$ array $\hat{\mathcal{R}}^{\mathrm{C}}[l,k]$. In the continuous Doppler–frequency (ν, f) domain, $\mathcal{R}^{\mathrm{C}}$ extends from $0 \leq \nu \leq N/(TQ)$ and $|f| \leq 1/2T$; $\hat{\mathcal{R}}^{\mathrm{C}}$ extends from $0 \leq l \leq N/(TN_{\mathrm{th}}+1)$ and $0 \leq f \leq 1/2T$.

$$\begin{aligned} \hat{\mathcal{R}}^{\mathrm{C}}[l,k] &= \mathcal{R}^{\mathrm{C}}[l,k], && 0 \leq l \leq Q_{\mathrm{h}}, \\ \hat{\mathcal{R}}^{\mathrm{C}}[N_{\mathrm{th}}-l,k] &= \left(\mathcal{R}^{\mathrm{C}}[l,N_{\mathrm{f}}+k]\right)^*, && 0 \leq l \leq Q_{\mathrm{h}}+g \end{aligned}$$

for $0 \leq k \leq N_{\mathrm{f}}-1$.

7. Recover the negative Doppler values from the positive ones:

$$\hat{\mathcal{R}}^{\mathrm{C}}[N_{\mathrm{t}}-l,k] = \left(\hat{\mathcal{R}}^{\mathrm{C}}[l,k]\right)^*, \quad 1 \leq l \leq N_{\mathrm{th}}+f$$

for $0 \leq k \leq N_{\mathrm{f}}-1$.

8. Transform the Doppler–frequency function $\hat{\mathcal{R}}^{\mathrm{C}}[l,k]$ to time–frequency domain to obtain the DTFD $\rho^{\mathrm{C}}[n,k]$:

$$\rho^{\mathrm{C}}[n,k] = \underset{l\to n}{\mathrm{IDFT}}\left(\hat{\mathcal{R}}^{\mathrm{C}}[l,k]\right).$$

The algorithm requires $(Q_{\mathrm{h}}+1) \times$ length-$2N$ FFTs plus $(Q_{\mathrm{h}}+1) \times$ length-$2N_{\mathrm{f}}$ FFTs plus $N_{\mathrm{f}}/2 \times$ length-N_{t} FFT operations to compute the $N_{\mathrm{t}} \times N_{\mathrm{f}}$ DTFD. When all parameter are at their largest values–that is, when $P = 2N$, $Q = N$, $N_{\mathrm{f}} = N$ and $N_{\mathrm{t}} = 2N$—then the maximum computational load for this algorithm is $3N/2 \times$ length-$2N$ FFT operations, which approximately equals the computational load for the nonseparable kernel.

F.5 Decimated LI- and DI-Kernel DTFD Algorithms

These kernel-specific algorithms compute the decimated DTFD, similar to the decimated DWVD-C algorithms in Section 5.4.1. See Chapter 5 for details about the decimated DTFD algorithms.

ALGORITHM-9: Decimated DI-kernel DTFD

- INPUT:
  - $2N$-point analytic signal $z[n]$;
  - P-point window function $g_2[m]$, where $P \leq 2N$;
  - parameter N_f, where $\lceil (P+1)/2 \rceil \leq N_\mathrm{f} \leq N$ when $P < 2N$ or $N_\mathrm{f} = N$ when $P = 2N$.
  - set of L time sample points $\{n_i\} = n_1, n_2, \ldots, n_L$, where $L \leq 2N$ and each time sample n_i from the set satisfies the inequality $0 \leq n_i \leq 2N-1$.
  - frequency-decimation factor b; b is an integer, $b \geq 1$, and $J = N_\mathrm{f}/b$ is also an integer.
- OUTPUT: $L \times J$ DTFD matrix $\rho^\mathrm{C}[n_i, bk]$.

1. Let $J_\mathrm{h} = \lceil J/2 \rceil$, $P_\mathrm{h} = \lfloor P/2 \rfloor$, $P_\mathrm{q} = \lceil P_\mathrm{h}/2 \rceil$, $N_\mathrm{fh} = \lceil N_\mathrm{f}/2 \rceil$, and $i = o(P_\mathrm{h})$.
2. Separate the time sample points $\{0, a, 2a, \ldots, (L-1)a\}$ into two sets: one set for even values of n_i, $\{n_{\mathrm{e}i}\}$ for $0 \leq i \leq L_\mathrm{e} - 1$; and one set for odd values of n_i, $\{n_{\mathrm{o}i}\}$ for $0 \leq i \leq L_\mathrm{o} - 1$. The value L_e is the number of even-valued time sample points and L_o is the number of odd-valued time sample points where $L_\mathrm{e} + L_\mathrm{o} = L$. Note that if a is even, $L_\mathrm{o} = 0$ as odd values do not exist in the set $\{0, a, 2a, \ldots, (L-1)a\}$ for a even.
3. Form the smoothed time–lag function for even–valued samples $n_{\mathrm{e}i}$ and odd-valued samples $n_{\mathrm{o}i}$:

$$
\begin{aligned}
R_\mathrm{etmp}[m] &= z[n_{\mathrm{e}i}/2 + m] z^*[n_{\mathrm{e}i}/2 - m] g_2[2m], \qquad 0 \leq m \leq (P_\mathrm{q} - 1 - i), \\
R_\mathrm{otmp}[m] &= z[(n_{\mathrm{o}i} - 1)/2 + m + 1] z^*[(n_{\mathrm{o}i} - 1)/2 - m] g_2[2m+1], \\
&\qquad 0 \leq m \leq P_\mathrm{q} - 1
\end{aligned}
$$

   and

$$
\begin{aligned}
R_\mathrm{etmp}[m] &= 0, \qquad (P_\mathrm{q} - i) \leq m \leq (N_\mathrm{f} - N_\mathrm{fh}) \\
R_\mathrm{etmp}[m] &= 0, \qquad P_\mathrm{q} \leq m \leq (N_\mathrm{f} - N_\mathrm{fh} - 1).
\end{aligned}
$$

   Next, recover the negative lag values from the positive ones

$$
\begin{aligned}
R_\mathrm{etmp}[N_\mathrm{f} - m] &= \left(R_\mathrm{etmp}[m]\right)^*, \qquad 1 \leq m \leq N_\mathrm{fh} - 1, \\
R_\mathrm{otmp}[N_\mathrm{f} - m - 1] &= \left(R_\mathrm{otmp}[m]\right)^*, \qquad 0 \leq m \leq N_\mathrm{fh} - 1.
\end{aligned}
$$

4. For the same sample points n_{ei} and n_{oi}, fold the functions K_{etmp} and K_{otmp}:

$$R_{\text{a}}^{\text{C}}[n_{\text{e}i}, m] = \sum_{p=0}^{b-1} R_{\text{etmp}}[pJ + m]$$
$$R_{\text{a}}^{\text{C}}[n_{\text{o}i}, m] = \sum_{p=0}^{b-1} R_{\text{otmp}}[pJ + m]$$

   over values $m = 0, 1, \ldots, J_{\text{h}}$ and then recover the negative lag values from the positive ones

$$R_{\text{a}}^{\text{C}}[n_{\text{e}i}, J - m] = \left(R_{\text{a}}^{\text{C}}[n_{\text{e}i}, m]\right)^*, \qquad 1 \le m \le J_{\text{h}} - 1,$$
$$R_{\text{a}}^{\text{C}}[n_{\text{o}i}, J - 1 - m] = \left(R_{\text{a}}^{\text{C}}[n_{\text{o}i}, m]\right)^*, \qquad 0 \le m \le J_{\text{h}} - 1.$$

5. Iterate the two previous steps over all values of $n_{\text{e}i}$ in the set $\{n_{\text{e}1}, n_{\text{e}2}, \ldots, n_{\text{e}L_{\text{e}}}\}$ and all the value of $n_{\text{o}i}$ from the set $\{n_{\text{o}1}, n_{\text{o}2}, \ldots, n_{\text{o}L_{\text{o}}}\}$ to produce the $L \times J$ time–lag function R_{a}^{C}.

6. Transform R_{a}^{C} to the time–frequency domain for even–odd values of n_i, using the method in Step 6 of ALGORITHM-7 from Section 5.3.2 by replacing $K_{\text{a}}^{\text{C}}[n, m]$ with $R_{\text{a}}^{\text{C}}[n, m]$ and $W^{\text{C}}[n, k]$ with $\rho^{\text{C}}[n, k]$.

The algorithm requires $L/2$ FFT$-J$ length-J FFT operations.

ALGORITHM-10: Decimated LI-kernel DTFD

- INPUT:
  - $2N$-point analytic signal $z[n]$;
  - parameter N_{t}, with $2Q \le N_{\text{t}} \le 2N$;
  - Q-point window function $G_1[l]$, with $Q \le N$;
  - time-decimation factor a, with a is an integer, $a \ge 1$, and $L = N_{\text{t}}/a$ is also an integer;
  - set of J frequency sample points $\{k_i\} = k_1, k_2, \ldots, k_J$, where $J \le N$ and each frequency sample k_i from the set satisfies the inequality $0 \le k_i \le N - 1$.
- OUTPUT: $L \times J$ DWVD $\rho^{\text{C}}[an, k_i]$.

1. Let $Q_{\text{h}} = \lfloor Q/2 \rfloor$, $N_{\text{th}} = \lfloor N_{\text{t}}/2 \rfloor$, and

$$Z[k] = \underset{n \to k}{\text{DFT}} \left(z[n]\right).$$

   Also, let $f = o(N_{\text{t}})$ and $g = o(Q)$, where the function $o(\cdot)$ is defined in (5.9).

2. Form the Doppler–frequency function for frequency sample point k_i

$$\begin{aligned}\mathcal{K}_{\mathrm{tmp}}[l] &= Z[k_i+l]Z^*[k_i-l]G_1[l], && 0 \le l \le Q_{\mathrm{h}},\\ \mathcal{K}_{\mathrm{tmp}}[N_{\mathrm{th}}-l] &= Z[k_i+N-l]Z^*[k_i-N+l]G_1[Q-l], && 1 \le l \le Q_{\mathrm{h}}+g\\ \mathcal{K}_{\mathrm{tmp}}[l] &= Z[k_i+N]Z^*[k_i-N]G_1[0], && l = N_{\mathrm{th}}.\end{aligned}$$

   and then recover the negative Doppler values from the positive ones

$$\mathcal{K}_{\mathrm{tmp}}[N_{\mathrm{t}}-l] = \left(\mathcal{K}_{\mathrm{tmp}}[l+1]\right)^*, \qquad 1 \le l \le N_{\mathrm{th}}+f.$$

3. For the same frequency sample point k_i fold the $\mathcal{K}_{\mathrm{tmp}}$

$$\mathcal{K}^{\mathrm{C}}[l,k_i] = \frac{1}{a}\sum_{p=0}^{a-1}\mathcal{K}_{\mathrm{tmp}}[pL+l], \qquad 0 \le l \le L_{\mathrm{h}}$$

   and then recover the negative Doppler values from the positive ones

$$\mathcal{K}^{\mathrm{C}}[L-l,k_i] = \left(\mathcal{K}^{\mathrm{C}}[l+1]\right)^*, \qquad 1 \le l \le L_{\mathrm{h}}-1.$$

4. Iterate the two previous steps over the set $\{k_i\}$ to produce the $L \times J$ Doppler–frequency function $\mathcal{K}^{\mathrm{C}}$.

5. Transform the Doppler–frequency function to the time–frequency domain

$$\rho^{\mathrm{C}}[an,k_i] = \underset{l\to n}{\mathrm{IDFT}}\left(\mathcal{K}^{\mathrm{C}}[l,k_i]\right)$$

   for all values in the set $\{k_i\}$.

The algorithm requires an $L \times J$ array and $J/2$ FFT$-L$ operations to compute the DWVD.

References

[1] B. Boashash, "Part I: Introduction to the concepts of TFSAP," in *Time–Frequency Signal Analysis and Processing: A Comprehensive Reference*, B. Boashash, Ed. Oxford, UK: Elsevier, 2003, ch. 1–3, pp. 3–76.

[2] W. Koenig, H. Dunn, and L. Lacy, "The sound spectrograph," *Journal of Acoustical Society of America*, vol. 18, no. 1, pp. 19–49, 1946.

[3] S. Mallat, *A Wavelet Tour of Signal Processing.* San Diego, USA: Academic Press, 1999.

[4] S. Chang, B. Yu, and M. Vetterli, "Adaptive wavelet thresholding for image denoising and compression," *Image Processing, IEEE Transactions on*, vol. 9, no. 9, pp. 1532–1546, Sep 2000.

[5] D. Donoho, "De-noising by soft-thresholding," *Information Theory, IEEE Transactions on*, vol. 41, no. 3, pp. 613–627, May 1995.

[6] H. Tong, *Non-linear Time Series: A Dynamical System Approach.* Oxford: Oxford University Press, 1990.

[7] L. Cohen, *Time–Frequency Analysis.* NJ 07458, USA: Prentice-Hall, 1995.

[8] B. Boashash, Ed., *Time–Frequency Signal Analysis and Processing: A Comprehensive Reference.* Oxford, UK: Elsevier, 2003.

[9] P. Flandrin, *Time–Frequency/Time-Scale Analysis.* San Diego: Academic Press, 1999, original French edition: *Temps-fréquence* (Paris: Hermès, 1993).

[10] J. Ville, "Théorie et applications de la notion de signal analytique," *Cables et Transmissions*, vol. 2A, no. 1, pp. 61–74, 1948, in French. English translation: I. Selin, *Theory and applications of the notion of complex signal*, Rand Corporation Report T-92 (Santa Monica, CA, August 1958).

[11] B. Boashash, "Note on the use of the Wigner distribution for time–frequency signal analysis," *IEEE Trans. Acoust., Speech, Signal Process.*, vol. 36, no. 9, pp. 1518–1521, 1988.

[12] E. Wigner, "On the Quantum Correction For Thermodynamic Equilibrium," *Physical Review*, vol. 40, no. 5, pp. 749–759, 1932.

[13] H.-L. Chan, J.-L. Lin, H.-H. Huang, and C.-P. Wu, "Elimination of interference component in Wigner–Ville distribution for the signal with $1/f$ spectral characteristic," *IEEE Trans. Biomed. Eng.*, vol. 44, no. 9, pp. 903–907, Sept. 1997.

[14] C. Richard, "Time–frequency based detection using discrete-time discrete-frequency Wigner distributions," *IEEE Trans. Signal Process.*, vol. 50, no. 9, pp. 2170–2176, Sep. 2002.

[15] L. Galleani and L. Cohen., "The Wigner distribution for classical systems," *Physics Letters, Section A: General, Atomic and Solid State Physics*, vol. 302, no. 4, pp. 149–155, sept. 2002.

[16] A. Monti, C. Medigue, and L. Mangin., "Instantaneous parameter estimation in cardiovascular time series by harmonic and time-frequency analysis," *IEEE Trans. Biomed. Eng.*, vol. 49, no. 12, pp. 1547–1556, Dec. 2002.

[17] P. J. Loughlin and L. Cohen, "A Wigner approximation method for wave propagation," *Journal of Acoustical Society of America*, vol. 118, no. 3, pp. 1268–1271, 2005.

[18] N. Majumdar, K. Pribram, and T. Barrett., "Time frequency characterization of evoked brain activity in multiple electrode recordings," *IEEE Trans. Biomed. Eng.*, vol. 53, no. 12, pp. 2516–2524, 2006.

[19] Y. Li and X. Zheng, "Spectral decomposition using Wigner–Ville distribution with applications to carbonate reservoir characterization," *The Leading Edge*, vol. 27, no. 8, pp. 1050–1057, 2008.

[20] L. Cohen, "Construction of time-frequency distributions for fields," in *Proceedings of SPIE - The International Society for Optical Engineering*, vol. 7074, no. 797400, San Diego, USA, Aug 2008.

[21] F. Harris, "On the use of windows for harmonic analysis with the discrete Fourier transform," *Proc. IEEE*, vol. 66, no. 1, pp. 51–83, 1978.

[22] C. Shannon, "A mathematical theory of communication," *Bell Syst Tech J*, vol. 27, no. 3, pp. 379–423, 1948.

[23] A. V. Oppenheim and R. W. Schafer, *Discrete-Time Signal Processing.* Englewood Cliffs, NJ 07458: Prentice-Hall, 1999.

[24] M. Frigo and S. G. Johnson, "The design and implementation of FFTW3," *Proceedings of the IEEE*, vol. 93, no. 2, pp. 216–231, 2005, special issue on "Program Generation, Optimization, and Platform Adaptation".

[25] S. L. Marple, Jr., "Computing the discrete-time 'analytic' signal via FFT," *IEEE Trans. Signal Process.*, vol. 47, no. 9, pp. 2600–2603, 1999.

[26] B. Boashash and G. R. Putland, "Computation of discrete quadratic TFDs," in *Time–Frequency Signal Analysis and Processing: A Comprehensive Reference*, B. Boashash, Ed. Oxford, UK: Elsevier, 2003, ch. 6, pp. 268–278.

[27] F. Peyrin and R. Prost, "A unified definition for the discrete-time, discrete-frequency, and discrete-time/frequency Wigner distributions," *IEEE Trans. Acoust., Speech, Signal Process.*, vol. 34, no. 4, pp. 858–866, Aug. 1986.

[28] D. Slepian, "On bandwidth," *Proc. IEEE*, vol. 64, no. 3, pp. 292–300, 1976.

[29] J. C. O' Neill and W. J. Williams, "Shift covariant time–frequency distributions of discrete signals," *IEEE Trans. Signal Process.*, vol. 47, no. 1, pp. 133–146, Dec. 1999.

[30] T. Claasen and W. Mecklenbräuker, "The Wigner distribution—a tool for time–frequency signal analysis. Part I: Continuous-time signals," *Philips J. Research*, vol. 35, pp. 372–389, 1980.

[31] D. Chan, "A non-aliased discrete-time Wigner distribution for time–frequency signal analysis," in *Proc. IEEE Int. Conf. on Acoustics, Speech and Signal Processing, (ICASSP-82)*, vol. 7, May 1982, pp. 1333–1336.

[32] M. Amin, "Time and lag window selection in wigner–ville distribution," in *Proc. IEEE Int. Conf. Acoust., Speech, Signal Processing, (ICASSP-87)*, vol. 12, apr 1987.

[33] W. Martin and P. Flandrin, "Wigner-Ville spectral analysis of nonstationary processes," *IEEE Trans. Acoust., Speech, Signal Process.*, vol. 33, no. 6, pp. 1461–1470, 1985.

[34] B. Boashash and A. Reilly, "Algorithms for time–frequency signal analysis," in *Time–Frequency Signal Analysis: Methods and Applications*, B. Boashash, Ed. Melbourne 3205: Wiley Press, 1992, ch. 7, pp. 163–181.

[35] B. Boashash and G. R. Putland, "Discrete time–frequency distributions," in *Time–Frequency Signal Analysis and Processing: A Comprehensive Reference*, B. Boashash, Ed. Oxford, UK: Elsevier, 2003, ch. 6, pp. 232–241.

[36] J. Jeong and W. Williams, "Alias-free generalized discrete-time time–frequency distributions," *IEEE Trans. Signal Process.*, vol. 40, pp. 2757–2765, Nov. 1992.

[37] J. C. O' Neill and W. J. Williams, "Aliasing in the AF-GDTFD and the discrete spectrogram," in *Proc. IEEE Int. Conf. Acoust., Speech, Signal Processing, (ICASSP-96)*, vol. 3, May 7–10, 1996, pp. 2610–2613.

[38] P. Duhamel and M. Vetterli, "Fast fourier transforms: a tutorial review and a state of the art," *Signal Processing*, vol. 19, pp. 259–299, 1990.

[39] A. H. Nuttall, "Alias-free Wigner distribution function and complex ambiguity function for discrete-time samples," Naval Underwater Syst. Cent. (NUSC), New London, CT, Tech. Rep., Apr. 1989, 8553.

[40] M. S. Richman, T. W. Parks, and R. G. Shenoy, "Discrete-time, discrete-frequency time–frequency analysis," *IEEE Trans. Signal Process.*, vol. 46, no. 6, pp. 1517–1527, Jun. 1998.

[41] T. Claasen and W. Mecklenbräuker, "The Wigner distribution—a tool for time–frequency signal analysis. Part II: discrete-time signals," *Philips J. Research*, vol. 35, pp. 276–350, 1980.

[42] J. C. O' Neill, P. Flandrin, and W. J. Williams, "On the existance of discrete Wigner distributions," *IEEE Signal Processing Letters*, vol. 6, no. 12, pp. 304–306, Dec. 1999.

[43] J. O' Toole, M. Mesbah, and B. Boashash, "A discrete time and frequency Wigner–Ville distribution: properties and implementation," in *Proc. Int. Conf. on Digital Signal Processing and Comm. Systems*, vol. CD-ROM, Noosa Heads, Australia, Dec. 19–21, 2005. [Online]. Available: http://eprints.qut.edu.au/2607/

[44] E. Chassande-Mottin and A. Pai, "Discrete time and frequency Wigner-Ville distribution: Moyal's formula and aliasing," *IEEE Signal Processing Letters*, vol. 12, no. 7, pp. 508–511, Jul. 2005.

[45] J. M. O' Toole, M. Mesbah, and B. Boashash, "A computationally efficient implementation of quadratic time–frequency distributions," in *Proc. Int. Sym. on Signal Processing and its Applications, ISSPA-07*, vol. I, Sharjah, United Arab Emirates, Feb. 12–15 2007, pp. 290–293.

[46] ——, "A new discrete analytic signal for reducing aliasing in the discrete Wigner–Ville distribution," *IEEE Trans. Signal Process.*, vol. 56, no. 11, pp. 5427–5434, Nov. 2008.

[47] ——, "A new discrete-time analytic signal for reducing aliasing in discrete time–frequency distributions," in *Proc. Fifteenth European Signal Processing Conf. EUSIPCO-07*, Poznań, Poland, Sep.3–7 2007, pp. 591–595.

[48] F. Peyrin, Y. Zhu, and R. Goutte, "A note on the use of analytic signal in the pseudo Wigner distribution," in *Proc. IEEE Int. Symp. on Circuits and Systems*, vol. 2, May 8–11 1989, pp. 1260–1263.

[49] J. M. O' Toole, M. Mesbah, and B. Boashash, "A new definition of discrete quadratic time–frequency distributions," in *Proc. Sixteenth European Signal Processing Conf. (EUSIPCO-08)*, Lausanne, Switzerland, Aug., 25–29 2008.

[50] ——, "Improved discrete definition of quadratic time–frequency distributions," *IEEE Trans. Signal Process.*, Nov. 2008, to be published.

[51] ——, "Efficient algorithms for discrete time–frequency distributions," in *Proc. Applied Computing Conf. (ACC'08).* Istanbul, Turkey: World Scientific and Engineering Academy and Society (WSEAS), May, 27–30 2008, pp. 310–315.

[52] ——, "Algorithms for discrete quadratic time–frequency distributions," *WSEAS Trans. Signal Processing, invited paper*, vol. 4, no. 5, pp. 320–329, May 2008.

[53] G. Cunningham and W. Williams, "Fast implementations of generalized discrete time–frequency distributions," *IEEE Trans. Signal Process.*, vol. 42, no. 6, pp. 1496–1508, 1994.

[54] S. Aviyente and W. Williams, "A centrosymmetric kernel decomposition for time–frequency distribution computation," *IEEE Trans. Signal Process.*, vol. 52, no. 6, pp. 1574–1584, 2004.

[55] J. O' Toole, M. Mesbah, and B. Boashash, "Neonatal EEG seizure detection using a time–frequency matched filter with a reduced template set," in *Proc. Int. Sym. on Signal Processing and its Applications, ISSPA-05*, Aug. 28–31, 2005, pp. 215–218.

[56] J. M. O' Toole, M. Mesbah, B. Boashash, and P. Colditz, "A new neonatal seizure detection technique based on the time–frequency characteristics of the electroencephalogram," in *Proc. Int. Sym. on Signal Processing and its Applications, ISSPA-07*, vol. III, Sharjah, United Arab Emirates, Feb. 12–15 2007, pp. 132–135.

[57] M. A. Poletti, "The development of a discrete transform for the Wigner distribution and ambiguity function," *J. Acoust. Soc. Am.*, vol. 84, no. 1, pp. 238–252, Jul. 1988.

[58] A. H. Costa and G. F. Boudreaux-Bartels, "An overview of aliasing errors in discrete-time formulations of time–frequency representations," *IEEE Trans. Signal Process.*, vol. 47, no. 5, pp. 1463–1474, May 1999.

[59] T. Claasen and W. Mecklenbräuker, "The aliasing problem in discrete-time Wigner distributions," *IEEE Trans. Acoust., Speech, Signal Process.*, vol. 31, no. 5, pp. 1067–1072, 1983.

[60] E. C. Bekir, "A contribution to the unaliased discrete-time Wigner distribution," *J. Acoust. Soc. Am.*, vol. 93, no. 1, pp. 363–371, Jan. 1992.

[61] A. Reilly, G. Frazer, and B. Boashash, "Analytic signal generation—tips and traps," *IEEE Trans. Signal Process.*, vol. 42, no. 11, pp. 3241–3245, 1994.

[62] B. Boashash and P. O' Shea, "A methodology for detection and classification of some underwater acoustic signals using time–frequency analysis techniques," *IEEE Trans. Acoust., Speech, Signal Process.*, vol. 38, no. 11, pp. 1829–1841, 1990.

[63] J. Jeong and W. Williams, "Time-varying filtering and signal synthesis," in *Time–Frequency Signal Analysis: Methods and Applications*, B. Boashash, Ed. Melbourne 3205: Wiley Press, 1992, ch. 17, pp. 389–405.

[64] G. Boudreaux-Bartels and T. Parks, "Reducing aliasing in the Wigner distribution using implicit spline interpolation," in *Proc. IEEE Int. Conf. Acoust., Speech. Signal Process.*, vol. 8, apr 1983, pp. 1438–1441.

[65] J. M. Morris and D. Wu, "On alias-free formulations of discrete-time Cohen's class of distributions," *IEEE Trans. Signal Process.*, vol. 44, no. 6, pp. 1355–1364, Jun. 1996.

[66] B. Boashash, "Time–frequency signal analysis," in *Advances in Spectrum Estimation*, S. Haykin, Ed. Englewood Cliffs, NJ: Prentice-Hall, 1991, ch. 9, pp. 418–517.

[67] V. Čížek, "Discrete Hilbert transform," *IEEE Trans. Audio Electroacoust.*, vol. 18, no. 4, pp. 340–343, Dec 1970.

[68] F. Bonzanigo, "A note on 'Discrete Hilbert transform'," *IEEE Trans. Audio Electroacoust.*, vol. 20, no. 1, pp. 99–100, Mar 1972.

[69] M. Elfataoui and G. Mirchandani, "A frequency domain method for generation of discrete-time analytic signals," *IEEE Trans. Signal Process.*, vol. 54, no. 9, pp. 3343–3352, 2006.

[70] J. M. O' Toole, M. Mesbah, and B. Boashash, "Proofs for discrete time–frequency distribution properties," UQ Centre for Clinical Research and Perinatal Research Centre, The University of Queensland, Australia, Tech. Rep. UQCCR-2009-06-09, June 2009. [Online]. Available: http://espace.library.uq.edu.au/view/UQ:178641

[71] B. Boashash and P. J. Black, "An efficient real-time implementation of the Wigner-Ville distribution," *IEEE Trans. Acoust., Speech, Signal Process.*, vol. 35, no. 11, pp. 1611–1618, 1987.

[72] M. Sun, C.-C. Li, L. N. Sekhar, and R. J. Sclabassi, "Efficient computation of the discrete pseudo-Wigner distribution," *IEEE Trans. Acoust., Speech, Signal Process.*, vol. 37, no. 11, pp. 1735–1742, 1989.

[73] S.-C. Chan and K.-L. Ho, "On computing the discrete Wigner-Ville distribution," *Electron. Lett.*, vol. 26, no. 10, pp. 636–638, May10 1990.

[74] J. R. O' Hair and B. W. Suter, "Kernel design techniques for alias-free time–frequency distributions," in *Proc. IEEE Int. Conf. Acoust., Speech, Signal Processing, (ICASSP-98)*, vol. 3, Apr. 1994, pp. 19–22.

[75] ——, "The Zak transform and decimated time–frequency distributions," *IEEE Trans. Signal Process.*, vol. 44, no. 5, pp. 1099–1110, May 1996.

[76] O. K. Ersoy, *Fourier-Related Transforms, Fast Algorithms and Applications.* New Jersey: Prentice-Hall, 1997.

[77] P. Duhamel, "Implementation of "split-radix" FFT algorithms for complex, real and real-symmetric data," *IEEE Trans. Acoust., Speech, Signal Process.*, vol. 34, no. 2, pp. 285–295, Apr. 1986.

[78] M. Frigo and S. G. Johnson, "FFTW: An adaptive software architecture for the FFT," in *Proc. IEEE Int. Conf. Acoust., Speech, Signal Processing, (ICASSP-98)*, vol. 3, 1998, pp. 1381–1384.

[79] B. Boashash and G. R. Putland, "Design of high-resolution quadratic tfds with separable kernels," in *Time–Frequency Signal Analysis and Processing : A Comprehensive Reference*, B. Boashash, Ed. Oxford, UK: Elsevier, 2003, ch. 5, pp. 213–222.

[80] B. R. Tharp, "Neonatal seizures and syndromes," *Epilepsia*, vol. 43, no. 3, pp. 2–10, 2002.

[81] M. V. der Bor, "The recongition and management of neonatal seizures," *Current Paediatrics*, vol. 12, pp. 382–387, Oct. 2002.

[82] R. R. Clancy, “Interictal sharp EEG transients in neonatal seizures,” *Journal of Child Neurology*, vol. 4, pp. 30–38, 1989.

[83] J. C. Rowe, G. L. Holmes, J. Hafford, B. Baboval, S. Robinson, A. Philipps, T. Ronsenkrantz, and J. Raye, “Prognostic value of the electroencephalogram in term and preterm infants following neonatal seizure,” *Electroencephalography and Clinical Neurophysiology*, vol. 60, pp. 183–196, 1985.

[84] S. Patrizi, G. L. Holmes, M. Orzalesi, and F. Allemand, “Neonatal seizures: Characteristics of EEG ictal activity in preterm and fullterm infants,” *Brain & Development*, vol. 20, pp. 427–437, 2003.

[85] A. J. Oliveira, M. L. Nunes, L. M. Haertel, F. M. Reis, and J. C. da Costa, “Duration of rhythmic EEG patterns in neonates: New evidence for clinical and prognostic significance of brief rhythmic discharges,” *Clinical Neurophysiology*, vol. 111, pp. 1646–1653, 2000.

[86] M. J. Aminoff, “Electroencephalography: General principals and clinical applications,” in *Electrodiagnosis in Clinical Neurology*, M. J. Aminoff, Ed. Oxford, UK: Churchill Livingstone, 1992, pp. 41–91.

[87] J. S. Hahn and B. R. Tharp, “Neonatal and pediatric electroencephalography,” in *Electrodiagnosis in Clinical Neurology*, M. J. Aminoff, Ed. Oxford, UK: Churchill Livingstone, 1992, pp. 93–141.

[88] C. T. Lombroso, “Neonatal EEG polygraphy in normal and abnormal newborns,” in *Electroencephalography: Basic Principles, Clinical Applications and Related Fields*, E. Niedermeyer and F. L. D. Silva, Eds. Oxford, UK: Williams & Wilkins, 1993, pp. 803–875.

[89] A. J. Oliveira, M. L. Nunes, and J. C. da Costa, “Polysomnography in neonatal seizure,” *Clinical Neurophysiology*, no. S2, pp. S74–S80, 2000.

[90] J. Gotman, D. Flanagan, J. Zhang, and B. Rosenblatt, “Automatic seizure detection in the newborn: Methods and initial evaluation,” *Electroencephalography and Clinical Neurophysiology*, vol. 103, pp. 356–362, 1997.

[91] L. G. Kiloh, A. J. McComas, and J. W. Osselton, *Clinical Electroencephalography*. London: Butterworth & Co., 1974.

[92] S. B. Wilson, M. L. Scheuer, C. Plummer, B. Young, and S. Pacia, “Seizure detection: correlation of human experts,” *Clinical Neurophysiology*, vol. 114, pp. 2156–2164, 2003.

[93] J. Gotman, “Automatic recognition of epileptic seizures in the EEG.” *Electroencephalography and Clinical Neurophysiology*, vol. 54, no. 5, pp. 530–40, 1982.

[94] A. Liu, J. Hahn, G. Heldt, and R. Coen, “Detection of neonatal seizures through computerised EEG analysis,” *Electroencephalography and Clinical Neurophysiology*, vol. 82, pp. 30–37, 1992.

[95] M. Roessgen, A. Zoubir, and B. Boashash, “Seizure detection of newborn EEG using a model based approach,” *IEEE Trans. Biomed. Eng.*, vol. 45, pp. 673–685, 1998.

[96] P. Celka and P. Colditz, “A computer-aided detection of EEG seizures in infants: A singular-spectrum approach and performance comparison,” *IEEE Trans. Biomed. Eng.*, vol. 49, pp. 455–462, 2002.

[97] H. Hassanpour, M. Mesbah, and B. Boashash, “Time–frequency feature extraction of newborn EEG seizure using svd-based techniques,” *EURASIP Journal on Applied Signal Processing*, vol. 16, pp. 2544–2554, 2004.

[98] ——, “Time–frequency based newborn EEG seizure detection using low and high frequency signatures,” *Physiological Measurement*, vol. 25, pp. 935–944, 2004.

[99] M. Navakatikyan, P. Colditz, C. Burke, T. Inder, J. Richmond, and C. Williams, “Seizure detection algorithm for neonates based on wave-sequence analysis.” *Clinical Neurophysiology*, vol. 117, pp. 1190–1203, Jun. 2006.

[100] S. Faul, G. Boylan, S. Connolly, L. Marnane, and G. Lightbody, “An evaluation of automated neonatal seizure detection methods,” *Clinical Neurophysiology*, vol. 116, no. 7, pp. 1533–1541, 2005.

[101] G. Boylan and J. Rennie, “Automated neonatal seizure detection,” *Clinical Neurophysiology*, vol. 117, pp. 1412–1413, Jul. 2006.

[102] N. B. Karayiannis, A. Mukherjee, J. R. Glover, P. Y. Ktonas, J. D. Frost Jr., R. A. Hrachovy, and E. M. Mizrahi, “Detection of pseudosinusoidal epileptic seizure segments in the neonatal EEG by cascading a rule-based algorithm with a neural network,” *IEEE Trans. Biomed. Eng.*, vol. 53, no. 4, pp. 663–641, Apr. 2006.

[103] B. Boashash and M. Mesbah, “Time–frequency methodology for newborn electroencephalographic seizure detection,” in *Applications in Time–Frequency Signal Processing*, A. Papandreou-Suppappola, Ed. CRC Press, 2003, ch. 9, pp. 339–369.

[104] ——, “A time–frequency approach for newborn seizure detection,” *IEEE Engineering in Medicine & Biology Magazine*, vol. 20, no. 5, pp. 54–64, September/October 2001.

[105] M. Mesbah and B. Boashash, “Performance comparsion of seizure dection methods using EEG of newborns for implementation of a DSP subsystem,” in *Proc. IEEE Int. Conf. on Acoust., Speech and Signal Processing (ICASSP’02)*, vol. 4, Orlando, FL, 13–17 May 2002, pp. 13–17.

[106] S. Nagasubramanian, B. Onaral, and R. Clancy, “On-line neonatal detection based on multi-scale analysis of EEG using wavelets as a tool,” in *Proc. IEEE Eng. in Med. and Bio. Society, (EMBS-97)*, vol. 3, 1997, pp. 1289–1292.

[107] P. Zarjam, M. Mesbah, and B. Boashash, "Detection of newborn EEG seizure using optimal features based on discrete wavelet transform," in *Proc. IEEE Int. Conf. on Acoust., Speech and Signal Processing (ICASSP'03)*, vol. 2, Hong Kong, 6–10 April 2003, pp. 265–268.

[108] L. Rankine, M. Mesbah, and B. Boashash, "Newborn EEG seizure detection using signal structural complexity," in *Proc. Thirteenth European Signal Processing Conf. (EUSIPCO-04)*, Vienna, Austria, Sep. 2004, pp. 2207–2210.

[109] ——, "Atomic decomposition for detecting signal structure changes : Application to EEG," in *Proc. Int. Conf. of Biomed. Eng., (BioMED-04)*, vol. CD-ROM, Innsbruck, Austria, Feb. 2004.

[110] P. J. Franaszczuk, G. K. Bergey, P. J. Durka, and H. M. Eisenberg, "Time–frequency analysis using the matching pursuit algorithm applied to seizures originating from the mesial temporal lobe," *Electroencephalography and Clinical Neurophysiology*, vol. 106, pp. 513–521, 1998.

[111] H. Hassanpour, W. J. Williams, M. Mesbah, and B. Boashash, "Time–frequency extraction of EEG spike events for seizure detection in neonate," in *Proc. Int. Sym. on Signal Processing and its Applications, (ISSPA-01)*, vol. 1, 2001, pp. 246–249.

[112] H. Hassanpour, M. Mesbah, and B. Boashash, "Comparative performance of time–frequency based newborn EEG seizure detection using spike signatures," in *Proc. Int. Sym. on Signal Processing and its Applications, (ISSPA-03)*, vol. 2, Hong Kong, 6–10 April 2003, pp. 389–392.

[113] ——, "Neonatal EEG seizure detection using spike signatures in the time–frequency domain," in *Proc. Int. Sym. on Signal Processing and its Applications, (ISSPA-03)*, vol. 2, 2003, pp. 41–44.

[114] L. Luke Rankine, "Newborn EEG seizure detection using adaptive time–frequency signal processing," Ph.D. dissertation, School of Engineering Systems, Queensland University of Technology, 2005.

[115] S. J. Schiff, D. Colella, G. M. Jacyna, E. Hughes, J. W. Creekmore, A. Marshall, M. Bozek-Kuzmicki, G. Benke, W. D. Gaillard, J. Conry, and S. R. Weinstein, "Brain chirps: spectrographic signatures of epileptic seizures," *Clinical Neurophysiology*, vol. 111, pp. 953–958, 2000.

[116] C. W. Helstrom, *Elements of Signal Detection and Estimation.* Englewood Cliffs, NJ 07632: Prentice Hall, 1995.

[117] P. Z. Peebles, *Probability, Random Variables, and Random Signal Principles.* Sinapore: McGraw-Hill, 1993.

[118] P. Flandrin, "A time–frequency formulation of optimum detection," *IEEE Trans. Acoust., Speech, Signal Process.*, vol. 36, no. 9, pp. 1377–1384, Sep. 1988.

[119] A. Sayeed, "Optimal time–frequency detectors," in *Time–Frequency Signal Analysis and Processing: A Comprehensive Reference*, B. Boashash, Ed. Oxford, UK: Elsevier, 2003, ch. 12, pp. 500–509.

[120] R. Chassande-Mottin and P. Flandrin, "On the time–frequency detection of chirps," *Applied and Computational Harmonic Analysis*, vol. 6, no. 2, pp. 252–281, Mar. 1999.

[121] B. Boashash and V. Sucic, "Resolution measure criteria for the objective assessment of the performance of quadratic time–frequency distributions," *IEEE Trans. Signal Process.*, vol. 51, no. 5, pp. 1253–1263, 2003.

[122] L. Rankine, N. Stevenson, M. Mesbah, and B. Boashash, "A nonstationary model of newborn EEG," *IEEE Trans. Biomed. Eng.*, vol. 54, no. 1, pp. 19–28, Jan. 2007.

[123] J. Jeong and W. Williams, "Kernel design for reduced interference distributions," *IEEE Trans. Signal Process.*, vol. 40, no. 2, pp. 402–412, 1992.

[124] B. Boashash, M. Mesbah, and P. Colditz, "Newborn EEG seizure pattern characterisation using time–frequency analysis," in *Proc. IEEE Int. Conf. on Acoust., Speech and Signal Processing (ICASSP'01)*, vol. 2, Salt Lake City, UT, 7–11 May 2001, pp. 1041–1044.

[125] P. Celka and P. Colditz, "Nonlinear nonstationary Wiener model of infant EEG seizures," *IEEE Trans. Biomed. Eng.*, vol. 49, pp. 556–564, 2002.

[126] G. Boudreaux-Bartels, "Mixed time–frequency signal transformations," in *The Transforms and Applications Handbook: Second Edition*, A. D. Poularikas, Ed. Boca Raton: CRC Press LLC, 2000, ch. 12.

[127] R. G. Baraniuk and D. L. Jones, "A signal-dependent time–frequency representation: Optimal kernel design," *IEEE Trans. Signal Process.*, vol. 41, no. 4, pp. 1589–1602, 1993.

[128] M. S. Scher, "Electroencephalography of the newborn: Normal and abnormal features," in *Electroencephalography: Basic Principles, Clinical Applications and Related Fields*, E. Niedermeyer and F. L. D. Silva, Eds. Philadelphia, USA: Lippincott Williams & Wilkins, 2003, pp. 937–989.

[129] Y. Zhao, L. E. Atlas, and R. J. Marks II, "The use of cone-shaped kernels for generalized time–frequency distributions of nonstationary signals," *IEEE Trans. Acoust., Speech, Signal Process.*, vol. 38, no. 7, pp. 1084–1091, 1990.

[130] Z. Hussain and B. Boashash, "Adaptive instantaneous frequency estimation of multicomponent FM signals using quadratic time–frequency distributions," *IEEE Trans. Signal Process.*, vol. 50, no. 8, pp. 1866–1876, 2002.

[131] B. Barkat and B. Boashash, "A high-resolution quadratic time–frequency distribution formulticomponent signals analysis," *IEEE Trans. Signal Process.*, vol. 49, no. 10, pp. 2232–2239, 2001.

[132] H. Choi and W. Williams, “Improved time–frequency representation of multicomponent signals using exponential kernels,” *IEEE Trans. Signal Process.*, vol. 37, no. 6, pp. 862–871, 1989.

[133] M. Mesbah, “Seizure detection in real newborn EEG data,” Signal Processing Research Centre, Queensland University of Technology, Tech. Rep., 2004.

[134] N. Stevenson, L. Rankine, M. Mesbah, and B. Boashash, “Newborn EEG seizure simulation using time–frequency signal synthesis,” in *Proc. APRS Workshop on Digital Image Computing*, Feb. 2005, pp. 145–151.

[135] A. Yasotharan and T. Thayaparan, “Optimum time–frequency distribution for detecting a discrete-time chirp signal in noise,” *IEE Proceedings-Vision, Image, and Signal Processing*, vol. 153, p. 132, 2006.

[136] J. S. Lim and A. V. Oppenheim, *Advanced Topics in Signal Processing.* Englewood Cliffs, NJ: Prentice-Hall, 1988.